THE UNIVERSITY
of EDINBURGH

Morphological Analysis of the Axon Initial Segment in Novel Monogenic Rat Models of Autism Spectrum Disorder and Intellectual Disability

Thesis submitted for the degree of Doctor of Philosophy

Shinjini Basu, ***B.Sc., M.Sc.***

THE UNIVERSITY *of* EDINBURGH

Biomedical Sciences

College of Medicine and Veterinary Medicine

University of Edinburgh

January 2020

Declaration

This work was carried out in the Centre for Discovery Brain Sciences, School of Biomedical Sciences at the University of Edinburgh as well as the Centre for Brain Development and Repair, National Centre for Biological Sciences, Bengaluru. I declare that this thesis was composed by myself and that the work contained herein is my own, unless otherwise stated and with exception of the following:

- Analysis of AIS length at the P28-32 age point in the mPFC, S1BF and V1 for *Syngap1*$^{+/\Delta Gap}$, *Syngap1*$^{+/-}$ *Nlgn3*$^{-/y}$, and *Nrx1*$^{+/-}$ were performed by BSc (Hons) students Ayisha Mahmood and Mary Mackay under my supervision
- Stereoteaxic Injections were carried out with the assistance of Dr. Adam Jackson
- Fear conditioning experiments for the *Syngap1*$^{+/\Delta Gap}$ model were performed with Dr. Sally Till
- Generalised Linear Mixed Modelling was performed by Zrinko Kozic and Dr. Owen Dando

No part of the work contained in this thesis has been submitted for any other degree or professional qualification.

Signed: ---------- Date: ----------

Acknowledgements

I've had the privilege of working in two wonderful (and big) labs so this bit is going to be a tad long but necessary. Let's start at the beginning with my supervisors, Prof Peter Kind and Prof Shona Chattarji. Thank you for your continuous support, critique, and insight over the past four years while I've tried to navigate my PhD with varying degrees of success. Another thank you to Peter for all the incredible comments and feedback on my thesis. Thank you to my additional supervisors Dr. Emily Osterweil, Dr. Paul Skehel, and Dr. Aditi Bhattacharya for all of your valuable inputs and suggestions over the four years.

A big thank you to Adam and Sally, for their infinite patience while teaching me how to do surgeries and behaviour and another thank you to Adam for all of the discussions that helped put a lot of this thesis into perspective. To Sam and Susana for teaching me perfusions, immunos, and slicing that make up the bulk of this thesis. And to Owen and Zrinko for running the GLMM analysis on all of my AIS data.

Anna, Katherine, and Tasha, the lovely YOHO (You only Hobo once) crew, thank you for drinking wine out of mugs while singing Disney tunes in four different languages while sat at our wee dining table in Bangalore. It made working the late nights and early mornings that much more fun. To Teresa, Farhana, Jesvin, Arnab, Giselle and Prabahan, thank you for making NCBS an incredibly fun year filled with intense discussions about science, life, and, of course, delicious food.

Thank you to members of the Kind-Wyllie, Osterweil, and Shona labs: David, Danai, Laura O, Laura B, Joanna, Lindsay, Lynsey, Raven, Tom, Anjie, Ali, Fliss, Neela, Katie M, Emma, Melania, Steph, Priya, Sarfaraz, Aiman, Vijay, Shashank, Arpita, Yogesh, Bharath, Rohit, Rohini, Shreya, Vaibhav, Zubin, and Priyal. The PhD would have been a lot less fun without all you lovely folks. A special thank you also to Fliss, Tasha, Adam, Ali, Sarah and Melanie for invaluable feedback on my thesis.

My honours and summer students, Mary, Alysia and especially Ayisha – you know my pain of measuring hundreds of AISs, so thank you for all your hard-work.

Konstanze, Iva, and Jet: Thank you for being the best room/ flat-mates I could have asked for and generally making sure I remembered to adult on a semi-regular basis. To all three of you and Agrima and Miriam for taking my 3 am panic stricken phone calls.

Maria, Jinty, Roanna, Emma and Angharad, thank you for being my partners in crime in all things outdoors from going on rather damp hikes to climbing trees and bouldering three too many times a week.

A thank you to Melanie for mentoring me over the past year and helping me see the silver lining over the dark clouds of the final year of my PhD. A wee thank you to New Scotland for giving me my weekly dancing fix, without which I would have lost what little sanity I do possess, a long time ago.

Thank you to Greg, for being there through all the anxiety, doubt, fatigue and joy over the past 3 years and having unlimited faith in me, especially when I didn't.

And lastly to my family. Dada and Aditi, thank you for being the sane (and occasionally sarcastic) voices that have helped me navigate adulthood. And to Ma and Baba, who have always believed in my ability to succeed in every hair-brained and half-baked adventure I have chosen to embark upon.

Lay Summary

Autism spectrum disorders, intellectual disabilities and childhood epilepsies have a prevalence of about 1-3% in the western child and adolescent populations with mutations in single genes being responsible for more than 60% of the more severe, low-functioning cases. However, the biological mechanisms underlying autism spectrum disorders and intellectual disabilities (ASD/IDs) remains largely unknown. Over the course of my PhD, I have used transgenic rats to model one such single-gene associated ASD/ID, *SYNGAP1*-mediated ID. The use of a laboratory rat as a pre-clinical model for this disorder will help us gain a better understanding of the cellular and molecular processes that cause altered behaviours observed in humans with this condition.

Neurons, the most abundant cell type in the brain, communicate with each other through short, electrical pulses at specialised junctions called synapses. Most neurons continually adapt the volume, speed, and frequency with which they communicate in response to external and internal cues. They do so by modulating some of their own features, including the number of incoming electrical pulses required before a neuron will conduct its own pulse to the next cell. This feature, termed 'cellular excitability', is very tightly regulated and is often found to be altered in ASD/ ID, including in rat models of *SYNGAP1*-mediated ID. One key regulator of cellular excitability is the site where these electrical pulses are generated, called the axon initial segment (AIS). The AIS controls cellular excitability by altering its length and its distance from the main body or 'soma' of the cell in response to incoming information. Thus, the key hypothesis explored in this thesis is that alterations in AIS length underlie the alterations in cellular excitability observed in the rat models of *SYNGAP1*-ID.

In order to test this hypothesis, first a characterisation of AIS lengths across six different brain regions was undertaken in rats that model *SYNGAP1*-ID and compared to control animals. The brain regions chosen included two sensory regions as well as four brain regions used for higher cognitive function as individuals with *SYNGAP1*-ID present with impaired cognitive function and altered responses to sensory stimuli including increased sensitivity to sound. Second, the ability of the AIS to adapt its length in response to stimuli was tested. This was done by subjecting *SYNGAP1*-ID and control rats to an anxiety-associated learning task followed by measuring and comparing changes in AIS lengths in two brain regions that are involved

in modulating fear and anxiety. An anxiety-associated learning task was chosen as fear and anxiety-related behaviours are known to be altered in individuals with *SYNGAP1*-ID.

Lastly my thesis has also explored the idea that different genetic causes of ASD/ID converge to result in similar changes to cellular function. As such, I hypothesize that alterations to AIS lengths might underlie alterations in cellular excitability across other single gene or monogenic causes of ASD/ID. In order to test this, I have examined AIS lengths in the same brain regions studied in the *Syngap1*-ID rat in six additional rat models of monogenic forms of ASD/ID. Convergence is a particularly attractive hypothesis because, if true, it would mean that the same drug might be beneficial to individuals with genetically distinct mutations that cause their ASD/ID. The results indicate that in almost all the brain-regions studied the AIS length remained unchanged between animals modelling ASD/ID and control animals. My thesis, therefore rejects the hypothesis that alterations in AIS length is a common pathway underlying changes in excitability across these models. However, the work documented here provides the first evidence of anxiety-induced alterations in AIS length in models of *SYNGAP1*-ID as well as differences in AIS length in a juvenile rat model of Fragile-X syndrome.

Scientific Abstract

Monogenic mutations in synaptic proteins are known to cause severe and low functioning cases of autism spectrum disorder and intellectual disability (ASD/ID) (Wright et al., 2018). One of the most prevalent monogenic causes of moderate to severe non-syndromic and syndromic ID with a high co-morbidity of seizures and altered sensory processing is *SYNGAP1* haploinsufficiency (Hamdan et al., 2009; Hoischen et al., 2014). Resulting from *de novo* truncating or frameshift mutations in the *SYNGAP1* gene on human chromosome 6, *SYNGAP1* haploinsufficiency leads to a 50% reduction of the encoded synaptic GTP-ase activating protein (SynGAP) (Hamdan et al., 2009).

Pre-clinical models of *Syngap1* haploinsufficiency have provided an invaluable tool to understand the underlying pathophysiology resulting from a reduction of SynGAP. The heterozygous mouse model of *Syngap1* haploinsufficiency (*Syngap1*$^{+/-}$) demonstrates a range of cellular, physiological and behavioural abnormalities from early development to adulthood (Chen et al., 1998; Kim et al., 1998; Komiyama et al., 2002; Rumbaugh et al., 2006; Muhia et al., 2010). Key among these phenotypes is brain region and cell-type specific hyper- and hypo-excitability, causing an excitation/inhibition imbalance which manifests as disrupted circuit function (Clement et al., 2012, 2013; Ozkan et al., 2014; Aceti et al., 2015; Berryer et al., 2016; Katsanevaki, 2017).

Neuronal excitability is defined as the probability of action potential (AP) generation in response to a given current. The site of AP generation is a specialised cellular compartment located between the somatodendritic and axonal compartments of a neuron, called the axon initial segment (AIS). The AIS is a dynamic structure, shown to alter its length and position along the axon in response to altered physiological and pathological conditions (for review see Rasband (2010)). Prolonged increase in neuronal activity causes shortening and a distal shift of the AIS (Evans et al., 2015; Grubb and Burrone, 2010) while extended periods of decreased neuronal activity result in lengthening and proximal shift of the AIS (Kuba et al., 2006; Kuba, 2012). The functional consequence of this morphological plasticity is altered intrinsic excitability such that neurons with distally located, shorter AISs exhibit increased AP threshold with subsequent production of fewer APs in response to a given current while neurons with longer, proximal AISs exhibit decreased AP threshold and increased frequency

of AP firing (Kuba et al., 2006; Grubb and Burrone, 2010; Kuba et al., 2010; Kuba, 2012; Evans et al., 2015). Given this ability of the AIS to alter cellular excitability and the evidence of altered excitability in pre-clinical models of *SYNGAP1* haploinsufficiency, this thesis tests the hypothesis that alterations in AIS length will underlie some the altered cellular excitability observed upon reduction of SynGAP.

In order to test this hypothesis, first a characterisation and comparison of AIS lengths between *Syngap1*$^{+/-}$ and control juvenile rats was undertaken across six brain regions previously known to exhibit altered cellular excitability or be involved in behaviours that are altered in *Syngap1* haploinsufficiency. These brain regions include the prelimbic medial prefrontal cortex (mPFC-PL), somatosensory cortex – barrel fields (S1BF), *Cornu Ammonis* 1 and 3 (CA1, CA3) sub-fields of the dorsal hippocampus, the lateral (LA) and basal (BA) nuclei of the amygdala and the primary visual cortex 1 (V1). Juvenile animals were chosen to reflect the developmental underpinnings of this disorder as *Syngap1*$^{+/-}$ mice exhibit alterations in synaptic physiology at this age (Barnes et al., 2015) and it coincides with the developmental critical period for some of the brain regions analysed, including the V1 and BLA. Further, the AIS has been shown undergo developmentally regulated alternations in its morphology during this time-period. Statistical analysis of results and post-hoc interactions of brain-region and genotype were analysed using a linear mixed modelling (LMM) approach to account for the non-normal distribution of the data-sets. Subsequently, the effects of *Syngap1* haploinsufficiency on morphological plasticity of the AIS was tested. This included analysis and comparison of genotype specific changes in AIS lengths over development and following a cued fear conditioning associative-learning paradigm. Lastly, as cell-type specific differences in cellular excitability have been noted in the *Syngap1*$^{+/-}$ mouse, AIS lengths were compared across genotypes in cells of the mPFC and BLA with specific projection targets. In addition to studying the difference of AIS length in rat models of *SYNGAP1* haploinsufficiency, a similar study was undertaken in this thesis in rat models of Fragile-X syndrome, Cowden's syndrome, *NLGN3*-associated non-syndromic ID, *NRXN1* and *CNTNAP2* associated ASD/ID. This work was undertaken to study the hypothesis that diverse genetic causes of ASD/ID converge onto common cellular pathways, and, as pre-clinical models of these disorders all exhibit evidence of altered cellular excitability, alterations in AIS length might underlie some of these changes.

The work documented in this thesis provides the first characterisation of AIS lengths across

pre-clinical models of *Syngap1* haploinsufficiency as well as across multiple monogenic rat models of ASD/ID. The results indicate that in almost all the brain-regions and models studied, AIS morphology remained unaltered between heterozygous/homozygous animals and their wild-type littermate controls, causing a rejection of the hypothesis that alterations in AIS morphology is a common cellular pathway underlying changes in cellular excitability across these models. However, provided here is the first evidence of AIS morphology in the mPFC-PL being differentially altered in *Syngap1* haploinsufficiency compared to control animals when subjected to a cued fear conditioning paradigm as well as alterations in AIS morphology in the mPFC, S1 and BA in a rat model of Fragile-X syndrome.

Contents

List of Abbreviations

ACSF	Artificial Cerebrospinal Fluid
ADHD	Attention Deficit Hyperactivity Disorder
AIS	Axon Initial Segment
AMPAR	α-amino-3-hydroxy-5-methyl-4-isoxazolepropionic acid receptor
AnkG	Ankyrin-G
AP	Action Potential
ASD/ID	Autism Spectrum Disorders and Intellectual Disability
BA	Basal Amygdala
BDNF	Brain-Derived Neurotrophic Factor
BFNIS	Benign Familial Neonatal-Infantile Seizure
C2	Calcium dependent Lipid Binding
CAM	Cell Adhesion Molecule
CamKII	Ca^{2+}/calmodulin-dependent protein kinase
CDK-5	Cyclin-Dependent Kinase 5
CeA	Central amygdala
CF	Characteristic Frequency
CNTNAP2	Contactin Association Protein-Like 2
CRF	Corticotropin Releasing Factor
CS	Conditioned Stimulus
D3	Dopamine Receptor 3
DDD	Deciphering Developmental Disorders
DfCS	Distance from Cell Soma
DG	Dentate Gyrus
E	Embryonic
EC	Entorhinal cortex
EPM	Elevated Plus Maze
EPSP	Excitatory Postsynaptic Potential
ERK 1/2	Extracellular-signal Regulated Kinases
FMR1	Fragile-X Mental Retardation Gene 1

FXS	Fragile X Syndrome
$GABA_A$	γ-Amino Butyric Acid
GEF	Guanine Exchange Factors
GLMM	Generalised Linear Mixed Modelling
GWAS	Genome Wide Association Studies
Het	Heterozygous
Het	Heterozygous
ICI	Inter-Conditioning Interval
IQ	Intelligent Quotient
ITI	Inter-Trial Interval
kDA	Kilo Dalton
L	Layer
LA	Lateral Amygdala
LEH	Long-Evans Hooded
LLPS	Liquid–liquid phase separation
LRRTM	Leucine Rich Repeat TransMembrane proteins
LRRTMs	Leucine-Rich Repeat Transmembrane Proteins
LTD	Long-Term Depression
LTP	Long Term Potentiation
MAGUK	Membrane-Associated Guanylate Kinases
MAPK	Mitogen-Activated Protein Kinases
mGluR	Metabotropic Glutamate Receptor
mGPSC	miniature $GABA_A$-mediated postsynaptic currents
mPFC	Medial Prefrontal Cortex
mTOR	Mammalian target of rapamycin
MWM	Morris Water Maze
NGS	Normal Goat Serum
NL	Nucleus Laminaris
NLGN3	Neuroligin-3
NM	Nucleus Magnocellularis
NMDAR	N-Methyl-D-Aspartate Receptors
NREM	Non-rapid eye movement
NRX1	Neurexin-1
NSID	Non-Syndromic Intellectual Disability
NT3	Neurotrophin 3
P	Postnatal day
PAG	Periaqueductal gray
PB	Phosphate Buffer
PBS	Phosphate Buffer Saline
PBS-T	Phosphate Buffer Saline with Tween-20
PCR	Polymerase Chain Reaction

PDD	Pervasive Developmental Disorders
PET	Positron Emission Tomography
PFA	Paraformaldehyde
PH	Pleckstrin Homolgy
PHTS	PTEN hamartoma tumour syndromes
PI3K	Phosphatidylinositol 3-phosphate kinase
PIP_2	Phosphatidylinositol4,5-bisphosphate
PIP_3	Phosphatidylinositol (3,4,5)-trisphosphate
PKB	Protein kinase B
PKC	Protein Kinase C
PPI	Pre-Pulse Inhibition
PSD	Post-Synaptic Density
PTEN	Phosphatase and Tensin Homolog
PTSD	Post Traumatic Stress Disorder
rsfMRI	resting State Functional Magnetic Resonance Imaging
S-ID	Syndromic Intellectual Disability
S1BF	Somatosensory Cortex - Barrel Fields
SD	Sprague-Dawley
TARP	Transmembrane AMPA-R Regulatory Proteins
TCA	Thalamo-Cortical Afferents
TS	Tuberous Sclerosis
TTX	Tetrodotoxin
US	Unconditioned Stimulus
USV	Ultra-Sonic Vocalisations
V1	Primary Visual Cortex 1
WT	Wild-type

List of Figures

List of Tables

Chapter 1

Introduction

1.1 Autism spectrum Disorder, intellectual disability & childhood epilepsy

Pervasive developmental disorders (PDDs), including autism spectrum disorders (ASD), intellectual disabilities (ID), attention deficit hyperactivity disorder (ADHD) and childhood epilepsies affect about 2-5% of the general western population (Chelly et al., 2006; Cooper et al., 2009; Shevell et al., 2003). Prevalence of these PDDs is estimated to be higher in low and middle-income countries where diagnosis, management, and support options are limited (Samadi and McConkey, 2011; Akhter et al., 2018).

As per the World Health Organisation's International Statistical Classification of Diseases and Related Health Problems (ICD-10), intellectual disability is defined as:

'A condition of arrested or incomplete development of the mind, which is especially characterized by impairment of skills manifested during the developmental period, skills which contribute to the overall level of intelligence, i.e. cognitive, language, motor, and social abilities' (World Health Organization, 1992).

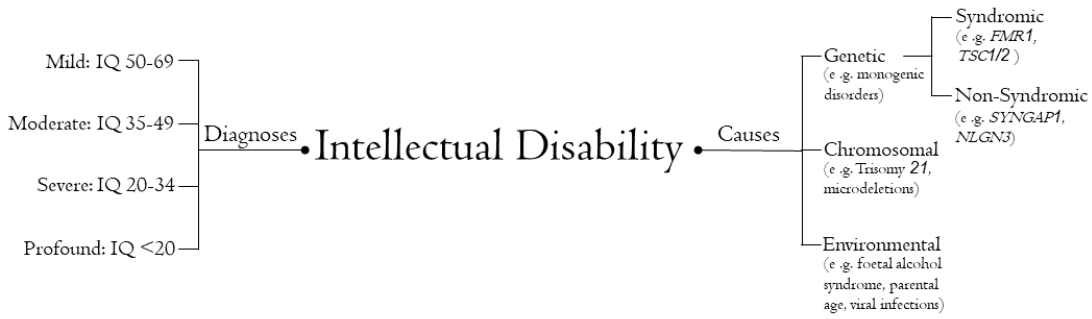

Figure 1.1: Diagnoses and Causes of Intellectual Disabilities (Left) A diagnosis of intellectual disabilities (ID) is classified using intelligence quotient (IQ) tests into mild (IQ 50-69), moderate (IQ 35-49), severe (IQ 20-34) or profound (IQ <20) (Right) The causes of ID are highly heterogeneous and include environmental, chromosomal and single gene mutations. Monogenic causes of ID are further divided in to syndromic and nonsyndromic forms of ID. Syndromic causes of ID are characterised by physical, metabolic and biological features and include Tuberous Sclerosis, Fragile X syndrome which are caused by mutations in the *TSC1/2* and *FMR1* genes respectively. In contrast, the only clinical manifestation associated with non-syndromic causes of ID is cognitive dysfunction, examples of which include mutations in *SYNGAP1* and *NLGN3* that encode the synaptic GTPase activating protein (SYNGAP) and NEUROLIGIN-3 that are crucial for normal synaptic functions.

Traditionally, ID severity was estimated using standardised intelligent quotient tests, with a positive diagnosis made in individuals presenting with an IQ score of <70 and onset before the age of 18. The diagnosis is further classified into mild (IQ 50-69), moderate (IQ 35-49), severe (IQ 20-34) or profound (IQ <20), and into syndromic (S-ID) or non-syndromic (NS-ID) intellectual disability (fig 1.1). In S-ID, patients present with one or multiple clinical features such as morphological (cranial, facial, and skeletal dysmorphisms), radiologic or metabolic abnormalities in addition to ID whereas patients with NS-ID present with intellectual disability as the sole clinical feature (Kaufman et al., 2010). More recently, the criteria for ID diagnosis has evolved to include the development of conceptual, social and practical skills, grounding its diagnosis in adaptive functioning.

ASD is characterised by deficits in social communication and social interaction, with restricted, repetitive patterns of behaviour, interests or activities (Harper, 2014). About 30% of individuals diagnosed with ASD also present with ID. While approximately 20% of individuals diagnosed with both ASD/ID present with epilepsy and 90% report altered sensitivity to various sensory and tactile stimuli (fig. 1.2) (Marco et al., 2011; Besag, 2018). An epilepsy diagnosis is applied to patients exhibiting two unprovoked seizures greater than 24 h apart (Fisher et al., 2014) with subsequent severe perturbations in neurobiological, cognitive, psychological, and social function (Scheffer et al., 2017). An epileptic seizure is a transient symptom state resulting

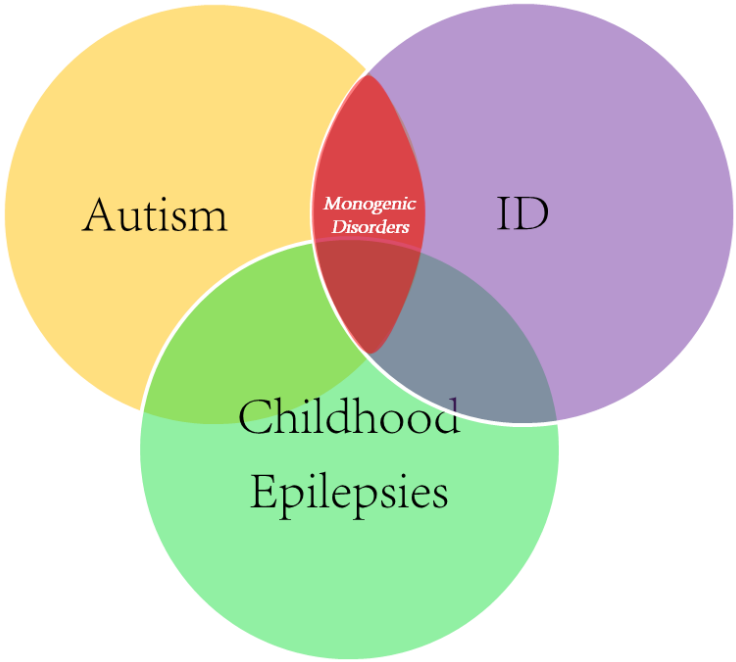

Figure 1.2: Neurodevelopmental Disorders Schematic Venn diagram of neurodevelopmental disorders (NDD) including autism spectrum disorders, intellectual disabilities (ID) and childhood epilepsies. Where these disorders overlap, the most severe, low functioning cases are found. Monogenic mutations have been found to be the predominant causative factor in these cases.

from abnormal, excessive, or synchronous neuronal activity in the brain and is characterized by abrupt and involuntary skeletal muscle activity (Klitten et al., 2011).

The impact on the life-span and quality of life for the individuals living with these disorders presents a major challenge to clinicians, geneticists and neuroscientists (Patja et al., 2001; Tyrer et al., 2007; Emerson and Baines, 2011; Dieckmann et al., 2015; Baxter et al., 2015). Current therapies focus on symptomatic relief of co-morbidities including seizures, anxiety, ADHD and mood disorders. Therefore, in order for us to better treat individuals with these disorders it is vital to understand its aetiology and pathophysiology.

1.1.1 Causes of ASD/ID

ASD/IDs present with complex aetiology, with causes being highly heterogeneous. These include both genetic and environmental factors that disrupt key neurodevelopmental processes during pre-, peri- and early post-natal life (Figure 1.1) (Chelly et al., 2006; Chiurazzi and Pirozzi,

2016). Acquired and environmental causes include maternal intoxication with alcohol or drugs (e.g. foetal alcohol syndrome), foetal infection (e.g, CMV, meningitis), vascular accidents and asphyxia. Genetic causes span chromosomal abnormalities and monogenic causes, with some studies suggesting they account for 25-50% of all ID cases (McLaren and Bryson, 1987; Kaufman et al., 2010). Chromosomal abnormalities include microdeletions, trisomy 21, and deregulation of imprinted genes causing syndromes such as Prader F Willi and Angelman syndrome. A recent Deciphering Developmental Disorders study (DDD) (Wright et al., 2018), has found that 42% of individuals of their 1,133 cohort with the most severe cases of ASD/ID all presented with mutations in a single gene. This is a 15% increase from the reported 27% in their initial 2011 study (Firth and Wright, 2011).

Despite the ever-increasing identification of genetic and environmental causes of ASD/ID, the underlying pathophysiology of these disorders remains poorly understood. Monogenic disorders are particularly attractive to study as not only do they account for the most severely affected individuals, but they can also be easily modelled in the lab *in vivo* (e.g. rodent models), *in vitro* (cell culture) and *in silico* (computational models). This allows for extensive pre-clinical examination and thus furthers our understanding of disease pathology.

SYNGAP1 haploinsufficiency, occurring in 0.75-1% of individuals with either epileptic encephalopathy (Carvill et al., 2013) or ID (Fitzgerald et al., 2015) and characterised by developmental delay (100% of individuals carrying pathogenic mutations), generalized epilepsy (~84%) and ASD ($\leq$50%) (Asadi, 2018), is one such single-gene disorder and forms the primary focus of this thesis.

1.2 *Syngap1* Haploinsufficiency linked to S-ID and NS-ID

The human *SYNGAP1* gene is present on chromosome 6p21.3 and encodes the ~135 kDa Synaptic GTP-ase Activating Protein (SynGAP). SynGAP is one of the most abundant proteins present in the post-synaptic density (PSD) of mammalian neurons, making up nearly 1-2% of all PSD-proteins (Kim et al., 1998). It is predominantly known for its negative regulation of the Ras/Rap pathway as part of the *N-methyl-D-aspartate* receptor (NMDAR) complex. The

structure and function of the *SYNGAP1* gene, and resulting protein, are further elaborated in section 1.3.

De novo mutations in the *SYNGAP1* gene were first identified as causative of NS-ID in 3 patients in Montreal by Hamdan et al. (2009). These mutations resulted in haploinsufficiency: The loss of one functional copy of the *SYNGAP1* gene and a consequent 50% reduction in protein level. Since then, mutations in *SYNGAP1* in patients with ID has been reported in over 18 studies (Vlaskamp et al., 2019). Hoischen et al. (2014) reported *SYNGAP1* as one of the most recurrent mutated genes with *de novo* mutations, in the form of truncating, missense, chromosomal translocations and micro-deletions, presenting in one of 8 patients with ID, ASD, schizophrenia and developmental and epileptic encephalopathy (fig. 1.3). The Deciphering Developmental Disorders (DDD) study led by Fitzgerald et al. (2015) identified *SYNGAP1* as one of the top 5 recurrently mutated genes in individuals with genetically-undefined developmental brain disorders. Lastly, the Simons Foundation Autism Research Initiative (www.sfari.org) listed *SYNGAP1* as one of 23 'high confidence' autism risk genes.

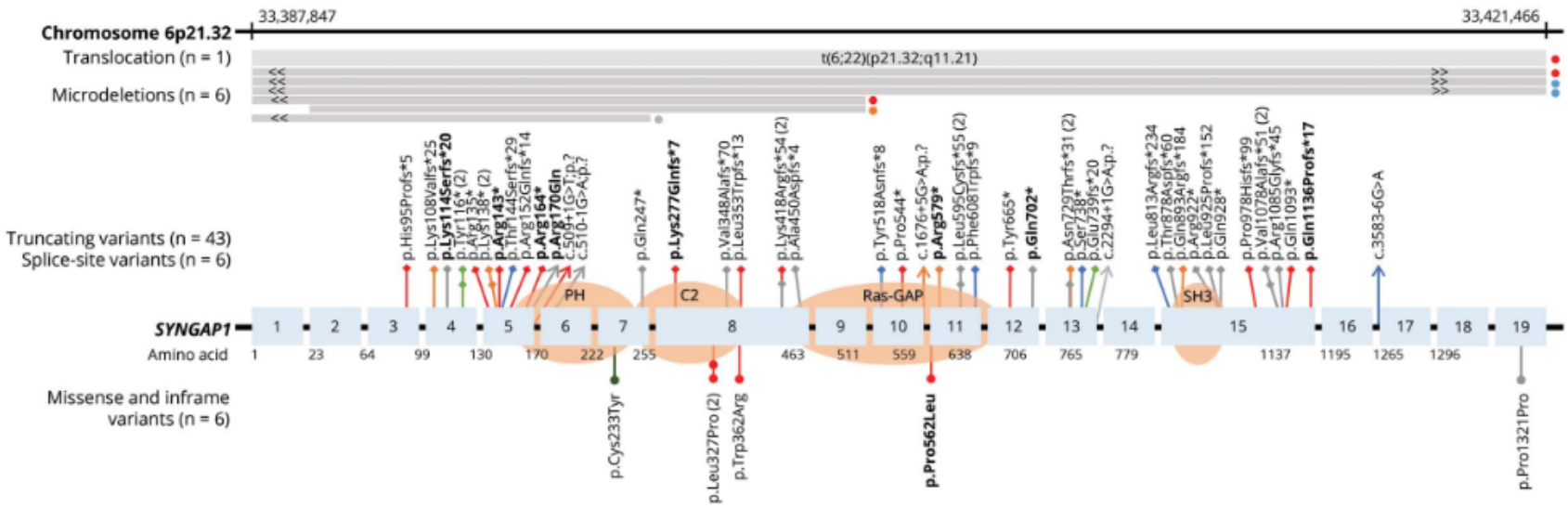

Figure 1.3: Schematic presentation of *SYNGAP1* mutations and micro-deletions previously published in the literature Chromosome 6p21.32 microdeletions including *SYNGAP1*, are presented as gray bars with «and »indicating that their breakpoints were outside the region presented here. Patient mutations include translocations, mirodeletions, truncating variants, splice-site variants, missense variants and inframe mutations. Colors of the lines represent the epilepsy syndrome phenotype: moderate to severe developmental and epileptic encephalopathy (red), moderate to severe developmental encephalopathy with epilepsy (orange), moderate to severe developmental encephalopathy with no epilepsy (blue), mild developmental and epileptic encephalopathy (light green), mild developmental encephalopathy with no epilepsy (dark green), and unknown/unclassified epilepsy (gray). Chromosomal coordinates were based on National Center for Biotechnology Information Build 37 [hg19] and *SYNGAP1* mutations, protein domains, and exons on the longest isoform 1 (NM 006772.2) Image from Vlaskamp et al. (2019).

Until 2015, *SYNGAP1* haploinsufficiency was linked solely to NS-ID. However, a study by Parker et al. (2015) presented the first evidence of 10 individuals with *SYNGAP1* haploinsufficiency presenting with clinically syndromic ID. A more recent study by Vlaskamp et al. (2019) identified 57 new patients with *de novo* mutations in *SYNGAP1*, 56 of whom presented with developmental and epileptic encephalopathy with eyelid myoclonia (65%), atonic seizures triggered by eating (25%) and ataxia and gait abnormalities (51%). 55 of the patients presented with ID (50 patients with moderate to severe ID), expanding the number of *SYNGAP1* haploinsufficiency individuals with S-ID.

Across multiple clinical case reports, the most recurrent pathologies reported in individuals with *SYNGAP1*-ID include: moderate to severe-ID, hyperactivity with ADHD, elevated anxiety, moderate to severe speech impairment, aggression towards care-givers, seizures including myoclonic seizure, absence seizures, drop attacks, generalised tonic-clonic seizures and photosensitive epilepsy. Parents and care-givers also note anecdotal evidence of increased pain-threshold, altered sleep patterns, gait abnormalities and hyperacusis (heightened sensitivity to sound) (Hamdan et al., 2009, 2011; Pinto et al., 2010; Parker et al., 2015; Krepischi et al., 2010; Zollino et al., 2011; Pinto et al., 2010; Klitten et al., 2011; De Ligt et al., 2012; Rauch et al., 2012; Berryer et al., 2013; Carvill et al., 2013; Writzl and Knegt, 2013; Redin et al., 2014; Von Stülpnagel et al., 2015; Mignot et al., 2016; Prchalova et al., 2017; Vlaskamp et al., 2019; Jimenez-Gomez et al., 2019).

Despite the increase in patient numbers presenting with autosomal dominant mutation-linked ID the numbers are quite small, partly due to the lowered reproductive fitness associated with these conditions, occluding linkage analysis. Therefore, pre-clinical models offer an excellent platform to gain a better understanding of complex pathophysiology underlying these disorders and new potential therapeutic targets.

1.3 SynGAP Protein: Expression, Structure and Function

1.3.1 Protein Expression

SynGAP was first identified in 1998 by two independent groups (Kim et al., 1998; Chen et al., 1998) in the PSDs of the rat forebrain. Found in a large complex with synapse associated protein (SAP102), PSD-95 and NMDARs, SynGAP protein expression was initially thought to be limited to the excitatory PSDs of mice (Kim et al., 1998; Chen et al., 1998; Knuesel et al., 2005; Clement et al., 2012, 2013; Ozkan et al., 2014). However, SynGAP was later shown to also be present in the PSDs of inhibitory GABAergic neurons of mice (Zhang et al., 1999; Moon et al., 2008; Ozkan et al., 2014; Berryer et al., 2016).

The earliest reported expression of *Syngap1* mRNA in mice is at embryonic (E) day 8.5 with whole-mount embryos showing expression throughout the developing neural tube, somites and heart (Porter et al., 2005). By E10.5 *Syngap1* mRNA expression extended to the developing limb-buds while expression in the cortex, basal ganglia and thalamus reported at E14.5. At E16.5, following the completion of neurogenesis, *Syngap1* expression is reported in the hippocampus and hypothalamus. In the cortex, protein expression peaks in the second week of post-natal development (P14) before being restricted to L2/3 and the boundary of L4/5 in the adults (>P60) (Barnett et al., 2006; Clement et al., 2012; McMahon et al., 2012). Lastly, in adult animals SynGAP protein is also expressed in the striatum, amygdala and olfactory bulbs but not in the thalamus, cerebellum, midbrain or brain stem (Porter et al., 2005).

1.3.2 Protein Structure

A highly-conserved gene, SynGAP has multiple amino- (N-) and carboxyl-terminal (C-) isoforms. The N-terminal isoforms include A, B, C and E and arise from alternative transcription start site while the C-terminal isoforms, arising from alternative splicing, include α1, α2, β1-4 and γ (Li et al., 2001; McMahon et al., 2012) (Figure 1.4). The different SynGAP isoforms show differential localisation, with the α1 isoform being found solely in excitatory neurons whereas the β isoform is found in both excitatory and inhibitory neurons. The β isoform is also found to

be distributed more along the dendritic tree compared to the α1 isoform in neuronal cell culture (Moon et al., 2008). Both the N- and C-terminal isoforms exert differential activity dependent functions, elaborated below (see section 1.3.3). Additionally, the C-terminus also acts as a classical small protein binding SH3 domain, mediating the formation of protein complexes via a proline-rich region (770 - 800) (Cohen et al., 1995).

The Pleckstrin Homology (PH) domain is a 100 amino acid region that binds the phosphatidylinositol of biological membranes. This domain is complete in the A, B and E isoforms, with a truncated domain present in the C isoform. The calcium dependent lipid binding (C2) domain forms part of the core-domain of the protein that is shared by all the isoforms. A study by Pena et al. (2008) showed that the C2 domain was crucial for the activity of SynGAP as a Rap-GTPase. The enzymatic 'GAP' domain of SynGAP defines it as a guanosine triphosphatase–activating protein and mediates the effect of SynGAP on downstream signalling pathways. This function is further elaborated below.

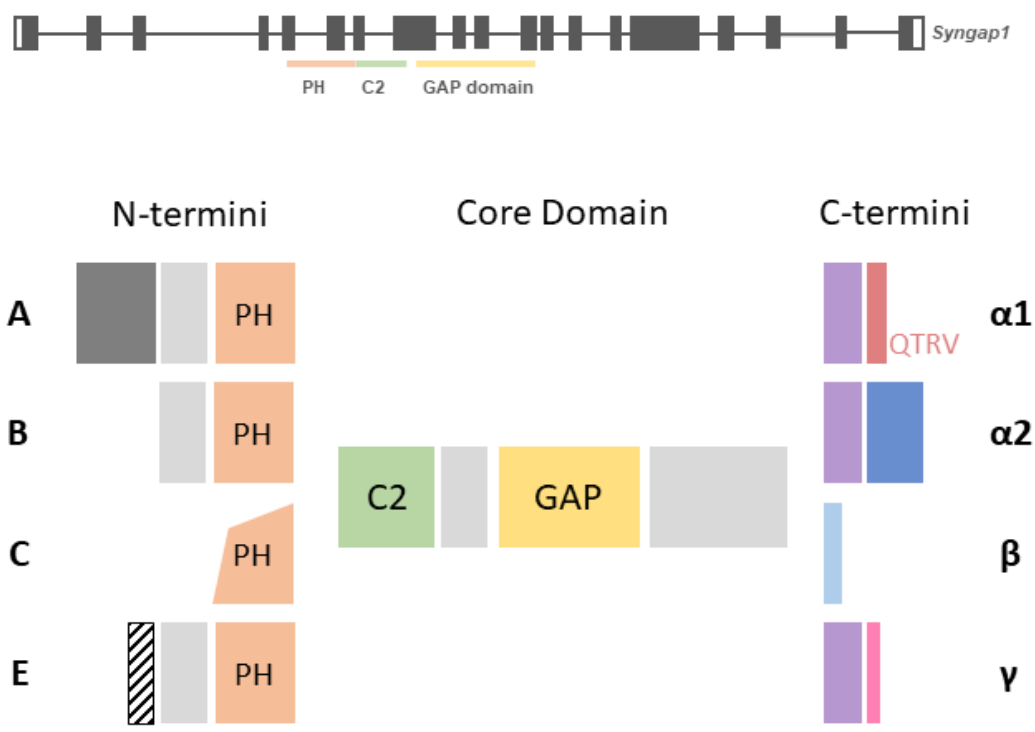

Figure 1.4: SynGAP Protein Structure (Top) *Syngap1* gene adapted from the online ENSEMBL database showing the exons coding for the PH, C2 and GAP domain (Bottom) SynGAP Protein showing the various N- and C-terminal Isoforms and the core functional protein domains

1.3.3 Protein Function

Protein Interactions

As previously stated, SynGAP forms part of the NMDAR protein complex. Its interactions as part of this complex affects downstream signalling cascades and synaptic plasticity in a GAP-domain dependent and independent manner.

Yeast two-hybrid screening studies revealed that SynGAP binds directly to the PDZ structural domains of membrane-associated guanylate kinases (MAGUKs) such as SAP102 and PSD-95. The same system also showed that PSD-95, via it's PDZ domain, directly binds to the GluN2B sub-unit of NMDARs (Kim et al., 1998). As the PSD-95 interaction provided a direct link between SynGAP and NMDARs, it was thought to be the main binding source localising SynGAP to the PSD. This binding is facilitated by the QTRV motif found in the $\alpha 1$ C-terminal isoform, making it the most studied of all SynGAP isoforms. However, experiments by Vazquez et al. (2004) showed that a mutation in the QTRV motif did not alter the presence of re-combinant protein in the spines and the β isoform, lacking the QTRV motif, is also isolated in the PSD fraction. These findings by Vazquez et al. (2004) can be partially explained by SynGAP's interaction with Ca^{2+}/calmodulin-dependent protein kinase (CamKII) (Kim et al., 1998; Chen et al., 1998). Indeed, SynGAP $\alpha 1$, $\alpha 2$ and β isoforms are all shown to directly interact with the α isoform of CamKII (Kim et al., 1998; Chen et al., 1998; Li et al., 2001).

Additionally, in neurons of the CA1 and CA3 sub-unit of the hippocampus, SynGAP is shown to interact with the ubiquitously expressed scaffolding protein MUPP1 (Krapivinsky et al., 2004). MUPP1 facilitates a direct physical interaction with CamKII, forming another link to NMDARs via CamKII's interaction to the GluN2B receptor sub-unit. This interaction, however, was shown to not be crucial for SynGAPs localisation to the PSD. Disruption of the MUPP1-SynGAP complex, using TAT-PDZ13 fusion protein, failed to alter SynGAP clusters at the PSD of cultured hippocampal neurons.

Activity Dependent Regulation

The regulation of synaptic strength by SynGAP is dependent on neuronal activity. McMahon et al. (2012) show that in mouse neuronal cultures, enhancing and inhibiting network activity produced differential expression of its N-terminal isoforms. Bath application of network enhancer bicuculline, a γ-amino butyric acid (a) ($GABA_A$) receptor agonist, increased mRNA levels of SynGAPs N-terminal B and C isoforms while reducing mRNA levels of the A isoform. Conversely, inhibiting network activity, via application of tetrodotoxin (TTX), reversed these changes. This form of network manipulation was not found to affect the mRNA levels of the C-terminal $\alpha 1$ or $\alpha 2$ isoforms. However, expression of $\alpha 1$, in combination with either A, B or C N-terminus, showed a 73% increase in the presence of 'silent synapses', measured as cells lacking mEPSCs. Expression of $\alpha 2$ did not show a similar increase, maintaining silent synapse percentages similar to wildtype levels of about 11%. Finally, $\alpha 2$ over-expression in combination with either the B or C N-terminal resulted in increased mEPSC amplitude and frequency whereas over-expression of $\alpha 1$ with the A N-terminal isoform resulted in decreased mEPSC amplitude.

In addition to regulating its synaptic strength, SynGAP localisation to the PSD is also regulated in an activity dependent manner. Typically SyNGAP expression is found in the PSD-core, the first 40 nm from the post-synaptic membrane, with more sparse expression 40-120 nm from the membrane (Yang et al., 2011). Yang et al. (2011, 2013) showed that upon depolarisation induced by application of K^+ or activation by application of NMDA, SynGAP $\alpha 1$ and $\alpha 2$ are relocated away from the PSD-core to the 40-120 nm region in PSD-fractions isolated from adult rat brains. This re-location is reversible and mediated by CamKII. Additionally, Araki et al. (2015) showed that during and following induction of chemical long-term potentiation (LTP) using glycine in cultured hippocampal neurons, CamKII mediates rapid dispersal of SynGAP away from spines. This is blocked if you inhibit CamKII or mutate its phosphorylating sites on SynGAP.

The predominant function of SynGAP is mediating synaptic plasticity via regulation of downstream signalling cascades and is discussed in the following section.

Downstream Signalling Cascades and Synaptic Plasticity

Upon activation of CamKII, either by Ca^{2+} entry to the PSD (predominantly via NMDAR activation) or Ca^{2+} independent auto-phosphorylation, CamKII binds to the phosphorylation sites present on the C-terminus of SynGAP (Oh et al., 2004). Phosphorylation of SynGAP activates the GTP-ase function of the protein. It acts in conjunction with guanine exchange factors (GEFs) to enhance the hydrolysis of GTP by de-phosphorylation of GTP-binding proteins. These GTP-binding proteins comprise of the Ras, Rap or Rho family of proteins and are known to activate multiple downstream signalling pathways (Palsson et al., 2000).

SynGAP was originally identified as an HRas-GAP (Chen et al., 1998; Kim et al., 1998) due to sequence and 3-D conformation homology with Ras-GAPs p120 and neurofibromin. Upon activation, SynGAP de-phosphorylates Ras from a GTP bound 'active' state to a GDP-bound 'inactive' state. GTP-bound Ras activates the extracellular-signal regulated kinases 1-and-2 (ERK 1/2) / mitogen-activated protein kniase (MAPK) pathway. Activation of the ERK1/2 / MAPK results in the phosphorylation of translation inhibitor 4E-BP, dis-inhibiting protein translation. Indeed, models of SynGAP haploinsufficiency including heterozygous (het) (*Syngap*$^{+/-}$) mice (Carlisle et al., 2008) and knock down neuronal cultures (Araki et al., 2015) show increased levels of Ras. Rumbaugh et al. (2006) showed increased phosphorylated (activated) ERK in cultures from *Syngap1*$^{-/-}$ mice while Komiyama et al. (2002) showed similarly high p-ERK levels in *Syngap*$^{+/-}$ adult mice. Both studies also found an increase in this elevated p-ERK level upon stimulation of NMDAR. Kim et al. (2003) showed that knock-down of SynGAP down using RNAi results in a sustained increase of p-ERK levels after NMDAR stimulation, instead of its typical transient activation. However, Ozkan et al. (2014) upon activating the NMDAR pathway showed no increase in elevated p-ERK levels. One possible explanation for this discrepancy, might be the stimulation protocols used. Ozkan et al. (2014) used a theta burst stimulation while Rumbaugh et al. (2006) used a low Mg^{2+}-high glycine media whereas Komiyama et al. (2002) bath applied NMDA. Further evidence of negative regulation of the ERK pathway by SynGAP was provided in a study by Berryer et al. (2013), in which neurons in organotypic slice cultures were transfected with either wild-type (WT) or mutated $^{\text{SYNGAP1}}$ with mutation loci matched to mutations found in patients. They found that upon transfection with WT *SYNGAP1*, the levels of p-ERK decreased whereas transfection with mutated $^{\text{SYNGAP1}}$ showed no change in p-ERK levels. Finally, Barnes et al. (2015) found

elevated levels of basal protein synthesis in juvenile *Syngap*$^{+/-}$ mice can be reversed to control levels by blocking the ERK1/2 pathway using U0126.

In addition to HRas, SynGAP also acts as a Rap1-GAP (Krapivinsky et al., 2004; Pena et al., 2008; Walkup et al., 2015). In fact, Krapivinsky et al. (2004) showed that in cultured rat hippocampal neurons SynGAP, as part of the MUPP1-SynGAP-CamKII complex, showed 10-fold stimulation of its Rap-GTPase activity compared to a two-fold stimulation of its Ras-GTPase activity. Rap is upstream of and shown to inhibit the p38-MAPK pathway (Palsson et al., 2000), therefore one would expect that loss of SynGAP would result in decreased p38-MAPK activity whereas increased SynGAP expression would cause the opposite. Indeed, Rumbaugh et al. (2006) showed that inducing SynGAP expression, by activation of NMDAR, resulted in increased p38-MAPK and these levels are reversed on knockdown of SynGAP using siRNA. Controversially, Krapivinsky et al. (2004) found that calmodulin mediated activation of CamKII led to a de-phosphorylation of SynGAP and attenuated the phosphorylation activity of p38-MAPK with no change in ERK activity. One possible explanation for this discrepancy is the use of different isoforms. The Rumbaugh et al. (2006) study specifically states the use of SynGAPα1, whereas the study by Krapivinsky et al. (2004) simply states the use of SynGAPα. Given the differential effect of α1 and α2 isoforms on synaptic strength, there is a possibility that the Krapivinsky et al. (2004) study used α2 and uncovered an isoform specific function.

Recently, Walkup et al. (2015), showed that the Ras-GAP versus Rap1-GAP activity of a recombinant SynGAP protein (r-SynGAP lacking 102 residues at the N-terminal) depended on its phosphorylation by cyclin-dependent kinase-5 (CDK-5) and CamKII. The study showed that phosphorylation of the C-terminal of r-SynGAP by CDK-5 preferentially promoted its Ras-GAP activity (98% compared to 25% Rap1-GAP activity) whereas phosphorylation by CamKII preferentially promoted its Rap1-GAP activity (76% to 25% Ras-GAP activity). This study provides the first evidence of SynGAP switching its Ras/Rap GTP-ase activity in a phosphorylation-partner dependent manner.

Ras and Rap are known to differentially control synaptic plasticity through control of α-amino-3-hydroxy-5-methyl-4-isoxazolepropionic acid (AMPA) receptor insertion dynamics at the post-synaptic membrane (Zhu et al. (2002)). Ras, through activation of the ERK1/2 pathway, drives long-cytoplasmic tail containing AMPA-R delivery to the membrane, enhancing

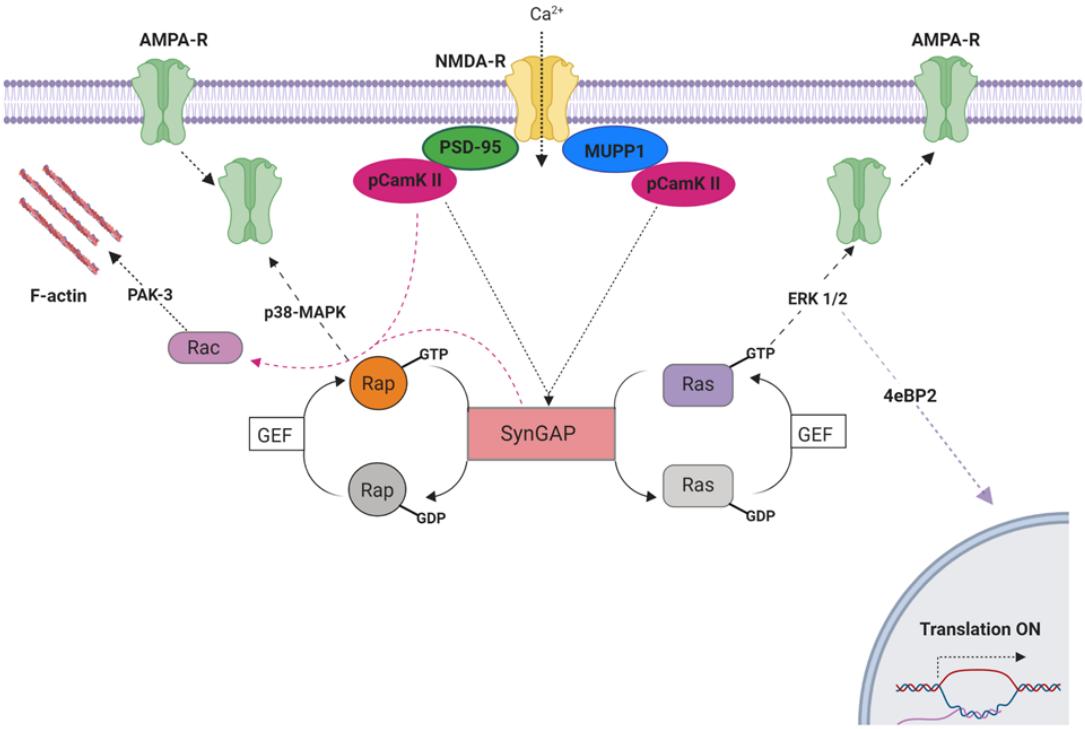

Figure 1.5: Downstream Signalling cascades mediated by SynGAP The Schematic shows the various Ras, Rap and Rac pathways activated by phosphorylation of SynGAP. Glutamate receptors, such as NMDAR and AMPAR, are clustered at the postsynaptic active zone with a dense matrix called PSD. Upon NMDAR activation, Ca^{2+} enters the postsynaptic cytosol, triggering phosphorylation of CaMKII, which in turn phosphorylates SynGAP. SynGAP regulates Ras-GTPases controlling actin dynamics and AMPARs insertion into the postsynaptic membrane. In Syngap1 Heterozygous mutation, the inhibition of Ras activation by SYNGAP1 is lost, which increases Ras activity, thereby increasing AMPAR exocytosis to the postsynaptic membrane. Phosphorylation of SynGAP by cyclin-dependent kinase 5 (CDK5) activates Rap1 that increases endocytosis of AMPAR. This schematic was made using Biorender software.

synaptic activity and facilitating LTP. In contrast, Rap promotes removal of short-tailed AMPA-Rs through the p38-MAPK, promoting activity induced synaptic long-term depression (LTD). Given its dual HRas and Rap1 function, one would expect loss of SynGAP to result in altered AMPAR mediated transmission, LTP and LTD. Komiyama et al. (2002) show that under basal conditions in *Syngap1*$^{-/-}$ mice, AMPAR transmission is unaffected. However, stimulation of LTP affects recruitment of AMPARs to the PSD, resulting in impaired LTP in the CA1 of the heterozygous mice. Given that this impairment in LTP is driven by Ras, one would expect *HRas*$^{-/-}$ mice to mimic this impairment. *HRas*$^{-/-}$ mice, infact, show enhanced AMPAR transmission following an LTP stimulation protocol. There appear to be two explanations for this observation: First, the loss of HRas maybe compensated for by other Ras subtypes and second, Ras-independent forms of LTP have been reported. Clement et al. (2013) measured an increased AMPA/NMDA ratio with decreased LTP in L4 stellate cells of the somato-sensory barrel cortex of P5 het mice. Ozkan et al. (2014) showed that tamoxifen-induced reversal of SynGAP levels in adult mice rescued the LTP deficit and lowered Ras and p-ERK levels. While the LTP deficits have been widely reproduced, studies on the surface expression of AMPA-R sub-units (GluR1, 2 and 3) has been more controversial. Rumbaugh et al. (2006) report decreased surface expression of GluR1 but increased number and size of GluR1 clusters in cultures from *Syngap1*$^{-/-}$ mice. Muhia et al. (2010) found a similarly increased size of GluR1 clusters in a conditional *Syngap1*-knockout mouse. However, Krapivinsky et al. (2004); Vazquez et al. (2004); Carlisle et al. (2008), and Araki et al. (2015) all report an increase in AMPAR concentration upon loss of SynGAP. Kim et al. (2003), further showed that transfecting cells lacking SynGAP with the full length SynGAP protein actively reduces surface AMPAR expression by about 33%.

In addition to impairments in LTP, models of *Syngap1* haploinsufficiency have also presented with altered LTD in a stimulation protocol-dependent manner. Upon chemical induction of LTD, using a high Ca^{2+} solution, reduced levels of LTD were reported in the CA1 region of 6-12 week old *Syngap1*$^{+/-}$ mice (Carlisle et al., 2008). Whereas LTD induction using a low-frequency paired-pulse protocol in the CA1 of similarly aged *Syngap1*$^{+/-}$ mice produced no LTD deficit (Kim et al., 2003). Induction of LTD by stimulating the metabotropic glutamate receptor-5 ($mGluR_5$) using DHPG showed exaggerated LTD in the CA1 of juvenile (P25-32) het mice (Barnes et al., 2015). Thus, while the exact mechanics are debated, SynGAP appears to mediate synaptic plasticity in an NMDAR-dependent manner through manipulation of AMPA-R

trafficking.

The studies so far discussed all report the influence of SynGAP on AMPAR trafficking via downstream signalling cascades, a GAP-domain dependent function. A study by Walkup et al. (2016) suggests an alternative C-terminus domain dependent mechanism by which SynGAP might influence AMPAR trafficking. At the post-synaptic membrane, AMPARs undergo a three-step immobilisation process that allows the docking of these receptors at the membrane. The three steps include insertion into the membrane, diffusion into the synapse and 'trapping' at the membrane (Opazo and Choquet, 2011). AMPAR trapping is mediated by proteins present in the post-synaptic density (PSD) including transmembrane AMPAR regulatory proteins (TARPs) and leucine rich repeat transmembrane proteins (LRRTMs). The PSD is a complex composed of signaling and scaffolding proteins present just below the post-synaptic membrane. The most abundant of its scaffolding proteins is PSD-95 that binds multiple PSD proteins, including TARPS, LRRTMs and SynGAP, via multiple PDZ protein domains. The Walkup et al. (2016) study postulates that since each PSD-95 molecules has a predefined number of PDZ binding domains, PSD proteins must compete with each other to fill these PDZ 'slots'. They further report that SynGAP, via its C-terminus QTRV motif, competes with PSD proteins like TARPs and LRRTMs to preferentially bind the PDZ slots of PSD-95, thereby restricting AMPAR docking at the PSD. Phosphorylation of SynGAP by CamKII and Polo-like Kinase 2 (PLK2) reduces its affinity to bind the PDZ domain of PSD-95, thereby freeing up PDZ-slots for other proteins, resulting in increased AMPARs at the PSD.

During synaptic plasticity, PSD size and composition are dynamically regulated with changes to synaptic strength. This change is thought to form the biophysical basis of LTP and LTD with recent *in vitro* super-resolution studies proposing a liquid–liquid phase separation (LLPS) model for this modulation. In the LLPS model, proteins are constantly diffusing between the dense LLPS 'core' structure formed by the protein-enriched cellular compartments beneath the post-synaptic membrane, and the less concentrated aqueous cytoplasm in synaptic spines (Feng et al., 2019; Zeng et al., 2016). SynGAP binding of PSD-95 induces phase separation, causing dispersion of the protein from the PSD complex into the cytoplasm, allowing for the recruitment and stabilization of AMPA receptors to the PSD thus controlling synaptic plasticity (Lautz et al., 2019). However, analysis of SynGAP protein concentrations from neurosynaptosomes and whole cell homogenates in rat models of *Syngap1* haploinsufficiency (S Nawaz, upublished)

found no differences in protein concentration, suggesting that altered protein phase does not underlie the aberrant synaptic plasticity in this model.

Both GAP-dependent and GAP-independent models of SynGAP function highlight the importance of this protein in controlling synaptic plasticity. However, it is still not known which of these modes of function is disrupted in individuals presenting with *SYNGAP1* haploinsufficiency mediated ID.

Lastly, SynGAP is also thought to mediate synaptic plasticity by regulating spine morphology. Actin regulation and dynamics can have both a physiological as well as a morphological effect on spines. The former is mediated by control of AMPA-R trafficking whereas the later through changes in architecture of spine shape, size, and turnover dynamics. F-actin is downstream of Ras and Rac-GTP and also associates with N-Cadherin which is downstream and activated by the AMPA-R subunit GluR2. Vazquez et al. (2004) first showed that cultures of *Syngap1*$^{+/-}$ neurons have increased spine number with larger head width. Carlisle et al. (2008) showed that at steady state, SynGAP regulates phosphorylation of the actin-binding protein cofilin in a Rac-PAK 1,3 kinase dependent manner. In *Syngap* $^{+/-}$ mice, levels of Rac-GTP, activated PAK and inactive (phosphorylated) cofilin were elevated. The same mice failed to show transient de-phosphorylation of cofilin upon activation of NMDARs and presented with increased spine number and spine head-width in the CA1 sub-region of the hippocampus. Clement et al. (2012) also show the similar increases in spine length, number and head width in the dentate gyrus (DG) of the hippocampus. Barnes et al. (2015) however, found no difference in either spine density or head width in the CA1 of the hippocampus using super-resolution STED microscopy. The study did, however, find an increase in spine neck length in the *Syngap1*$^{+/-}$ mice compared to WT controls, indicating an increase in compartmentalisation factor. The compartmentalisation factor shows the impact of morphological change on biochemical diffusion coupling and is calculated as head volume x head neck length / area of spine neck cross-section (Wijetunge et al., 2014). In the case of *Syngap1*$^{+/-}$ mice it would indicate altered biochemical coupling of the spine to the parent dendritic shaft. McMahon et al. (2012) also found no effect of specific isoforms on spine, density, width or length in SynGAP knockout neuronal cultures. The discrepancies between the studies maybe accounted for by a few reasons. First, all studies were done at different ages, Carlisle et al. (2008) at 3-6 months, Clement et al. (2012) at P14 and Barnes et al. (2015) at P35. Secondly, the Clement et al. (2012) study was performed

at a different sub-region of the hippocampus, the DG, compared to the CA1 in the Barnes et al. (2015) study. Third, spines on different dendrites were chosen for analysis: Barnes et al. (2015) measured apical dendrites whereas Carlisle et al. (2008) measured spines on the basal dendrite. However, the most pronounced reason for the discrepancies in the findings reported is the use of a spine categorisation system employed in the Carlisle et al. (2008) and Clement et al. (2012) studies. This system differentiates spines into 'stubby', 'mushroom' and 'filopodia' depending on on its morphology, and both studies state that the differences reported are for the 'mushroom' spines. However, spine morphology is shown to cover a continuum of shapes and sizes uncorrelated to function, making the rather simple classification obsolete (Wijetunge et al., 2014), and it therefore is unclear if genotype differences would persist with this categorisation removed. Additionally, Clement et al. (2012) use spine number (ranging from 2383 to 2788 spines) as their independent metric or 'n' for statistics. Spine numbers are dependent on the animal, therefore using it as the 'n' conflates statistical significance. Another study by Aceti et al. (2015) found an increase in spine length and density in L5 of the primary somato-sensory cortex of *Syngap1*$^{+/-}$ mice at P21 that is lost by P60. Using time-lapse microscopy they also show decreased spine turnover at P21-23 and P30-32 suggesting accelerated maturation. Clement et al. (2012) show increased spine motility in the DG of *Syngap1*$^{+/-}$ mice at P14. This evidence suggests that SynGAP has a role in altering spine turnover dynamics during critical periods of development, but these might be distinct across brain regions.

1.4 Modelling *SYNGAP1* haploinsufficiency

In order to understand the pathophysiology of complex disorders, it is vital that we are able to successfully model them in a pre-clinical setting. The original definition of an 'ideal' pre-clinical model of human psychiatric disorders was coined by (McKinney and Bunney, 1969). They required that for a model to be relevant to human pathology it must show analogous of symptoms with existence of observable and measurable behavioral changes, that was agreed upon amongst multiple observers. The model must also be reproducible and show similar response to treatments. The original 5-point criteria has since been adapted to three core criteria of validity (Belzung and Lemoine, 2011):

Construct validity refers to the human-model similarity of the genetic predisposition that participates in the etiology of the disease. In the case of *SYNGAP1* haploinsufficiency this would require that the animal model present with a 50% reduction in SynGAP protein resulting from loss of one copy of the *Syngap1* gene.

Face validity is the similarity of observable ethologically-relevant pathological behaviours in the model compared to the human disorder. In modelling social isolation of individuals with ASD/ID, one would look for altered social behaviours in the animal model. Face validity is sometimes extended to also include 'biomarker' validity, wherein functionally-related biological markers of the modeled condition are present in the pre-clinical model. For example, when modelling post-traumatic stress disorder in rodents, a surge in glucocorticoids is measured despite the fact that they do not come in the same form in human subjects (cortisol) and in rodents (corticosterone).

Predictive validity refers to the ability of the model to predict both behavioural and pharmacological outcomes of the condition it is modelling. In cases of epilepsy, a model with predictive validity would inform the experimenter of the efficacy of an anti-epileptic drug being tested.

The most widely used model of *SYNGAP1*-ID at present is a heterozygous mouse model while in this thesis, I use two novel monogenic rat models of *Syngap1* haploinsufficiency. However, as behavioural, circuit and electro-physiological characterisation of the rat models occurred concurrently with the work outlined in this thesis, the behaviour and circuit deficits of only the *Syngap1* mouse model and how it compares to patient co-morbidities is outlined below.

1.4.1 Mouse Model of *SYNGAP1* haploinsufficiency

Cellular and Synaptic Deficits

The first knock-out mouse model of *Syngap1* was published by Komiyama et al. (2002). They noted that mice homozygous for the *Syngap1* deletion (*Syngap1*$^{-/-}$) died between P2 to P5. However, Kim et al. (2003) and Barnett et al. (2006)) found that reducing litter sizes

by selective removal of litter-mates allowed *Syngap1*$^{-/-}$ to survive till P7. The lethality of the deletion may explain why no individuals with a homozygous deletion in *SYNGAP1* have been reported.

One of the most reported features of individuals with *SYNGAP1* haploinsufficiency is presence of cortical generalized seizures (Carvill et al., 2013; Berryer et al., 2013). To analyse the presence of spontaneous seizures, Ozkan et al. (2014) performed video-monitored electroencephalography (EEG) in adult (>12 weeks) WT and het mice. While no seizure-like motor events were observed in the video recordings, high amplitude cortical discharges were recorded in the EEG from the het mice but not from the WT littermates. These epileptiform discharges were intermittent, ranging in frequency from 1 to 681/hour (mean of 81/hr). They also found a decreased threshold of flurothyl induced clonus and tonic-clonic seizures in the het mice. Additionally, Clement et al. (2012) reported an increased incidence of audiogenic seizures at P21-25 in the het mice. 100% of the hets in their behaviour cohort showed wild-running, consisting of intense running mixed with high jumps, compared to 50% of the WTs, and 66% of the hets had seizures. While both these studies are encouraging of the face validity of the mouse model, the data should be interpreted with caution as the power of the experiments is low. The Ozkan et al. (2014) study employed an n=3 and n=2 for the het and WT mice respectively while the Clement et al. (2012) study used an n=6 per genotype.

A significant number of individuals with *SYNGAP1*-ID present with altered sensory perception, predominantly increased sensitivity to sound (hyperacusis) and photosensitive epilepsy (Parker et al., 2015; Klitten et al., 2011). While the exact biomechanics underlying these alterations is yet to be elucidated, they are thought to result from impaired connectivity and processing within neuronal networks. This typically manifests as an impaired excitatory/inhibitory (E/I) balance and given the abundance of SynGAP at glutamatergic synapses, its loss is hypothesised to result in increased excitatory activity (Lee et al., 2017). In support of this, Clement et al. (2012) showed that photostimulation-evoked signals, measured using fast voltage-sensitive dye imaging, originating in the dentate gyrus (DG) of het mice were amplified, instead of attenuating, as they spread through the hippocampus. Using a similar imaging approach Ozkan et al. (2014), also reported increased excitability in the medial-prefrontal cortex of adult (8-10 weeks) het mice. While both these studies have focused on increased glutamatergic neuronal activity, another possible explanation for increased excitability is the loss of inhibition. Berryer et al.

(2016) used an optogenetic approach with a conditional mouse line to selectively knock-out *Syngap1* from GABAergic inhibitory cells derived from the medial ganglionic eminence. They found that *Syngap1* haploinsufficiency significantly reduced the formation of perisomatic innervations by parvalbumin-positive basket cells, impairing their connectivity and reducing inhibitory synaptic activity and cortical gamma oscillation power in the somatosensory cortex. The studies so far present evidence of a shift in the E/I balance towards increased excitation, either by a direct increase of glutamatergic activity or reduced GABAergic inhibition. Recent evidence by Michaelson et al. (2018) suggests that these shifts might be circuit specific. They report reduced cortical activity in the upper lamina of the somatosensory cortex-barrel field (S1BF) of adult *Syngap1*$^{+/-}$ mice. This suggests a circuit hypo-excitability might underlie altered thigmotaxis (altered movement of an animal in response to a touch stimulus (Simon et al., 1994; Walz et al., 2016)) which has been reported in 20 of 48 patients in the same study. These deficits are particularly confounding as a previous study by Aceti et al. (2015) found accelerated maturation of dendritic spines and synaptic pruning during critical periods in the S1BF of het mice. Additionally, Barnett et al. (2006) showed that while complete loss of SynGAP resulted in more serious barrell-loss phenotypes, het mice show normal but delayed formation of barreloids in L4 of the S1BF. They found partial segregation of the thalamocortical afferents (TCA) from the whiskers into barreloids in the thalamus in P5-7 *Syngap1*$^{-/-}$ mice. These afferents further made it into L4 of the S1Bf but lost cellular segregation, resulting in a lack of barrels in the S1. The discrepancies between the studies can, to some extent, be attributed to the difference in age between the studies. The study by Aceti et al. (2015) used animals between P14-21 while the Michaelson et al. (2018) study used adult mice.

Sensory hypersenstitivites may also arise from an inability to filter or prioritize incoming sensory stimuli, thus leading to a 'overload' of sensory information. This process, termed 'sensorimotor gating', is tested using the 'Pre-pulse inhibition' (PPI) test and is known to rely on fore-brain circuitry (Braff et al., 2001). The PPI test is based on the principle that pre-exposure to weaker stimulus, the 'pre-pulse', dampens the response to an immediately followed (within 150 ms) stronger stimulus. Guo et al. (2009) performed an acoustic PPI and startle test in *Syngap1* het mice and WT controls using a pre-pulse sound of 4KHz presented at 4-16 dB above background noise followed by a 120ms delayed startle sound of 120 dB. For the general startle response, naïve mice were subjected to increasing amplitudes of white noise ranging form 70-120 dB. They found that the het mice presented with both reduced inhibition

to the startle response and a generally heightened startle response, measured as amplitude of the evoked potential using an EEG.

Behavioural Deficits

In addition to altered excitability in models of *Syngap1* haploinsufficiency, a number of cognitive and behavioural deficits have also been observed in these mice. These deficits have been observed in both lines with complete germline mutations (Komiyama et al., 2002; Muhia et al., 2009, 2010; Clement et al., 2012; Ozkan et al., 2014; Berryer et al., 2016) as well as lines where SynGAP has been deleted in a cell-type and age dependent manner (conditional mutants) (Muhia et al., 2012; Ozkan et al., 2014; Berryer et al., 2016).

Hyperactivity & Anxiety

One of the most consistent behavioural findings reported in *Syngap1* het mice is increased locomotor activity (Guo et al., 2009; Muhia et al., 2009, 2010, 2012; Clement et al., 2012; Berryer et al., 2016). Hyperactivity is measured by calculating total distance travelled and moving speed of the mouse when exposed to an open field environment (Guo et al., 2009; Muhia et al., 2010; Ozkan et al., 2014; Berryer et al., 2016). This increased locomotion is suggested to be due to increased glutamatergic activity, rather than loss of inhibitory activity, with a resultant disruption in the E/I balance of the circuit. Evidence for this comes from the Berryer et al. (2016) and Ozkan et al. (2014) studies, where no increase in locomotion was observed in mice where SynGAP was conditionally deleted in GABAergic neurons arising from the MGE, while hyperactivity was observed in mice with SynGAP conditionally knocked out in glutamatergic neurons of the fore-brain. The Ozkan et al. (2014) study also performed a 'rescue' experiment, wherein they found that reversing SynGAP levels in the adults rescued the cellular phenotypes outlined in section 1.3.3 but did not alter the increased locomotion levels observed in these mice. Suggesting that reversal of cellular and synaptic abnormalities does not reverse the pleiotropic compensatory changes which together contribute to the pathology of *SYNGAP1*-ID. Guo et al. (2009) also noted an increase in 'stereotypy' behaviours in the het mice, a characteristic widely reported in individuals with autism and schizophrenia (Randrup

and Munkvad, 1974). Scored as bouts of repetitive movements without purpose, presence of these behaviours in the het mice confers further face validity to this model.

In addition to hyperactivity, a decrease in anxiety-related behaviours is also widely reported in the *Syngap1* het mice. Most endogenous measures of anxiety utilize the rodent instinct to preferentially spend time in shaded/covered regions as opposed to open/exposed regions. In the open field arena, anxiety levels are scored by comparing the amount of time the mouse spends in the walled periphery to the amount of time spent in the exposed (arbitrarily defined) centre. Another widely used behavioural task to measure anxiety in rodents is the elevated plus maze (EPM). The arena for the EPM consists of safe 'closed' arms with high side walls crossed with unsafe 'open' arms without any side walls to form a plus shaped elevated platform. Anxiety in this task is measured as amount of time spent in the closed arm compared to time spent in the exposed open arm (Lister, 1987; Peier, 2000). In addition to time spent in the open arms/centre, another measure of anxiety is the number of entries into the centre (open field) or the open arm (EPM). In both tasks, *Syngap1* het mice show reduced anxiety with increased amounts of time spent and entries into the 'centre' of the open field (Guo et al., 2009; Muhia et al., 2010) as well as the 'open arms' of the EPM (Muhia et al., 2010; Ozkan et al., 2014; Berryer et al., 2016). Contrary to the observations made in mice, most individuals with *SYNGAP1*-ID show elevated levels of anxiety (Krepischi et al., 2010; Klitten et al., 2011). Given that the above described tasks used to measure anxiety levels in the rodent models are dependent, to some degree, on the animal's movement, the hyperactivity observed in the het mice might offer an explanation for the discrepant anxiety phenotypes between the mouse model and human patients.

Social Function

Impaired social interaction and communication are key features observed in individuals with ASD. To test if the *Syngap1* het mice present with similar social impairments, studies used the 3-chamber social interaction task to assess social interaction, social isolation and preference for social novelty (Guo et al., 2009; Berryer et al., 2016). The 3-chamber task utilizes the wild-type rodent preference for sociability, the choice of spending more time with another rodent as opposed to an object, and social novelty, preferentially investigating a new intruder placed in the arena compared to a familiar one (Nadler et al., 2004; Bolivar et al., 2007). Accordingly, time spent in the central 'neutral' chamber as opposed to chambers with rodents in them is scored as 'social isolation'. Both studies found that *Syngap1* het mice showed decreased preference for social novelty without any change in social interaction. Guo et al. (2009) also report increased social isolation. Social interaction is scored by counting the number of entries into the specific chamber as well as time spent 'sniffing' the con-specific animal. Therefore, one explanation for decreased social novelty memory might be impaired olfactory processing in the het mice. However, Guo et al. (2009) found no olfactory deficits in these mice, suggesting that the observed phenotypes were in fact social deficits. These studies indicate that reduced SynGAP function results in a significant cognitive defect altering social interactions.

Cognition & Memory

Most individuals with *SYNGAP1*-ID present with moderate to severe ID (for review see Vlaskamp et al. (2019)), therefore testing cognition and memory in the *Syngap1* het mice is crucial for the face validity of the model. A brain structure vital for the acquisition and consolidation of spatial memory is the hippocampus (Hodges, 1995) and the *Syngap1* het mice show impaired NMDAR mediated LTP and exaggerated $mGluR_5$ mediated LTP in the CA1 sub-region of the hippocampus. These impairments have previously been associated with deficits in spatial reference memory. As such, Komiyama et al. (2002) and Muhia et al. (2010) tested hippocampal-dependent spatial memory in these mice using the Morris Water Maze (MWM). A spatial reference-memory version of the task was used wherein the latency of the animal to find a platform using distal visual cues was measured. Both tests reported mildly impaired spatial memory retrieval in the het mice with no difference in memory acquisition or extinction. Muhia et al. (2010) also reported a decrease in time spent in the 'correct' platform quadrant by the het

mice when the platform is removed. However, this deficit was only found in the first 15 s of the 60 s testing period.

Muhia et al. (2010) also assessed reference and working memory in the *Syngap1* het mice using a baited version of the dry-land radial-arm maze. In this test, alternate arms of the maze were 'baited' with reward food pellets. Following an initial training phase where a 'reference memory' (RM) was acquired, RM errors were defined as initial entry into an unbaited arm. Following this phase, the number of re-entries into a baited arm after reward consumption and entries into a never baited arm were assessed as errors in 'working memory' (WM). They report that the het mice showed impaired acquisition and retrieval of RM as well as increased WM errors.

The most widely reported spatial memory deficit in the *Syngap1* het mice is the loss of spontaneous alternation in the T-maze. Rodents innately explore novelty in their environment. The unforced T-maze, which is dependent on a pre-frontal cortex-hippocampus network, assesses this exploratory behaviour by measuring the entries of the rodent into each arm of the maze (Deacon and Rawlins, 2006). While WT mice naturally alternate between the arms entered, the *Syngap1* het mice fail to do so above chance (Guo et al., 2009; Muhia et al., 2010; Berryer et al., 2016). Given that this task involves the recognition of novelty (un-entered arm) over familiarity (just entered arm), novel object recognition was also assessed in thees animals. However, no deficits were observed in this task (Muhia et al., 2010).

In addition to spatial reference memory, the *Syngap1* het mice have also been tested in associative memory paradigms. Clement et al. (2012) showed that *Syngap1* het mice exhibit lowered freezing compared to WT mice in a hippocampal-dependent contextual fear paradigm. In this paradigm, rodents are exposed to an aversive context 'A', where they receive aversive stimuli like footshocks, followed by exposure to a neutral context 'B'. The animals are then returned to context 'A' and their aversive behaviour (typically presenting as freezing behaviour in mice) is scored as a % of time. A similar result was reported by Ozkan et al. (2014) but only in a conditional mutant where SynGAP was deleted from GABA-ergic neurons, using a *Gad2*-cre driver line, and not in the mutant where SynGAP was deleted from excitatory glutamatergic neurons. Guo et al. (2009), however found no differences in freezing behaviour of the *Syngap1* het mice when using contextual fear conditioning. This result is unsurprising as the WT mice

in the study by Clement et al. (2012) showed very little reduction in % time spent freezing over the course of the entire protocol, suggesting a generalised fear response as opposed to the more widely reported reduction in freezing over time. Guo et al. (2009), however, did report reduced freezing in *Syngap1* het mice following a cued-fear conditioning paradigm. In this paradigm, a specific cue (called the conditioned stimulus or CS), like a tone, is associated with an aversive stimulus (called the unconditioned stimulus or US), like a foot-shock, and is dependent on a pre-frontal cortex-amygdala interaction as opposed to hippocampal interactions.

Un-modelled Alterations

While a majority of the neurological and behavioural presentations of *SYNGAP1*-ID have been modelled in the mice, others have not been as extensively characterised. Increased pain tolerance has been reported in individuals with *SYNGAP1*-ID, but the *Syngap1*$^{+/-}$ mice show no altered sensitivity to thermal stimulation (Muhia et al., 2010). Individuals also present with altered sleep patterns, but circadian rhythm abnormalities yet to be studied in the *Syngap1*$^{+/-}$ mouse model.

1.4.2 Using Rats to Model ASD/ ID

A number of factors have led to mice being the most widely used model organism in biomedical research (Mayford et al., 1997). These include the availability of a diverse genetic toolbox to create transgenic lines with precise spatial and temporal control of loss of function mutations as well as rescue experiments (Lipp and Wolfer, 1998), a short reproductive cycle making them more cost-effective to maintain in the lab (Siglin and Baker, 2001) and better performance, compared to other rodent models, on tasks involving touch-screens (Bussey et al., 2008). However, within the framework of 'bench top to bedside' translational medicine, modelling ASD/IDs in mice presents with some limitations. Behaviourally, mice show limited cognitive flexibility, thereby restricting the battery of tests that can be used to study a disorder that predominantly presents as deficits in cognition (Ellenbroek and Youn, 2016). They also show increased impulsivity, introducing greater variability in datasets of more challenging tasks Ellenbroek and Youn (2016). Ethologically, male mice show limited social interactions, living in single-male territorial structures (called 'demes') that is founded by an alpha that mates

with multiple females (Van zegeren, 1979). As a result, interactions between males are much rarer and, when they occur, are more aggressive and territorial in nature (Schmid-Holmes et al., 2001). In accordance with this observation, studies investigating home-cage relations in WT mice have revealed aggressive behaviour between con-specifics. This presents a challenge when modelling disorders where impaired social interaction is at the diagnostic core.

Using the Norway rat, *Rattus norvegicus*, as a model organism mitigates a few of these limitations. First, rats offer greater cognitive flexibility as witnessed in operant tasks to self-administer drugs (Parker et al., 2014). They also perform better, with smaller reported variability, in a number of cognitive flexibility and attention tasks including attention shifting, delayed attention and delayed (non) matching to sample tasks Ellenbroek and Youn (2016). Given that ADHD is a highly reported co-morbidity of ASDs (Leitner, 2014), it is crucial that the model used is able to perform complex attention tasks, especially when testing drug efficacy. Specifically for mood disorders, another common comorbidity to ASD/ ID, rats and mice show distinct neurochemical profiles, with the rat profile being more closely matched to human physiology. For example, in a restrained-stress paradigm Konstandi et al. (2000) showed that rats and mice evoked differential transmission of noradrenaline, dopamine and serotonin. Further, Larm et al. (2003) performed a comparative study looking at the expression profiles of serotonergic neuropeptide galanin and its receptor GalR1 (Misane et al., 1998). Galanin and Galr1 have been implicated in regulating cellular processes underlying anxiety and depression. The study showed that mice lack these molecules in the dorsal raphé nucleus, a brain region key for regulating mood disorders. Consistent with this finding, studies by Blanchard et al. (1997) and Griebel et al. (1997) found that drugs acting on the serotonergic pathway had anxiolytic and panicolytic effects in rats but not in mice. These neurochemical differences between rats and mice extend to the effect of corticotropin releasing factor (CRF). CRF expression in the brain stem is a key regulator of fear and anxiety (Van'T Veer et al., 2012) whereas its expression in the cortex is associated with cognition and stereotyped motor behaviours (Binder and Nemeroff, 2010; Crawley et al., 1985; Dunn and Swiergiel, 2008) showed intra-cerebroventricular administration CRF lead to a reduction of depression like behaviours in rats but not mice. Given the potential pharmacological implications of species choice on the predictive value of the model, efforts must be made to find a balance between high-throughput models with human-relevant physiology.

Specifically for ASDs, the aspect where rats most prove their superiority over mice as the model of choice is social cognition and behaviour. Ethologically, rats live in complex hierarchical colonies but dominance structure amongst the males is less rigid, with all males often mating with all females. This fluid structure acts to reduce aggression and territorial instincts between males (Blanchard et al., 1997) and increases natural social interaction. The increased sociability of rats, compared to mice, is supplemented by observations of juvenile rats in 'rough and tumble' play and wrestle behaviour (Siviy and Panksepp, 2011). In humans, peer-play is an integral part of childhood development, and children with ASD and ADHD often experience social isolation. Play behaviour in rats typically comprises of non-serious chasing, fighting and rolling around together accompanied by emission of high frequency (50kHz) ultrasonic vocalisations (USVs). Play has been shown to promote growth factor expression in the brain (Gordon et al., 2003), with rats that were isolated showing increased play behaviour upon restoration of sociability (Burgdorf et al., 2013). Social interaction was also found to be the preferred reward, compared to a cocaine reward, in rats (79%) when compared to mice (22%) (Kummer et al., 2014; Zernig and Pinheiro, 2015). In addition to play rats also exhibit 'empathy', another sophisticated and nuanced behaviour. Sato et al. (2015) tested the presence of altruistic intentions in rats using a witness to distress paradigm. In this setting, rats were placed in a plexiglass box divided into two compartments with entry between sides restricted by a hatch. In one half of the compartment, the rat was subjected to a forced swim test with steadily rising water levels. The only way for the 'forced-swim' rat to escape was if the observer rat released the hatch separating the two sides. The results from the experiments showed that the observer rat only released the hatch when the 'forced-swim' rat was in distress. Additionally, if the observer had previously been subjected to the forced swim paradigm the rat learnt to release the hatch, and save the cage-mate, faster than one that had never been soaked. These, more sophisticated, empathy experiments have so far only been possible in rats compared to other laboratory rodents. Thus, when modelling disorders like ASD/ID where impairments in social cognition and interaction is a key feature of the diagnosis, using the rat over the mouse might be preferred.

Rats also provide a number of auxiliary benefits. They weigh about 10 times more than mice, with the rat brain weighing 4 times more than the mouse brain (Ellenbroek and Youn, 2016). This increased size leads to larger tissue samples and increased blood volume, reducing the number of animals needed, particularly when measuring low-abundance molecules. The

increased size also aides technically complicated procedures like surgeries, allowing better targeting of smaller brain structures, like the thalamus, and implantation of *in vivo* micro-electrodes as early as P14 (Langston et al., 2010). The latter is particularly advantageous when studying NDDs as it allows for longitudinal studies within the same animal, providing unique insights into the developmental trajectory of these disorders. In addition to the rat brain weighing more than the mouse brain, the cortex is 40% thicker. This allows for about 10x improved spatial resolution in non-invasive imaging studies using positron emission tomography (PET) (Zheng et al., 2016). Another popular imaging technique widely used to study brain dynamics is resting state functional magnetic resonance imaging (rsfMRI). While rats and mice show similar spatial resolution in this technique, the variability in the acquired datasets is much lower in the rat (Jonckers et al., 2011). Finally, rats are also shown to better recapitulate gender differences of human clinical conditions including inflammatory diseases and cardiovascular diseases (Paul et al., 1994; Taurog et al., 1999).

The predominant drawback of using rats, compared to mice, is the limited availability of sophisticated genetic manipulation tools and the increased cost of maintenance. However, recent advances in zinc-finger nuclease and CRISPR/Cas9 technology have allowed for the generation of rat knock-out models of ASD/ID including *Fmr1, MeCP2, Nlgn3, Nrxn1, GRM5, Pten* and *CNTNAP2* (Horizon Discovery). The use of these models is already expanding our current understanding of these disorders (Engineer et al., 2014; Till et al., 2015).

Given the improved translational attributes of rats outlined above, this thesis uses two novel rat models to study *SYNGAP1* haploinsufficiency mediated ID. The first shares construct validity with the human and mouse models, being heterozygous for the entire protein ($Syngap1^{+/-}$). The second model has a specific deletion of the GAP domain ($Syngap1^{+/\Delta GAP}$), seeking to delineate what attributes of the disorder are specifically contributed to by the loss of the GAP domain.

1.5 Convergence in models of ASD / ID

Despite the genetic heterogeneity of ASD/ID the disorders manifest with substantially overlapping behavioural abnormalities. This, in turn, might indicate mutually affected molecular

pathways and circuits in the pathophysiological axis of these disorders. Indeed, bioinformatics analysis of common and rare variants of genes causative of ASD/ID has identified biological sub-networks where a significant number of these genes cluster (Hormozdiari et al. (2015), De La Torre-Ubieta et al. (2016)). One such predominant cluster is genes involved in synaptic function (Figure 1.6). This cluster includes modulators of biochemical pathways that control protein turn-over including protein translation (*SYNGAP1, FMR1, TSC1/2, PTEN*) and degradation (*UBE3A*) as well as adhesion (*NRX* and *NLGN*) and cytokeletal (*CNTNAP2*) molecules that control synapse formation, maintenance and neuronal conduction. The net effect of these mutations is altered synaptic strength, which, in turn affects circuit excitability (Lee et al., 2017).

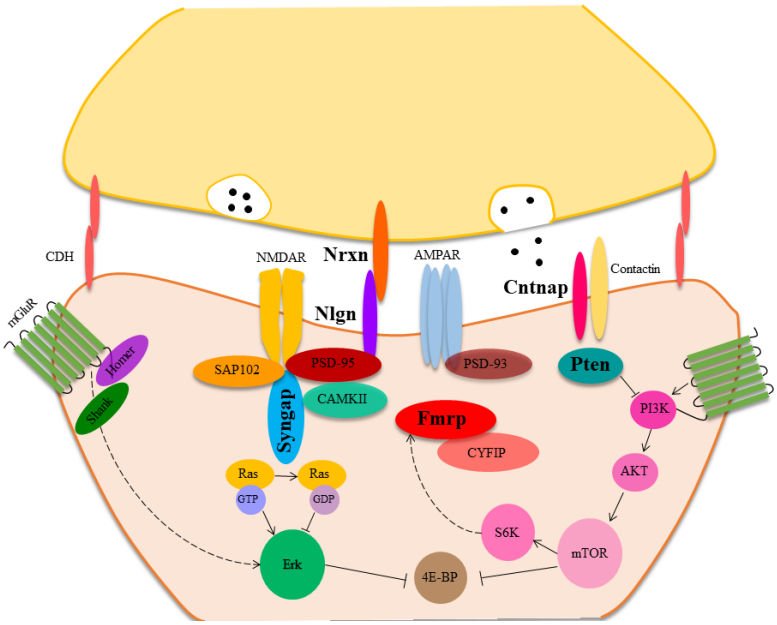

Figure 1.6: Synapse schematic A schematic of an excitatory pre and post-synaptic compartments showing proteins implicated in ASD/ ID that will be investigated in this thesis highlighted in bold.

Experimental evidence of this idea of biochemical and molecular convergence is found in a number of animal models of ASD/ ID (Auerbach et al., 2011; Baudouin et al., 2012; Zoghbi and Bear, 2012; Costa-Mattioli and Monteggia, 2013; Krumm et al., 2014; Pinto et al., 2014; De Rubeis et al., 2014; Barnes et al., 2015). One such node of convergence is dysregulation of local protein turnover, wherein mouse models of fragile-X syndrome (FXS), *SYNGAP1*-haploinsufficiency, *Eif4ebp2*-deletion show exaggerated protein synthesis (Osterweil et al., 2010; Barnes et al., 2015; Gkogkas et al., 2013), models of tuberous sclerosis (TS) show reduced protein synthesis (Auerbach et al., 2011) and models of Angelman's syndrome show

enhanced protein degradation (LaSalle et al., 2015). Another node of convergence is altered synaptic function leading to exaggerated or impaired LTP and LTD associated with changes in cellular and circuit excitability. Group 1 metabotropic glutamate receptor ($mGluR_{1/5}$) mediated LTD is found to be exaggerated in mouse models of FXS (Huber et al., 2002), *SYNGAP1*-haploinsufficiency (Barnes et al., 2015), Angelman's syndrome (hui Jiang et al., 1998) and occluded in models of TS (Auerbach et al., 2011), *NLGN3* associated NSID (Baudouin et al., 2012), Cowden syndrome (Butler et al., 2005). Similarly LTP is found to be impaired in models of FXS, Noonan syndrome, Neurofibromatosis 1 and *SYNGAP1*-haploinsufficiency while LTP is enhanced in Costello syndrome (Louros and Osterweil, 2016).

From a therapeutic standpoint, mechanistic convergence is a particularly attractive hypothesis. If true, this would save considerable time and resources in drug-safety and clinical trial studies as the same drug could be administered to individuals with genetically distinct causes of ASD/ID. Pre-clinical evidence of this was shown in Barnes et al. (2015), where they found that acute application of drugs that have previously been used to ameliorate phenotype in mouse models of FSX including CTEP ($mGluR_5$ inhibitor), lovastatin (indirect Ras inhibitor) and U0126 (ERK1/2 inhibitor), successfully lowered basal protein synthesis levels in a mouse model of *SYNGAP1*-haploinsufficiency.

Given that altered cellular excitability provides another possible avenue of convergence, this thesis looks at a key controller of this excitability - the axon initial segment.

1.6 The Axon Initial Segment

Neurons, the most abundant cell type in the brain, are composed of two functionally distinct compartments (Figure 1.7): The somatodendritic compartment which is composed of the cell body and dendritic arbor, receives inputs from the surrounding cells, and the axonal compartment, the main output compartment, propagates action potentials generated by the neuron to trigger synaptic release onto downstream projections. At the junction of the two compartments, just beyond the axon-hillock, sits the axon initial segment (AIS). First described over fifty years ago, the AIS is the site of action potential (AP) generation (Palay et al., 1968; Peters et al.,

1968). In the years since, its unique molecular architecture and functions have been extensively studied.

Described below is a brief overview highlighting the key structural components and function of the AIS with emphasis on its morphological plasticity in response to physiological manipulations and pathological conditions.

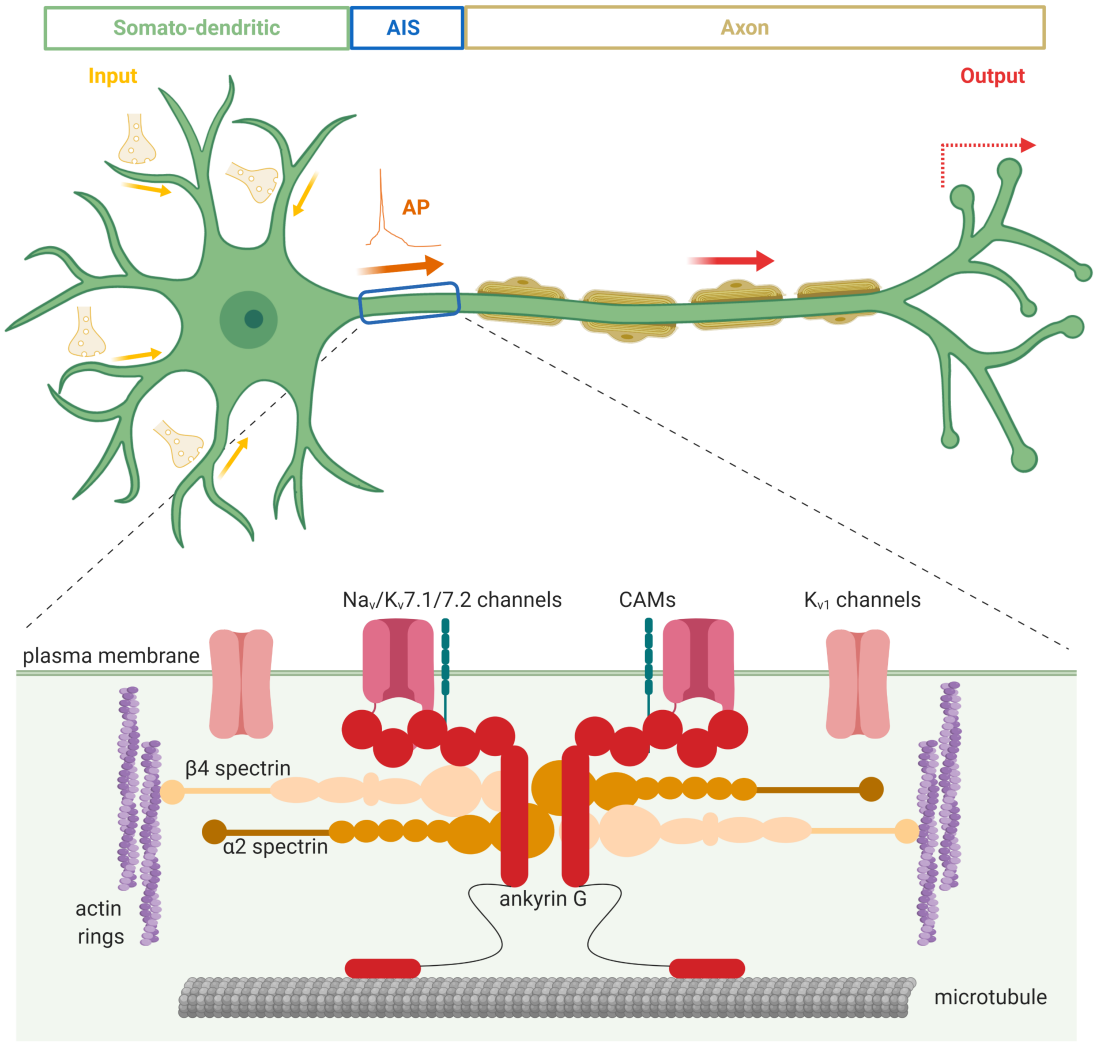

Figure 1.7: Axon initial segment structure The Axon Initial segment lies between the somatodendritic input compartment and axonal output compartments of the neuron (Upper panel). AIS membrane is composed of voltage-gated ion channels (Na$_v$, K$_v$7) and cell adhesion molecules (CAMs) that are bound to the underlying microtuble fascicles by anchoring protein Ankyrin-G. The submembrane complex of the AIS consists of $\alpha 2/\beta 4$ spectrin tetramers that connect actin rings spanning $\sim$190 nm with Ankyrin-G lying in the middle of this tetrameric complex (lower panel). This schematic was made using the Biorender software and components are adapted from Leterrier and Dargent (2014); Leterrier (2018).

1.6.1 Molecular Composition of the AIS

Studies using electron microscopy first identified the AIS in the rat cerebral cortex as a structure present along the first 20-60 μm of the axon shaft. Its identification was based on the presence of three distinct morphological features (Palay et al., 1968; Peters et al., 1968):

- The presence of *fascicles*: bundles of 3-10 microtubules
- A ~50 nm-thick undercoat lining the plasma membrane, which abruptly disappears at the onset of myelination
- A complete lack of ribosomes

The AIS has a layered molecular and cytoskeletal scaffold that extends from the microtubule fascicles to the plasma membrane. The organisation of this sophisticated network of submembrane and transmembrane proteins is predominantly achieved by the anchoring protein Ankyrin-G (AnkG). Outline below is an overview of two key components that make-up the AIS membrane complex, AnkG and voltage-gated ion channels.

Ankyrin-G (AnkG)

Ankyrins are peripheral membrane proteins with extensive tissue-specific isoforms arising from alternative mRNA processing (Lambert and Bennett, 1993; Bennett, 1992). Two serine-rich nervous tissue specific isoforms, encoded by the gene *ankyrin-G* or *ANK3*, of 480 and 270 kDa were first isolated from the human frontal cortex and termed AnkG (Kordeli et al., 1995). AnkG clusters at the site of AIS formation in the proximal axon between E13.5 and P1 *in vivo* or 3-4 days *in vitro* in neuronal cultures (Galiano et al., 2012; Gutzmann et al., 2014; Le Bras et al., 2014). Starting at the N-terminus, AnkG comprises of a 24 ankyrin-repeat membrane binding domain, a spectrin binding domain, a serine rich domain, an unstructured tail and a carboxyl-terminal. This modular structure allows AnkG to interact with and organise all layers of the AIS scaffold, earning it the title of 'master-organiser' (Bennett and Baines, 2001) and the most vital constituent of the AIS (Jones and Svitkina, 2016).

At the surface of the plasma-membrane AnkG, via its membrane-binding domain, forms the archetypal AIS membrane protein complex consisting of voltage-gated ions channels and cell adhesion molecules (CAMs) such as neurofascin 186 (NF-186) and Nuronal CAM (Nr-CAM) (Figure 1.7). Voltage-gated sodium (Na_v), potassium (K_v) and calcium (Ca_v) channels bind AnkG through their ankyrin targeting motifs. The expression, distribution and function of the various channel sub-types is further discussed in section 1.6.1. The spectrin binding domain of AnkG binds to the underlying actin/spectrin sub-membrane complex, thus inserting its entire amino-terminal, including the membrane-protein complex, into the plasma membrane. Details of the arrangement of this complex were resolved using a combination of platinum replica electron microscopy and stochastic optical reconstruction microscopy (Leterrier, 2018; Vassilopoulos et al., 2019). The actin/spectrin sub-membrane complex is composed of actin rings, ~190 nm apart, connected by spectrin tetramers. This complex presents along the entire length of the axolemma, conferring structural rigidity to the axons (Xu et al., 2013; D'Este et al., 2015; Leterrier et al., 2015). The spectrin tetramer composes of 2 α and 2 β sub-units, with β4 being the predominant isoform in the AIS and β2 being the predominant isoform in the distal axon. AnkG recruits β4-spectrin to the AIS in a phosphorylation dependent manner (Dzhashiashvili et al., 2007; Yang et al., 2007; Jenkins et al., 2015) and binds repeats 14-15 of β4-spectrin (Komada and Soriano, 2002), positioning itself and its bound ion channels and CAMs midway between the actin rings (Xu et al., 2013; Leterrier et al., 2015; D'Este et al., 2017). The carboxyl-terminal tail of AnkG extends to a maximum depth of 140 nm into the intracellular AIS shaft and connects the actin/spectrin complex to the underlying microtubules. The interaction with microtubules is mediated via microtubule associated proteins including end-binding protein 1/3 (EB1/3) (Leterrier et al., 2011) and nuclear distribution element-like 1 (Ndel1) (Kuijpers et al., 2016).

The domains and processes resulting in recruitment of AnkG to the AIS are unclear. Schultz et al. (2006) suggests that AnkG recruitment is dependent on phosphorylation of pIκBα, a phosphorylation inhibitor of nuclear factor-κB, while He et al. (2012) suggests that AnkG recruitment and stability is dependent on palmitoylation of cysteine-70 of its membrane binding domain. Further, Galiano et al. (2012) and Zhong et al. (2014) suggest that, in cortical neurons, the formation of the AIS is dependent on the distal axon cytoskeletal protein complex of actin/β2-spectrin and ankyrin-B. While the precise temporal dynamics of AIS assembly are yet to be revealed, the importance of AnkG in AIS formation and maintenance has been

demonstrated by a number of groups. Loss of AnkG *in vivo* (*ankyrinG*$^{-/-}$) results in a loss of 'AIS compartment' proteins including β4-spectrin, Na_v, NF-186 and NrCAM (Zhou et al., 1998; Jenkins and Bennett, 2001; Jenkins et al., 2015). The cells of *ankyrinG*$^{-/-}$ mice present altered physiological proprieties including increased threshold for AP initiation, reduced firing rate with sporadic firing and decreased gamma oscillations (Zhou et al., 1998; Jenkins et al., 2015). *In vitro* silencing of AnkG in hippocampal cultures using short-hairpin RNA (Jenkins et al., 2015) or RNA-interference (Hedstrom et al., 2008) results in a similar loss of 'AIS compartment' proteins along with loss of axonal identity, as observed by the localisation of dendritic post-synaptic markers including microtubule-associated protein 2 (MAP2), K^+/Cl^- co-transporter (KCC2), PSD-95 and 'spines' in the proximal axon (Hedstrom et al., 2008; Rasband, 2010; Jenkins et al., 2015).

Although AnkG is not needed for axon formation (Galiano et al., 2012; Jenkins et al., 2015), it provides the selective advantage of formation of the AIS, in turn allowing rapid and precise control over AP generation and neuronal signalling. Given the specialised and vital role of AnkG in AIS assembly and maintenance of neuronal polarity this thesis uses AnkG as a marker to identify the AIS.

Ion Channels at the AIS

High-density clustering of voltage-gated ion channels, including sodium (Na_v), potassium (K_v) and calcium (Ca_v) channels, is the hallmark of the AIS (Rasband, 2010; Kole and Stuart, 2012; Jones and Svitkina, 2016; Nelson and Jenkins, 2017; Leterrier, 2018).

Na_v channels are made up of four transmembrane domains and localise to the AIS through binding of AnkG to a nine amino-acid sequence in the cytoplasmic-loop connecting its trans-membrane domains II and III (JoséGarrido et al., 2003). $Na_v1.1$, $Na_v1.2$ and $Na_v1.6$ channels localise along the length of the AIS in a cell-type and developmental age dependent manner (Kole and Stuart, 2012). $Na_v1.1$ is expressed in GABAergic cells, retinal ganglion cells and spinal-cord motor neurons (Van Wart et al., 2007; Lorincz and Nusser, 2008; Duflocq et al., 2008). In retinal ganglion cells, $Na_v1.2$ is expressed in early development while expression of $Na_v1.6$ coincides with the onset of repetitive firing (Boiko et al., 2003). Whereas in cortical

pyramidal cells of P14-16 rats, $Na_v1.2$ is located at the proximal (to the cell soma) end of the AIS whereas $Na_v1.6$ is located at its distal end (Hu et al., 2009). Overall, Na_v's are responsible for the local inward ion current at the AIS where $Na_v1.6$ channels are responsible for AP generation whereas $Na_v1.2$ are involved in their back-propagation to the soma (Hu et al., 2009).

K_v channels at the AIS suppress neuronal excitability and regulate AP repolarisation, thus determining AP threshold, inter-spike interval, and firing frequency of the neuron (Brown and Adams, 1980; Pan et al., 2006). The most abundant K_v channels present at the AIS are the low threshold $K_v1.1$ and $K_v1.2$ channels (Dodson et al., 2002; Goldberg et al., 2008; Inda et al., 2006; Lorincz and Nusser, 2008; Ogawa et al., 2008; Van Wart et al., 2007). These channels localise to the distal AIS through binding of PSD-93, instead of AnkG (Ogawa et al., 2008; Duflocq et al., 2011), and influence AP firing frequency and waveform. K_v channels 7.2 and 7.3 (KCNQ2/3) cluster at the AIS of pyramidal neurons using a Na_v-homologous AnkG-targeting motif present on its C-terminus (Pan et al., 2006). These channels generate a slowly activating and non-inactivating M-type current which controls spike-frequency adaptation.

Ca^{2+} sequestering cisternal organelles were identified at the AIS by Peters et al. (1968). While it was hypothesized that these organelles must sequester local Ca^{2+} entering via Ca_v channels, the presence of these Ca_v channels at the AIS was not shown until 1996. Callewaert et al. (1996) were the first to show the presence of P/Q-type Ca^{2+} ($Ca_v2.1$ and 2.2) channels in the AIS of cerebellar purkinje cells. More recently, Bender and Trussell (2009) showed the localisation of T- and R-type Ca^{2+} channels ($Ca_v2.3$, 3.1 and 3.2) in the AIS of dorsal cochlear nucleus interneurons, cortical layer 5b pyramidal cells and cerebellar purkinje cells while Yu et al. (2006) showed the presence of N-type Ca^{2+} channels in cortical pyramidal cells. These channels served to boost membrane depolarization and are essential for the generation and timing of action potential bursts known as complex spikes.

1.6.2 AIS Function

Diffusion Barrier and Maintenance of Neuronal Polarity

Directional propagation of action potentials in neurons results from anatomical and functional polarity of its compartments. In the mouse cortex, the onset of this polarity is rapid, occurring between embryonic day (E) 14-18 (Barnes and Polleux, 2009). The AIS is tasked with maintenance of this polarity throughout post-natal life (Rasband, 2010). Kobayashi et al. (1992) hypothesised that it does so by forming a 'diffusion barrier'. They showed that in cultured hippocampal neurons, fluorescent membrane-bound phospholipids in the distal axon were unable to diffuse into the somatodendritic compartment. In addition to lipids, lateral diffusion of membrane-bound proteins NCAM-L1 and THY1 are also restricted at the AIS (Winckler et al., 1999). Pharmacological disruption of the actin filaments increases mobility of both proteins and lipids, as observed by single-particle tracking (Nakada et al., 2003). These observations led to the proposal of a 'fence and pickets' model of the AIS diffusion barrier where the 'pickets' are the trans-membrane ion-channels and cell adhesion molecules that are themselves immobilized by the underlying Ank-G-actin-spectrin 'fence'.

While the existence of this barrier controls the diffusion of membrane components in the proximal axon, how does it mediate the trafficking of intra-cellular cargo and distinguish between axon-destined and dendrite-destined cargo? AIS control of intra-cellular trafficking was first proposed by Song et al. (2009), who measured the diffusion rates of fluroescently labelled dextrans of varying molecular weights from the soma to the axons in cultured hippocampal neurons. They found that dextran movement was restricted in a weight-dependent manner, with only the smaller dextrans visible in the axonal compartment. This led to the proposal that the actin-cytoskeleton of the AIS acts as a 'size sieve'. Indeed, disruption of actin filament polymerisation by latrunculin A allowed for rapid dispersion of previously-excluded large-dextran molecules to the axon. As well, Farías et al. (2015) propose a 'pre-axonal exclusion zone', a TRIM-46 positive region in the axon-hillock at the start of the AIS that actively recruits axonal cargo while rejecting somatodendritic cargoes. While the formation of this region is shown to be Ank-G dependent (Van Beuningen et al., 2015), Gumy et al. (2017) showed that pre-axonal exclusion occurs in Ank-G-lacking neurons of the the dorsal root ganglion. Nirschl et al. (2017)

propose a retrieval mechanism for mistargeted cargoes within the AIS. This follows a two-step protocol where mistargeted cargo is first stalled by actin followed by either dynein or dynamin-mediated retrieval. Evidence for the actin-based stalling comes from the works of Lewis et al. (2009) and Watanabe et al. (2012). They showed that somatodendritic proteins selectively bind to the motor myosin V (Lewis et al., 2009) which, in turn, binds to the actin patches at the AIS, causing cargo immobilisation (Watanabe et al., 2012; Balasanyan et al., 2017; Janssen et al., 2017). The dynein-mediated retrieval is dependent on CDK5-phosphorylation of dynein activator NDel1 and its binding partner LIS1 (Klinman et al., 2017), whereas dynamin-mediated retrieval is controlled by Rab5 and its effector FHF (Guo et al., 2016).

While the hypotheses above propose mechanisms of keeping somatodendritic cargo out, the AIS is also proposed to recruit axonal cargo via selective binding of AIS microtubules to anterograde kinesin motors like KIF5 (Nakata and Hirokawa, 2003).

Morphological Plasticity and AP Dynamics

In addition to maintaining neuronal polarity, the AIS is widely implicated in regulating neuronal excitability in a homeostatic manner (Kuba et al., 2006, 2010; Grubb and Burrone, 2010; Evans et al., 2015). This regulation ranges from modulation of surface ion-channel expression at the AIS in the short-term (miliseconds to minutes) to morphological changes including alteration of AIS length and position along the axon in the long-term (hours to days) (Petersen et al., 2017).

Short-term 'fast' modulation of the AIS is mediated either by Ca^{2+} influx into the AIS (Del Puerto et al., 2015; Martinello et al., 2015; Benned-Jensen et al., 2016) or by neurotransmitters acting on receptors located at or near the AIS (Bender et al., 2010; Cotel et al., 2013; Ko et al., 2016; Yang et al., 2016; Yin et al., 2017). In cultured hippocampal neurons, sustained glutamatergic stimulation of NMDARs leads to an elevation of intracellular Ca^{2+}, inducing rapid (5-10 min) endocytosis of $Na_v1.2$ and $K_v7.2/7.3$ ion-channels at the AIS (Benned-Jensen et al., 2016). This endocytosis, mediated by calpain, is thought to be neuroprotective against excitotoxcity as it suppresses AP generation and further glutamate release (Benned-Jensen et al., 2016). In dentate granule cells from acute brain slices, electrical stimulation (8 x 40 kHz, 125

ms inter-burst interval) of cholinergic fibres is sufficient to activate the muscarinic M1 receptor leading to intracellular Ca^{2+} influx into the AIS via $Ca_v3.2$ (Martinello et al., 2015). This results in a suppression of K_v7 mediated M-current, decreased spike-threshold and increased priming of cells to fire APs for up to 30 min post-stimulation. Neurotransmitters that affect AIS ion-channel expression include dopamine and serotonin (Bender et al., 2010; Cotel et al., 2013; Yang et al., 2016; Ko et al., 2016; Yin et al., 2017). In dorsal cochlear nucleus cartwheel interneurons, Bender et al. (2010) showed that activation of dopamine receptors specifically inhibited Ca_v3 channels at the AIS through activation of protein kinase C (PKC) ultimately reducing the AP output of these neurons. Yang et al. (2016), similarly show that dopamine receptor 3 (D3) activation inhibits Ca_v3 channels at the AIS, through non-canonical β-arrestin mediated signalling. Cotel et al. (2013) showed that prolonged activation of serotonin receptor 5-HT_{1A} in motor neurons, inhibits Na^+ channel mediated spike initiation at the AIS while Yin et al. (2017) showed that activation of 5-HT_{1A} in pyramidal neurons of the prefrontal cortex lead to selective inhibition of $Na_v1.2$ channels, decreasing AP back propagation which may result in sustained neuronal firing through integration of excitatory post-synaptic potentials (EPSPs). In addition to modulation of Na_v channels, serotonin activation also hyperpolarises HCN channels at the AIS in the principal neurons of the medial superior olive lowering AP threshold (Ko et al., 2016). Together, activity of these ion-channels work to homeostatically regulate neuronal excitability, preventing excitotoxicity or prolonged suppression of activity, in response to incoming stimuli.

Long-term structural plasticity of the AIS presents as modulation of its length and position along the axon over the course of normal development (Cruz et al., 2009; Le Bras et al., 2014; Yamada and Kuba, 2016; Gutzmann et al., 2014; Schlüter et al., 2017; León-Espinosa et al., 2018), in response to altered neuronal activity (Kuba et al., 2010; Grubb and Burrone, 2010; Chand et al., 2015; Wefelmeyer et al., 2016; Horschitz et al., 2015) or pathology (Yoshimura and Rasband, 2014; Yamada and Kuba, 2016; Jamann et al., 2018). While this occurs in a brain-region and cell-type specific manner, all things being equal, longer AISs increase cellular excitability whereas shorter AISs restrict cellular excitability. Similarly, more distally located AISs decrease neuronal excitability whereas more proximally located AISs increase neuronal excitability. While the exact mechanisms for these changes in unknown, elongation of AIS length is expected to increase the number of ion-channels while relocation of the AIS further from the soma increases its electrical isolation, allowing synaptic signal processing to occur

independently of the dendrites and soma.

The modulation of AIS morphology to fine-tune neuronal activity was first shown in the avian auditory system, specifically in the nucleus magnocellularis (NM) and nucleus laminaris (NL) of the chicken (Kuba et al. (2006), Kuba and Ohmori (2009)). Neurons in these regions respond only to sounds of a 'characteristic' frequency (CF), and are arranged in a tonotopic fashion with high-frequency recognising cells present more rostro-medially and low-frequency recognising cells present more caudo-laterally (Parks and Rubel (1975)). NM cells receive input directly from the auditory nerve and generate spikes at a particular phase of the sound wave to convey temporal information to the NL. This system allows for accurate estimation of interaural time difference and localisation of the sound source. In the NM, neurons detecting low-frequencies ($\sim$0.2 kHz) have about 2-fold longer AIS length, and increased number of Na_v channels, than those detecting high-frequencies ($\sim$4 kHz) (Kuba and Ohmori (2009)). Characteristically, high-CF NM neurons receive a single-large input from the auditory nerve whereas low-CF NM neurons receive multiple small synaptic inputs, with AP being generated by input summation. The difference in AIS length allows the low-CF NM neurons to compensate for Na^+ current inactivation during this slow depolarisation. Thus, the length of the AIS changes with the number and size of synaptic inputs and ensures reliable and precise firings in NM neurons. Unilateral removal of the cochlea resulted in a >50% increase in AIS length, measured by changes in both Ank-G labelling as well as a pan-Na_v marker, and neuronal excitability of NM neurons compared to the intact side within 7-days (Kuba et al. (2010)). Additionally, auditory deprivation at any stage of development resulted in a similar elongation of AIS length in NM neurons. This structural elongation is complemented by a near-simultaneous redistribution of K_v channels, switching predominant channel subtypes from $K_v1.1$ to $K_v7.2$. The slow activation kinetics of $K_v7.2$ reduces the shunting conductance during AP initiation at the AIS and enhances neuronal excitability (Kuba et al. (2015)). In the NL, high-CF neurons continue to be $\sim$2-fold shorter than low-CF neurons, but unlike NM neurons the high-CF NL neurons also show increased distance from the cell soma (Kuba et al. (2006)). This increased distance electrically isolates the AIS from the capacitive and conductive loads that result from temporal summation of high-CF inputs to the soma and dendrities, allowing AP generation from small Na^+ conductances and accurate coincidence detection. During early development of NL neurons, the AIS (stained with Ank-G and pan-Na_v markers) appears at E9 and is of comparable length across neurons of all CF. The AIS elongates until E15, following which a CF-specific shortening

occurs. This shortening is shown to be activity dependent as bilateral removal of the otocyst (precursor to the inner-ear), which ablates afferent inputs to the NL, resulted in longer AIS lengths in high-CF neurons (Kuba et al., 2014). The distance of the AIS from the soma, however, was not affected by otocyst removal. Therefore, regulation of AIS length and position along the axon is regulated developmentally in both an activity-dependent and independent manner.

In cultures, neurons show specific adaptation of AIS length and location upon chronic depolarisation (24-48 h) with either high extracellular K^+ or optogenetic manipulation (Grubb and Burrone, 2010; Evans et al., 2013; Chand et al., 2015; Evans et al., 2015). In dissociated hippocampal cultures, elevating neuronal activity by 48 h treatment with 15 mM K^+ or bursts of photostimulation (5 flashes at 20 Hz every 5s for 48 h) results in a distal shift, relative to cell soma, in all AIS components including AnkG, βIV-spectrin and Na_v, specifically in excitatory neurons with GAD-65 positive GABAergic interneurons showing no such shift (Grubb and Burrone, 2010). This relocation results in decreased neuronal excitability, as evidenced by increased current threshold and current threshold density for firing an AP (Grubb and Burrone, 2010). Functionally, this relocation was shown to be dependent on L-type Ca_v channel (Ca_v1) activation, as pharmacological block of Ca_v1 abolished AIS relocation. Downstream of Ca_v activation, AIS relocation is mediated by the Ca^{2+}-sensitive phosphatase calcineurin, as similar pharmacological blockage of this molecule prevents AIS relocation upon high-K^+ or photostimulation mediated depolarisation (Evans et al., 2013). In cultures of dopaminergic neurons from the rat olfactory bulb, however, chronic depolarisation induced by 24 h treatment with 15 mM K^+, resulted in increased length and proximal relocation of the AIS (Chand et al., 2015). This inverse plasticity was also found to be Ca_v1 dependent but is not accompanied by alterations in AP firing properties. The above studies suggest that perturbed network inputs induce activity-dependent changes of AIS structure to allow altered axonal transport and/or axonal growth dynamics (Marik et al., 2010; Chand et al., 2015). Additionally, cell-type specific AIS plasticity has also been observed *in vitro* (Evans et al., 2015). Optogenetically and phamaracologically induced depolarisation over a 'short' time-scale (3h) showed significant reduction in AIS length without any relocation only in neurons from hippocampal dentate granule cell cultures and not in neurons from hippocampal CA1 or CA3 cell cultures (Evans et al., 2015). Shortening of the AIS resulted in reduced neuronal excitability, particularly repetitive firing. This 'rapid' shortening was also found to be mediated by calcineurin, and reversed by

CDK5 and re-phosphorylation of Na_v. In addition to Ca^{2+} signaling, Guo et al. (2016, 2017) proposed that secretory-signalling molecules, brain-derived neurotrophic factor (BDNF) and neurotrophin 3 (NT3), underlie AIS structural plasticity. In hippocampal cultures, elevation of extracellular BDNF or NT3 results in proximal (to the cell soma) relocation of the AIS with increased neuronal excitability whereas knockdown of neurotrophin receptors TrkB and TrkC causes distal relocation of the AIS with a reduction in neuronal excitability (Guo et al., 2017). Thus, while activity-dependent alterations in AIS length and location have been widely reported the exact signalling cascades underlying this structural plasticity are still being identified. These studies reveal that the AIS is not just a trigger zone for AP generation, but plays a key role in regulating the integration of synaptic input and neurotransmitter release resulting in alteration of intrinsic cellular excitability.

Distinct AIS lengths and structural plasticity are also observed *in vivo* during normal development (Fried et al., 2009; Cruz et al., 2009; Le Bras et al., 2014; Gutzmann et al., 2014), artificial reduction of sensory input (Gutzmann et al., 2014; Schlüter et al., 2017) as well as in periods of naturally reduced activity like hibernation (León-Espinosa et al., 2018). In the New Zealand white rabbit, different sub-types of retinal ganglion cells, with distinct visually-responsive properties, have AISs of distinct length and proximity to the soma (Fried et al., 2009). Notably, directionally selective (DS) ganglion cells and brisk transient/alpha (BT) light-intensity sensitive ganglion cells differed significantly in average AIS length (DS: 28.6 ± 4.8 μm; BT: 40.6 ± 5.39 μm; P= <0.001) while proximity to the cell soma differed significantly between DS/BT cells and unspecified ganglionic cells (DS: 22.8 ± 6.4 μm; BT 26.9 ± 5.5 μm; unspecified cells: 0-40 μm). In rhesus macaque monkeys, the AIS of pyramidal neurons in the prefrontal cortex shortened in length during the first 6 post-natal months, following which the length remained stable through adolescence and adulthood (Cruz et al., 2009). However, the AIS lengths of gephyrin-positive GABAergic chandelier neurons in the same region and model showed marked shortening only during adolescence (2-3 years) (Cruz et al., 2009). Taken together these studies indicate that not only do cells with distinct spiking properties show differences in AIS length and location along the axon (Fried et al., 2009) but also that the AIS lengths of different cell types within the same brain region undergo distinct developmental trajectories (Cruz et al., 2009). In motor neurons of the mouse embryo, AnkG is observed as early as E9.5 and found to be homogeneously distributed throughout the developing axon, with expression restricted to the proximal axon by E11.5 (Le Bras et al., 2014). In the mouse primary visual

cortex, Gutzmann et al. (2014) showed that AIS length is dynamically regulated from E14.5 into adulthood. From when the AIS first appears at E14.5, a steady increase in its length is observed, peaking at P10-15, coincidental with eye-opening. This is followed by significant shortening during the critical period of ocular dominance plasticity (commencing around P21, for review see Espinosa and Stryker (2012)), with shortest lengths being observed at P28 (Gutzmann et al., 2014). In the adult visual cortex, AIS lengths were longer than those observed at P28, but still significantly shorter than those observed at P10-15, providing the further evidence that neurons of different brain regions show differential developmental trajectories of AIS length. Dark rearing of mice from birth abolished the dynamic shortening of AIS lengths observed between P10-15 and P21-28. This shortening was later shown to depend on the presence of the cisternal organelle (Schlüter et al., 2017), as mice lacking synaptopodin, a marker for the cisternal organelle, showed AIS shortening at P21-28 despite being dark-reared. Given that the cisternal organelle is known to mediate Ca^{2+}-trafficking, it maybe speculated that this form of AIS structural plasticity is Ca^{2+} dependent, however direct evidence for this remains to be shown. While there is evidence in the literature of reduced cellular excitability upon dark-rearing (Fagiolini et al., 1997; Morales et al., 2002; Heinen et al., 2004; Funahashi et al., 2013), the causal role of dynamic AIS regulation on reduced cellular excitability upon dark-rearing is yet to be shown. In addition to sensory deprivation, environmental modifications including enrichment have been shown to shorten AIS length in the murine frontal cortex (Nozari et al., 2017). Lastly, León-Espinosa et al. (2018) showed that during innate prolonged states of reduced neuronal and metabolic activity, like hibernation, the AIS in the somatosensory cortex and CA1 regions of the Syrian hamster elongate. This elongation is likely compensatory for the reduced states of synaptic and neuronal activity, though there is speculation that it serves a neuroprotective function to ishaemic insults as a results of hibernation accompanied hypothermia (León-Espinosa et al., 2018). However, the direct effects of elongates AIS lengths during hibernation on cellular excitability are yet to be shown.

Given that AIS structure is influenced by network input, Gulledge and Bravo (2016) proposed that neurons intrinsically optimise their excitability by modifying AIS location and length in a manner that is closely correlated with neuronal morphology. Using a computational model of realistic somatodendritic morphologies, they showed that small neurons (like dentate granule cells) exhibited maximal excitability when AIS is of intermediate length (60-65μm) and located adjacent to the soma. While larger cells (like pyramidal neurons) were maximally excitable

when the AIS was long (100μm) and located more distally. They also altered the capacitance and conductance of the dendritic compartment and found that the former played a more central role in influencing AP generation at the AIS. Their results also suggest that alterations to AIS length, rather than location - when paired with corresponding changes in Na^+ conductance - modified neuronal excitability more effectively.

In addition to physiological changes during development, the AIS is also shown to be modified during various pathological conditions, particularly epilepsy and ischaemia/ stroke. These alterations are discussed below.

1.6.3 AIS in Disease Pathology

Altered network activity is a hallmark of multiple nervous system disorders. Given that the AIS influences cellular excitability, it is unsurprising that aberrant AIS morphology and plasticity is implicated in neuronal disorders and injury (Fig.1.8). Discussed below are some such findings.

Epilepsy

AIS function, particularly its control of neuronal excitability is heavily dependent on the density and composition of ion-channels present at this site. Malfunction of these channels, particularly Na^+, $GABA_A$ and K^+ channels, have been associated various forms of epilepsy (insert all the reference). Thus, Wimmer et al. (2010) proposed that the AIS was a 'common node' in the pathophysiology of epilepsy, where heterogeneous mutations converge, alter AIS structure and influence neuronal excitability. The first evidence of the 'common node' hypothesis comes from a study by Ribak (1985). NF-186, a cell-adhesion molecule found at the AIS, is shown to target axo-axonic GABA-ergic synapse formation at the AIS (Ango et al., 2004; Kriebel et al., 2011). The Ribak (1985) study found that in primate models of temporal lobe epilepsy, there was a loss of GABAergic inhibition targeting the AIS. This loss resulted from degeneration of axo-axonic chandelier cells in the epileptic foci and resulted in reduced inhibition of cortical pyramidal cells.

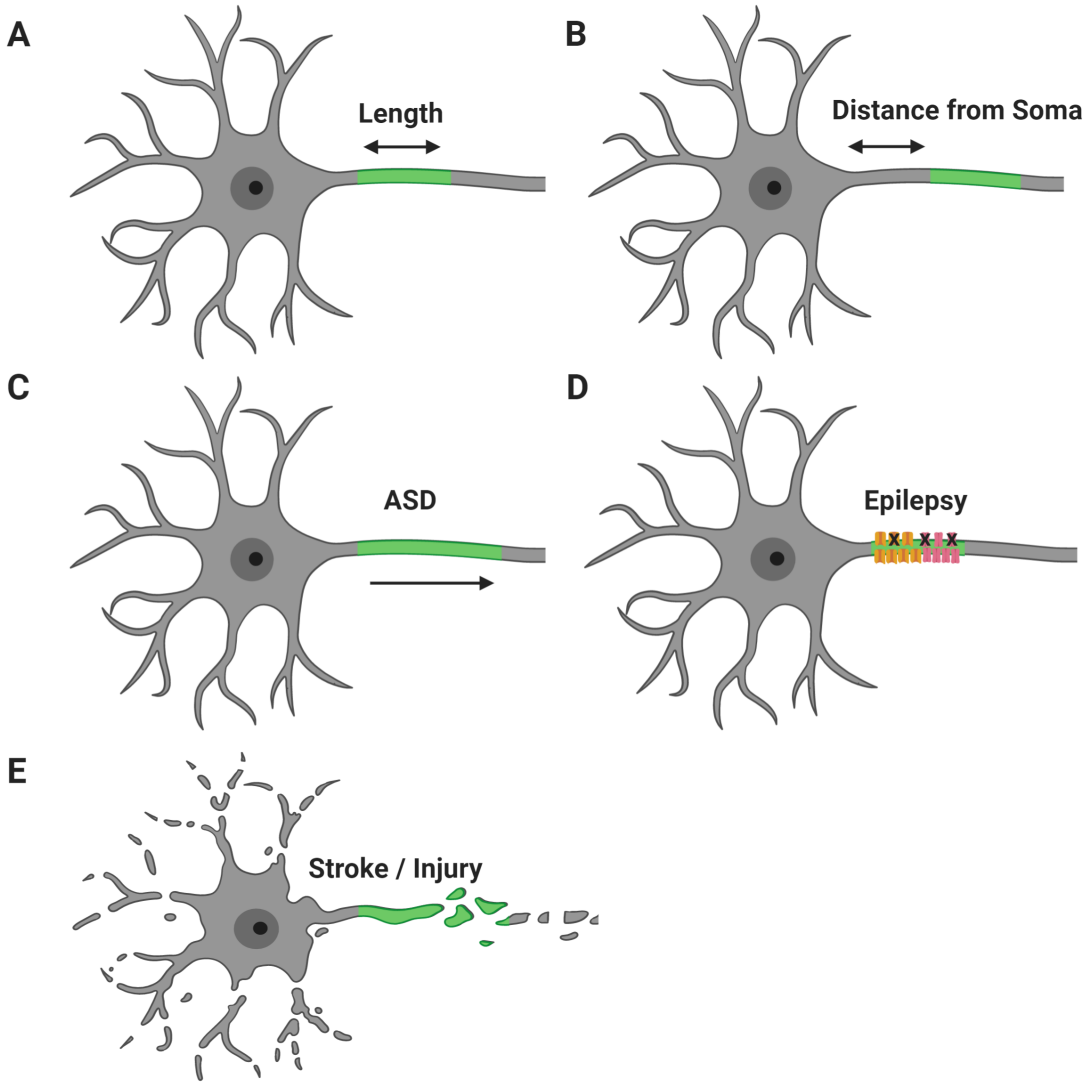

Figure 1.8: Structural changes to the AIS in Plasticity and Pathology (A, B) The AIS alters its length and position along the axon, measured as altered distance from the soma, in an activity dependent manner (C) There is evidence of elongated AIS lengths mouse models of Fragile-X Syndrome (Booker et al., 2019) and Angelman's syndrome (Kaphzan et al., 2011) (D) Evidence of increased number of ion-channels present at the AIS as well as decreased number of functional ion-channels at the AIS have been presented in cases of epilepsy (Rasband, 2010) (E) In cases of stroke and traumatic brain injury degradation of the AIS and the axon have been indicated (Schafer et al., 2009). This schematic was made using the Biorender and scidraw softwares and parts were adapted from Rasband (2010).

Moving on to ion-channels, the most prominent AIS localising single-channel mutation associated with epilepsy is $Na_v1.1$. Mutations in this channel cause a phenotypic spectrum of epilepsy from mild febrile seizures (Wallace et al., 1998) to severe myoclonic epilepsy of infancy (Dravet syndrome) (Scheffer et al., 2009, 2007). $Na_v1.1$ is coded by the gene *SCN1A* and localises exclusively to the AIS of GABAergic neurons. Mouse models of Dravet syndrome (*Scn1a*$^{-/-}$) exhibit loss of Na^+ current with significantly reduced firing of GABAergic neurons in the hippocampus without altered activity in excitatory neurons (Yu et al., 2006; Ogiwara et al., 2007; Kalume et al., 2007). Suggesting that reduced inhibition might underlie neuronal hyperactivity in this model. Missense mutations in $Na_v1.2$ are causative of a milder form of childhood epilepsy, benign familial neonatal-infantile seizure (BFNIS) as well as refractory seizures (Berkovic et al., 2004; Ogiwara et al., 2009). Whereas mutations in $Na_v1.6$, encoded by *SCN8A*, are thought to be neuroprotective against development of epileptic phenotypes. Evidence for the neuroprotective function is two-fold. First, in heterozygous knock-out mouse models of *Scn8a*$^{+/-}$, animals exhibited reduced seizure susceptibility (Blumenfeld et al., 2009), whereas double-knockout *Scn1a*$^{-/-}$;*Scn8a*$^{+/-}$ ameliorated seizure severity and lethality of the *Scn1a*$^{-/-}$ mice (Martin et al., 2007). The mutations discussed above are in the pore-forming α sub-unit of Na channels, and typically Na channels also comprise of two auxiliaryβ sub-units (Catterall, 2000). Mutations in $\beta 1$ (*SCN1B*) have been reported in patients with generalised epilepsy with febrile seizures as well as in some patients with Dravet's syndrome (Wallace et al., 1998; Scheffer et al., 2007; Patino et al., 2009). However, neurons in mice with complete loss of *Scn1b* (*Scn1b*$^{-/-}$) were found to be hypoexcitable (Brackenbury et al., 2010).

In addition to Na_v channels, mutations in K_v expressed at the AIS have also been associated with epilepsy. Mutations in $K_v1.1$ is associated with episodic ataxia. Given that this channel controls AP waveform and synaptic efficiency, epilepsy mutations could result in increased firing by altering axonal AP (Kole et al., 2007). Mutations in $K_v7.2$ and 7.3 lead to reduced surface expression of these channels, with reduced M-current generation, in patients with benign familial neonatal seizures (Browne et al., 1994; Jentsch, 2000; Chung et al., 2006; Miceli et al., 2009).

Finally, gain of function mutations in $Ca_v3.2$, resulting in increased Ca^{2+} influx, is associated with idiopathic generalised epilepsy with absence seizures (Chen et al., 2003; Heron et al., 2004, 2007; Khosravani et al., 2004, 2005; Vitko et al., 2005). While loss of $Ca_v2.3$ increased

limbic seizure resistance (Weiergräber et al., 2006).

Thus, while multiple ion-channels present at the AIS are implicated in epileptic etiology, direct evidence of altered AIS structure or function in the above stated models is still required.

Stroke and Traumatic Brain Injury

Ischaemic injury following stroke results in widespread neurological dysfunction. A major contributor to this dysfunction is excito-toxicity resulting from a sudden and large influx of Ca^{2+}. Schafer et al. (2009) showed that in *in vivo* and *in vitro* models of stroke this increase in intracellular Ca^{2+} activates the protease calpain and results in irreversible breakdown of the AIS cytoskeleton and loss of Na_v clusters. This breakdown occurs independently of and prior to wide-spread cell death that is also characteristic of stroke. Loss of the AIS results in loss of neuronal polarity with somatodendritic markers like MAP2 being found in the former axon while pharmacological inhibition of calpain blocks AIS disassembly following neuronal injury (Schafer et al., 2009). Concomitant with this increased excitation at the site of injury, areas adjacent to it (the peri-infarct cortex) increase GABAergic mediated tonic-inhibition in an attempt to curb excito-toxicity. Hinman et al. (2013) showed that neurons in the peri-infarct cortex reduce their AIS length along with a loss of axo-axonic synapses resulting in reduced cellular excitability. Counter intuitively, blocking this increased inhibition either by blocking GABA mediated downstream signalling or stimulating glutamate signalling aides recovery post-stroke. Together, the data suggests that structural changes to the AIS are a core pathophysiology of stroke, its morphological plasticity may contribute to poststroke changes in neuronal excitability and this may provide a potential pharmacological target to enhance recovery from stroke.

Autism Spectrum Disorders

The first evidence of altered AIS morphology in a model of ASD comes from the works of Kaphzan et al. (2011). They report that in the CA1 of a mouse model of Angelman's syndrome the AIS is elongated along with increased expression of $Na_v1.6$ at the AIS. The altered AIS

morphology was accompanied by changes to the intrinsic electrophysiological properties in these cells including increased action potential amplitude and increased threshold potential.

Additionally, studies using genome wide association (GWAS) and whole exome sequencing have identified mutations in AIS protein coding genes as causative for ASD/ID in a number of cases. Sanders et al. (2012) performed whole exome sequencing in 928 individuals including 200 discordant sibling pairs. In their pool of 279 *de novo* coding mutations they identified two independent nonsense variants in the gene *SCN2A*, encoding the AIS channel $Na_v1.2$, present in probands but not in the siblings. Bi et al. (2012) performed whole exome sequencing on 67 individuals with ASD and identified three different missense mutations in *ANK3*, which codes the AIS master organiser ankyrin-G, from four unrelated individuals with ASD. Iqbal et al. (2013) report one case of a chromosomal translocation causing heterozygous disruption of *ANK3* in a patient with ADHD and ASD as well as a familial cases of autosomal recessive ID, hypotonia, spasticity and sleep disturbances resulting from a homozygous frameshift mutation in *ANK3*. RNAi silencing of the Drosophila homolog of *ANK3* resulted in short-term memory loss, supporting the importance of this gene in cognition (Iqbal et al., 2013). Most recently, Kloth et al. (2017) used trio-whole-exome sequencing to identify a heterozygous *de novo* nonsense mutation in *ANK3* in an individual presenting with speech impairment, intellectual disability, macrocephaly, chronic hunger and an altered sleeping pattern.

While AIS dysfunction is yet to be reported in these cases, the presence of these mutations in AIS specific proteins underscores the importance of this structure in cognition and makes it an attractive structure to study in the the context of ASD/ID.

Other Neuropsychiatric Disorders

In addition to the above stated disorders, mutations in *ANK3* have been associated by GWAS to patients with bipolar disorder (Ferreira et al., 2008; Leussis et al., 2012; Wang and Miller, 2018). In schizophrenic patients with reduced GABA activity, a upregulation of the AIS specific $\alpha 2$ subunit of $GABA_A$ receptors is observed in pyramidal cells of the prefrontal cortex (Lewis et al. (2005)). While in patients with multiple sclerosis, there is evidence of increased antibodies against the AIS-CAM NF-186 (Mathey et al., 2007).

1.7 Aims of this thesis

Two groups of studies were critical to the formulation of the hypothesis tested in this thesis: First, an increase in AIS length was observed in pyramidal cells of the *stratum radiatum* in the CA1 of mouse models of Angelman's syndrome (Kaphzan et al., 2011) and Fragile-X syndrome (FXS) (Booker et al., 2019) with the increased length underlying cellular hyperexcitability (Booker et al., 2019). Second, mouse models of FXS and *SYNGAP1* haploinsufficiency show convergent cellular and molecular deficits (Barnes et al., 2015) with cellular deficits observed in the FXS mouse model persisting in a rat model of FXS (Till et al., 2015). Given the extensive cellular excitability deficits reported across multiple brain-regions upon reduction of SynGAP, reports of convergent synaptic pathophysiology between models of FXS and *SYNGAP1*-ID as well as the ability of AIS morphology to influence cellular excitability the **chief hypothesis** tested in this thesis is:

Haploinsufficiency of *Syngap1* will result in alterations of AIS length. These alterations may be one underlying mechanism for the altered cellular excitability observed in animal models of *Syngap1* haploinsufficiency.

Further studies show that a reduction in the levels of SynGAP alters spine maturation dynamics (Aceti et al., 2015; Clement et al., 2012). Spines are the first point of information input in the neuron, with the density and functionality of spines playing a critical role in shaping intrinsic cellular excitability and shaping the properties of the axon initial segment (Kole and Stuart, 2012; Wefelmeyer et al., 2016; Bolós et al., 2019), lending support to the hypothesis that the AIS length maybe altered in models of *Syngap1* haploinsufficiency.

In order to test this hypothesis, in **chapter 3**, I undertake a comprehensive a characterisation and comparison of AIS lengths between *Syngap1*$^{+/-}$ and control juvenile (P28-35) rats was undertaken across six brain regions previously shown to exhibit altered cellular excitability or be involved in behaviours that are altered in *Syngap1* haploinsufficiency (for review see Jeyabalan and Clement (2016)). These brain regions include the prelimbic medial prefrontal cortex (mPFC PL), somatosensory cortex – barrel fields (S1BF), *Cornu Ammonis* 1 and 3 (CA1, CA3) sub-fields of the dorsal hippocampus, the lateral (LA) and basal (BA) nuclei of the

amygdala and the primary visual cortex 1 (V1). Juvenile rats were chosen for the experiments as the convergent pathhophysiology between the FXS and *Syngap1* mouse models as well as the alteration in AIS length in the FXS mouse model were observed at this age. Additionally, this developmental period coincides with the critical window for some of the brain regions being studied including the V1 and BLA. The first model, *Syngap1*$^{+/-}$, shares construct validity with the heterozygous mouse model and most patient mutations of *SYNGAP1*-ID, a similar characterisation is undertaken in a second model which selectively lacks the GAP enzymatic domain and models patients with point mutations that selectively remove GAP domain function, *Syngap1*$^{+/\Delta Gap}$. This dual approach allows delineation of the function of the GAP domain versus the scaffolding function of SynGAP in particular cellular and behavioural processes.

In **chapter 4**, I test the hypothesis that reduction in SynGAP alters *in vivo* morphological plasticity of the AIS. Specifically, analysis and comparison of genotype specific changes in AIS lengths over development was undertaken in neurons of the mPFC PL and the BLA. Subsequently, adaptation of AIS length following a cued fear conditioning associative-learning paradigm was analysed in both models of *Syngap1* haploinsufficiency compared to controls. Lastly, as cell-type specific differences in cellular excitability have been noted in the *Syngap1*$^{+/-}$ mouse and reciprocal mPFC-BLA projection neurons are crucial for the formation and retrieval of fear memory, AIS lengths in this specific sub-population were analysed across genotypes.

In **chapter 5**, I test the hypothesis that genetically heterogenous causes of ASD/ID result from common alterations in cellular pathways. To this effect, I repeated the analysis performed in chapter 3 hlwhile expanding the scope of the analysis to include 5 monogenic rat models of ASD/ID. All five genes chosen are found at the post-synapse and include models of Fragile-X syndrome (*Fmr1*$^{-/y}$), Cell adhesion molecule associated non-syndromic ID (*Nlgn3*$^{-/y}$, *Nrx1*$^{+/-}$, *Cntnap2*$^{+/-}$) and a model of Cowden Syndrome that has been linked to ASD (*Pten*$^{+/-}$).

Chapter 2

Materials and Methods

2.1 Animals

2.1.1 Housing and breeding

All animals used were bred and maintained across two different sites: The University of Edinburgh, Scotland, United Kingdom and the National Centre for Biological Sciences, Tata Institute of Fundamental Research, Bangalore, India. The *Fmr1* 'knockout' (*Fmr1*$^{-/y}$), *Syngap* 'Gap deletion' (*Syngap1*$^{+/\Delta gap}$), and *Syngap* 'full-knockout' rats (*Syngap1*$^{+/-}$) were group housed and bred in accordance with the United Kingdom Home office regulations and Animals (Scientific Procedures) Act 1986 (ASPA 1986). They were maintained in a facility that was kept on a 12:12 hour light/ dark cycle with food and water *ad libitum*.

The *Nlgn3*$^{-/y}$, *Nrx1*$^{+/-}$, *Cntnap2*$^{+/-}$, and *Pten*$^{+/-}$ transgenic rats were bred and maintained in agreement with ethical guidelines approved by the Institutional Animal Ethics Committee (National Centre for Biological Sciences, Tata Institute of Fundamental Research, Bangalore, India). These animals were group-housed and maintained in a facility on a 14:10 hour light/ dark cycle with food and water available *ad libitum*.

For experimental results detailed in chapter 3, rats of both sexes were used whereas experiment and analysis was limited to male rats in chapters 4 and 5. Further, juvenile (P28-35) animals were used to obtain results detailed in chapters 3 and 5, while adult (P90-120) rats were used in chapter 4.

2.1.2 Generation of rat models

The transgenic animal models were generated by Sigma Advanced Genetic Engineering (SAGE) laboratories (St. Louis, MO, USA), now part of Horizon Discovery, using zinc-finger nuclease technology with the exception of the *Syngap1*$^{+/-}$ animals, which were generated using CRISPR-interference. The *Fmr1*$^{-/y}$, *Syngap1*$^{+/\Delta gap}$, and *Syngap1*$^{+/-}$ transgenic animals were created on a Long-Evan Hooded (LEH) background while the *Nlgn3*$^{-/y}$, *Nrx1*$^{+/-}$, *Cntnap2*$^{+/-}$, and *Pten*$^{+/-}$ transgenic animals were created on a Sprague-Dawley (SD) background.

Generation of *Fmr1* LEH rats

The *Fmr1* knockout (KO) rats were custom generated by insertion of an eGFPnlsSV40pA cassette in the coding region of exon 1 which resulted in a loss of the FMR protein (Fig. 2.1).

Generation of *Syngap1*$^{+/\Delta Gap}$ LEH rats

The *Syngap1*$^{+/\Delta Gap}$ mutants were designed by Prof Peter Kind and Dr. Sally Till. Transgenic animals were generated by selective deletion of 3584 base pairs (bp) and simultaneous insertion of a 'CAC' 3 bp between intron 7 and exon 12 of the *Syngap1* gene, resulting in deletion of the GTPase Activating Protein (GAP) domain of the SynGAP protein (Fig. 2.2).

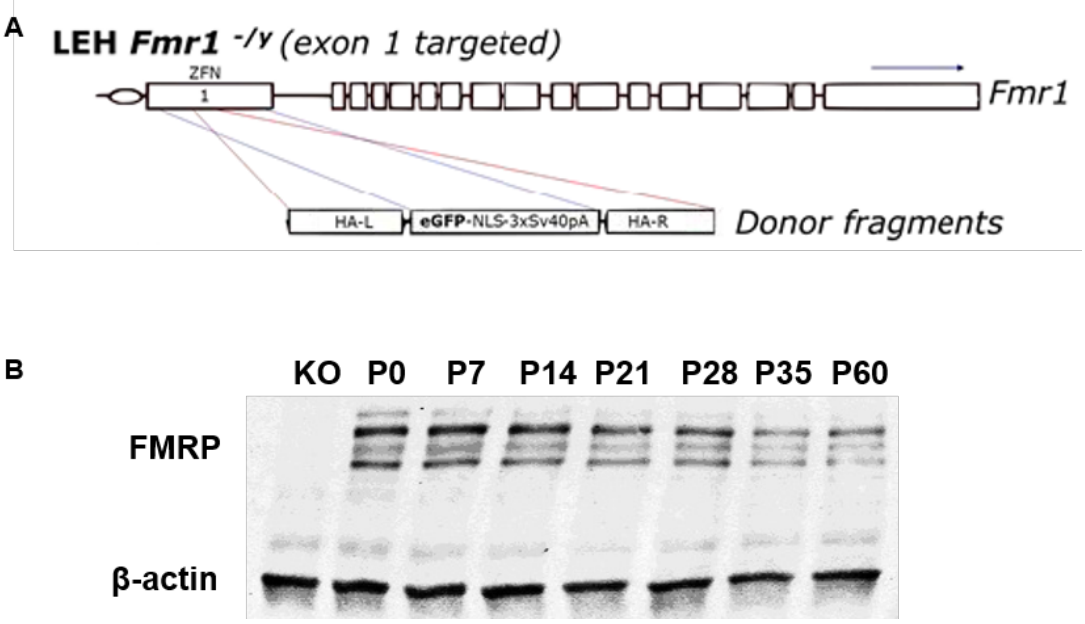

Figure 2.1: Generation of the custom *Fmr1* rat model (A) Diagram of ZFN left and right homology arms (HA-L, HA-R) cleavage sites (selection) for the custom made *Fmr1* KO LEH rats showing that the open reading frame of *Fmr1* gene was interrupted in exon 1 by a eGFP gene cassette (B) Western blot showing the loss of FMRP in the KO animals but not at any developmental stage of the wildtype littermate controls. Western Blot experiments performed by Dr Sally Till.

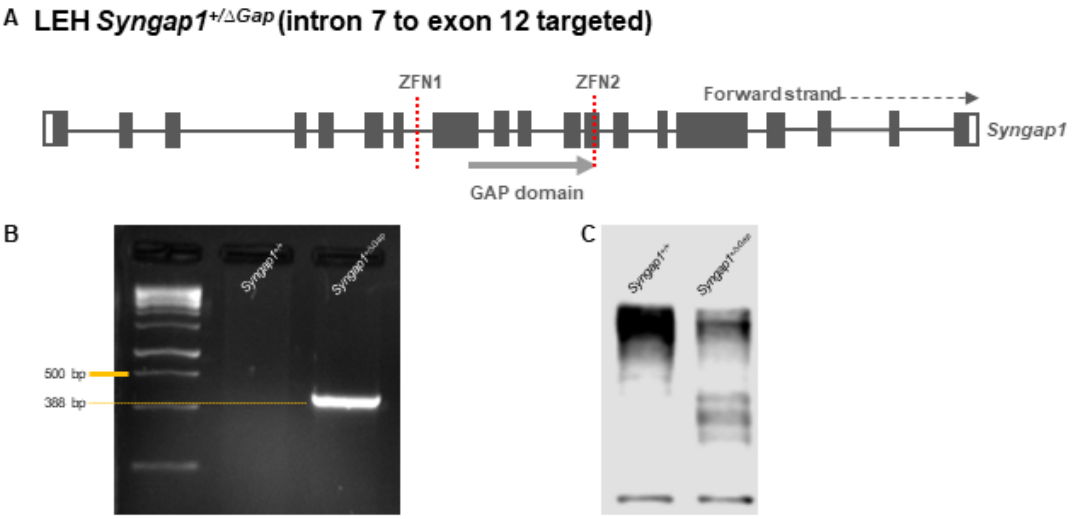

Figure 2.2: Generation of the custom *Syngap1*$^{+/\Delta Gap}$ rat model (A) Schematic of the *Syngap1* gene showing the locations of the two ZFN sites used to create a selective C2 and GAP domain deletion. Arrow indicates the coding region of the GAP domain from exon 8-12 (B) Gel showing the results of the genotyping strategy used to identify heterozygous *Syngap1*$^{+/\Delta Gap}$ rats, as only these animals showed presence of a 388 bp band that was absent in the wildtypes. (C) Western blot showing the ~140 kDa wildtype band only in the *Syngap1*$^{+/+}$ animals whereas *Syngap1*$^{+/\Delta Gap}$ rats show a reduction in protein level of the ~140 kDa full length protein with the presence of additional smaller molecular weight GAP-inactivated SynGAP proteins

Generation of *Syngap1*$^{+/-}$ LEH rats

The *Syngap1*$^{+/-}$ mutant animals were also designed by Prof Peter Kind and Dr Sally Till. Transgenic animals were generated using a single-guide RNA targeted to exon 8 of the *Syngap1* gene. This caused a 2 bp deletion and 1 bp insertion, resulting in the generation of a premature stop codon and loss of Syngap protein (Fig. 2.3).

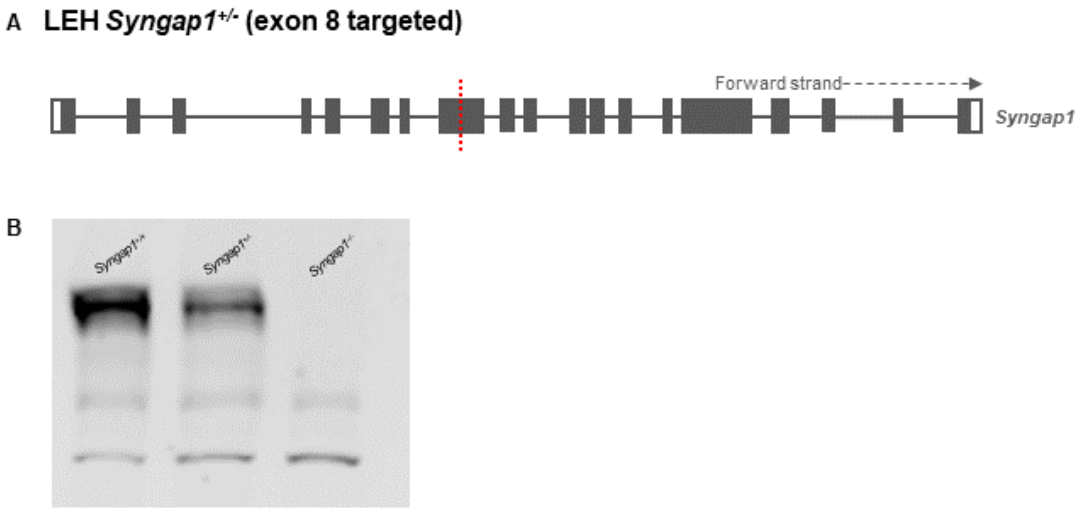

Figure 2.3: Generation of the custom *Syngap1*$^{+/-}$ rat model (A) Schematic of the *Syngap1* gene showing the deletion region in exon 8 that was targeted using CRISPR-Cas9 technology. (B) Western blot from P5 hippocampal lysates showing the ~140 kDa wildtype band in the *Syngap1*$^{+/+}$ animals, while the *Syngap1*$^{+/-}$ rats show a reduction in protein level of the ~140 kDa full length protein and the full length protein band is completely absent in *Syngap1*$^{-/-}$ rats.

Generation of *Nlgn3*$^{-/y}$ SD rats

The *Nlgn3*$^{-/y}$ knockout rats were generated by selective deletion of 58 bp of exon 5 of the *Nlgn3* gene resulting in a complete loss of Nlgn3 protein (Fig. 2.4).

Generation of *Nrx1*$^{+/-}$ SD rats

The *Nrx1*$^{+/-}$ mutant rats were generated by selective deletion of 16 bp of exon 1 of the *Nrx1* gene resulting in a premature stop codon and loss of Nrx1 protein (Fig. 2.5).

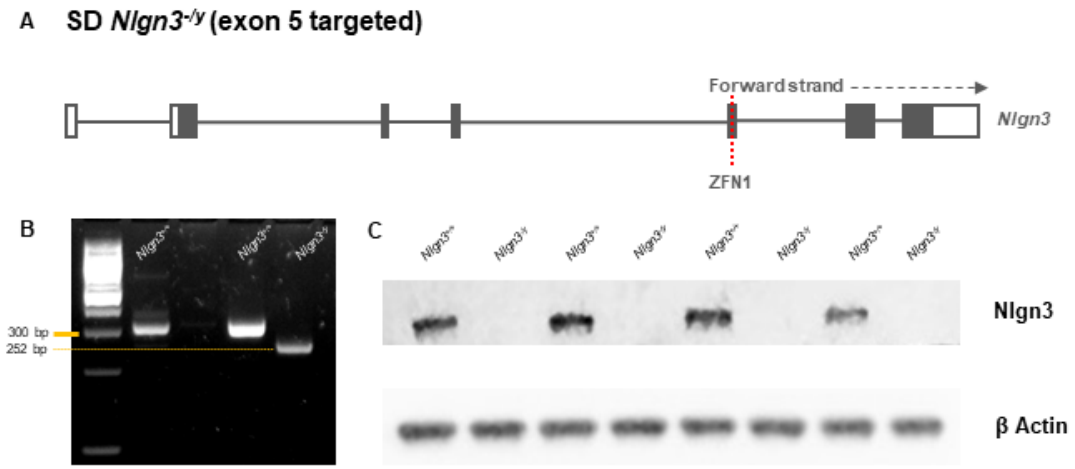

Figure 2.4: Generation of the *Nlgn3* rat model (A) Schematic of the *Nlgn3* gene showing the location of the ZFN site targeting exon 5 (B) Gel showing the results of the genotyping strategy used to differentiate between $Nlgn3^{-/y}$ and wildtype rats, wildtype rats showed a 300bp band while KO rats showed a 252bp band (C) Western blot showing the 110kDa wildtype band only in the $Nlgn3^{+/y}$ animals whereas $Nlgn3^{-/y}$ rats show no protein band when probed with the same antibody. Western blots performed by Aiman Kayenaat.

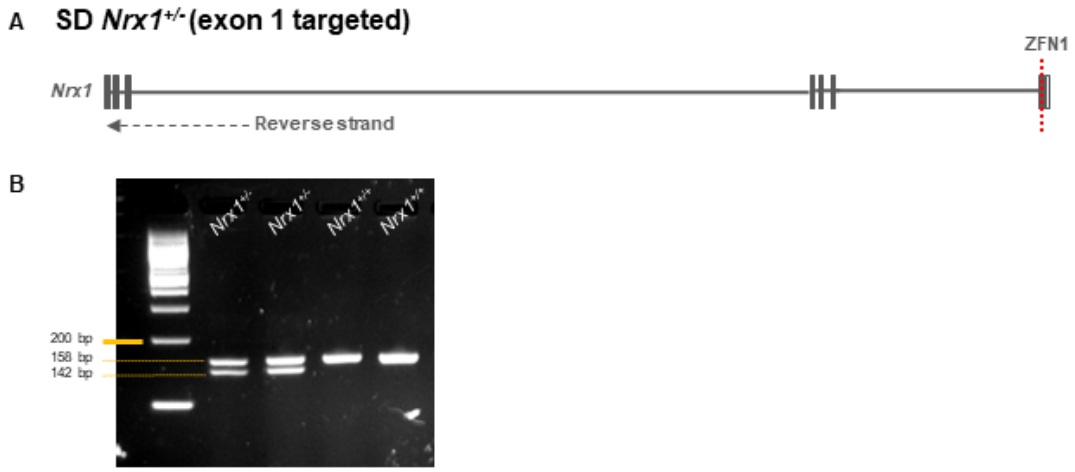

Figure 2.5: Generation of the *Nrx1* rat model (A) Schematic of the *Nrx1* reverse strand gene showing the location of the ZFN site targeting exon 1 (B) Gel showing the results of the genotyping strategy used to differentiate between $Nrx1^{+/-}$ and wildtype rats, wildtype rats showed a 158 bp band while heterozygous rats show the WT 158 bp band as well as the mutant 142 bp band.

Generation of *Cntnap2*$^{+/-}$ SD rats

The *Cntnap2*$^{+/-}$ mutant rats were generated by deletion of 5 bp of exon 6 of the *Cntnap2* gene resulting in a premature stop codon and loss of Cntnap2 protein (Fig. 2.6).

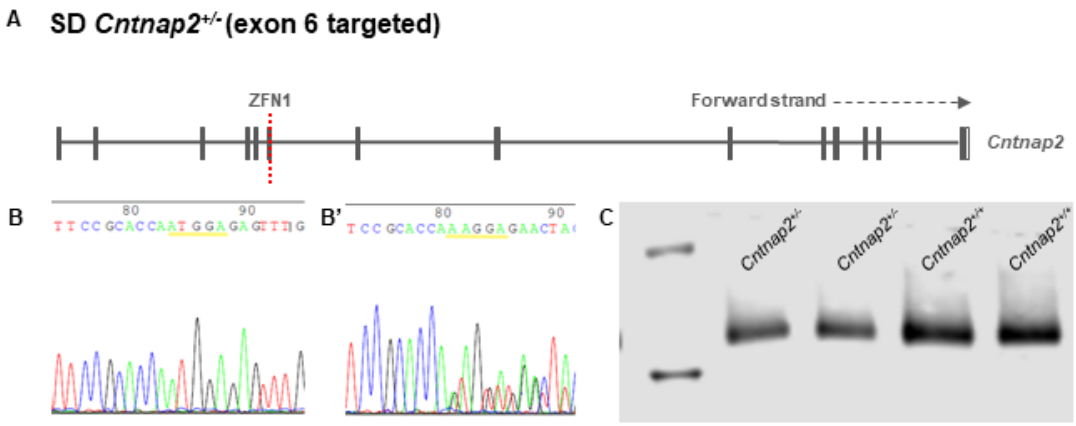

Figure 2.6: Generation of the *Cntnap2* rat model (A) Schematic of the open reading frame of the *Cntnap2* gene showing the ZFN site targeting exon 6. Sequencing chromatographs from wildtype (B) and *Cntnap2*$^{+/-}$ (B') rats with the yellow line showing the 5 bp ATGGA site targeted by the ZFN that is altered in the heterozygous animals (C) Western blot showing a reduction of Cntnap2/Caspr2 in the *Cntnap2*$^{+/-}$ animals but not in wildtype (*Cntnap2*$^{+/+}$) littermate controls.

Generation of *Pten*$^{+/-}$ SD rats

The *Pten*$^{+/-}$ mutants were generated by deletion of 7 bp of exon 7 of the *Pten* gene resulting in a premature stop codon and loss of Pten protein (Fig. 2.7).

2.1.3 Genotyping

2.1.4 DNA extraction

Tissue was collected at P14 in the form of ear notches for animal identification and genotyping. DNA was extracted using the Qiagen DNEasy Blood & Tissue kit (#69506) for DNA Isolation. Tissue was lysed in a mixture of extraction buffer ATL and proteinase K by incubating overnight at 56 °C. The lysis reaction was stopped by adding Buffer AL and 100% Ethanol. The

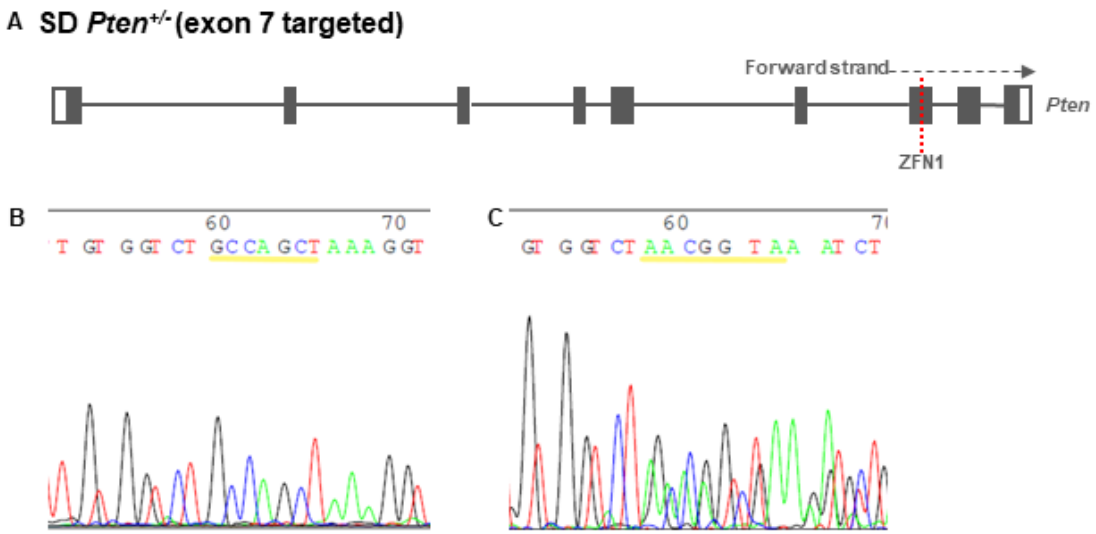

Figure 2.7: Generation of the *Pten* rat model (A) Schematic of the open reading frame of the *Pten* gene showing the ZFN site targeting exon 7. Sequencing chromatographs from wildtype (B) and $Pten^{+/-}$ (C) rats with the yellow line showing the 7 bp GCCAGCT site targeted by the ZFN that is altered in the heterozygous animals.

vortexed solution was then transferred to a spin-column and centrifuged at 6000 x *g* for 1 min to allow the DNA to bind to the spin-column membrane. The bound DNA was then washed with wash buffer AW1 by adding and centrifuging at 6000 x *g* for 1 min. The DNA membrane was then dried by adding buffer AW2 and centrifuging at 20,000 x *g* for 3 min. Finally, the DNA was eluted in 80-100 μl of double-distilled water (ddH_2O) at an approximate concentration of 1 μg/μl and stored at -20 °C till further use.

2.1.5 Polymerase chain reaction for *Syngap1*$^{+/\Delta gap}$, *Nlgn3*$^{-/y}$ and *Nrx1*$^{+/-}$

The genotype of each animal was confirmed using a PCR containing 6 μl of Thermofisher Scientific DreamTaq Green PCR Master Mix (#K1081), 1 μM forward primer, 1 μM reverse primer and 0.8-1 μg of purified DNA. PCR products were then run on a 4% agarose gel. A full list of primers and thermal cycling conditions are outlined below in Table 2.1 and Table 2.2.

Table 2.1: Primers for Genotyping

Animal Model	Primer Name	Sequence - 5'-3'
Pten	Cell f	AAGCAGTCAGTGTGAAGAATTTTG
	Cell r	AAGCAAAAGGGCTGTGGTTA
Cntnap2	Cell f	TTCCCACTACTCAGGAAGCAA
	Cell r	AAGAAGGAAGGAAAAGGGGC
Nrxn1	Sm del f1	GCAGCTCAGCTTCTCCATCT
	Sm del r1	ACTTGACCTCCACCCACTTG
Nlgn3	Cel-1 f	CATCCGAGACAGTGGTGCTA
	Cel-1 r	AGAAAGCCCTTGGTATTCGG
Syngap1$^{+/\Delta gap}$	Lg f1	GGCACCTTCCCCAAGTAAGT
	Cel1 r	TCACTTGGTGAGTGAGTGCC
Syngap1$^{+/-}$	Cel-1 f	GGGAGTGGTGGACGCTATTA
	Cel-1 r	GGGGTACCACTGCTCTGTGA
Fmr1	Gfpf1	ACGTAAACGGCCACAAGTTC
	Gfpr1 r	ATGCCGTTCTTCTGCTTGTC
	Celf1	CGAGGAAGGACGAGAAGATG
	Celr1	CCGCTTCCCTGACTGAAC

Table 2.2: Thermocycling conditions for *Syngap1*$^{+/\Delta gap}$, *Nlgn3*$^{-/y}$ and *Nrx1*$^{+/-}$ primers

Cycle Step	Temp (°C)	Time	
1	95	5 min	
2	95	30 s	x 35 cycles
3	60	30 s	
4	68	40 s	
5	68	5 min	

2.1.6 Genotyping for *Fmr1*$^{-/y}$, *Syngap1*$^{+/-}$, *Cntnap2*$^{+/-}$, and *Pten*$^{+/-}$ animals

Tissue samples from animals were sent directly to Transnetyx (Cordova, Tennessee, USA) for genotyping. Genomic DNA was extracted, genotyped and sequenced using proprietary methods. Primers used for genotyping are found in Table 2.1.

2.1.7 Western Blotting

Tissue preparation

Animals were overdosed with either Isoflurane or Haloethane, released as fumes from liquid stock, and killed by decapitation. Brains were collected using a spatula in pre-oxygenated ice-cold artificial cerebrospinal fluid (ACSF) (Table 2.3). 500 μM dorsal hippocampus slices were dissected using a Stoelting tissue chopper, snap frozen on dry ice and stored at -80 °C.

Tissue homogenisation

Each 500 μM slice was lysed in 150 μl Homogenisation buffer (Table 2.3) using a 200 μl pipette followed by vortexing. 30 *mu*l of the sample was reserved separately for the protein concentration assay. 50 μl of 4x Laemlli buffer (Sigma Aldrich) containing 10% β-mercaptoethanol was added to the remaining sample to break the disulphide bonds in the proteins and coat them in a negative charge to facilitate the Western blotting. Samples were then denatured by boiling at 85 °C for five minutes.

Protein concentration assay

The protein concentration of each sample was determined using a Pierce^{TM} BCA Protein Assay Kit (Thermo Fisher Scientific #23227). Initially, BSA standards were made using a 20 mg/ml BSA stock which was diluted with ddH2O to make a 2 mg/ml solution. This 2 mg/ml solution was serially diluted in ddH_2O to give a range of BSA standards from 2 mg/ml to 0.625 mg/ml. For the assay, 5 μl of either BSA standard or protein sample were added to a 96-well Nunc plate in triplicate. Next, the BCA working reagent was prepared by mixing Reagent A with Reagent B (50:1) and 200 μl was added to 10μl of each albumin standard and each diluted protein sample. The plate was incubated for 30 minutes at 37 °C and a FluoStar Optima plate reader (BMG Labtech) was used to read the plate at an absorbance of 570 nm. Protein concentrations for each sample were then calculated based on the BSA standard curve.

Running the Western blot

Prior to loading samples were boiled again for five minutes and briefly spun down. 5 μl of protein ladder (PageRulerPlus Prestained Protein Ladder, Thermo Scientific #26620) and 10 μg of each sample was loaded into a well of 12% Mini-PROTEAN TGX Precast Gels (Bio-Rad #4561045). The gels were run in running buffer (table 2.3) at a constant voltage of 100 V until the markers separated (approximately 15-20 min) and then at 200V until the dye front just ran off the bottoms of the gels (approximately 25-30 min).

Transfer steps

The samples were transferred to nitrocellulose membrane (Bio-Rad #1620112) in transfer buffer (table 2.3) at either 85 V for 2 hours at room temperature or 35 V overnight at 4 °C.

Antibody steps

The nitrocellulose membranes were briefly rinsed in ddH_2O and 0.1M Phosphate Buffer Saline (PBS) (table 2.3) before staining with Pierce Reversible Protein Stain Kit (Thermo Fisher Scientific, #24580) according to the manufacturer's instructions to visualise the protein bands and check the quality of the transfer. The blot was then cut at specific molecular weights (50, 75 or/and 100 kDA) so that multiple proteins could be probed for on the same membrane.

The blots were rinsed further for upto three times with 0.1 M PBS plus 0.1% Tween-20 (PBS-T) and blocked in 'blocking solution', a 1:1 mixture of Odyssey Blocking Buffer (Li-COR Biosciences #927-40000) and 0.1 M PBS-T (Thermo Fisher Scientific, #85113), for 1 hour at room temperature. Blocking solution was poured off and the blots were incubated overnight at 4°C in primary antibody diluted in 'blocking solution'.

The primary antibody was discarded and membranes were washed three times with PBS-T and incubated in the dark at room temperature in secondary antibody diluted in blocking solution (Table 4) for 60-90 minutes.

Table 2.3: Solutions for Western Blotting and Immunohistochemistry

Solutions	
ACSF	124 mM NaCl (Sigma Aldrich) 1.25 mM NaH_2PO_4 (Sigma Aldrich) 3 mM KCl (Sigma Aldrich) 26 mM $NaHCO_3$ (Sigma Aldrich) 10 mM Glucose (Sigma Aldrich) 2 mM $CaCl_2$ (Sigma Aldrich) 1 mM $MgCl_2$ (Sigma Aldrich)
Homogenisation Buffer	10 mM HEPES (Sigma Aldrich) 150 mM NaCl (Sigma Aldrich) 2 mM EDTA (Sigma Aldrich) 2 mM EGTA (Sigma Aldrich) Phosphatase Inhibitor Cocktail Sets II and III (Merck Millipore)
Running Buffer	25 mM Tris (Sigma Aldrich) 190 mM Glycine (Sigma Aldrich) 0.1% Sodium Dodecylsulphate (2BScientific Ltd)
Transfer Buffer	25 mM Tris (Sigma Aldrich) 190 mM Glycine (Sigma Aldrich) 20% Methanol (Fisher Scientific)
PBS	10mM Sodium Phosphate 2.60 mM KCl 140 mM NaCl
0.1M PB	75.4 mM NaH_2PO_4 (Sigma Aldrich) 24.6 mM Na_2HPO_4 (Sigma Aldrich)

Secondary antibody solution was poured off and the blots were washed 2 times in PBS-T and further rinsed in 0.1 M PBS. Membranes were imaged on an Odyssey infrared imaging system (Li-COR Bioscience) and bands were visualised on Image Studio Lite v5.0 (Li-COR Bioscience).

Table 2.4: Antibodies for Western Blotting

Primary Antibodies for Western Blotting			
Antibody Name (Supplier)	Catalogue Number	Animal	Dilution
Pan-Syngap (Abcam)	AB77235	Rabbit	1:2000
Cntnap2 (Merck Millipore)	AB5886	Rabbit	1:1000
Secondary Antibodies for Western Blotting			
IRDye 800CW H+L (Li-COR Biosciences)	926-32211	Goat anti-Rabbit	1:5000
IRDye 680RD H+L (Li-COR Biosciences)	926-68070	Goat anti-Mouse	1:5000

2.2 Immunohistochemistry

2.2.1 Tissue processing

Perfusions

Animals were sedated with approximately 2 ml of Haloethane/Isoflurane and terminal anaesthesia using either a Ketamine/Xylazine mixture or Sodium pentobarbital was administered via intraperitoneal (IP) injection (Ketamine 100-200 mg/kg; Xylazine 5-16 mg/kg; Sodium pentobarbital 27.5 g/kg body weight). Animals were then trans-cardially perfused with ice-cold PBS followed by 4% paraformaldehyde (PFA) in 0.1 M PB (table 2.3), pH 7.2-7.4 with volumes approximately equalling the blood volume of the animal. Brains were then removed with a spatula and post-fixed in 4% PFA for up to 2-3 hours at room temperature. If not immediately sectioned, brains were washed twice for 10 min in 0.1 M PBS and stored in 0.025% Na-Azide in PBS at 4 °C.

Vibratome sectioning

Brains were sectioned into 50 μm coronal sections using a vibratome (Leica VT 1200S). Sectioning was performed in 0.1 M PB and the vibratome was set at an amplitude of 1 mm with a sectioning speed of 0.2-0.3 mm/s. Areas of interest were identified using a rodent brain atlas (Paxinos and Watson (2007)) and sections were stored in 0.025% Na-Azide in PB at 4 °C

2.2.2 Immunofluorescent labelling

Sections were washed 3 times in 0.1 M PBS. Non-specific labelling was blocked with a solution containing 10% normal goat serum (NGS), 0.3% Triton-X to permeablise cells (Jamur and Oliver (2010)), 0.05% Sodium Azide for its bacteriostatic qualities, in PBS for 1hr at room temperature. Sections were then incubated in primary antibodies (table 2.5) in the above

solution, except NGS concentration was reduced to 5%, for 24-72 hours at 4 °C.

Sections were then washed 3 times in PBS and incubated in secondary antibodies (table 2.5) in solution containing 3% NGS, 0.1% Triton-X, 0.05% Sodium Azide in PBS for 3 hours at room temperature or overnight at 4°C. Sections were then washed twice in PBS and once in PB to prevent NaCl crystallisation and subsequently mounted in either Vectashield anti-fade hard-set mounting medium (Vector Labs #H-1400) or for sections containing retrobeads (see section 2.3.2) Fluoromount Aqueous Mounting Medium (Merck Millipore, #F4680).

Primary Antibodies for Immunofluorescence			
Antibody Name (Supplier)	Catalogue Number	Animal	Dilution
Ankyrin-G (Antibodies Incorporated)	75-146	Mouse	1:500
NeuN (Merk Millipore)	634301	Rabbit	1:500
Secondary Antibodies for Immunofluorescence			
Alexa Fluor 405 (Thermo Fisher Scientific)	A-31556	Goat anti-Rabbit	1:500
Alexa Fluor 488 (Thermo Fisher Scientific)	A-11001	Goat anti-Mouse	1:500
Alexa Fluor 568 (Thermo Fisher Scientific)	A-11011	Goat anti-Rabbit	1:500
Alexa Fluor 647 (Thermo Fisher Scientific)	A-21235	Goat anti-Mouse	1:500

Table 2.5: Antibodies for Immunofluorescence

2.3 Stereotaxic injections

Surgeries were performed by the author under the supervision of Dr Adam Jackson.

2.3.1 Anaesthesia and preparation

Prior to surgery, 8-10 week old rats were weighed, placed in a plexiglass chamber and anaesthetised using a mixture of air and isoflurane (5%, 0.4 l/min). When the breathing rate had slowed to approximately 1 Hz, rats were transferred to a stereotaxic frame (David Kopf, CA, US) where anaesthesia was continued through a mask (1.5–3.5%, 0.4 l/min). Rats were placed on a heat-mat to regulate body temperature. Anaesthesia level was constantly monitored throughout the experiment through observation of breathing rate and loss of toe pinch reflex. Ear bars were placed into the skull indentation on the inter-aural line to fix the head in place.

The fur on the head was shaved using an electric razor and the scalp was swabbed with iodine solution. Viscotears liquid gel (Bausch & Lomb) was added to the eyes to prevent drying and the following analgesics and anti-inflammatory drugs were injected subcutaneously: Veteregesic, buprenorphine, 0.1 mg/kg of body weight; Dexamethasone, 2 μg; Carpofen, 0.15 mg. An additional injection of 1 ml saline solution was administered subcutaneously to prevent dehydration. All surgical tools were washed and autoclaved prior to surgery. In the event of multiple surgeries on the same day, instruments were sterilised using a bead steriliser between surgeries. Injection pipettes were produced from boroscillate glass capillaries (Harvard apparatus, UK) using a vertical puller (P-1000 Flaming Brown, Sutter Instruments, US).

2.3.2 Stereotaxic surgery

A small incision was made along the medial axis of the scalp and the skull exposed by clamping the skin with forceps. The skull was cleaned to expose the lambda and bregma with any ruptured blood vessels cauterised. The skull and surrounding skin was kept hydrated using saline solution throughout the experiment. Bregma and lambda co-ordinates were established and the nose bar adjusted to ensure they were in the same horizontal plane. Sterotaxic co-ordinates for the injection site were adapted from the Paxinos and Watson (2007) atlas and identified relative to the Bregma. The skull was thinned using a microdrill, following which a small gauge needle was used to perforate the skull and remove it. Any ensuing blood flow was cleaned and stemmed before proceeding with the injections.

Red Retrobeads IX (Lumafluor) were diluted 1:4 in saline and infused into the mPFC (AP +3.00 mm, ML +0.6 mm, DV -2.0 mm) of the right hemisphere. Green Retrobeads IX (Lumafluor) were used undiluted and infused into the BLA (AP -3.3 mm, ML -5.0 mm, DV -8.1 mm) of the left hemisphere. All DV co-ordinates were measured relative to dura. Retrobeads were injected using a micromanipulator and a pipette with a 20 μm tip diameter (Nanoject, Drummond Scientific, PA) at a speed of 9.2 nl/min. After the infusion of 50nl, injection was stopped and the pipette left in place for a further 10 mins before removing it from the brain. The skull was sealed using bone wax and the scalp sutured (VICRYL, Ethicon) and treated with povidone-iodine solution.

Animals were single-housed post-surgery and allowed to recover for at least 7 days before perfusion.

2.4 Behaviour

Behaviour experiments of the *Syngap1*$^{+/\Delta gap}$ strain of animals were performed in conjunction with Dr. Sally Till. All other experiments were performed solely by the author.

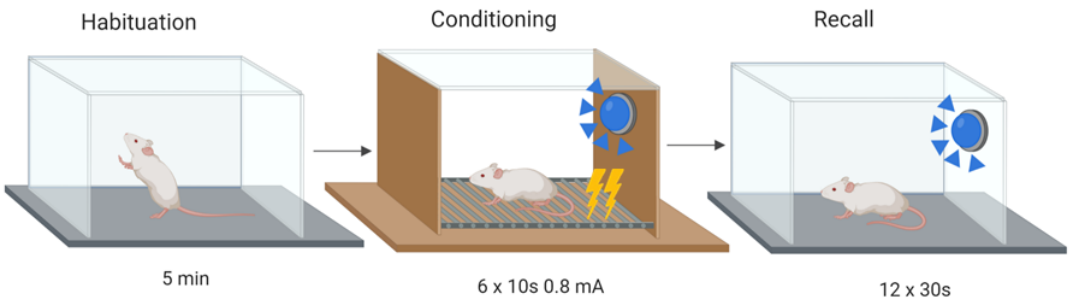

Figure 2.8: Fear Conditioning Paradigm Schematic showing the fear conditioning behavioural paradigm. Animals were habituated for 5 min on two non-consecutive days. Conditioning took place in a different box and 6 presentations of a 10 seconds neutral flashing blue light (CS) co-terminating with a 1s 0.8mA footshock (US). During Recall, animals were returned to the habituation chamber and presented with 12 iterations of the 30 seconds of the CS. This figure was made using the Biorender student package.

2.4.1 Handling and habituation

Behaviour was carried out on adult rats (P80-120) that were housed in groups of 2-4 rats per cage. All animals were handled and tails marked at least 3 days prior to the start of the experiment and in a separate holding room. Animals were then habituated for 5 min on non-consecutive days to the testing context in the experiment room. The recall context was a modified Colbourne box with black and white checked/striped place-mat curved to cover the clear back and a smooth plastic excrement tray that was cleaned/sprayed with 70% Ethanol.

2.4.2 Fear conditioning assay

After the two days of habituation, animals were subjected to a classical Pavlovian conditioning paradigm. Conditioning took place in a Colbourne box without any inserts and with an electrical grid that was cleaned with Distel (Tristel) disinfectant wipes. Animals were allowed to explore the box for 3 min before being presented with 6 iterations of a 10 second neutral flashing blue light, the conditioned stimulus (CS), that co-terminated with a 1s 0.8 mA non-harmful foot-shock, the unconditioned stimulus (US). The interval between the CSs were varied in length to avoid anticipatory freezing (CS on at 180, 360, 490, 770, 980, and 1280 seconds). Following conditioning, animals were immediately returned to their home-cage. Additionally, the first animal of every cage, counter-balanced for genotype, was a CS-only control that was presented with the flashing light without the presentation of the foot-shock.

2.4.3 Recall

24 hours following conditioning, the rats were put into the testing context, allowed to explore the context for 2 min and then given 12 presentations of the CS. Each CS 'light-on' presentation was 30 seconds and was interleaved with 30 seconds of 'light-off'. Approximately 2 hours after fear recall animals were terminated by perfusion fixation (see section 2.2.1).

2.4.4 Behavioural analysis

All analysis was done with experimenter being blind to genotype. The primary behaviour scored was 'freezing' defined as: *A complete suppression of spontaneous locomotor activity, and of all movements except those needed for respiration (S. Fanselow (1984)).* The animal had to show 2 seconds of complete immobility following a bout of movement before it was counted as 'freezing'. Behaviour was scored manually by the experimenter using a stop-watch and rounded down to the nearest second.

Freezing was then calculated as a % of time using the following equation:

$$\%Freezing = \frac{Time\ Frozen\ (sec)}{Total\ Time\ in\ Interval\ (sec)} \times 100 \tag{2.1}$$

Spearman's correlation analysis was performed for AIS recall and extinction exhibited per animal. These were calculated as follows:

$$\%Recall = Mean\ \%Freezing\ during\ the\ first\ 3\ CS\ presentations\ (CS1\text{-}3) \tag{2.2}$$

$$\%Extinction = Mean\ \%Freezing\ CS1\text{-}3 - Mean\ \%Freezing\ CS10\text{-}12 \tag{2.3}$$

Intervals for conditioning and re-call were as follows:

Conditioning Intervals	**Recall Intervals**
Pre 180s	Pre 120s
Inter-Conditioning Interval (ICI)	Trial 1-12 30s
ICI 1 170s	Inter-Trial interval
ICI 2 120s	(ITI) 1-11 30s
ICI 3 270s	
ICI 4 200s	
ICI 5 290s	

Table 2.6: Conditioning and Recall Intervals

2.5 Imaging

All image acquisition and analysis was done blinded to experiment conditions and genotype.

2.5.1 Confocal imaging

Immunolabelled slices were imaged using standard multi-channel confocal microscopy. Experiments performed in Bengaluru (for strains *Fmr1, Cntnap2, Nrx1, Nlgn3, Pten*) were imaged on an inverted Leica SP5 confocal microscope while those performed in Edinburgh (*Syngap1*) were imaged on an upright Zeiss LSM800 confocal microscope under oil immersion 60x/1.4 or 63x/1.4 objective. Z-stacks of 1 μm steps were taken through the 50μm section and 2 images per region per experimental animal were taken for the CA1, CA3, BA and LA. For the mPFC, tiles spanning the entire cortical column of the pre-limbic region were chosen. Typically 7 tiles per row and 2 rows were imaged from the midline to layer (L) 6/white matter. Similarly for the S1BF, the entire cortical column was imaged, ensuring that the images were within the whisker barrels. Barrels were identified using a lower magnification lens (20x) and tiles were taken from the cortical edge to L6. Akin to S1, the V1 images were tiled from cortical surface to L6. Cortical areas were identified using a standard adult rat brain atlas (Paxinos and Watson, 2006).

2.5.2 Image analysis

Images were analysed using FIJI (Image J) software. For cortical tiled images, L2/3, L4 and L5 were identified based on proximity to midline (mPFC) or slice surface (S1BF, V1), cell density and cell soma size. The latter was identified using a neuronal marker 'NeuN' that stains the perisoma. AISs were identified on the basis of Ankyrin-G (AnkG) staining and measured from their proximal to distal end (Fig 2.9). Approximately 70-100 AISs were traced per region, per animal for all the base-line measurements. This value was chosen arbitrarily to allow enough values for bootstrapping analysis. Bootstrapping analysis was performed by Dr. Owen Dando, and showed that for a statistically significant difference of approximately 3 μm or higher, a minimum of 25 AIS measurements were sufficient. In accordance with this, in animals with retro-bead injections at least 25 AISs were measured per region per animal while for those that underwent behaviour 50 AISs were traced through the z-stack per region per animal.

Exclusion criteria included AISs that were cuts off either at the top or bottom of the section,

continued off of the edge of the image or were occluded by blood vessels (Fig 2.9).

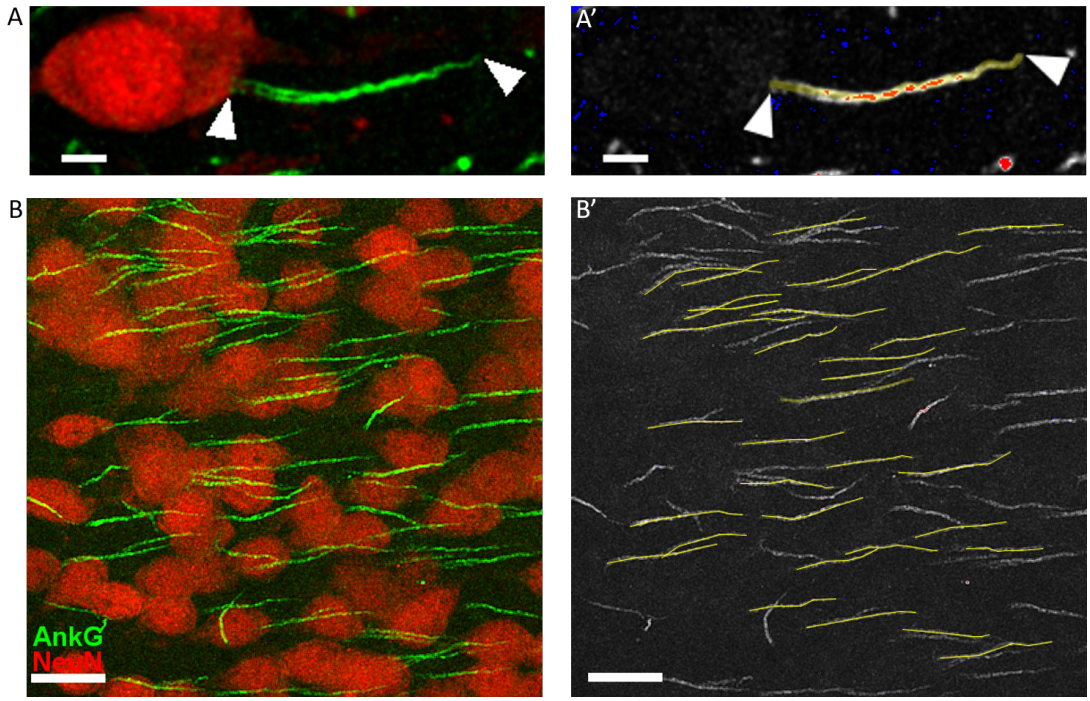

Figure 2.9: AIS Analysis Criteria (A) Representative image of a single AIS with arrows pointing to the proximal and distal ends (scale bar = 5 μm) (A') Yellow line shows a traced AIS (scale bar = 5 μm) (B) Representative image of the mPFC showing multiple AISs (scale bar = 20 μm) (B') Yellow lines showing traced AISs that met the selection criteria for measurement of representative figure B (scale bar = 20 μm).

2.6 Statistics

All the base-line AIS data was statistically analysed by Zrinko Kozic using a generalised linear mixed modelling (GLMM) approach. Briefly, using the 'R' package 'lme 4' differences in AIS length between genotypes and across brain regions were analysed per model. Further, using the R package 'car' for analysis of deviance, type III ANOVA with post-hoc correction for multiple comparisons (Tukey's) was used to identify statistically significant differences. Use of the GLMM approach allowed for higher statistical sensitivity, when compared to traditional non-parametric statistical tests, for evaluation of data trends and significance while simultaneously using animal number as the statistical metric 'n' thus avoiding pseudoreplication.

For behaviour, a Two-Way ANOVA with Bonferroni's correction for post-hoc multiple

comparisons was used. Comparison to measure statistical significance were differences between genotypes and condition (CS only VS CS+US) at each ICI during conditioning and at each trial and ITI during re-call.

Chapter 3

Characterisation of AIS lengths in juvenile rat models of *Syngap1* haploinsufficiency

3.1 Introduction

SYNGAP1 haploinsufficiency, causing a 50% reduction in levels of the protein SynGAP, is a leading cause of syndromic and non-syndromic intellectual disability (Hoischen et al., 2014). Clinically, *SYNGAP1*-ID is often accompanied by developmental and epileptic encephalopathies including generalised seizures, sensory hypersensitivities, such as hyperacusis and altered response to tactile-stimuli, and photosensitive epilepsy (Parker et al., 2015; Klitten et al., 2011; Carvill et al., 2013; Berryer et al., 2013). Pre-clinical murine models of *Syngap1* haploinsufficiency present with similar seizure and altered sensory processing phenotypes: Mice heterozygous for the *Syngap1* gene (*Syngap1*$^{+/-}$), consequently lacking 50% of the SynGAP protein, exhibit an average of 81 absence seizure-like epileptoform discharges per hour (Ozkan et al., 2014), increased incidence of audiogenic seizures and decreased threshold for fluorothyl induced tonic-clonic seizures (Clement et al., 2012). Abnormal sensory processing in the *Syngap1*$^{+/-}$ mice include reduced pre-pulse inhibition, exaggerated startle response to auditory stimuli and altered thigmotaxis (Guo et al., 2009).

These seizure and altered sensory processing phenotypes suggests an increase in network excitability. A long-standing model thought to drive this circuit hyperexcitability in ASD is a change in the excitation to inhibition ratio (E/I) in the cerebral cortex (Rubenstein and Merzenich, 2003). Evidence from pre-clinical models for the altered E/I ratio hypothesis in the field of ASD has been mixed with reports ranging from reduced inhibition (Wallace et al., 2012; Liang et al., 2015; Mao et al., 2015) to reduced excitation (Dani et al., 2005; Wood and Shepherd, 2010; Delattre et al., 2013) to increased inhibition (Tabuchi et al., 2007; Harrington et al., 2016). This altered circuit excitability is itself underscored by alterations in cellular excitability. In the *Syngap1*$^{+/-}$ mouse model of *SYNGAP1*-ID, alterations in cellular and network excitability appear to be brain-region and cell-type specific. For instance, neurons in the medial prefrontal cortex (mPFC), a brain region involved in higher cognitive function, attention and goal-directed behaviour (Ostlund and Balleine, 2005), and the dentate gyrus (DG), a hippocampal sub-region involved in formation of episodic memory (Kesner, 2007), of *Syngap1*$^{+/-}$ mice show increased activity in excitatory glutamatergic neurons (Clement et al., 2012; Ozkan et al., 2014). Similarly cells in layer (L) 4 of the somatosensory barrel cortex (S1BF), a primary sensory region, of *Syngap1*$^{+/-}$ mice were found to be hyperexcitable, due to reduced synaptic activity of GABAergic inhibitory neurons (Berryer et al., 2016). However, cells in L2/3 of the S1BF were found to be hypoexcitable in adult *Syngap1*$^{+/-}$ mice (Michaelson et al., 2018). While cellular hyperexcitability of the mPFC and DG are thought to underlie the seizure phenotypes observed in *Syngap1*$^{+/-}$ animals (Ozkan et al., 2014), hypoexcitability of S1BF L2/3 cells is thought to underlie their disrupted thigmotaxis (Michaelson et al., 2018).

Defined as a propensity of the neuron to generate, beyond a certain threshold, an action potential (AP) from a given input signal (usually an excitatory postsynaptic potential or EPSP), the excitability of a neuron is dependent on a number of intrinsic physiological features including the number and type of voltage-gated ion channels present at the dendrites, soma and axon initial segment (AIS) (Daoudal and Debanne, 2003). Mechanistically, the ion channels of the somatodendritic compartment serve to amplify (via persistent sodium current and T-type calcium channels) or attenuate (via A-type K^+ current and H-type cationic current) the amplitude of the incoming EPSP (Reyes, 2001) while those at the AIS are responsible for the initiation of the AP (Kole and Stuart, 2012). This input-output coupling is fundamental to the function of the neuron, and cells are known to alter AIS location, length and ion-channel density, influencing the threshold and frequency of AP generation, in response to physiological stimuli and

pathology (Kuba et al., 2006; Rasband, 2010; Kole and Stuart, 2012). Specifically in ASD/ID, altered AIS morphology has been noted in mouse models of Angelman's syndrome (Kaphzan et al., 2011) and Fragile-X syndrome (Booker et al., 2019). In both models, mutant mice exhibited longer AISs in the CA1 sub-region of the dorsal hippocampus compared to wild-type controls accompanied by reduced AP voltage threshold, reduced minimal current amplitude for AP generation (rheobase) and increased firing frequency.

Given the extensive excitability deficits reported across multiple brain-regions in mouse models of *SYNGAP1*-haploinsufficiency and reports of convergent synaptic pathophysiology between mouse models of Fragile-X syndrome (*Fmr1*$^{-/y}$) and *SYNGAP1*-ID (*Syngap1*$^{+/-}$) (Barnes et al., 2015), in this chapter I investigate the hypothesis that the convergence of cellular phenotypes would translate between the mouse and rat models and, similar to the *Fmr1*$^{-/y}$ mice, alterations in AIS length would be observed in rat models of *SYNGAP1*-ID. Additional support for this hypothesis comes from studies that show a reduction in levels of SynGAP accelerates spine maturation and increases dendritic spine length in L5 pyramidal cells of the S1BF Aceti et al. (2015), while increase in spine motility is noted in the DG (Clement et al., 2012). Spines are the first point of information input in the neuron, with the density and functionality of spines playing a critical role in shaping intrinsic cellular excitability and shaping the properties of the axon initial segment (Kole and Stuart, 2012; Wefelmeyer et al., 2016; Bolós et al., 2019). In order to address this hypothesis, I undertook a comprehensive characterisation of AIS lengths in periadolescent rats (P28-35) of *Syngap1* haploinsufficiency across neo-cortical and archicortical regions where excitability deficits have previously been observed in *Syngap1*$^{+/-}$ mice. Described below is a brief summary of the brain regions selected, their function and the excitability deficits observed upon reduction of SynGAP.

The first brain region inspected was the medial prefrontal cortex (mPFC). The mPFC is associated with a diverse range of cognitive and emotional function, exerting 'top-down' control on attentional processes, visceromotor activity, decision making, goal-directed behaviour, and working memory (Ostlund and Balleine, 2005). Anatomically the rat mPFC comprises of four divisions, the medial (frontal) agranular, anterior cingulate, prelimbic (PL), and infralimbic (IL) cortices, each of which is involved in distinct cognitive processes (Hoover and Vertes, 2007). Here, I focused on the pre-limbic (PL) division of the mPFC, a brain region implicated in working memory (Ragozzino et al., 1998; Floresco et al., 1997; Delatour and Gisquet-Verrier,

2000, 1999, 1997, 1996; Seamans et al., 1995; Brito and Brito, 1990) as increased cellular excitability has previously been reported in mPFC glutamatergic neurons (Ozkan et al., 2014) in *Syngap1*$^{+/-}$ mice, along with marked deficits in working memory tasks (Muhia et al., 2010).

Next, AIS lengths in two primary sensory cortices were measured which included the barrel fields of the somatosensory cortex (S1BF) and the visual cortex (V1). The primary somatosensory cortex in rodents is organised into somatotopic maps, wherein peripheral features such as facial whiskers (mystacial vibrissae) are isomorphically recapitulated onto the cortical surface (Belford and Killackey, 1979; Woolsey and Van der Loos, 1970). This recapitulation is driven by thalamocortical afferents (TCAs) and the faithful representation of the rodent whisker pad is termed the 'barrel field' such that each individual whisker is represented by its own neuronal cluster or 'barrel'. Normal development of the barrel fields starts with tangential TCA overlap in L4 followed by activity-dependent developmental events that involve axonal and dendritic elaboration and synaptic development culminating in barrel segregation (Rebsam et al., 2002). Microcircuitry within the barrels typically consists of information from the trigeminal nerve reaching L4 through the TCAs, which is then relayed to L2/3 and finally to L5/6, the main output layer of the barrel cortex (Chen-Bee et al., 2012; Petersen, 2007). In mouse models of *SYNGAP1*-ID, mice lacking SynGAP (*Syngap1*$^{-/-}$) failed to show barrel segregation whereas mice heterozygous for SynGAP (*Syngap1*$^{+/-}$) show partial segregation of the TCAs into barreloids in the thalamus and retarded segregation at L4 (Barnett et al., 2006). Additionally, in *Syngap1*$^{+/-}$ mice cells of S1BF L2/3 are hypoexcitable (Michaelson et al., 2018) while those in L4 are hyperexcitable (Berryer et al., 2016). The primary visual cortex (V1)is another sensory system that is shaped by experience-dependent synaptic modifications and shown to be affected in ASD (Frenkel and Bear, 2004). In a clinical setting, individuals with *SYNGAP1* encephalopathy are reported to have photosensitivity (Vlaskamp et al., 2019) while in a pre-clinical setting neurons in L2/3 of the primary visual cortex (V1) in *Syngap1*$^{+/-}$ mice show increased excitability during locomotion (Katsanevaki, 2017), making both the S1BF and the V1 important target brain regions to study in the context of modified AIS lengths.

Finally, two key brain-regions of the limbic system were chosen for AIS analysis; the dorsal hippocampus and the basolateral amygdala. The hippocampus is the seat for novel memory formation, particularly episodic memory and spatial cognition (for review see Hannula and Duff (2017)). In a 'typical' hippocampal circuit, external information from L2/3 of entorhinal

cortex (EC) is relayed to the CA3 and DG via the perforant pathway. The CA3 subsequently relays information onto CA1 and CA2 via the schaffer collaterals. Finally, the CA1 closes the circuit by projecting to L5 of the EC (Hannula and Duff, 2017). Plasticity of CA3-CA1 synapses have previously been shown to be disrupted in models of ASD, including *Fmr1*$^{-/y}$ and *Syngap1*$^{+/-}$ mice (Barnes et al., 2015). These disruptions in *Syngap1*$^{+/-}$ mice include attenuated LTP (Komiyama et al., 2002), attenuated NMDAR-LTD (Carlisle et al., 2008) and exaggerated mGluR-LTD (Barnes et al., 2015) in the CA1. While these are examples of deficits in plasticity, which typically arise from altered synaptic efficacy (Debanne, 2009), alterations in the AIS, which in-turn influence AP generation thresholds, may contribute to the altered plasticity. Accompanying the cellular deficits, *Syngap1*$^{+/-}$ mice show deficits in long-term spatial memory tasks (Komiyama et al., 2002; Muhia et al., 2010), further underscoring the importance of investigating AIS lengths in the dorsal CA1 and CA3.

Altered emotional state, including elevated anxiety and stress levels, is a common co-morbidity of *SYNGAP1* haploinsufficiency (Hamdan et al., 2009; Parker et al., 2015; Jeyabalan and Clement, 2016; Asadi, 2018). These behaviours indicate a dysfunction in the amygdala, a part of the limbic system that is involved in the acquisition, expression and storage of fear-related memories (Forster L. et al., 2012; Davis, 2006). The amygdala comprises of various nuclei, but the basolateral nucleus (BLA) is believed to play a key role in fear learning across various species (LeDoux et al., 1990). The BLA comprises of the lateral amygdala (LA), which receives sensory afferents from the thalamus and cortex and plays a key role in fear acquisition (Romanski and LeDoux, 1992). The basal amygdala (BA) is involved in memory storage and fear expression and projects to other cortical and sub-cortical components of the fear circuit including the ventral CA1, mPFC and central amygdala (Gale et al., 2004; Anglada-Figueroa and Quirk, 2005). In rodents, fear memory is classically studied using fear conditioning paradigms (Marchand et al., 2003). While no direct evidence of altered amygdala function has been reported in the *Syngap1*$^{+/-}$ mice, these mice do show reduced levels of anxiety in contextual fear conditioning paradigms (Clement et al., 2012). This evidence in conjunction with the patient co-morbidities makes the BLA an interesting target to study in the context of altered cellular excitability and modified AIS lengths.

The AIS length analysis was performed across two distinct rat models of *Syngap1* haploinsufficiency, one mutant specifically lacking 50% of the GAP domain (*Syngap1*$^{+/\Delta Gap}$) and the

other lacking 50% of the full length protein (*Syngap1*$^{+/-}$) in order to delineate the contribution of the GAP domain to any observed phenotypes.

3.2 Results

3.2.1 mPFC L2/3 and L5

Within the PL, AIS lengths of neurons from both L2/3 and L5 were analysed as it has previously been shown that neurons from the different layers have distinct electrophysiological properties (Song and Moyer, 2018), arguing that they may have distinct alterations in AIS length. No difference in average AIS length or cumulative distribution of AIS lengths was observed in neurons of either L2/3 (fig. 3.1 F *Syngap1*$^{+/+}$= 28.75 μm $\pm$ 0.85 μm n=11, *Syngap1*$^{+/\Delta gap}$= 28.31 μm $\pm$ 0.81 μm n=8, *Syngap1*$^{+/-}$= 28.73 μm $\pm$ 0.69 μm n=11 animals) or L5 of the mPFC PL between animals of either genotype compared to wildtype littermate controls (fig.3.1 K; *Syngap1*$^{+/+}$= 28.99 μm $\pm$ 0.55 μm n=11, *Syngap1*$^{+/\Delta gap}$= 29.19 μm $\pm$ 0.67 μm n=8, *Syngap1*$^{+/-}$= 28.73 μm $\pm$ 0.79 μm n=11 animals).

3.2.2 S1BF L2/3, L4 and L5

As both AIS length and S1BF show experience/activity-dependent alterations, and *Syngap1*$^{-/-}$ and *Syngap1*$^{+/-}$ mice show abnormal barrel segregation as well as altered cellular excitability, I looked for alterations to baseline AIS lengths across L2/3, L4 and L5 in *Syngap1*$^{+/\Delta Gap}$ and *Syngap1*$^{+/-}$ rats compared to controls. I found no change in average AIS length or cumulative distribution of AIS lengths across all layers examined in either model compared to age-matched, littermate control (fig.3.2; L2/3 (F) *Syngap1*$^{+/+}$= 27.48 μm $\pm$ 0.76 μm n=13, *Syngap1*$^{+/\Delta Gap}$= 25.98 μm $\pm$ 0.51 μm n=9, *Syngap1*$^{+/-}$= 27.12 μm $\pm$ 0.58 μm n=12; L4 (K) *Syngap1*$^{+/+}$= 21.31 μm $\pm$ 0.42 μm n=13, *Syngap1*$^{+/\Delta Gap}$= 21.29 μm $\pm$ 0.59 μm n=9, *Syngap1*$^{+/-}$= 20.62 μm $\pm$ 0.51 μm n=12; L5 (P) *Syngap1*$^{+/+}$= 27.56 μm $\pm$ 0.74 μmn=13, *Syngap1*$^{+/\Delta Gap}$= 27.94 μm $\pm$ 0.53 μm n=9, *Syngap1*$^{+/-}$= 28.01 μm $\pm$ 0.36 μm n=12 animals).

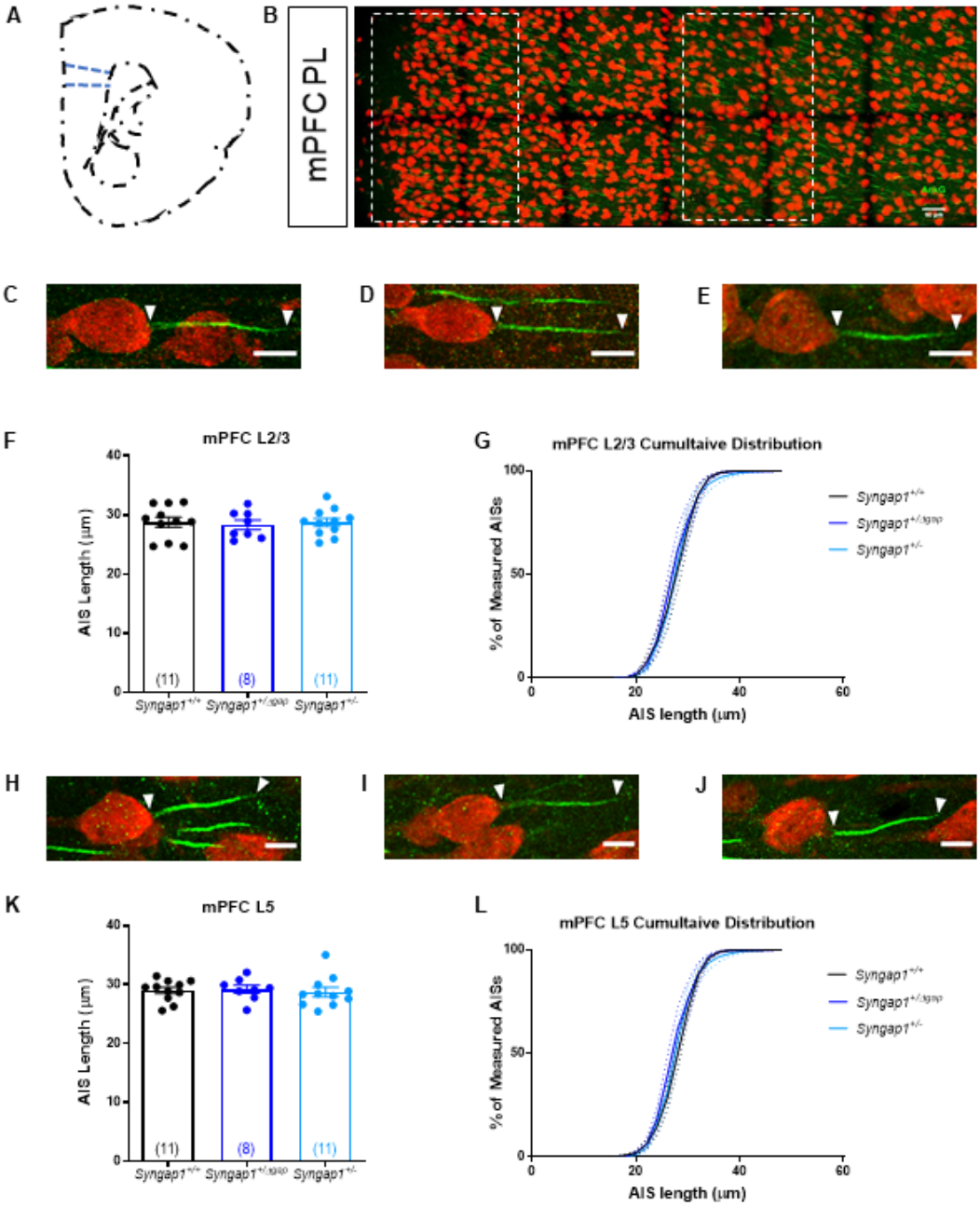

Figure 3.1: AIS lengths are unchanged in L2/3 and L5 of the mPFC in P28-35 *Syngap1*$^{+/\Delta Gap}$ and *Syngap1*$^{+/-}$ rats (A) Schematic of a coronal section of the mPFC. Blue lines highlight the region of the PL imaged. (B) Representative image of the cortical stack acquired for analysis. Cell bodies visualised using NeuN (red) and AIS using AnkG (green). White boxes demarcate the regions selected for analysis of L2/3 (left) and L5 (right). Representative single AISs with arrows representing the proximal and distal ends from L2/3 and L5 of *Syngap1*$^{+/+}$ (C, H), *Syngap1*$^{+/\Delta Gap}$ (D, I) and *Syngap1*$^{+/-}$ (E, J) rats. Scale bar=10 μm. (F, G) No change in average AIS length (*Syngap1*$^{+/+}$= 28.75 $\pm$ 0.85 μm n=11, *Syngap1*$^{+/\Delta Gap}$= 28.31 $\pm$ 0.81 μm n=8, *Syngap1*$^{+/-}$= 28.73 $\pm$ 0.69 μm n=11 animals) or cumulative distribution of AIS lengths was observed in mPFC L2/3 between genotypes. (K, L) No change in average AIS length (*Syngap1*$^{+/+}$= 28.99 $\pm$ 0.55 μm n=11, *Syngap1*$^{+/\Delta Gap}$= 29.19 $\pm$ 0.67 μm n=8, *Syngap1*$^{+/-}$= 28.73 $\pm$ 0.79 μm n=11 animals) or cumulative distribution of AIS lengths in mPFC L5 was observed between genotypes.

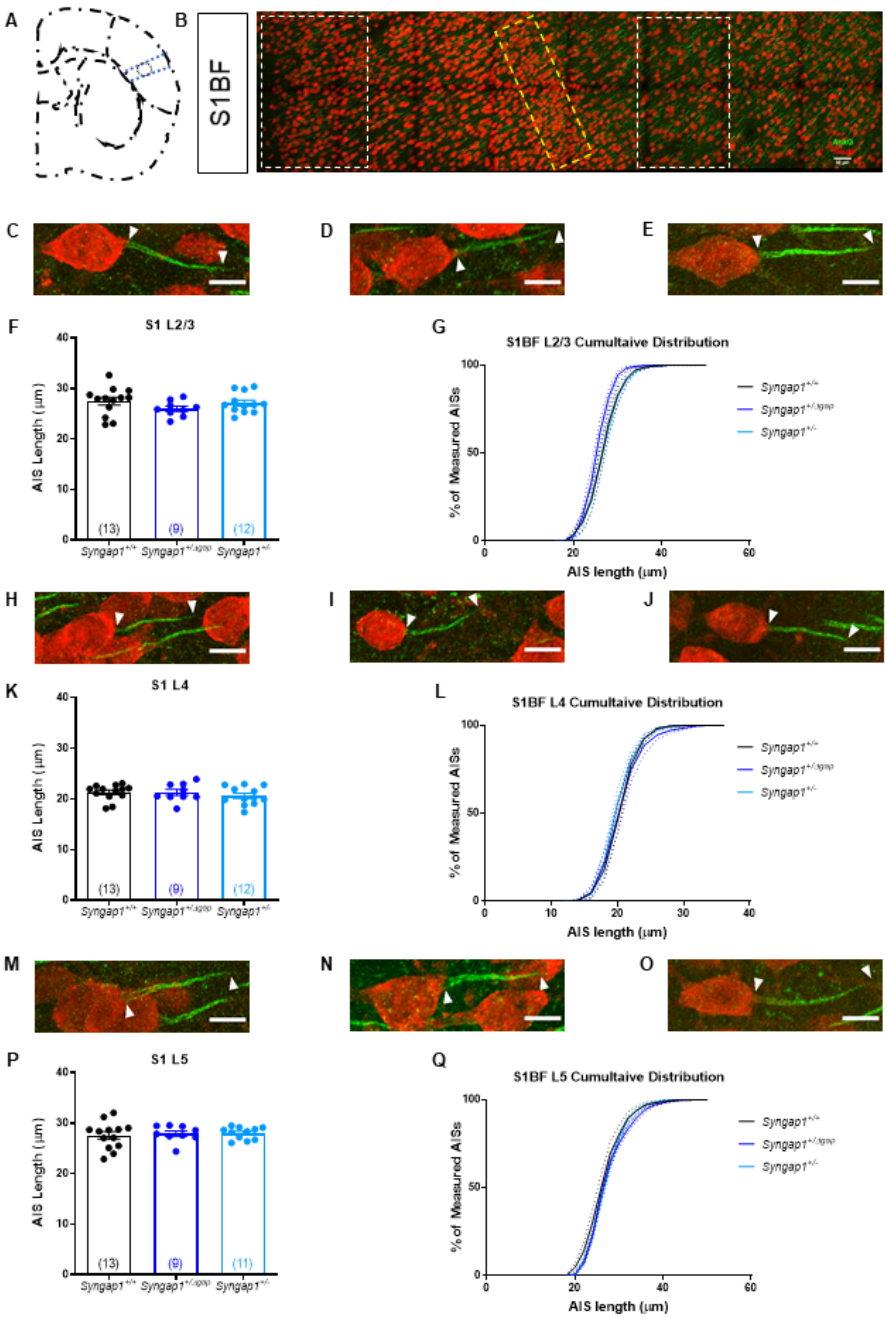

Figure 3.2: AIS lengths are unchanged in L2/3, L4 and L5 of the S1 in P28 *Syngap1*$^{+/\Delta Gap}$ and *Syngap1*$^{+/-}$ rats
(A) Schematic of S1BF. Blue lines highlight the imaged region. (B) Representative image of the cortical stack with boxes demarcating regions selected for analysis of L2/3 (left), L4 (middle) and L5 (right). Representative single AISs with arrows representing the proximal and distal ends from L2/3 (C-E), L4 (H-J) and L5 (M-O) of *Syngap1*$^{+/+}$ (C, H, M), *Syngap1*$^{+/\Delta Gap}$ (D, I, N) and *Syngap1*$^{+/-}$ (E, J, O) rats. Scale bar=10 μm. No change in average AIS length was observed in S1 L2/3 (F; *Syngap1*$^{+/+}$= 27.48 $\pm$ 0.76 μm n=13, *Syngap1*$^{+/\Delta Gap}$= 25.98 $\pm$ 0.51 μm n=9, *Syngap1*$^{+/-}$= 27.12 $\pm$ 0.58 μm n=12 animals), L4 (K; *Syngap1*$^{+/+}$= 21.31 $\pm$ 0.42 μm n=13, *Syngap1*$^{+/\Delta Gap}$= 21.29 $\pm$ 0.59 μm n=9, *Syngap1*$^{+/-}$= 20.62 $\pm$ 0.51 n=12 μm animals) or L5 (P; *Syngap1*$^{+/+}$= 27.56 $\pm$ 0.74 μm n=13, *Syngap1*$^{+/\Delta Gap}$= 27.94 $\pm$ 0.53 μm n=9, *Syngap1*$^{+/-}$= 28.01 $\pm$ 0.36 μm n=12 animals). Cumulative distribution of AIS lengths was unchanged in L2/3 (G), L4 (L) and L5 (Q) between genotypes.

3.2.3 V1 L2/3 and L5

Given the evidence of altered cellular excitability in V1 L2/3 neurons by Katsanevaki (2017) I reviewed the AIS lengths in L2/3 as well as L5 of the rat V1. No change in average AIS length or cumulative distribution of AIS lengths was found in *Syngap1*$^{+/\Delta Gap}$ and *Syngap1*$^{+/-}$ rats in either layer compared to controls (fig. 3.3; L2/3 (F) *Syngap1*$^{+/+}$= 25.59 μm $\pm$ 0.75 μm n=12, *Syngap1*$^{+/\Delta Gap}$= 24.97 μm $\pm$ 0.94 μm n=9, *Syngap1*$^{+/-}$= 26.42 μm $\pm$ 0.63 μm n=11; L5 (K) *Syngap1*$^{+/+}$= 27.38 μm $\pm$ 0.60 μm n=12, *Syngap1*$^{+/\Delta Gap}$= 26.63 μm $\pm$ 0.71 μm n=9, *Syngap1*$^{+/-}$= 26.63 μm $\pm$ 0.71 μm n=9 animals).

3.2.4 Dorsal Hippocampus CA1 and CA3

AIS lengths were measured in both the CA1 and CA3 sub-regions of the dorsal hippocampus but no alterations in average length or distribution of lengths were found in either region of *Syngap1*$^{+/\Delta Gap}$ and *Syngap1*$^{+/-}$ rats compared to controls (fig.3.4; CA1 (F) *Syngap1*$^{+/+}$= 31.72 μm $\pm$ 0.89 μm n=13, *Syngap1*$^{+/\Delta Gap}$= 33.09 μm $\pm$ 0.84 μm n=8, *Syngap1*$^{+/-}$= 31.45 μm $\pm$ 1.04 μm n=11; CA3 (M) *Syngap1*$^{+/+}$= 44.77 μm $\pm$ 2.01 μm n=13, *Syngap1*$^{+/\Delta Gap}$= 45.6 μm2 $\pm$ 1.99 μm n=8, *Syngap1*$^{+/-}$= 43.82 μm $\pm$ 2.17 μm n=9 animals).

3.2.5 Basolateral Amygdala

Finally, I analysed the average and cumulative distribution of AIS lengths in both the LA and the BA but found no changes in either parameter in *Syngap1*$^{+/\Delta Gap}$ and *Syngap1*$^{+/-}$ rats compared to controls (Fig 3.5; LA (G) *Syngap1*$^{+/+}$= 24.43 μm $\pm$ 1.06 μm n=8, *Syngap1*$^{+/\Delta Gap}$= 25.45 μm $\pm$ 0.82 μm n=7, *Syngap1*$^{+/-}$= 23.71 μm $\pm$ 0.96 μm n=6; BA (O) *Syngap1*$^{+/+}$= 33.21 μm $\pm$ 1.84 n=8, *Syngap1*$^{+/\Delta Gap}$= 32.83 μm $\pm$ 1.69 μm n=7, *Syngap1*$^{+/-}$= 30.94 μm $\pm$ 2.26 μm n=7 animals).

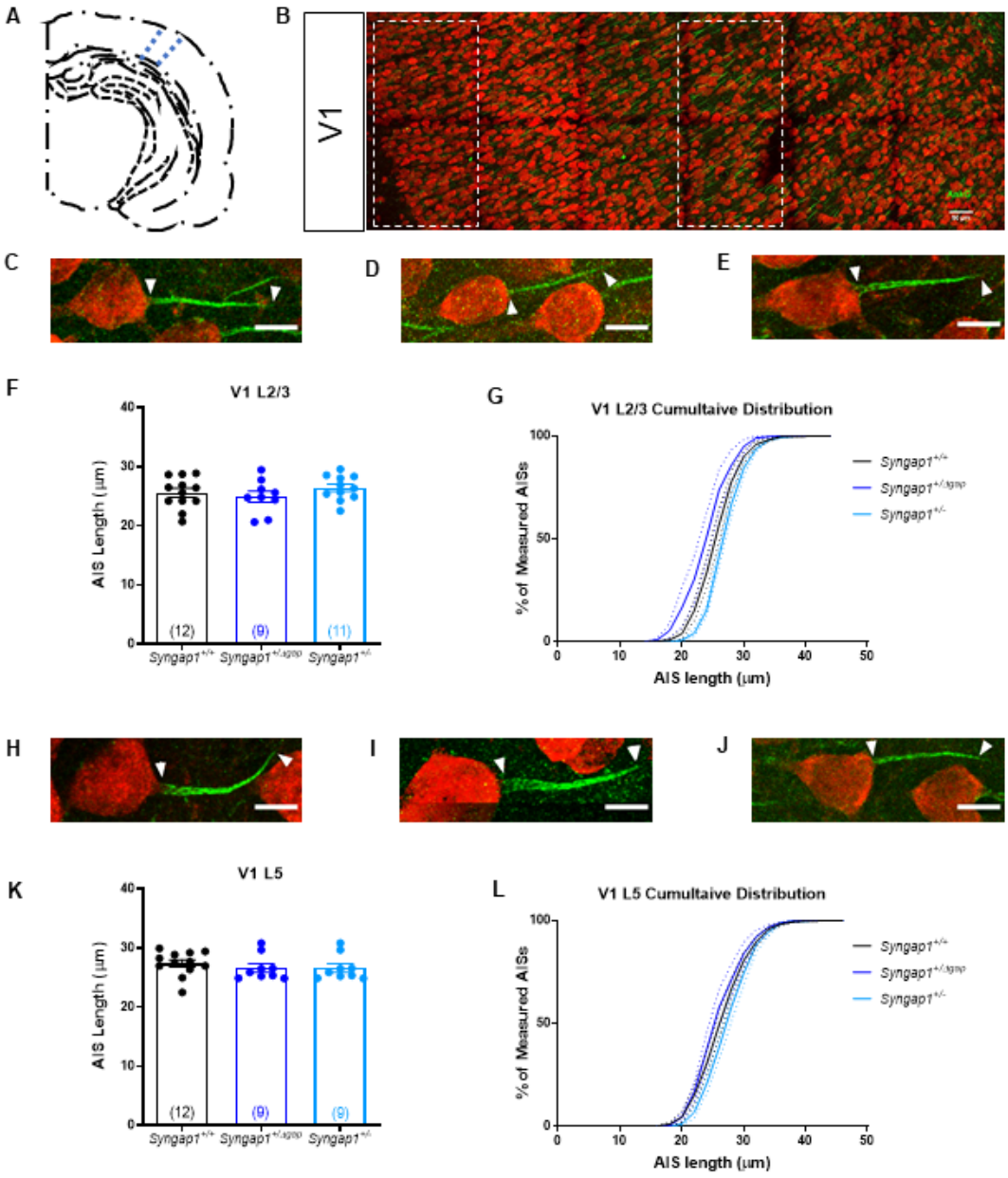

Figure 3.3: AIS lengths are unchanged in L2/3 and L5 of the V1 in P28 *Syngap1*$^{+/\Delta Gap}$ and *Syngap1*$^{+/-}$ rats (A) Schematic of V1. Blue lines highlight the imaged region. (B) Representative image of the cortical stack with boxes demarcating regions selected for analysis of L2/3 (left) and L5 (right). Representative single AISs with arrows representing the proximal and distal ends from L2/3 (C-E) and L5 (H-J) of *Syngap1*$^{+/+}$ (C, H), *Syngap1*$^{+/\Delta Gap}$ (D, I) and *Syngap1*$^{+/-}$ (E, J) rats. Scale bar=10 μm. No change in average AIS length was observed in V1 L2/3 (F; *Syngap1*$^{+/+}$= 25.59 $\pm$ 0.75 μm n=12, *Syngap1*$^{+/\Delta Gap}$= 24.97 $\pm$ 0.94 μm n=9, *Syngap1*$^{+/-}$= 26.42 $\pm$ 0.63 μm n=11 animals) or L5 (K; *Syngap1*$^{+/+}$= 27.38 $\pm$ 0.60 μm n=12, *Syngap1*$^{+/\Delta Gap}$= 26.63 $\pm$ 0.71 μm n=9, *Syngap1*$^{+/-}$= 26.63 $\pm$ 0.71 μm n=9 animals). Cumulative distribution of AIS lengths was unchanged between genotypes in L2/3 (G) and L5 (L).

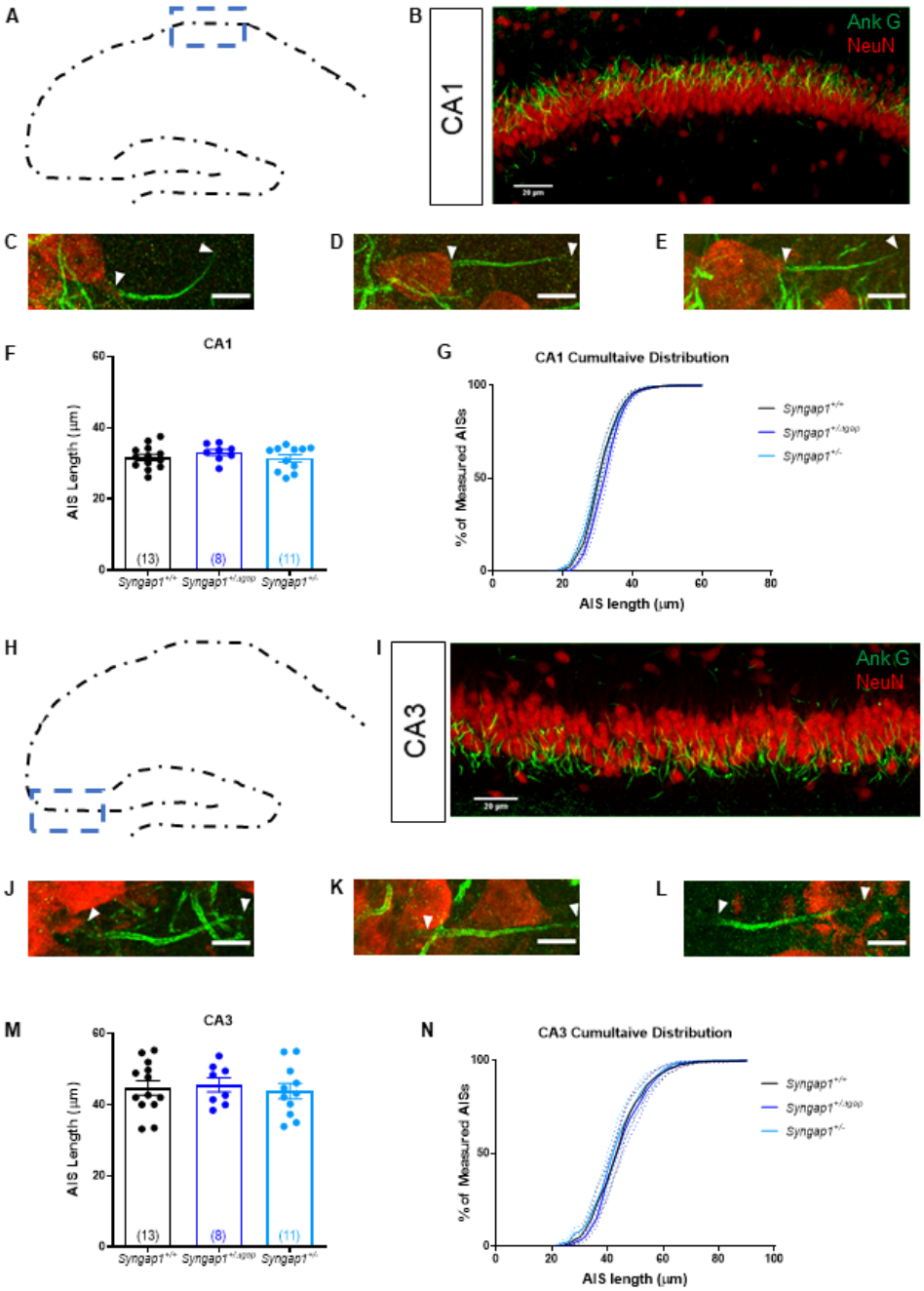

Figure 3.4: AIS lengths are unchanged in the CA1 and CA3 of P28 *Syngap1*$^{+/\Delta Gap}$ and *Syngap1*$^{+/-}$ rats Schematic of CA1 (A) and CA3 (H). Blue boxes highlight the imaged region. Representative low magnification image of CA1 (B) and CA3 (I). Representative single AISs with arrows representing the proximal and distal ends from CA1 (C-E) and CA3 (J-L) of *Syngap1*$^{+/+}$ (C, J), *Syngap1*$^{+/\Delta Gap}$ (D, K) and *Syngap1*$^{+/-}$ (E, L) rats. Scale bar=10 μm. No change in average AIS length was observed in CA1 (F; *Syngap1*$^{+/+}$= 31.72 $\pm$ 0.89 μm n=13, *Syngap1*$^{+/\Delta Gap}$= 33.09 $\pm$ 0.84 μm n=8, *Syngap1*$^{+/-}$= 31.45 $\pm$ 1.04 μm n=11 animals) or CA3 (M; *Syngap1*$^{+/+}$= 44.77 $\pm$ 2.01 μm n=13, *Syngap1*$^{+/\Delta Gap}$= 45.62 $\pm$ 1.99 μm n=8, *Syngap1*$^{+/-}$= 43.82 $\pm$ 2.17 μm n=9 animals). Cumulative distribution of AIS lengths was unchanged across genotypes in CA1 (G) and CA3 (N).

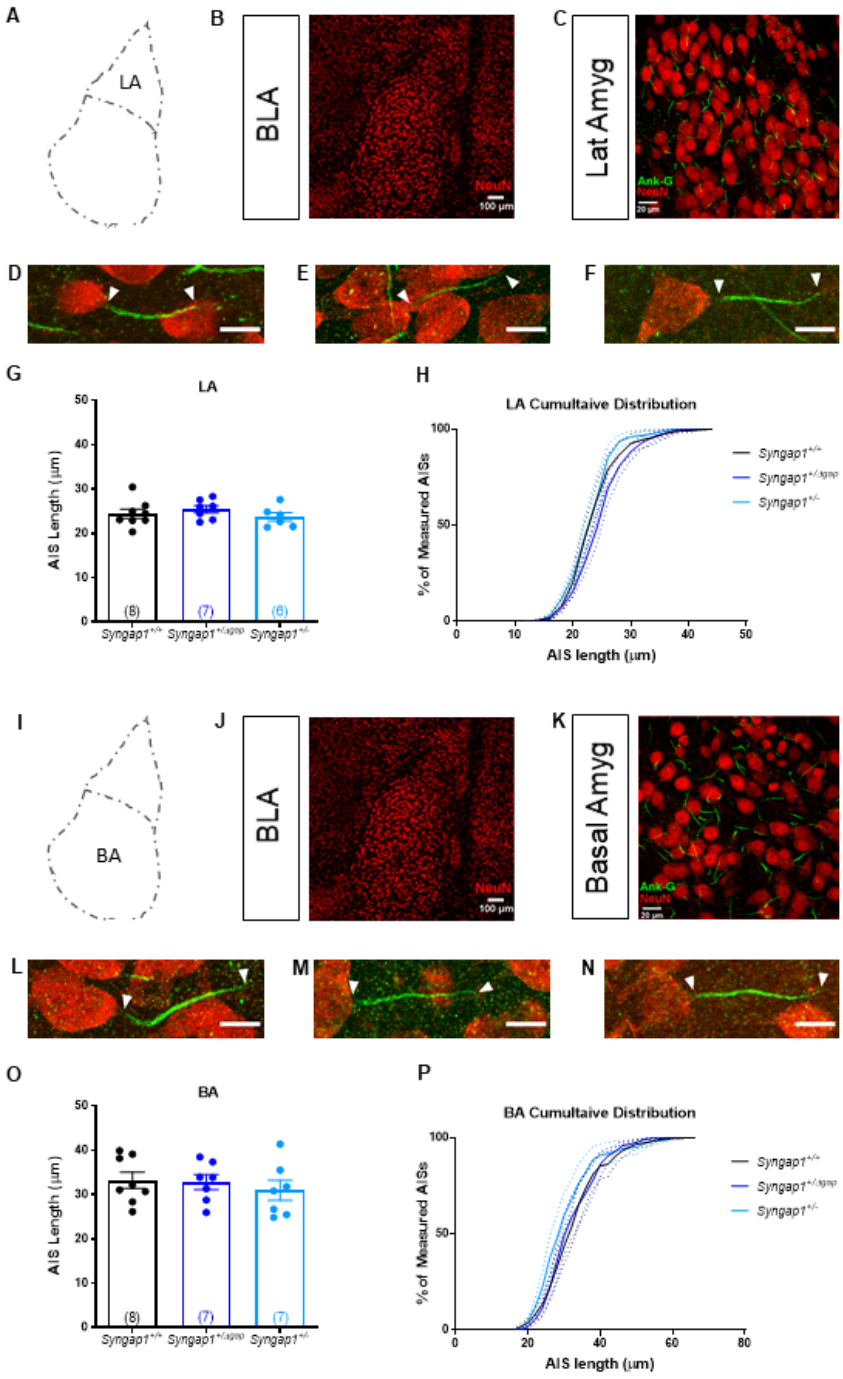

Figure 3.5: AIS lengths are unchanged in the BA and LA of P28 *Syngap1*$^{+/\Delta Gap}$ and *Syngap1*$^{+/-}$ rats Schematic of LA (A) and BA (I). Representative low magnification (B, J) and high magnification (C, K) of the BLA nucleus. Representative single AISs with arrows representing the proximal and distal ends from LA (D-F) and BA (L-N) of *Syngap1*$^{+/+}$ (D, L), *Syngap1*$^{+/\Delta Gap}$ (E, M) and *Syngap1*$^{+/-}$ (F, N) rats. Scale bar=10 μm. No change in average AIS length was observed in the LA (G; *Syngap1*$^{+/+}$= 24.43 $\pm$ 1.06 μm n=8, *Syngap1*$^{+/\Delta Gap}$= 25.45 $\pm$ 0.82 μm n=7, *Syngap1*$^{+/-}$= 23.71 $\pm$ 0.96 μm n=6 animals) or BA (O; *Syngap1*$^{+/+}$= 33.21 $\pm$ 1.84 μm n=8, *Syngap1*$^{+/\Delta Gap}$= 32.83 $\pm$ 1.69 μm n=7, *Syngap1*$^{+/-}$= 30.94 $\pm$ 2.26 μm n=7 animals). Cumulative distribution of AIS lengths was unchanged between genotypes in the LA (H) and BA (P).

3.3 Discussion

The body of work in this chapter presents the first comprehensive analysis of AIS lengths across multiple brain regions in a rat model of ASD/ID. However, in all the brain regions analysed no genotype specific differences in AIS length were observed. Specifically, I have looked at two complementary models of *SYNGAP1* haploinsufficiency that were jointly designed by Professor Peter Kind and Dr. Sally Till. The *Syngap*$^{+/-}$ rats carry a point mutation in exon 8 and share construct validity with protein-truncating nonsense and frameshift mutations observed in clinical presentations of *SYNGAP1*-ID, and similar to the *Syngap*$^{+/-}$ mice, lack 50% of the full-length protein (fig.2.3). In addition to protein truncating mutations, seven pathogenic *de novo* missense mutations have been identified in the *SYNGAP1* gene, including 3 in the catalytic GAP domain and 2 in the C2 domain (Berryer et al., 2013; O'Roak et al., 2014; Parker et al., 2015; Mignot et al., 2016). Introduction of two of these *de novo* missense mutations (p.W362R in C2 domain, p.P562L in GAP domain) in cortical organotypic cultures resulted in the presence of multiple enzymatically inactive proteins in addition to the wildtype (~140 kDa) protein. Enzymatic ability was measured by the extent of inhibition to ERK activation in transfected cultures (Berryer et al., 2013). Thus, the *Syngap1*$^{+/\Delta Gap}$ rats were designed with a heterozygous deletion of the C2 and catalytic GAP domain of the protein. In hippocampal homogenates from these rats, similar to the transfected organotypic cortical cultures and in contrast to *Syngap*$^{+/-}$ mice and rats, there is a reduction of the full-length (~140 kDa) protein coupled with the presence of additional, enzymatically inactive, bands of lower molecular weight (fig.2.2), a phenomenon not observed in wildtype age-matched and littermate (*Syngap1*$^{+/+}$) controls. Therefore using both *Syngap*$^{+/-}$ and *Syngap1*$^{+/\Delta Gap}$ rat models offers a unique insight into the phenotypic spectrum associated with domain-specific mutations in *SYNGAP1*-linked ID.

Due to protein localisation at the PSD (Chen et al., 1998; Kim et al., 1998) and its role in regulating AMPA-receptor trafficking (Komiyama et al., 2002; Clement et al., 2012), neuronal excitability alterations in mouse models of *Syngap1s* haploinsufficiency have traditionally been attributed to alterations in synaptic properties and plasticity. Conventionally, SynGAP's control of synaptic plasticity is mediated through its GTP-ase (GAP domain dependent) activity on Ras and Rap with subsequent downregulation of ERK1/2 and p38MAPK signalling pathways (Kim et al., 2003; Krapivinsky et al., 2004; Rumbaugh et al., 2006; Carlisle et al., 2008).

An additional mechanism of SynGAP's control of synaptic plasticity proposed that SynGAP regulates PSD composition, including expression of surface AMPARs, in a GAP-independent mechanism through its C-terminal PDZ binding domain (Walkup et al., 2016). Thus the use of both *Syngap1*$^{+/\Delta Gap}$ and *Syngap*$^{+/-}$ rats renders the additional advantage of a direct comparison of cellular and behavioural deficits elicited by the loss of the enzymatic GAP domain compared to loss of the full length protein.

The conception of this project was based on two key pieces of evidence: First, an increase in AIS length was observed in pyramidal cells of the *stratum radiatum* in the CA1 of a mouse models of Angelman's syndrome (Kaphzan et al., 2011) and Fragile-X syndrome (FXS) (Booker et al., 2019). Subsequently, in the *Fmr1*$^{-/y}$ mice, this increase was shown to underlie the hyperexcitability observed in these cells (Booker et al., 2019). Second, a previous publication showed convergent cellular and molecular deficits between mouse models of FXS and *SYNGAP1* haploinsufficiency (Barnes et al., 2015) with cellular deficits observed in the FXS mouse model persisting in a rat model of FXS Till et al. (2015). Given the extensive alterations in cellular excitability observed across multiple brain regions in the*Syngap1*$^{+/-}$ mice, I tested the hypothesis that these deficits would translate to the rat models of *SYNGAP1*-ID and an alteration in AIS length might underlie some of these observed deficits. Additionally, as most current work on SynGAP function has focused on altered synaptic properties that affect integration of input, the work in this chapter would be the first to assess for alterations at a site key for generation of neuronal output. Since previous AIS length analysis in ASD models were conducted in juvenile animals (P26-32) and is a developmental critical period of sensory cortices (De Villers-Sidani et al., 2008), I used a similar age range in my project (P28-35).

3.3.1 Rat v/s mouse models of *SYNGAP1* haploinsufficiency

In parallel to the work described in this chapter, extensive characterisation of both *Syngap1* rat models was undertaken by other members of the lab. While there are some notable similarities between the rat and mouse models of *SYNGAP1* haploinsufficiency, such as elevated levels of basal protein synthesis, they also exhibit distinct cellular, molecular and behavioural phenotypes. Some of these differences in key cellular and behavioural phenotypes across the models, and the interpretation of my data in the context of these results is discussed below.

Notably, the comparatively high through-put nature of AIS analysis allowed the examination of more brain regions than were characterised by electrophysiology. However, no genotype specific differences in average AIS length were observed in all the regions studied.

Cellular excitability

Characterisation of intrinsic physiology and cellular excitability, including measuring the firing and associated action potential properties as well as passive membrane properties were undertaken in pyramidal cells of mPFC PL, CA1, BA and LA. Firing and AP properties included measurement of the minimal current required to elicit an action potential (AP) (rheobase), the voltage at which AP was elicited (AP threshold) and analysis of the AP waveform including amplitude and half-width while passive membrane properties included measuring resting membrane potential, input resistance, membrane capacitance and sag (a measure of hyperpolarization-activated cation current I_h). Notably, Booker et al. (2019) found that in CA1 pyramidal cells of *Fmr1*$^{-/y}$ mice exhibited increased firing, reduced rheobase and AP threshold compared to controls without alterations in any passive membrane properties. Similarly, Kaphzan et al. (2011) found that in a mouse model of Angelman's syndrome, pyramidal cells from the CA1 also show reduced AP threshold, increased firing and increased AP amplitude with a small hyperpolarisation of the resting membrane potential. Both studies further showed that this increase in cellular excitability could be explained by an increase in AIS length found in these cells. Therefore, in our rat models of *Syngap1*-haploinsufficiency I was particularly interested in regions that showed altered evoked firing properties without modifications in intrinsic membrane properties.

While the *Syngap1*$^{+/-}$ mice exhibit increased evoked excitability in pyramidal glutamatergic cells of mPFC L2/3 (Ozkan et al., 2014) neither the *Syngap1*$^{+/\Delta Gap}$ nor the *Syngap*$^{+/-}$ rats exhibited any alterations in firing or AP properties in mPFC PL cells. This lack of altered single-cell excitability in the mPFC agrees well with the unchanged AIS lengths observed in both genotypes compared to controls. Similarly, no changes in passive membrane and active AP properties were found in pyramidal cells of the CA1 in *Syngap1*$^{+/-}$ rats, in agreement with the lack of genotype specific alterations in AIS length in these animals. A key objective of this project was to establish if cellular phenotypes convergent between the mouse models of FXS and *SYNGAP1*-ID would extend to altered AIS length and translate to the rat models of

Syngap1 haploinsufficiency. Both the electrophysiological and AIS data would indicate that this is not the case for the *Syngap1*$^{+/-}$ rats. The *Syngap1*$^{+/\Delta Gap}$ rats do show a reduction in AP threshold, however this change is not accompanied by an increased firing rate, alteration in passive membrane properties or any change in AIS length. While this indicates that perhaps additional factors, such as axonal diameter (Radivojevic et al., 2017), maybe responsible for the change in AP threshold observed, the functional consequences of this change remains to be established.

The final region characterised electrohpysiologically was the basolateral nucleus of the amygdala. While intrinsic cellular excitability in this brain region has not previously been characterised in the *Syngap1*$^{+/-}$ mouse, these mice do present with altered amygdalar-dependent behaviours, such as decreased anxiety, suggesting altered neuronal and circuit excitability (Guo et al., 2009; Muhia et al., 2010; Ozkan et al., 2014; Berryer et al., 2016). In our rat models, the *Syngap1*$^{+/-}$ rats exhibit increased firing rate in the LA but not in the BA while the *Syngap1*$^{+/\Delta Gap}$ rats exhibit decreased firing rate with increased rheobase in the BA but not in the LA. These changes in firing properties are not accompanied by any change in passive membrane properties, indicative of AIS length change mediated dysfunction. However, a lack of statistically significant change in average AIS length across genotypes would indicate that alterations in AIS length are not responsible for the observed altered cellular firing. This lack of statistical significance can partly be explained by the wide range of average lengths across animals observed in the BLA compared to other brain regions (LA *Syngap1*$^{+/+}$ P28-35= 10.14 μm, *Syngap1*$^{+/\Delta Gap}$= 5.81 μm, *Syngap1*$^{+/-}$ P28-35= 6.23 μm; BA *Syngap1*$^{+/+}$ P28-35= 13.77 μm, *Syngap1*$^{+/\Delta Gap}$= 12.54 μm, *Syngap1*$^{+/-}$ P28-35= 16.54 μm). The BLA projects to, and receives projections from, multiple brain regions with projection targets known to shape cellular excitability (Song et al., 2015). A contributing factor to this increased range of AIS lengths maybe the current analytical approach, which does not distinguish between, thus diluting out, sub-population specific effects. This idea is further discussed in section 3.3.2 below.

In addition to cellular excitability, both mouse and rat models of *SYNGAP1* haploinsufficiency exhibit impairments in synaptic plasticity. Prominently, *Syngap1*$^{+/-}$ mice show impaired long-term potentiation (LTP) in the CA1 sub-region of the hippocampus (Komiyama et al., 2002), a deficit which is reversed upon restoration of SynGAP to wildtype protein levels in adults (Ozkan et al., 2014). Impaired LTP is also observed in L4 stellate cell in the S1BF of

Syngap1$^{+/-}$ mice (Clement et al., 2013). Finally, *Syngap1*$^{+/-}$ mice also show altered long-term depression (LTD) in an age and protocol dependent manner (Kim et al., 2003; Carlisle et al., 2008; Barnes et al., 2015). Similar to the *Syngap1*$^{+/-}$ mice, *Syngap1*$^{+/-}$ rats also show impaired LTP in the CA1 with impaired LTP in the mPFC L5 and thalamic inputs to the amygdala being observed in both the *Syngap1*$^{+/\Delta Gap}$ and *Syngap1*$^{+/-}$ rats. While there are no direct established links between altered synaptic efficacy and the axon initial segment, Evans et al. (2015) propose that calcineurin and CDK5, molecules known to alter SynGAP activity Walkup et al. (2015), modulate AIS length and may have a marked effect on multiple firing, a feature that is crucial for LTP.

Behavioural phenotypes

Similar to inconsistencies in cellular excitability deficits, the *Syngap1* mouse and rat models also exhibit differences in behavioural phenotypes. Hyperexcitability with increased locomotion has been widely reported in *Syngap1*$^{+/-}$ mice (Guo et al., 2009; Muhia et al., 2010; Clement et al., 2012; Berryer et al., 2016) and is thought to be driven by increased activity of glutamatergic neurons (Ozkan et al., 2014). While the *Syngap1*$^{+/-}$ rats appear hyperactive, the *Syngap1*$^{+/\Delta Gap}$ rats appear to be hypoactive, suggesting distinct alterations to circuit excitability between the models. In addition to hyperactivity, the *Syngap1*$^{+/-}$ rats show sustained impaired motor co-ordination in an accelerating rotarod task, a phenomenon that is not observed in the *Syngap1*$^{+/-}$ mice (Muhia et al., 2010). Individuals with *SYNGAP1*-ID are reported to have an increased pain tolerance, a feature that is not observed in the *Syngap1*$^{+/-}$ mice (Muhia et al., 2010). Reminiscent of clinical reports, *Syngap1*$^{+/-}$ rats show an increased threshold for thermal pain while *Syngap1*$^{+/\Delta Gap}$ rats show decreased pain threshold, further suggesting model specific alterations to underlying circuitry. A point of cross-species conservation of behavioural phenotypes is deficits in spatial memory. The *Syngap1*$^{+/-}$ mice show impaired spatial memory in a prefrontal-hippocampal dependent alternated T-maze (Deacon and Rawlins, 2006) while both *Syngap1*$^{+/-}$ and *Syngap1*$^{+/\Delta Gap}$ rats show impaired long-term (24 hour delay) hippocampal based spatial memory in an object location task (Warburton and Brown, 2015). While individuals with *SYNGAP1*-ID show increased anxiety related behaviours, nascent anxiety like behaviours tested in an open field and elevated plus maze show reduced anxiety levels in *Syngap1*$^{+/-}$ mice (Guo et al., 2009; Muhia et al., 2010). Similar to the patient phenotype, both *Syngap1*$^{+/-}$ and *Syngap1*$^{+/\Delta Gap}$

rats show elevated levels of nascent and novelty induced anxiety as measured using a marble interaction paradigm, suggesting hyperactivity of the underlying circuit.

While at present there is no direct evidence linking altered behavioural states to changes in AIS length, altered behaviour is indicative of underlying circuit hyper- or hypo-excitability (Nelson and Valakh, 2015). This altered circuit excitability may, in turn, be caused by alterations in cellular excitability, which is known to be influenced by alterations to AIS length (Kuba et al., 2006; Grubb and Burrone, 2010). However, as no changes in average AIS length were observed between rats of either *Syngap1* haploinsufficiency genotype and controls in brain-regions implicated in the altered behaviours, other regulators of learning and memory, such as altered synaptic plasticity, must underlie the observed behavioural phenotypes. Observed LTP deficits in the CA1, mPFC and amygdala without alterations in intrinsic cellular excitability support this conclusion. Of note, AIS length measurements in this chapter were performed at an age-point earlier than the behavioural characterisation, with the assumption that any alterations in AIS length and subsequent cellular excitability would precede behavioural abnormalities. However, the change in cellular excitability and adaptation of AIS length following subjection to behavioural paradigms has not been assessed.

3.3.2 Limitations in experimental design

Having discussed the sparse cellular excitability deficits in our *Syngap1* rat models, it is unsurprising that the AIS length remained unchanged specifically in mPFC L5, CA1 and BLA. However, one cannot exclude the possibility that technical and experimental design choices attributed to the lack of phenotypes observed. Some of these variables include sex of experimental animal, experimental age and analysis approach and are discussed below.

Sex differences

Animals of both sexes from both models were used in the experiments outlined above. While there is evidence in literature of differential hippocampal function between male and female rats, most of these differences are noted in adult animals (>P60), which is outwith the age of the experimental animals used here (Maren et al., 1994; Oberlander and Woolley, 2016; Yang et al., 2004; Choleris et al., 2018). One study, however, did find enhanced perforant

pathway-LTP in male but not female peri-adolescent (P35) rats (Maren et al., 1994), which is the upper limit of the age range used here. However, within the context of published *Syngap1* research both male and female animals have extensively been used to characterise cellular excitability deficits in the *Syngap1*$^{+/-}$ mice (Rumbaugh et al., 2006; Clement et al., 2012, 2013; Ozkan et al., 2014) with only one report of male-specific reduction in mEPSC amplitude in parvalbumin positive interneurons in the S1 (Berryer et al., 2016). Due to the possibility of sex-specific alterations in AIS length, 'sex' was used as a random variable in the generalised linear mixed model and separation of data by sex determined no significant contribution of this variable on observed results. Therefore, it would appear unlikely that the use of rats of both sexes significantly impacted the results outlined in this chapter. However, as work in subsequent chapters is performed either in adult animals where sex-specific differences are better delineated or in animals containing X-linked mutations, work has been restricted to male rats.

Experimental age

The experimental age chosen in this chapter, P28-35, was based off the age at which the AIS changes in *Fmr1*$^{-/y}$ mice were found (Booker et al., 2019), the age at which convergence of cellular and molecular phenotypes was observed between *Fmr1*$^{-/y}$ and *Syngap1*$^{+/-}$ mice (Barnes et al., 2015) and as it is a developmental critical period for sensory cortices (De Villers-Sidani et al., 2008). However, published literature on cellular and excitability deficits in mouse models of *Syngap1* haploinsufficiency use a wide range of ages. In wildtype mice, expression of SynGAP increases postnatally, peaking at P14 (Clement et al., 2012; McMahon et al., 2012). Concomitant with this increase, a number of excitability and spine-turnover deficits in the *Syngap1*$^{+/-}$ mice have been noted from P5-P14, especially in the S1BF and the dentate gyrus of the hippocampus (Clement et al., 2012, 2013; Aceti et al., 2015). Notably, AIS lengths are most dynamically regulated in the second post-natal week (Gutzmann et al., 2014). Therefore, P13-15 may have been a more suitable time-point to assess alterations in AIS length. However, analysis of intrinsic excitability in the CA1 and BLA at P14 of *Syngap1*$^{+/-}$ and *Syngap1*$^{+/\Delta Gap}$ rats revealed no changes in firing rates in pyramidal cells of these regions (Toft, 2019; Mizen, 2017).

Altered cellular phenotypes have also been noted in adult *Syngap1*$^{+/-}$ mice, including impaired CA1 LTP (Komiyama et al., 2002), increased spine-density (Carlisle et al., 2008) and increased firing in the mPFC L2/3 cells (Ozkan et al., 2014). Additionally, spontaneous absence-

like seizures have only been noted at >12 weeks of age in *Syngap1*$^{+/-}$ mice (Ozkan et al., 2014). Since cellular excitability alterations have not been characterised in adults in our rat models of *SYNGAP1*-ID and there is an increase in AIS length in adults mice compared to juveniles (Gutzmann et al., 2014), in chapter 4 I investigated alterations to AIS length at in male rats aged P90-120.

AIS analysis

A key technical limitation of the current analysis is the 'blanket' approach, wherein AISs that met the criteria outlined in chapter 2 were analysed without drawing a distinction between cells that project to, or receive projections from, specific other brain regions. While this approach is suitable for areas such as the CA1, CA3, S1 L2/3 and L4 and V1 L2/3, that have fairly conserved inputs and laminar distribution of connections (Chen-Bee et al., 2012; Petersen, 2007; Hannula and Duff, 2017; Nowak and Bullier, 1997), it is less suitable for cortical output layers (L5) in the mPFC, S1, V1 and the BA. This is especially important in the light of circuit-specific long-range hypoconnectivity in models of ASD/ID (Moseley et al., 2015). This may, to an extent, explain the increased range of average AIS lengths observed in the BA of our rat models. In order to address this limitation, in chapter 4 I have focused analysis of AIS lengths on reciprocal connections between mPFC PL and the BLA.

Lastly, the AIS is also shown to impact cellular excitability by altering its position along the axon (Grubb and Burrone, 2010; Evans et al., 2013, 2015). However, relative distance of the start of the AIS from the cell soma were not measured here for a number of reasons. First, in both the FXS (Booker et al., 2019) and Angelman's syndrome mouse models (Kaphzan et al., 2011), no alterations in distance from cell soma (dfcs) were reported. Secondly, in my analysis of dfcs in other models of ASD/ID, no changes were observed between genotypes (see appendix fig.S4). In addition, the average observed dfcs in appendix fig.S4 were much smaller that those previously reported in cultures (Grubb and Burrone, 2010; Evans et al., 2013, 2015). Thus, while alterations to dfcs may contribute to some aspects of altered cellular excitability, such as the reduced AP threshold in the CA1 of *Syngap1*$^{+/\Delta Gap}$ rats, the significantly smaller magnitude of any observed changes would make these connections more tenuous.

Chapter 4

In vivo morphological plasticity of the AIS in rat models of *Syngap1* haploinsufficiency

4.1 Introduction

ASDs have widely been considered a condition lacking central cognitive coherence as a result of altered neural functional connectivity (Frith, 2003; Belmonte et al., 2004; Barttfeld et al., 2011; Moseley et al., 2015). Studies using fMRI and EEG have reported a double dissociation in connectivity patterns in individuals with ASD compared to age matched controls: During 'rest', where participants are not engaged in any particular task, long-range connections, particularly fronto-occipital connections, show functional hypoconnectivity (Assaf et al., 2010; Barttfeld et al., 2011; Moseley et al., 2015) while short-range connections show hyperconnectivity (Barttfeld et al., 2011). During periods of attention, however, brain-network connectivity appears to increase if the target of attention is internal (e.g. focusing on respiration) whereas connectivity is decreased if the attention target is external (e.g. external auditory stimulus or task) (Barttfeld et al., 2012). Therefore, functional connectivity defects in ASD appear to be state dependent. However, individual component analysis has revealed that compared to controls, the mPFC of individuals with ASD appears to be functionally under-connected to multiple brain regions both at rest (Carper and Courchesne, 2005) and during attention states (Kawakubo

et al., 2009; Castelli, 2002), making it an interesting target region to study in the context of ASD/ IDs.

Situated at the rostral tip of the frontal lobe, the mammalian prefrontal cortex (PFC) is a key player in complex cognitive processes that are known to be disrupted in neurodevelopmental disorders including decision making, attention states and working memory (Miller, 2000; Testa-Silva et al., 2012). Studies in *Syngap1*$^{+/-}$ mice revealed deficits in PFC-dependent working memory (Muhia et al., 2010) as well as increased glutamatergic activity in the medial prefrontal cortex (mPFC) of adult (>9 weeks) *Syngap1*$^{+/-}$ mice compared to controls (Ozkan et al., 2014). While no such increase in glutamatergic activity was found in the *Syngap1*$^{+/-}$ rats, impairments in translaminar long-term potentiation (LTP), a form of hebbian synaptic plasticity that forms the neural basis for learning and memory (Hebb, 1949; Nabavi et al., 2014; Langille and Brown, 2018), have been found in the mPFC of juvenile and adult *Syngap1*$^{+/-}$ rats. Anatomically, the mPFC is divided into four sub-regions each with distinct long-range projection targets (Vertes, 2004). These long-range targets drive the formation of distinct mPFC sub-networks by defining the morphology and intrinsic physiology of pyramidal cells in the chief cortical output layer of the mPFC, layer 5 (L5), as well as their local inhibitory micro-circuit (Wang et al., 2006; Brown and Hestrin, 2009; Dembrow et al., 2010). A sub-region of the mPFC crucial for limbic-cognitive functions, including fear mediated learning, is the pre-limbic cortex (PL) (Hoover and Vertes, 2007). Fear related behaviours are altered in models of *SYNGAP1*-ID such that *Syngap1*$^{+/-}$ mice exhibit impaired acquisition of fear memory (Clement et al., 2012) whereas *Syngap1*$^{+/-}$ rats exhibit exaggerated recall of fear memory (see section 4.2.2). Reciprocal glutamatergic connections between the PL and the basolateral nucleus of the amygdala (BLA) underlie the formation, consolidation, recall and extinction of fear and anxiety associated memories (Vidal-Gonzalez et al., 2006; Laviolette et al., 2005; Corcoran and Quirk, 2007). Similar to the mPFC, LTP deficits accompanied by altered cellular excitability is observed in BLA of juvenile *Syngap1*$^{+/-}$ rats (Toft, 2019). These excitability deficits might alter the maturation dynamics of the prefrontal-amygdala connectivity and underlie the abnormal expression of fear behaviour, making it a valid candidate circuit to study in the context of altered neural functional connectivity in our model of ASD.

Altered functional connectivity observed in fMRI studies, typically results from altered circuit activity. Mechanisms underlying circuit dysfunction range from alterations in the ex-

pression or activity of ion channels to changes in neurotransmitters and receptors that affect excitability at a cellular level (Contractor et al., 2015). One ion-channel rich neuronal compartment that influences cellular excitability is the axon initial segment (AIS). The AIS is a plastic structure, modifying it's morphology, particularly it's length, over the course of normal development (Fried et al., 2009; Cruz et al., 2009; Le Bras et al., 2014; Gutzmann et al., 2014), in response to varying environmental stimuli (Schlüter et al., 2017; Gutzmann et al., 2014) and in pathology (Ferreira et al., 2008; Schafer et al., 2009; Kaphzan et al., 2011; Kloth et al., 2017). *In vitro* and *in vivo* studies in non-mammalian systems have shown that this adaptation of AIS length and location along the axon is activity dependent and modifies the intrinsic excitability of cells (Kuba et al., 2006; Kuba and Ohmori, 2009; Grubb and Burrone, 2010; Evans et al., 2013; Chand et al., 2015; Evans et al., 2015). Preliminary data from the laboratory of Professor Andreas Lüthi has found that upon fear conditioning in wild-type adult mice, the AIS of BA cells that project to the PL elongate (personal correspondence).

Taken together, the alterations in cellular excitability previously noted in the prefrontal cortex and basolateral amygdala in our rat models of *Syngap1* haploinsufficiency, exaggerated recall of mPFC-BLA circuit dependent fear memory in these animals coupled with impaired and not exaggerated LTP and evidence of a role of non-synaptic AIS plasticity in fear memory consolidation and recall, advocates for a closer inspection of AIS plasticity in a model that presents with perturbed fear memory. The hypothesis tested in this chapter is that a reduction in SynGAP protein levels results in altered development and experience-dependent changes in AIS length. In order to test this hypothesis, first I analysed and compared AIS lengths in the PL and the BLA, in adult versus juvenile *Syngap1*$^{+/-}$ rats to determine age-dependent alterations in AIS length. Following this, I analysed the effects of fear-conditioning on AIS lengths in *Syngap1*$^{+/-}$ and *Syngap1*$^{+/\Delta gap}$ rats in both the PL and the BLA. Finally, as the alterations in AIS length following fear conditioning from the laboratory of Professor Andreas Lüthi is specifically in BA cells that project to the mPFC, I analysed AIS lengths of the sub-population of cells that project specifically from the BLA to the PL in *Syngap1*$^{+/-}$ rats. A further argument to look at these specific sub-populations comes from previous work in the lab where in a rat model of Fragile-X syndrome a decrease in AIS length is found specifically in PL cells that project to the BLA (Jackson, 2016) (see appendix fig.S1). Given previous evidence of convergence between mouse models of FXS and *SYNGAP1*-ID (Barnes et al., 2015), I also analysed AIS lengths of cells of the mPFC that project to the BLA.

4.2 Results

4.2.1 Age dependent changes to AIS length

Structural plasticity of AIS length with age have been previously reported in mice and monkeys. Data from wildtype (WT) mouse primary visual cortex showed an increase in AIS length in adulthood (>P60) compared to juvenile (P28) animals (Gutzmann et al., 2014). In rhesus macaque monkeys, the AIS of pyramidal neurons in the prefrontal cortex (PFC) shortened in length during the first 6 post-natal months, as animals transitioned from childhood to adolescence (Cruz et al., 2009). However, the AIS lengths of gephyrin-positive GABAergic chandelier neurons in the same region and model showed marked shortening only during adolescence (2-3 years) (Cruz et al., 2009). Taken together these studies indicate that AIS lengths are dynamically regulated during development as well as AISs of different cell types within the same brain region undergo distinct developmental trajectories. Given this evidence of *in vivo* plasticity of AIS morphology, I first analysed genotype specific differences in AIS length with age between adult (P90-120) (*Syngap1*$^{+/+}$) and *Syngap1*$^{+/-}$ rats in the pre-limbic (PL) region of the mPFC and the basal and lateral nucleus of the amygdala (BLA). The AIS length measurements in the adults were further compared to those obtained in juvenile (P28-32) rats of both genotypes in chapter 3. These particular brain regions were chosen for their role in the ontogenesis of fundamental behaviours that are disrupted in *SYNGAP1* haploinsufficiency linked ASD/ID (Hamdan et al., 2011; Parker et al., 2015; Prchalova et al., 2017; Vlaskamp et al., 2019; Jimenez-Gomez et al., 2019) such as threat learning (Deal et al., 2016; Akers et al., 2012; Rudy, 1993; Arruda-Carvalho et al., 2017) and social interaction (Panksepp, 1981; Siviy and Panksepp, 2011).

PL L2/3 and L5

As AIS lengths of both WT (*Syngap1*$^{+/+}$) and *Syngap1*$^{+/-}$ rats at P28-32 were measured in chapter 3, here I measured AIS lengths in the PL L2/3 and L5 in animals at P90-120 and analysed the developmental trajectory and genotype differences between WT and HET (*Syngap1*$^{+/-}$) rats (figs. 4.1 & 4.2). Unlike previous data from the mouse cortex (Gutzmann et al., 2014), WT animals did not show any significant difference in mean AIS length in cells of L2/3 (*Syngap1*$^{+/+}$ P28-35= 28.75 $\pm$ 0.85 μm, P90-120= 31.55 $\pm$ 0.37 μm) or L5 (*Syngap1*$^{+/+}$ P28-35= 28.99 $\pm$ 0.55 μm , P90-120= 32.14 $\pm$ 0.65 μm) with age. Interestingly, in both layers the shortest (minimum) measured AIS length was significantly increased in adult WT (P90-120) animals compared to juveniles (P28-35) with no change in the longest (maximum) measured length and a concomitant decrease in the range of measured AIS lengths. Changes in AIS length with age in the mouse primary visual cortex shows that cells at the later age point, considered functionally mature, have longer AISs (Gutzmann et al., 2014). Within this context, the increase in minimum AIS length and decrease in range of AIS lengths without any change in average or maximum measured AIS lengths in the PL of WT rats suggests that the population of cells sampled at the juvenile age are at different stages of maturity while those in the adult animals are more closely matched.

AIS lengths in PL L5 of *Syngap1*$^{+/-}$ rats followed similar alterations to the WT animals with no age-dependent change in mean or maximum measured AIS length, increased minimum measured AIS length, decreased range and a shift in the cumulative distribution towards longer AIS lengths (see fig. 4.2 B, B' & table 4.2), indicating that haploinsufficiency of SynGAP does not affect developmental alterations in AIS length in PL L5. AIS lengths in cells of PL L2/3 of *Syngap1*$^{+/-}$ rats did not show any difference in mean AIS length with age and, similar to *Syngap1*$^{+/+}$ rats, showed decreased range with increased minimum measured AIS lengths. However, these cells did not follow the WT developmental trajectory of the shift in the cumulative AIS lengths towards increased length which was further accompanied by decreased maximum measured AIS length (see fig. 4.2 A, A' & table 4.1).

Further, genotype specific analysis revealed a trend of reduced average AIS length (fig.4.1D *Syngap1*$^{+/+}$= 31.55 $\pm$ 0.37 μm n=4, *Syngap1*$^{+/-}$= 29.05 $\pm$ 0.63 μm n=4 animals, p=0.0571) and a significant difference in the cumulative distribution (fig.4.1E p=<0.0001 using a Kolmogorov-

Smirnov test) of AIS lengths in L2/3 of *Syngap1*$^{+/-}$ rats compared to WT controls at P90-120. No genotype specific change, however, was observed in L5 either at the level of average AIS length (fig.4.1H *Syngap1*$^{+/+}$= 32.14 $\pm$ 0.65 μm n=4, *Syngap1*$^{+/-}$= 31.06 $\pm$ 0.49 μm n=4 animals) or in the cumulative distribution of AIS lengths (fig.4.1I) of P90-120 *Syngap1*$^{+/-}$ rats compared to controls.

PL L2/3			
		Syngap1$^{+/+}$	*Syngap1*$^{+/-}$
Mean Length	P28-35	28.75 μm	28.73 μm
	P90-120	31.55 μm	29.05 μm
Min Length	P28-35	24.66 μm	25.24 μm
	P90-120	30.59 μm	28.36 μm
Max Length	P28-35	32.18 μm	33.11 μm
	P90-120	32.39 μm	30.95 μm
Range	P28-35	7.52 μm	7.86 μm
	P90-120	1.80 μm	2.59 μm

Table 4.1: Comparison of AIS lengths in PL L2/3 at P28-35 and P90-120

PL L5			
		Syngap1$^{+/+}$	*Syngap1*$^{+/-}$
Mean Length	P28-35	28.99 μm	28.73 μm
	P90-120	33.14 μm	31.06 μm
Min Length	P28-35	25.57 μm	25.43 μm
	P90-120	30.52 μm	30.29 μm
Max Length	P28-35	31.43 μm	35.03 μm
	P90-120	33.66 μm	32.43 μm
Range	P28-35	5.86 μm	9.60 μm
	P90-120	3.13 μm	2.13 μm

Table 4.2: Comparison of AIS lengths in PL L5 at P28-35 and P90-120

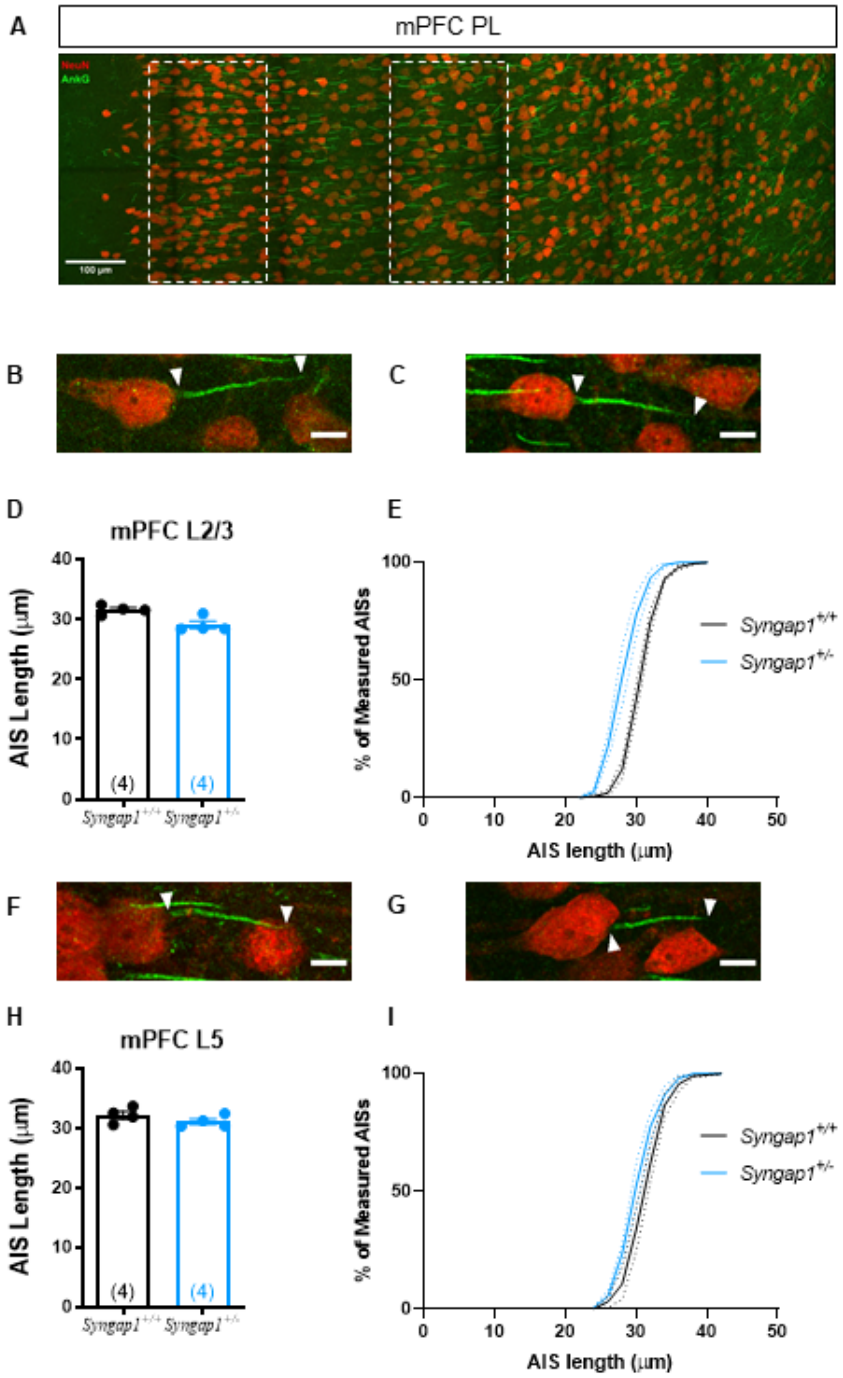

Figure 4.1: AIS lengths in PL L2/3 and L5 of P90-120 *Syngap1*$^{+/+}$ and *Syngap1*$^{+/-}$ rats (A) Representative image of the cortical stack acquired for analysis. Cell bodies visualised using NeuN (red) and AIS using AnkG (green). White boxes demarcate the regions selected for analysis of L2/3 (left) and L5 (right). Representative single AIS with arrows indicating the proximal and distal ends from *Syngap1*$^{+/+}$ (L2/3 B, L5 F) and *Syngap1*$^{+/-}$ (L2/3 C, L5 G) rats. Scale bar=10 μm. (D, E) Trend of reduced average AIS length (*Syngap1*$^{+/+}$= 31.55 $\pm$ 0.37 μm n=4, *Syngap1*$^{+/-}$= 29.05 $\pm$ 0.63 μm n=4 animals, p=0.0571) and significantly shifted cumulative distribution of AIS lengths was observed in PL L2/3 of *Syngap1*$^{+/-}$ rats compared to controls p=<0.0001 using a K-S test. (H, I) No change in average AIS length (*Syngap1*$^{+/+}$= 32.14 $\pm$ 0.65 μm n=4, *Syngap1*$^{+/-}$= 31.06 $\pm$ 0.49 μm n=4 animals) or cumulative distribution of AIS lengths was observed in in PL L5 of *Syngap1*$^{+/-}$ rats compared to controls.

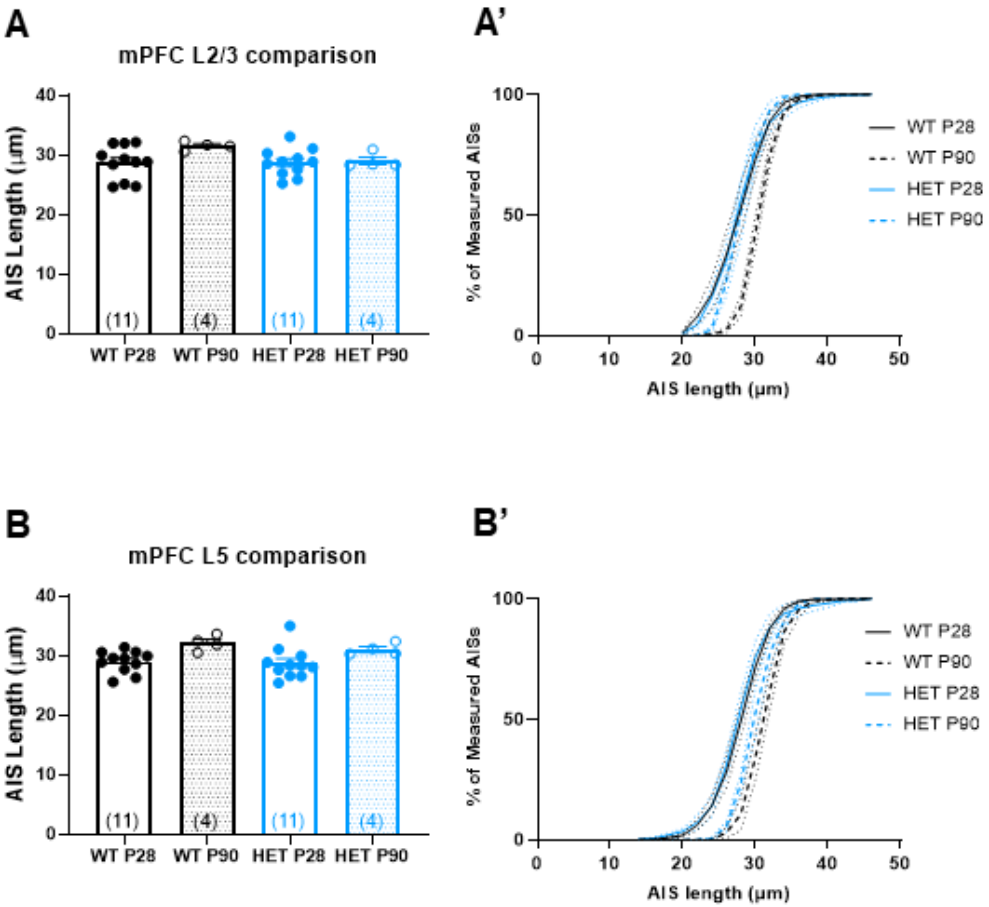

Figure 4.2: Comparative AIS lengths between P28-35 and P90-120 *Syngap1*$^{+/+}$ and *Syngap1*$^{+/-}$ rats in L2/3 and L5 of the mPFC Comparison of mean and cumulative distribution of AIS lengths across age and genotype indicate that (A, A') in cells of mPFC PL L2/3 *Syngap1*$^{+/+}$ (WT) animals show no significant difference in average AIS length but a shift in the overall distribution of AIS lengths towards longer AISs while AIS lengths of *Syngap1*$^{+/-}$ (HET) rats do not exhibit a similar shift in AIS length distribution towards longer AISs (B, B') Cells of PL L5 show no significant change in mean AIS length with age but both WT and HET animals show a shift in cumulative distribution of AIS lengths towards longer AISs.

BA and LA

Similar to the PL, AIS lengths across genotypes in both the LA and the BA in animals at P90-120 (fig. 4.3 & 4.4) were measured and compared to changes observed at P28-32 (fig. 3.5). In the LA of WT rats mean AIS length was significantly increased in adult animals compared to juveniles (*Syngap1*$^{+/+}$ P28-35= 24.43 $\pm$ 1.06 μm, P90-120= 29.13 $\pm$ 0.74 μm, p=0.0243). This increase in average length appeared to be predominantly driven by increased minimum measured AIS length at P90-120 as maximum measured AIS length was comparable across ages (see table 4.3 & 4.4 A, A'). Similar to the results obtained in the WT animals, average AIS length measured in the LA of *Syngap1*$^{+/-}$ rats was significantly increased (P28-35= 23.71 $\pm$ 0.96 μm, P90-120= 28.31 $\pm$ 0.75 μm, p=0.0389). This increase again was driven by increased minimum measured length at P90-120 as maximum measured AIS length remain unchanged with age (see table 4.3 & 4.4 A, A'). Following on from the interpretation of this data in the PL, it would imply that cells in the LA in juvenile animals showed more heterogenous functional maturity while those in the adult animals were more homogenous and a reduction in SynGAP levels did not affect this maturation (Two-Way ANOVA, GenotypexAge F(1, 18)=0.002392, p=0.9615; Age F(1, 18)=18.76, p=0.0004).

As with the LA, average AIS length (*Syngap1*$^{+/+}$ P28-35= 33.21 $\pm$ 1.84 μm, P90-120= 40.07 $\pm$ 2.88 μm) and minimum measured AIS length was increased between P28-32 and P90-120 in cells of the BA in WT rats. Interestingly however the maximum measured AIS length was also increased with no change in range of lengths measured in WT animals at P90-120 compared to P28-32 (see table 4.4 & 4.4 B, B'). The overall increase in average AIS length (*Syngap1*$^{+/-}$ P28-35= 30.94 $\pm$ 2.26 μm, P90-120= 38.42 $\pm$ 1.57 μm) and minimum measured AIS length in BA cells of WT P90-120 rats (compared to P28-32 rats) extended to the *Syngap1*$^{+/-}$ rats. However, maximum measured AIS length was unchanged with subsequent decrease in range of AIS lengths measured across ages in these animals (see table 4.4 & 4.4 B, B'). The interpretation of cells at P90-120 having longer AISs and being functionally more mature could be extended to the BA of both WT and *Syngap1*$^{+/-}$ rats in that there is increased minimum measured AIS length (Two-Way ANOVA, GenotypexAge F(1, 19)=0.01699, p=0.8977; Age F(1, 19)=9.492, p=0.0062). However, the the unaltered range of AIS lengths measured in the WT BA cells would imply that additional factors affect the AIS length of a cell. Given that AIS structure, particularly length, is known to be dependent on synaptic input (Kuba et al., 2006;

Fried et al., 2009) and that excitability of BA cells is dependent on its projection target (Paré and Gaudreau, 1996), the unchanged range of AIS lengths measured in the WT rats at P90-120 can be attributed to sampling a mixed population of cells that project to or receives projections from different brain regions. Given that *Syngap1* haploinsufficiency causes a reduction in the range of AIS lengths measured, it might imply that AIS lengths of a particular sub-population are differentially affected. Genotype specific differences in AIS lengths in one such sub-population is elaborated on in section 4.2.3.

Lastly, no genotype specific changes were observed in average AIS length in the BA (fig.4.3D *Syngap1*$^{+/+}$= 40.07 $\pm$ 2.88 μm n=4, *Syngap1*$^{+/-}$= 38.42 $\pm$ 1.57 μm n=4 animals) or LA (fig.4.3I *Syngap1*$^{+/+}$= 29.13 $\pm$ 0.74 μm n=4, *Syngap1*$^{+/-}$= 28.31 $\pm$ 0.75 μm n=4 animals), nor were there any changes to cumulative distribution of AIS lengths (fig. 4.3E, J) seen in either region rats aged P90-120 *Syngap1*$^{+/-}$ compared to WT litter-mate controls.

LA			
		Syngap1$^{+/+}$	*Syngap1*$^{+/-}$
Mean Length	P28-35	24.43 μm	23.71 μm
	P90-120	29.13 μm	28.31 μm
Min Length	P28-35	20.33 μm	21.41 μm
	P90-120	28.07 μm	26.60 μm
Max Length	P28-35	30.48 μm	27.64 μm
	P90-120	31.30 μm	29.88 μm
Range	P28-35	10.14 μm	6.23 μm
	P90-120	3.28 μm	3.27 μm

Table 4.3: Comparison of AIS lengths in LA at P28-35 and P90-120

BA			
		Syngap1$^{+/+}$	*Syngap1*$^{+/-}$
Mean Length	P28-35	33.21 μm	30.94 μm
	P90-120	40.07 μm	38.42 μm
Min Length	P28-35	26.15 μm	24.86 μm
	P90-120	31.53 μm	35.54 μm
Max Length	P28-35	39.92 μm	41.40 μm
	P90-120	43.69 μm	41.80 μm
Range	P28-35	13.77 μm	16.54 μm
	P90-120	12.16 μm	6.26 μm

Table 4.4: Comparison of AIS lengths in LA at P28-35 and P90-120

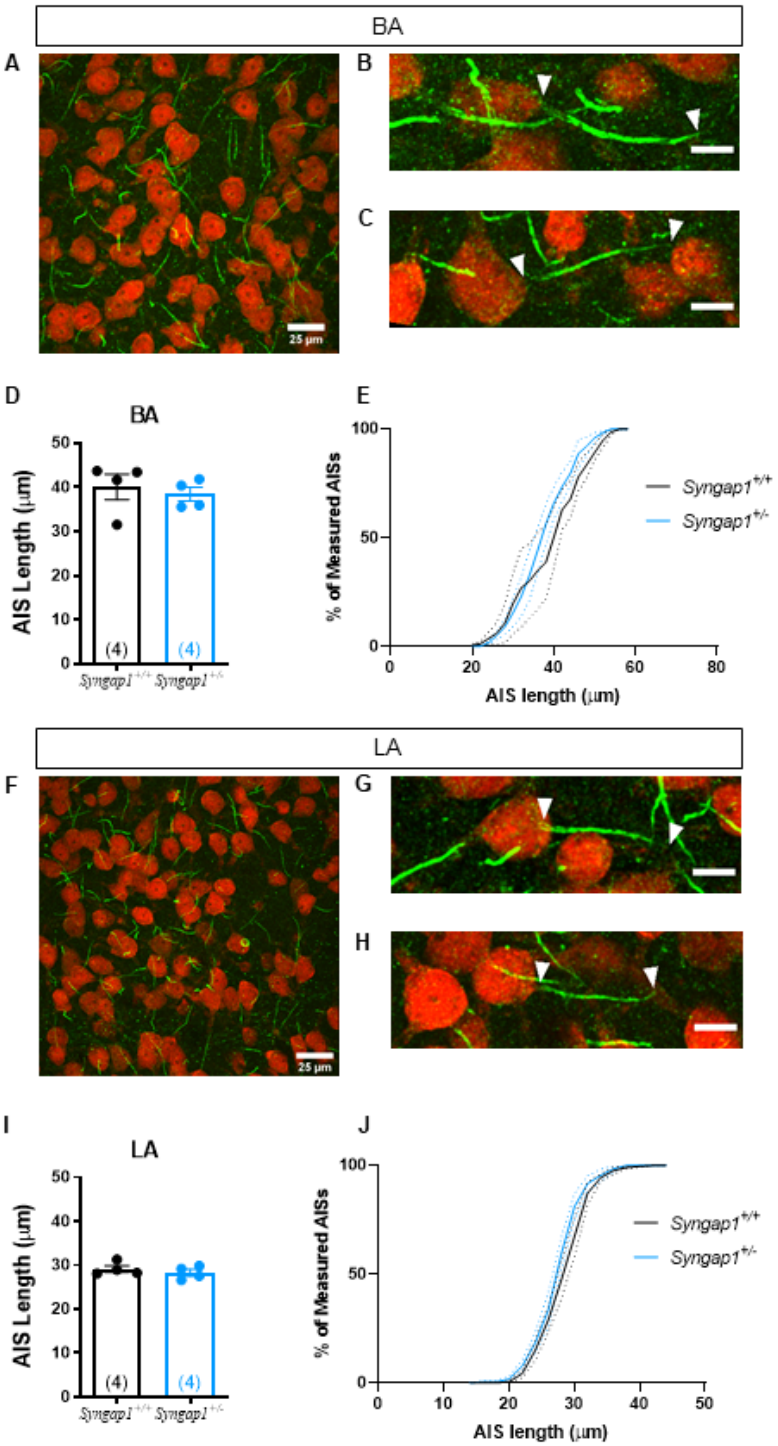

Figure 4.3: AIS lengths in BA and LA of P90-120 *Syngap1*$^{+/+}$ and *Syngap1*$^{+/-}$ rats (A) Representative image of the BA used for analysis. Cell bodies visualised using NeuN (red) and AIS using AnkG (green). Representative single AISs with arrows representing the proximal and distal ends from BA and LA respectively of *Syngap1*$^{+/+}$ (B, G) and *Syngap1*$^{+/-}$ (C, H) rats. Scale bar=10 μm. (D, E) No change in average AIS length (*Syngap1*$^{+/+}$= 40.07 $\pm$ 2.88 μm n=4, *Syngap1*$^{+/-}$= 38.42 $\pm$ 1.57 μm n=4 animals) or cumulative distribution of AIS lengths was observed in BA of *Syngap1*$^{+/-}$ rats compared to controls. (F) Representative image of the LA used for analysis. (I, J) No change in average AIS length (*Syngap1*$^{+/+}$= 29.13 $\pm$ 0.74 μm n=4, *Syngap1*$^{+/-}$= 28.31 $\pm$ 0.75 μm n=4 animals) or cumulative distribution of AIS lengths in LA L5 was observed in *Syngap1*$^{+/-}$ rats compared to controls.

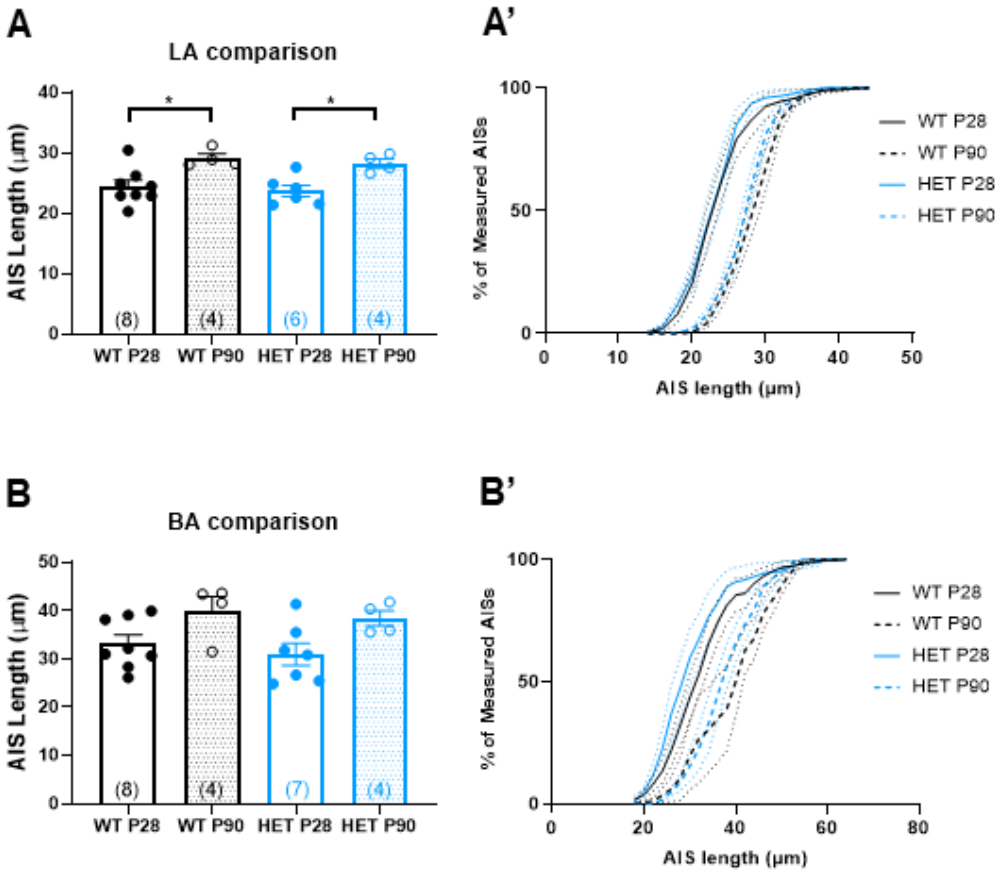

Figure 4.4: Comparative AIS lengths between P28-35 and P90-120 *Syngap1*$^{+/+}$ and *Syngap1*$^{+/-}$ rats in the BLA Comparison of mean and cumulative distribution of AIS lengths across age and genotype indicate that cells in the (A, A') LA, Two-Way ANOVA, GenotypexAge F(1, 18)=0.002392, p=0.9615; Age F(1, 18)=18.76, p=0.0004 and (B, B') BA, Two-Way ANOVA, GenotypexAge F(1, 19)=0.01699, p=0.8977; Age F(1, 19)=9.492, p=0.0062 show increased mean length and a shift in cumulative distribution towards increased AIS lengths in both *Syngap1*$^{+/+}$ (WT) and *Syngap1*$^{+/-}$ (HET) rats.

4.2.2 Experience-dependent changes to AIS length

Experience-dependent plasticity of AIS morphology has been previously shown in neurons of avian and murine sensory systems (Kuba et al., 2010; Gutzmann et al., 2014; Schlüter et al., 2017). In chick embryos, auditory deprivation resulted in an elongation of AIS length, with increased cellular excitability, in neurons of the cochlear nucleus magnocellularis (Kuba et al., 2010). Similarly, dark rearing of mouse pups resulted in elongated AIS lengths and increased cellular excitability in neurons of the mouse primary visual cortex (Gutzmann et al., 2014; Schlüter et al., 2017). Additionally, preliminary work from the laboratory of Professor Andreas Lüthi has found an increase in AIS length in basal amygdalar cells following an associative learning (cued fear conditioning) paradigm. Unpublished results from our laboratory show that rat models of *Syngap1* haploinsufficiency have exaggerated recall of fear memory in an associative learning/ cued fear conditioning paradigm. Given the potential of a role of non-synaptic AIS plasticity in fear memory consolidation and recall, here I analysed AIS plasticity in a model that presents with perturbed fear memory. As recall of fear memory is dependent on the mPFC-BLA circuit (Song et al., 2015; Saha et al., 2018) and altered cellular excitability has been noted in the prefrontal cortex and basolateral amygdala (Toft, 2019) in our rat models, post-behaviour AIS analysis was limited to these two brain regions.

Fear memory in *Syngap1*$^{+/-}$ rats

For assessment of fear memory acquisition and recall, adult (P80-120) WT and *Syngap1*$^{+/-}$ rats were subjected to classic pavlovian conditioning. Briefly, animals were habituated to the testing 'neutral' context for 5 min on two non-consecutive days. 24h after the second day of habituation animals were placed in a different context and subjected to a visually cued fear conditioning paradigm where each animal received 6 presentations of a 10s flashing blue light (the conditioning stimulus or CS) which co-terminated with a 1s 0.8 mA footshock (the unconditioned stimulus or US). During the conditioning phase, acquisition of fear memory was assessed as percentage time spent by the animal in the 'freezing' behavioural state. Freezing state was defined as a complete suppression of spontaneous locomotor activity, and of all movements except those needed for respiration (S. Fanselow, 1984). Both WT and *Syngap1*$^{+/-}$ subjected to

the CS-US pairings (referred to as fear-conditioned or FC) animals showed comparable levels of freezing, which were significantly higher than control animals which were presented only with the flashing blue light (CS) without pairing with the footshock (US) (referred to as CS only) (fig.4.5A, Two-Way ANOVA CSx Genotype p=0.0001, $F_{(15, 70)}$=3.673). Additionally, rats of neither genotype showed evidence of generalised anxiety as % freezing prior to the presentation of the first CS was negligible (*Syngap1*$^{+/+}$= 0.093% $\pm$ 0.093, *Syngap1*$^{+/-}$= 0.71% $\pm$ 0.234). These results concur with previous findings from the laboratory (S Till, unpublished) and indicate that *Syngap1* haploinsufficiency does not affect acquisition of fear memory.

Following conditioning, re-exposure to the CS induces conditioned fear 'freezing' response, which represents a reliable measure of the learned association. Here, 24h after conditioning animals were placed in the neutral context to which they were habituated and tested for re-call and extinction of fear memory. During this phase, animals were presented with 12 iterations of the CS for 30s with a 30s inter-trial interval (ITI) and % freezing over time was used as the behavioural read-out. In a typical wild-type animal subjected to this paradigm, % freezing will be highest in the initial three or four CS presentations and is classed as re-call or fear memory (Pavlov, 1927). With subsequent presentations of the CS without US pairing, the % freezing exhibited by the animal decreases as it forms a new association of the CS with the absence of US. This is classed as extinction learning (for review see Shechner et al. (2014); Bouton (2004)). Here, the average of % freezing exhibited during the first three CS presentations (CS1-3) was classed as fear recall while the difference in average % freezing between the first three and last three CS presentations (CS1-3 - CS10-12) was classed as extinction. *Syngap1*$^{+/-}$ FC rats re-called at levels similar to WT rats (Fig.4.5B, *Syngap1*$^{+/+}$= 59.78% $\pm$ 9.70, *Syngap1*$^{+/-}$= 65.21% $\pm$ 9.03) with animals of both genotypes showing significantly higher levels of freezing compared to CS only controls (Two-Way ANOVA CSxGenotype p=<0.0001, $F_{(36, 360)}$=3.084). Following re-call, animals were subjected to further presentations of the CS to test for extinction learning. While WT FC animals showed a reduction in freezing over the course of the CS presentations (extinction = 28.11% $\pm$ 8.76%), this was lower than the levels typically seen in literature (Chang et al., 2009). Additionally, while 'typical' WT rodents would show modulation of the freezing response during the inter-trial intervals (ITI), the WT FC rats in this behavioural cohort showed a low degree of modulation of freezing response during the ITIs (fig. S3). In *Syngap1*$^{+/-}$ FC rats, % freezing was reduced only modestly over the course of the CS presentations (extinction = 11.54% $\pm$ 6.20%) with animals failing to show modulation of the freezing response during

the ITIs (fig. S3). As with the conditioning, the animals of both genotypes did not show a generalised anxiety response prior to the onset of the first CS (fig.4.5B pre-stim freezing *Syngap1*$^{+/+}$=16.08% $\pm$ 5.77%, *Syngap1*$^{+/-}$= 32.88% $\pm$ 8.36%, Two-Way ANOVA p=0.6832). In agreement with previous data from the lab, this would imply that haploinsufficiency of SynGAP leads to exaggerated re-call of fear memory causing an attenuation of extinction learning.

AIS lengths post fear conditioning in *Syngap1*$^{+/-}$ rats

Following behaviour, I analysed AIS lengths in the pre-limbic mPFC (PL) and basolateral amygdala (BLA) of animals subject to the fear-conditioning paradigm and compared the results obtained to CS only controls for both genotypes. The PL and BLA are known to play a fundamental role in the acquisition and re-call of fear memory (Herry and Johansen, 2014). Given that *Syngap1*$^{+/-}$ rats show exaggerated fear re-call and AIS alterations in the BA have previously been found post fear conditioning, the selection of these two brain regions was appropriate.

In PL L2/3, a trend of reduced average AIS length between WT FC and *Syngap1*$^{+/-}$ FC rats (fig.4.5G, *Syngap1*$^{+/+}$= 30.00 *pm* 0.49 μm n=7, *Syngap1*$^{+/-}$ = 27.98 *pm* 0.54 μm n=9 animals, p=0.0595) while a shift towards shorter AIS lengths in the cumulative distribution was observed in *Syngap1*$^{+/-}$ FC rats compared to WT FC rats (fig.4.5H). Further, no statistically significant differences were observed in either WT or *Syngap1*$^{+/-}$ FC rats compared to the CS only controls (*Syngap1*$^{+/+}$ CS only= 29.82 $\pm$ 0.56 μm n=3, *Syngap1*$^{+/-}$ CS Only= 27.95 $\pm$ 0.74 μm n=4 animals).

In PL L5, no change in average AIS length or cumulative distribution of AIS lengths was observed across rats of either genotype that were subjected to fear conditioning (FC) or in comparison to CS only control animals (Fig.4.5M, N *Syngap1*$^{+/+}$ CS only= 29.29 $\pm$ 0.79 μm n=3, *Syngap1*$^{+/+}$= 29.41 *pm* 0.47 μm n=8, *Syngap1*$^{+/-}$ CS Only= 29.26 $\pm$ 0.56 μm n=4 and *Syngap1*$^{+/-}$= 29.30 *pm* 0.42 μm n=9 animals). Similarly no change in average AIS length or cumulative distribution of AIS lengths was found across genotype or condition (FC compared to CS Only) in either the LA or the BA (LA fig.4.6E, F *Syngap1*$^{+/+}$ CS only= 26.45 $\pm$ 0.15 μm n=3, *Syngap1*$^{+/+}$= 26.38 *pm* 0.3 μm n=7, *Syngap1*$^{+/-}$ CS Only= 25.40 $\pm$ 0.69 μm n=4 and

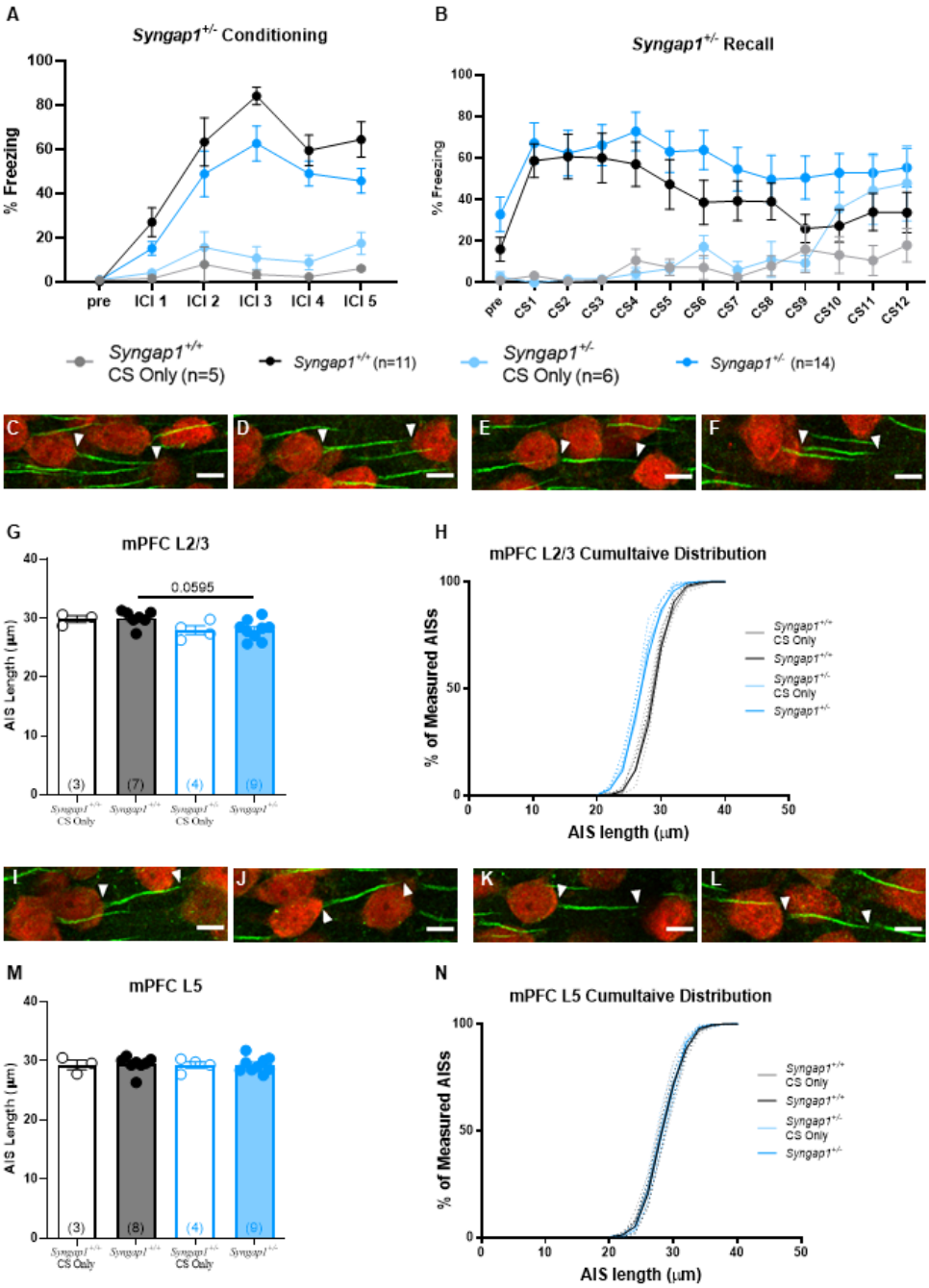

Figure 4.5: AIS lengths in mPFC PL L2/3 and L5 of fear conditioned *Syngap1*$^{+/+}$ and *Syngap1*$^{+/-}$ rats (A) Fear conditioning (FC) (*Syngap1*$^{+/+}$ CS only n=5, *Syngap1*$^{+/+}$ FC n=11, *Syngap1*$^{+/-}$ CS only n=6, *Syngap1*$^{+/-}$ FC n=14) show that *Syngap1*$^{+/-}$ rats freeze at comparable levels to *Syngap1*$^{+/+}$ levels (B) Fear Recall /Extinction shows that *Syngap1*$^{+/-}$ FC rats recall at levels similar to *Syngap1*$^{+/+}$ rats and significantly higher than CS only controls (Two-Way ANOVA P=<0.0001).(C-F) Representative single AISs with arrows representing the proximal and distal ends from PL L2/3 of *Syngap1*$^{+/+}$ CS only (C), *Syngap1*$^{+/+}$ (D), *Syngap1*$^{+/-}$ CS only (E) and *Syngap1*$^{+/-}$ (F) rats. Scale bar=10 μm. (G, H) Trend of reduced average AIS length and cumulative distribution of AIS lengths was observed in PL L2/3 of *Syngap1*$^{+/-}$ FC rats compared to *Syngap1*$^{+/+}$ FC rats. (I-L) Representative single AISs with arrows representing the proximal and distal ends from PL L5 of *Syngap1*$^{+/+}$ CS only (I), *Syngap1*$^{+/+}$ (J), *Syngap1*$^{+/-}$ CS only (K) and *Syngap1*$^{+/-}$ (L) rats. Scale bar=10 μm. (M, N) No change in average AIS length or cumulative distribution of AIS lengths in PL L5 was observed in rats of either genotype or condition.

Syngap1$^{+/-}$ = 26.26 *pm* 0.52 μm n=8; BA fig.4.6K, *Syngap1*$^{+/+}$ CS only= 40.18 $\pm$ 4.16 μm n=3, *Syngap1*$^{+/+}$= 37.17 *pm* 2.29 μm n=7, *Syngap1*$^{+/-}$ CS Only= 36.64 $\pm$ 2.57 μm n=4 and *Syngap1*$^{+/-}$= 38.30 *pm* 2.09 μm n=8).

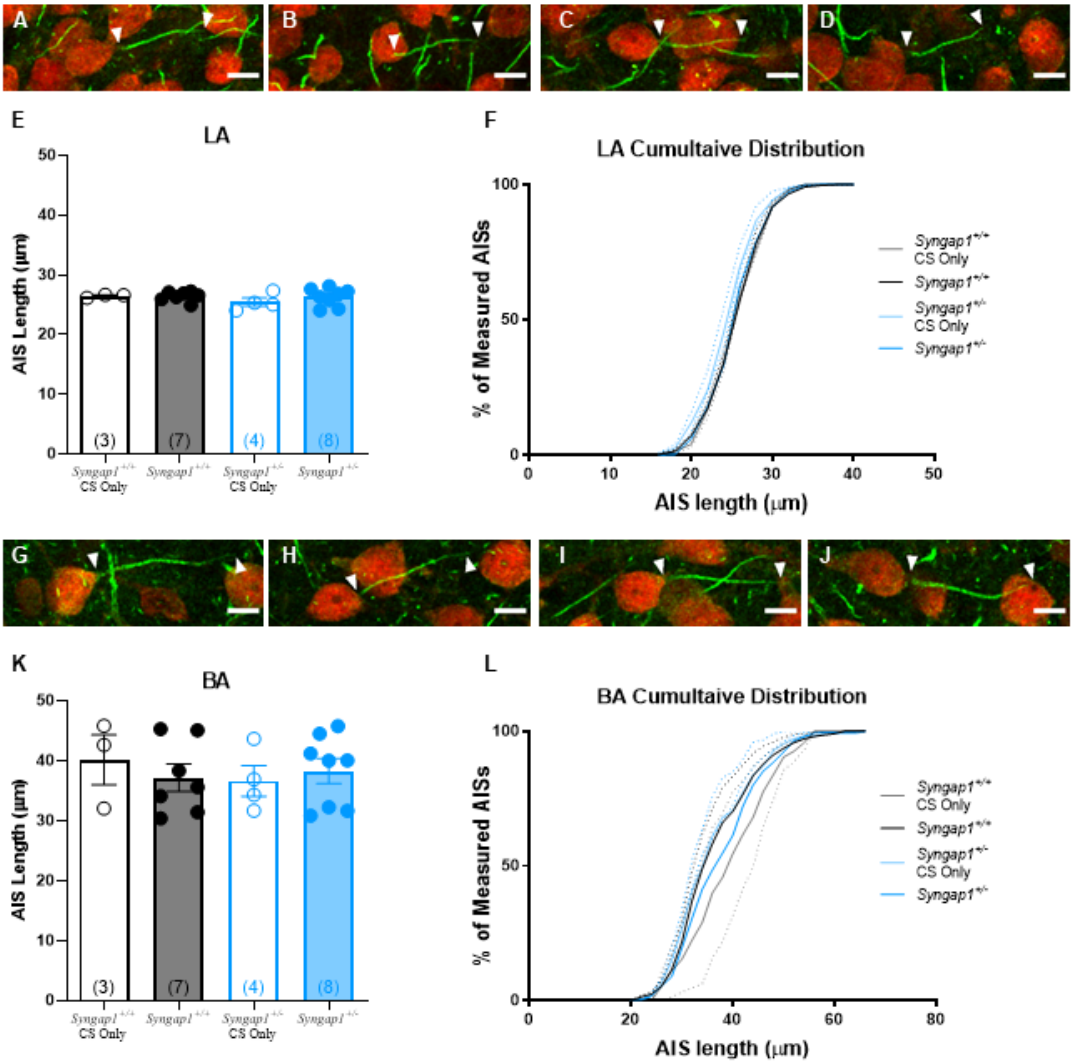

Figure 4.6: AIS lengths in LA and BA of fear conditioned *Syngap1*$^{+/+}$ and *Syngap1*$^{+/-}$ rats (A-D) Representative single AISs with arrows representing the proximal and distal ends from the LA of *Syngap1*$^{+/+}$ CS only (A), *Syngap1*$^{+/+}$ (B), *Syngap1*$^{+/-}$ CS only (C) and *Syngap1*$^{+/-}$ (D) rats. Scale bar=10 μm. (E, F) No change in average AIS length (*Syngap1*$^{+/+}$ CS only= 26.45 $\pm$ 0.15 n=3, *Syngap1*$^{+/+}$= 26.38 *pm* 0.3 n=7, *Syngap1*$^{+/-}$ CS Only= 25.40 $\pm$ 0.69 n=4 and *Syngap1*$^{+/-}$ = 26.26 *pm* 0.52 n=8 animals) or cumulative distribution of AIS lengths was observed in rats of either genotype or condition. (G-J) Representative single AISs with arrows representing the proximal and distal ends from the BA of *Syngap1*$^{+/+}$ CS only (G), *Syngap1*$^{+/+}$ (H), *Syngap1*$^{+/-}$ CS only (I) and *Syngap1*$^{+/-}$ (J) rats. Scale bar=10 μm. (K, L) No change in average AIS length (*Syngap1*$^{+/+}$ CS only= 40.18 $\pm$ 4.16 n=3, *Syngap1*$^{+/+}$= 37.17 *pm* 2.29 n=7, *Syngap1*$^{+/-}$ CS Only= 36.64 $\pm$ 2.57 n=4 and *Syngap1*$^{+/-}$= 38.30 *pm* 2.09 n=8 animals) or cumulative distribution of AIS lengths was observed in rats of either genotype or condition

Fear memory in *Syngap1*$^{+/\Delta Gap}$ rats

Patients with *SYNGAP1*-ID typically present with protein truncating mutations resulting in haploinsufficiency (Hamdan et al., 2009; Krepischi et al., 2010; Klitten et al., 2011; Hamdan et al., 2011; Carvill et al., 2013). The *Syngap1*$^{+/-}$ rats show haploinsufficiency of the full-length protein in a fashion similar to these clinical patients, thus showing construct validity. However, in addition to protein truncating mutations, seven pathogenic *de novo* missense mutations, with three being in the catalytic GAP domain, have also been identified in the *SYNGAP1* gene in patients presenting with ID (Berryer et al., 2013; O'Roak et al., 2014; Parker et al., 2015; Mignot et al., 2016). These missense mutations result in the presence of enzymatically inactive forms of the SynGAP protein, leading to a 50% reduction in GAP function without a 50% reduction in total protein levels (Berryer et al., 2013). Further, SynGAP acts both in a GAP-domain dependent and independent manner at the post-synaptic density to regulate downstream signalling pathways and synaptic plasticity (Walkup et al., 2015, 2016, 2018). Therefore, in order to further our understanding of the contributions of the various SynGAP protein domains to *SYNGAP1*-ID pathophysiology with specific focus on the GAP domain, fear memory acquisition and recall were assessed in a rat model containing a specific deletion of the GAP domain (*Syngap1*$^{+/\Delta Gap}$).

During the conditioning phase, *Syngap1*$^{+/\Delta Gap}$ rats (n=8) show fear memory acquisition at a rate comparable to WT animals (*Syngap1*$^{+/+}$, n=9) as measured by % freezing over the course of the protocol (fig.4.7A, Two-Way ANOVA p=0.8250, $F_{(5, 25)}$=0.4276). Animals of both genotypes show significantly higher freezing than CS only controls (Two-Way ANOVA CSxGenotype p=0.0045) and no evidence of generalised anxiety as indicated by low % freezing levels prior to the on-set of the first CS-US pairing (Fig.4.7A, % freezing pre-stimulus *Syngap1*$^{+/+}$= 0.556% $\pm$ 0.55%, *Syngap1*$^{+/\Delta Gap}$= 4.028% $\pm$ 1.44%, p=0.5447 Bonferroni's multiple comparisons test). Thus haploinsufficiency of the GAP domain, similar to haploinsufficiency of the full-length SynGAP protein, causes no impairments in acquisition of fear memory.

During the recall phase, % freezing exhibited by an animal were measured across twelve CS presentations and the inter-trial intervals. *Syngap1*$^{+/\Delta Gap}$ rats showed higher, but statistically non-significant, % freezing during the first three CS presentations compared to WT fear-

conditioned (WT FC) rats (Fig.4.7B, *Syngap1*$^{+/+}$= 67.78% ± 7.80%, *Syngap1*$^{+/\Delta Gap}$= 81.11% ± 9.08%, Two-Way ANOVA p=>0.999) with fear conditioned (FC) animals of both genotypes showing significantly higher % freezing compared to CS only controls (Fig.4.7A, Two-Way ANOVA CSxGenotype p=<0.0001, $F_{(36, 240)}$=2.891). Similar to the conditioning phase, neither WT nor *Syngap1*$^{+/\Delta Gap}$ FC rats showed evidence of generalised anxiety as measured by % freezing exhibited prior to the first CS presentation (Fig.4.7B pre-stim freezing *Syngap1*$^{+/+}$= 1.67% ± 5.02%, *Syngap1*$^{+/\Delta Gap}$= 33.96% ± 10%, p=0.4396 Bonferroni's multiple comparisons test). Over the course of the 12 CS presentations, WT FC animals showed progressively reduced % freezing, which is measure classically used as evidence of extinction learning (Chang et al., 2009). Here, 'extinction' was measured as the difference in % freezing exhibited by an animal between CS1-3 and CS10-12 and for WT FC animals was 43.70% ± 5.78%. *Syngap1*$^{+/\Delta Gap}$ FC rats, however, showed significantly lower levels of 'extinction' compared to WT FC animals (% freezing during CS1-3 - CS10-12= 10.28% ± 8.59, Two-Way ANOVA p=0.0148), mimicking the exaggerated fear memory recall phenotype of the *Syngap1*$^{+/-}$ rats. Differing from the phenotype of *Syngap1*$^{+/-}$ rats, the *Syngap1*$^{+/\Delta Gap}$ showed modulation of their freezing response during inter-trial intervals (see appendix fig.S3).

AIS lengths post fear conditioning in *Syngap1*$^{+/\Delta Gap}$ rats

Given the similarly exaggerated fear recall in *Syngap1*$^{+/\Delta Gap}$ and *Syngap1*$^{+/-}$ FC rats, the role of the medial prefrontal cortex (mPFC) and the basolateral amygdala in fear memory recall (Herry and Johansen, 2014) and evidence of AIS plasticity in the basal amygdala post fear-conditioning (A Lüthi), I analysed and compared AIS lengths in both these brain regions in animals subjected to the fear-conditioning paradigm to CS only controls across both genotypes.

In the mPFC, average AIS lengths and cumulative distribution of AIS lengths was assessed in L2/3 and L5 of the pre-limbic sub-region as this region has previously been shown to be crucial for fear memory recall (Corcoran and Quirk, 2007). No difference in either average AIS length or cumulative distribution of AIS lengths in observed in cells of PL L2/3 between animals subjected to FC compared to CS only control animals, or between genotypes (Fig.4.7G, H *Syngap1*$^{+/+}$ CS only= 29.78 ± 1.41 μm n=2, *Syngap1*$^{+/+}$= 29.59 *pm* 0.47 μm n=7, *Syngap1*$^{+/\Delta Gap}$ CS Only= 27.81 ± 0.89 μm n=3 and *Syngap1*$^{+/\Delta Gap}$ = 30.06 *pm* 0.56 μm n=6

animals). In cells of PL L5, increased average AIS length and altered cumulative distribution of AIS lengths was observed in *Syngap1*$^{+/\Delta Gap}$ FC rats compared to *Syngap1*$^{+/+}$ FC (Fig.4.7M, N *Syngap1*$^{+/+}$= 30.23 *pm* 0.32 μm n=7, *Syngap1*$^{+/\Delta Gap}$= 31.62 *pm* 0.35 μm n=6 animals, p=0.04) and CS only control rats (Fig.4.7M, N *Syngap1*$^{+/\Delta Gap}$ CS Only= 29.16 $\pm$ 0.50 μm n=3 and *Syngap1*$^{+/\Delta Gap}$= 31.62 *pm* 0.35 μm n=6 animals, p=0.0049).

In the lateral and basal nuclei of the amygdala, no changes in either average AIS length or cumulative distribution of AIS lengths was observed between animals subjected to fear conditioning and CS only controls or between genotypes in either condition (LA fig.4.8E, F *Syngap1*$^{+/+}$ CS only= 27.35 $\pm$ 1.84 μm n=2, *Syngap1*$^{+/+}$= 27.82 *pm* 0.80 μm n=7, *Syngap1*$^{+/\Delta Gap}$ CS Only= 27.59 $\pm$ 0.84 μm n=3 and *Syngap1*$^{+/\Delta Gap}$ = 28.35 *pm* 0.39 μm n=6; BA fig.4.8K, L *Syngap1*$^{+/+}$ CS only= 36.62 $\pm$ 7.01 μm n=2, *Syngap1*$^{+/+}$= 35.59 *pm* 1.76 μm n=7, *Syngap1*$^{+/\Delta Gap}$ CS Only= 36.69 $\pm$ 4.14 μm n=3 and *Syngap1*$^{+/\Delta Gap}$ = 38.04 *pm* 1.31 μm n=6).

Inevitably, within the cohorts of fear conditioned animals the % freezing exhibited during CS presentations that was used to measure recall and extinction was varied. Given that plasticity of AIS morphology is dependent on the experience of each individual animal, I wanted to assess if the AIS lengths measured in a given brain-region were correlated with the amount of % freezing exhibited by that animal during recall and extinction. Therefore, I ran a Spearman's correlation analysis of the measured AIS lengths in all four regions with the % freezing exhibited by an animal during recall and extinction (fig.4.9). The analysis revealed that in WT FC animals of both *Syngap1*$^{+/-}$ and *Syngap1*$^{+/\Delta Gap}$ cohorts, no significant correlations were found between AIS lengths in any of the brain regions and % freezing exhibited during recall or extinction (fig.4.9A, B). However, *Syngap1*$^{+/-}$ FC rats showed a significant, negative correlation between % freezing exhibited during recall (r^2=-0.934, p=0.002, n=8) and extinction (r^2= -0.766, p=0.032) and measured AIS lengths in PL L2/3. In *Syngap1*$^{+/\Delta Gap}$ FC rats, AIS lengths in the BA were negatively and significantly correlated with % freezing exhibited by an animal during recall (r^2= -0.943, p= 0.017). Further, both *Syngap1*$^{+/-}$ and *Syngap1*$^{+/\Delta Gap}$ CS only control animals did not show any significant correlations of AIS length and % freezing during recall or extinction, ensuring that the correlations obtained were dependent on animal experience and could not be explained by genotype (*Syngap1*$^{+/-}$ CS only recall-PL L2/3 r^2= 0.316, p=0.667, extinction-PL L2/3 r^2= 0.800, p=0.333; *Syngap1*$^{+/\Delta Gap}$ CS only recall-BA r^2=0.500, p=1.00).

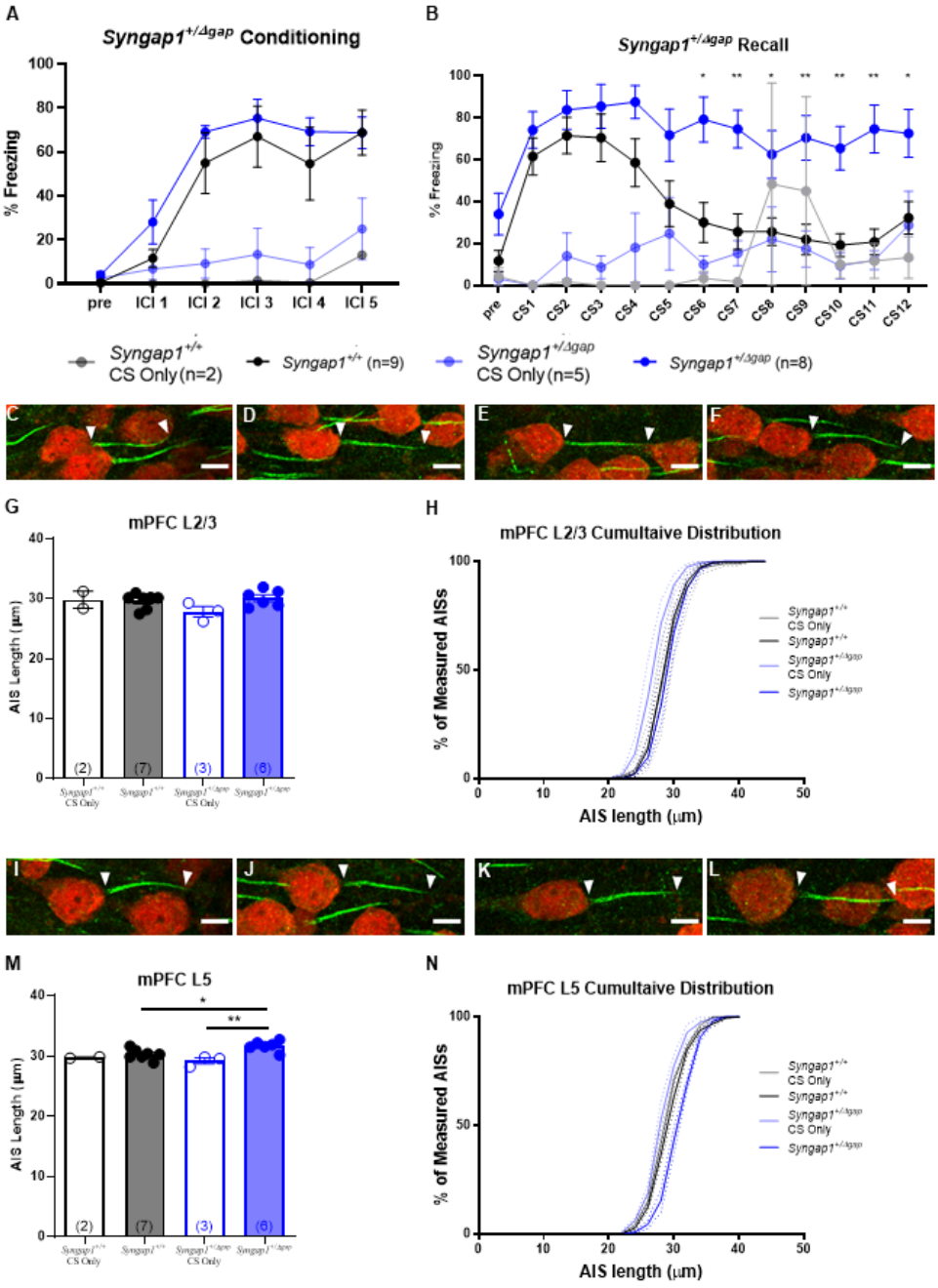

Figure 4.7: AIS lengths in mPFC PL L2/3 and L5 of fear conditioned *Syngap1*$^{+/+}$ and *Syngap1*$^{+/\Delta Gap}$ rats (A) FC shows that *Syngap1*$^{+/\Delta Gap}$ rats freeze at comparable levels to *Syngap1*$^{+/+}$ levels (*Syngap1*$^{+/+}$ CS only n=2, *Syngap1*$^{+/+}$ FC n=9, *Syngap1*$^{+/\Delta Gap}$ CS only n=5, *Syngap1*$^{+/\Delta Gap}$ FC n=8) (B) Fear Recall /Extinction shows that *Syngap1*$^{+/\Delta Gap}$ FC rats recall at levels similar to *Syngap1*$^{+/+}$ rats and significantly higher than CS only controls (C-F) Representative single AISs with arrows representing the proximal and distal ends from PL L2/3 of *Syngap1*$^{+/+}$ CS only (C), *Syngap1*$^{+/+}$ (D), *Syngap1*$^{+/\Delta Gap}$ CS only (E) and *Syngap1*$^{+/\Delta Gap}$ (F) rats. Scale bar=10 μm. (G, H) No change in average AIS length or cumulative distribution of AIS lengths was observed in PL L2/3 of rats of either genotype or condition. (I-L) Representative single AISs with arrows representing the proximal and distal ends from PL L5 of *Syngap1*$^{+/+}$ CS only (I), *Syngap1*$^{+/+}$ (J), *Syngap1*$^{+/\Delta Gap}$ CS only (K) and *Syngap1*$^{+/\Delta Gap}$ (L) rats. Scale bar=10 μm. (M, N) Average AIS length and cumulative AIS lengths were significantly increased in *Syngap1*$^{+/\Delta Gap}$ FC rats compared to *Syngap1*$^{+/\Delta Gap}$ CS only rats as well as *Syngap1*$^{+/+}$ FC rats.

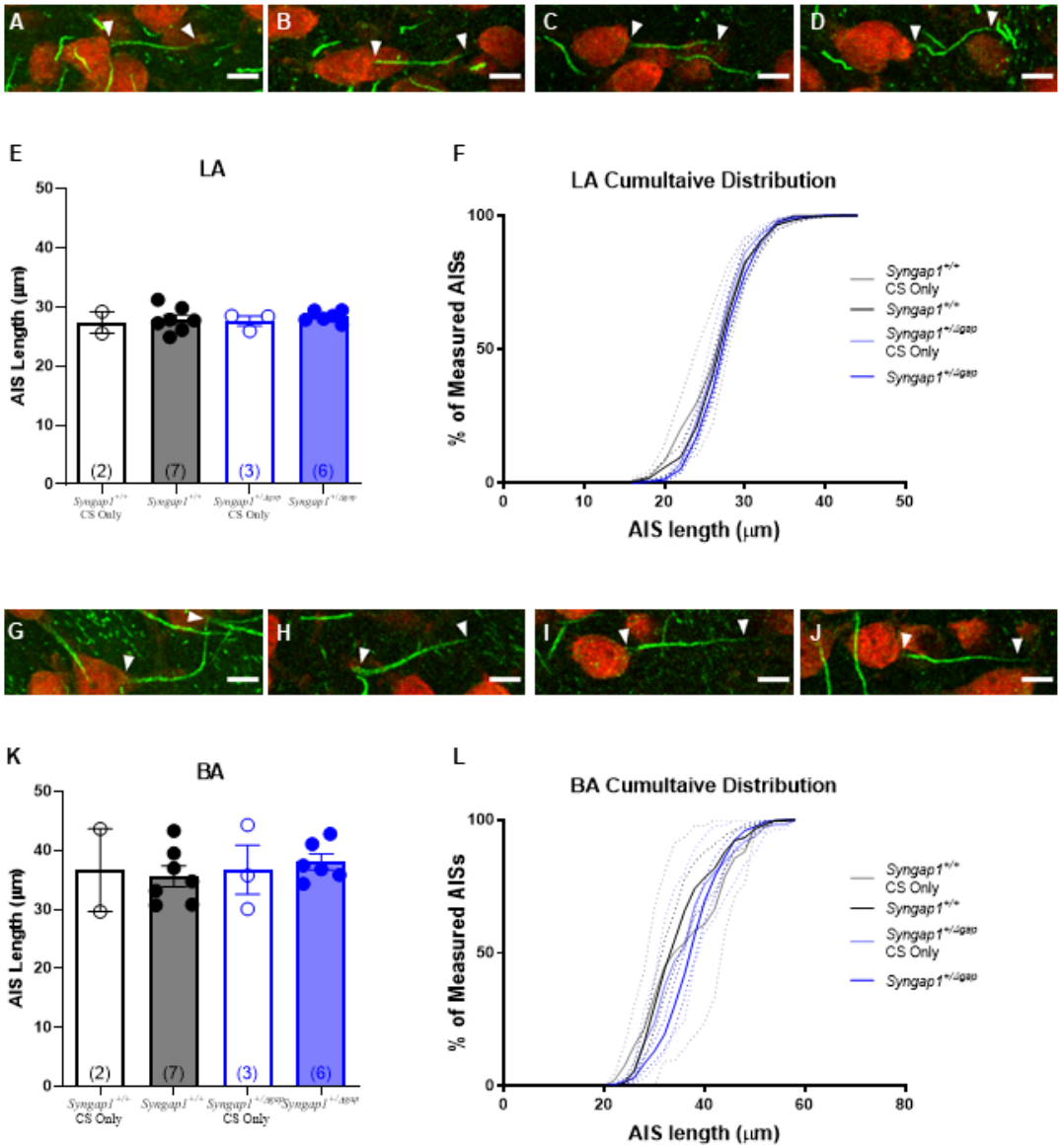

Figure 4.8: AIS lengths in LA and BA of fear conditioned *Syngap1*$^{+/+}$ and *Syngap1*$^{+/\Delta Gap}$ rats (A-D) Representative single AISs with arrows representing the proximal and distal ends from the LA of *Syngap1*$^{+/+}$ CS only (A), *Syngap1*$^{+/+}$ (B), *Syngap1*$^{+/\Delta Gap}$ CS only (C) and *Syngap1*$^{+/\Delta Gap}$ (D) rats. Scale bar=10 μm. (E, F) No change in average AIS length (*Syngap1*$^{+/+}$ CS only= 27.35 $\pm$ 1.84 n=2, *Syngap1*$^{+/+}$= 27.82 *pm* 0.80 n=7, *Syngap1*$^{+/\Delta Gap}$ CS Only= 27.59 $\pm$ 0.84 n=3 and *Syngap1*$^{+/\Delta Gap}$ = 28.35 *pm* 0.39 n=6 animals) or cumulative distribution of AIS lengths was observed in rats of either genotype or condition. (G-J) Representative single AISs with arrows representing the proximal and distal ends from the BA of *Syngap1*$^{+/+}$ CS only (G), *Syngap1*$^{+/+}$ (H), *Syngap1*$^{+/\Delta Gap}$ CS only (I) and *Syngap1*$^{+/\Delta Gap}$ (J) rats. Scale bar=10 μm. (K, L) No change in average AIS length (*Syngap1*$^{+/+}$ CS only= 36.62 $\pm$ 7.01 n=2, *Syngap1*$^{+/+}$= 35.59 *pm* 1.76 n=7, *Syngap1*$^{+/\Delta Gap}$ CS Only= 36.69 $\pm$ 4.14 n=3 and *Syngap1*$^{+/\Delta Gap}$ = 38.04 *pm* 1.31 n=6 animals) or cumulative distribution of AIS lengths was observed in rats of either genotype or condition

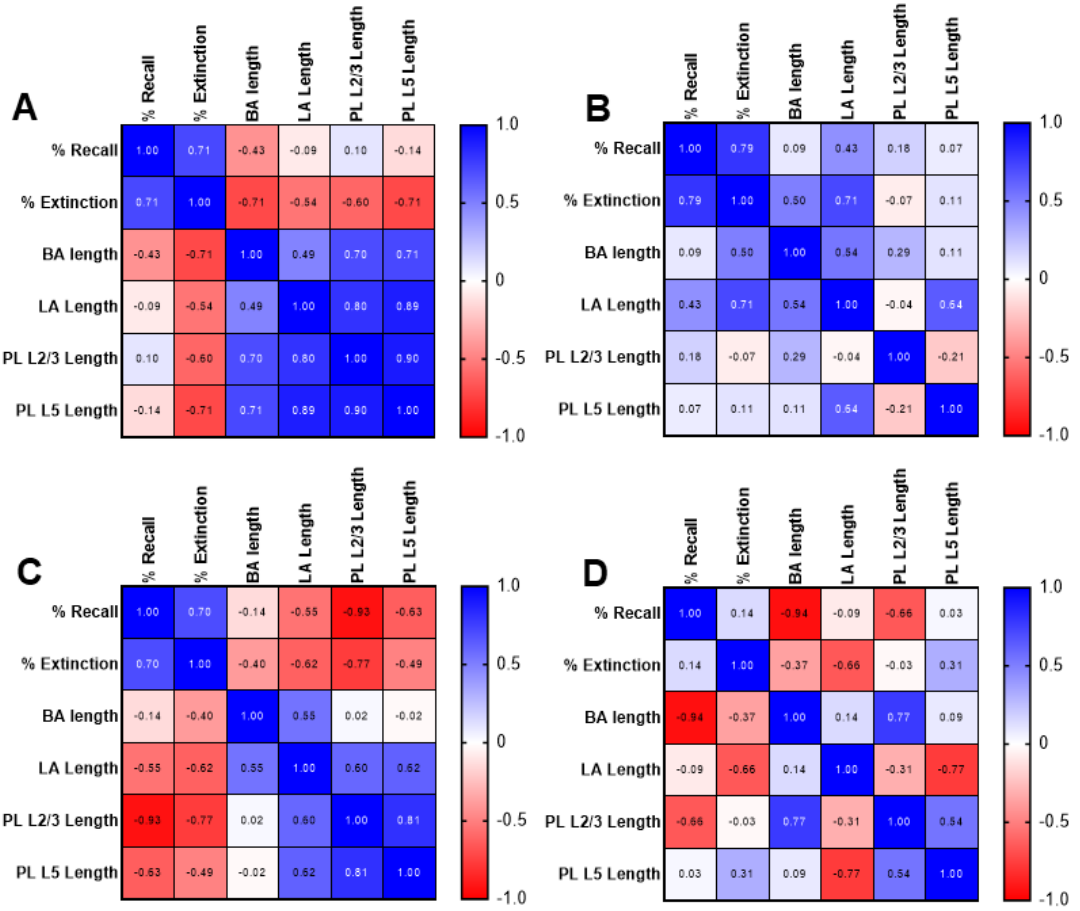

Figure 4.9: Spearman's correlation data of AIS lengths with fear recall and extinction in *Syngap1*$^{+/-}$ and *Syngap1*$^{+/\Delta Gap}$ rats No significant correlation of AIS lengths in any of the brain regions analysed to %Recall or %Extinction in WT FC rats from either the *Syngap1*$^{+/-}$ cohort, *n=6* (A) or the *Syngap1*$^{+/\Delta Gap}$ cohort, *n=7* (B) (C) Statistically significant negative correlation was found between PL L2/3 AIS length with both %Recall (r^2= -0.934, p= 0.002) and %Extinction (r^2= -0.766, p=0.032) in *Syngap1*$^{+/-}$ FC rats, *n=8* (D) Statistically significant negative correlation was seen between BA AIS length with %Recall (r^2= -0.943, p= 0.017) in *Syngap1*$^{+/\Delta Gap}$ FC rats, *n=6*.

4.2.3 Sub-Population Specific changes to AIS length

Reciprocal monosynaptic connectivity between the mPFC and the BLA (Bacon et al., 1996; Verwer et al., 1996; Mcdonald et al., 1996; Krettek and Price, 1977; Gabbott et al., 2005; Hoover and Vertes, 2007) is crucial for mediating fear-associated learning, memory consolidation and emotional regulation (Burgos-Robles et al., 2017; Klavir et al., 2017; Davis and Whalen, 2001). Disruption of this circuit has been implicated in a variety of anxiety-related disorders including post-traumatic stress disorder (PTSD) (Burghy et al., 2012) and obsessive-compulsive disorder (Sun et al., 2019). Altered anxiety states are a common comorbidity of ASD/ID (for review see Kerns and Kendall (2012)), and perturbations in mPFC and BLA circuits in pre-clinical models of these disorders has previously been reported (Markram et al., 2008; Rinaldi et al., 2008; Testa-Silva et al., 2012; Selleck et al., 2018). Moreover, fear-conditioning in rodents has specifically been shown to alter the intrinsic excitability of mPFC-BLA projection neurons (Song et al., 2015) and a key regulator of intrinsic cellular excitability is the axon initial segment (for review see (Kole and Stuart, 2012)). The AIS is known to regulate its length in an activity dependent manner and in mice fear conditioning is shown to result in the elongation of the AIS in BA-mPFC projection neurons. Further, in a rat model of Fragile-X syndrome that is known to have impaired fear-associated learning (see appendix fig.S2), mPFC-BLA projection neurons are shown to have shorter AISs compared to wildtype controls (see appendix fig.S1, Jackson (2016)). Given that the rat models of *Syngap1* haploinsufficiency present with altered fear-memory and mouse models of FXS and *SYNGAP1*-ID have previously been shown to have convergent cellular phenotypes, I hypothesized that AIS lengths specifically within mPFC-BLA and BLA-mPFC projection neurons would be differentially altered at a baseline condition (without being subjected to any learning paradigms) in our rat model.

In order to test this hypothesis, I used a retrograde tracing approach (fig.4.10A, fig4.11A). Physiologically inert beads tagged with rhodamine fluorophores were stereotaxically injected into the mPFC and BLA to study reciprocal connectivity within the same subject. 'Red' beads (excitation wavelength 530nm) were injected into the mPFC of the right hemisphere (fig.4.10B, C) while 'green' beads (excitation wavelength 460nm) were injected into the BLA of the left hemisphere (fig.4.11B, C). Due to previously reported inter-hemispheric asymmetry in amygdala size (Jung et al., 2018) and connectivity (Polli et al., 2009), the same hemispheres were injected in all animals. AIS lengths in the BLA and mPFC of the ipsilateral hemisphere to

the site of injection were measured.

AIS lengths in BLA-mPFC projection neurons

Injection of retrobeads into the mPFC showed that cells projecting to this region were found predominantly in the basal nuclei of the BLA (fig.4.10A-D), as has previously been shown (Song et al., 2015; McGarry and Carter, 2017; Sun et al., 2019). No change in average AIS length or cumulative distribution of AIS lengths was observed in BLA-mPFC projection neurons in adult (P90-120) *Syngap1*$^{+/-}$ rats compared to wildtype, littermate controls (fig.4.10G, *Syngap1*$^{+/+}$= 42.20 $\pm$ 1.37 n=6, *Syngap1*$^{+/-}$= 40.99 $\pm$ 1.03 n=8 animals). However, the sub-population of BLA-mPFC projection neurons of both WT and *Syngap1*$^{+/-}$ rats showed differential distribution of AIS lengths compared to those of the whole-population BA neurons. In WT animals, values for mean, minimum and maximum measured AIS lengths showed a slight increase in BLA-mPFC neurons accompanied by decreased overall range of AIS lengths (table. 4.5), however the difference in mean AIS length values was not statistically significant (Two-way ANOVA with Bonferroni's correction for multiple comparisons, p=0.8092). Similar to WT animals, BLA-mPFC projection neurons in *Syngap1*$^{+/-}$ rats showed slightly increased, but not statistically significant (Two-way ANOVA with Bonferroni's correction for multiple comparisons, p=0.6722), average AIS lengths (table. 4.5). Minimum and maximum measured AIS lengths were also increased in *Syngap1*$^{+/-}$ rats, similar to WT animals, while the range showed a ~2μm increase than those measured in age-matched whole-population BA neurons of *Syngap1*$^{+/-}$ rats. In both genotypes, mean AIS lengths of BLA-mPFC neurons were significantly higher than whole-population LA neurons (Two-way ANOVA with Bonferroni's correction for multiple comparisons, p=<0.0001). Overall, the data indicates that within AIS lengths of BLA-mPFC sub-population neurons was not significantly different from the general population of BA neurons and that *Syngap1* haploinsufficiency did not cause a sub-population specific alteration in AIS length in BLA-mPFC neurons.

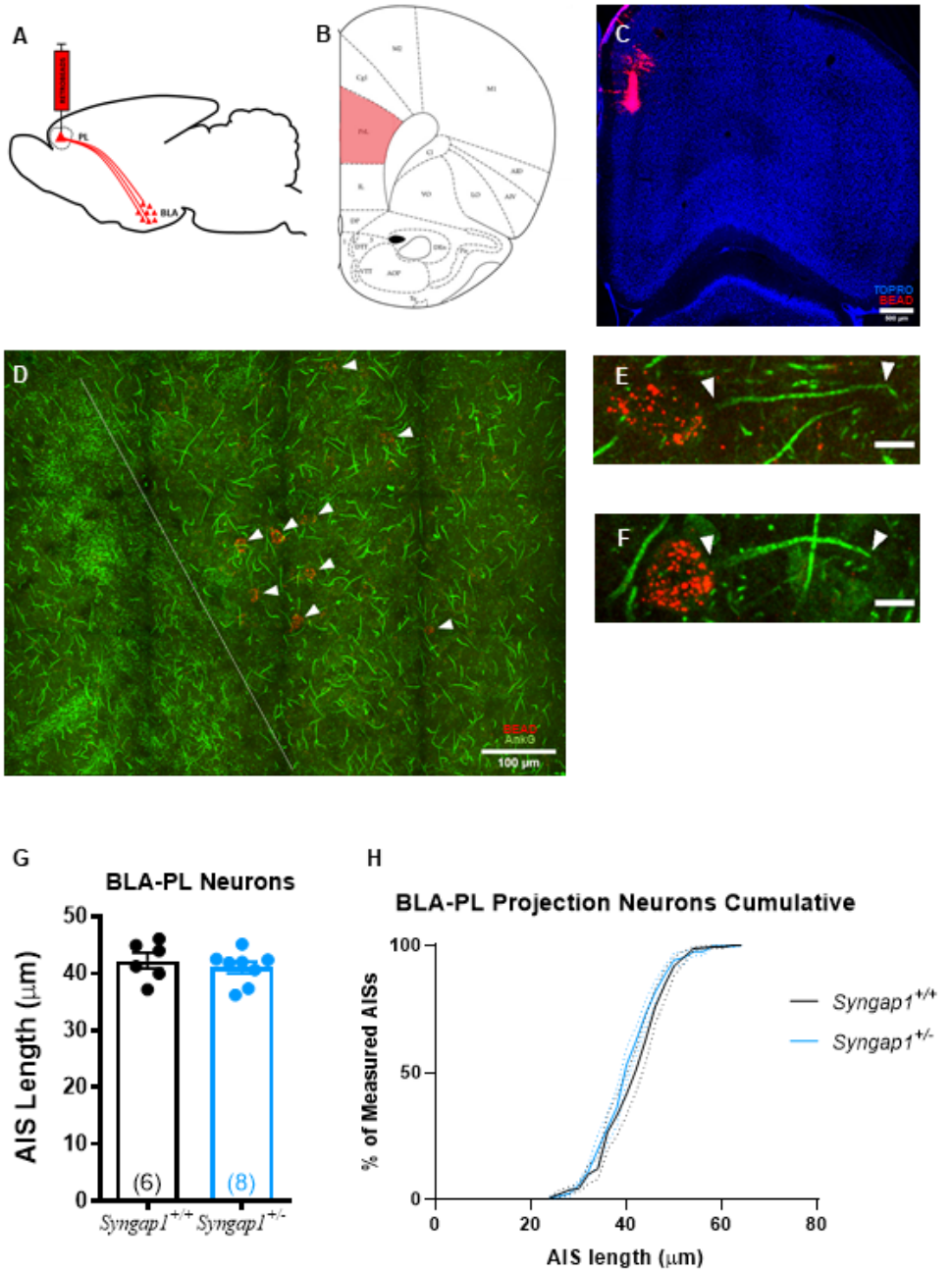

Figure 4.10: AIS lengths in BLA-PL projecting neurons of *Syngap1*$^{+/+}$ and *Syngap1*$^{+/-}$ rats (A) Schematic showing the retrograde labelling strategy (B) Schematic of a coronoal section of the rat brain at AP = +3.00, DV = $\pm$0.6 with the red region highlighting the region of the PL targeted by the stereotaxic injection (C) Example image of injection site targetting the PL. Beads contain a 530 fluorophore, counter-stained with TOPRO (D) Representative stitched imafe of the BLA used for analysis. White arrows identify successfully labelled cells and the white dashed line denotes the external capsule. (E-F) Representative single AISs with arrows representing the proximal and distal ends of *Syngap1*$^{+/+}$ (E) and *Syngap1*$^{+/-}$ (F) rats. Scale bar=10 μm. (G, H) No change in average AIS length (*Syngap1*$^{+/+}$= 42.20 $\pm$ 1.37 n=6, *Syngap1*$^{+/-}$= 40.99 $\pm$ 1.03 n=8 animals) or cumulative distribution of AIS lengths was observed in *Syngap1*$^{+/-}$ rats compared to controls

BLA-mPFC vs BLA			
		Syngap1$^{+/+}$	*Syngap1*$^{+/-}$
Mean Length	BLA-mPFC	42.20 μm	40.99 μm
	BA	40.07 μm	38.42 μm
	LA	29.13 μm	28.31 μm
Min Length	BLA-mPFC	37.14 μm	36.18 μm
	BA	31.53 μm	35.54 μm
	LA	28.07 μm	26.60 μm
Max Length	BLA-mPFC	46.04 μm	45.11 μm
	BA	43.69 μm	41.80 μm
	LA	33.66 μm	32.43 μm
Range	BLA-mPFC	8.89 μm	8.93 μm
	BA	12.16 μm	6.26 μm
	LA	3.28 μm	3.27 μm

Table 4.5: Comparison of AIS lengths in BLA-mPFC projecting cells and whole-population BLA cells

AIS lengths in PL-BLA projection neurons

Injection of the retrobead into the BLA showed that cells of both PL L2/3 and L5 project to the BLA (fig.4.11A-D), as has been previously shown (Hoover and Vertes, 2007). No differences in either average AIS length or cumulative distribution of AIS lengths was observed in *Syngap1*$^{+/-}$ rats compared to WT controls (fig.4.11G, H *Syngap1*$^{+/+}$= 29.24 $\pm$ 0.73 μm n=5, *Syngap1*$^{+/-}$= 28.67 $\pm$ 0.41 μm n=8 animals). Compared to the measurements of AIS length made in neurons of PL at a whole-population level in adult WT animals, PL-BLA projection neurons showed significantly reduced mean AIS length compared to the mean in PL L5 neurons (*Syngap1*$^{+/+}$ PL-BLA= 26.80 $\pm$ 0.7306 μm, L2/3= 30.59 $\pm$ 0.3717 μm, L5= 30.52 $\pm$ 0.6533 μm, p=0.0206) but not PL L2/3 neurons (p=0.0931). This decrease in average length was accompanied by decreased minimum measured AIS length in PL-BLA projection neurons compared to neurons in both PL L2/3 and PL L5 while overall range of AIS lengths was increased (see table.4.6). Similarly in *Syngap1*$^{+/-}$ rats, average AIS length of PL-BLA projection neurons was significantly reduced in comparison to average length of PL L5 neurons (*Syngap1*$^{+/-}$ PL-BLA= 28.67 $\pm$ 0.4140 μm, L2/3= 29.05 $\pm$ 0.6352 μm L5= 31.06 $\pm$ 0.4998 μm, p=0.0435) but not neurons of PL L2/3 (p=0.9959). Minimum and maximum measured AIS length in PL-BLA neurons of *Syngap1*$^{+/-}$ rats also matched those of WT PL-BLA neurons and were shorter than those measured in PL L2/3 or L5 whole-population neurons with an increased range of measured AIS lengths. Overall the data indicates that *Syngap1* haploinsufficiency did not result in altered mean AIS length in PL-BLA projection neurons when compared to the

same sub-population in wildtype littermate controls or when compared to mean AIS lengths of PL L2/3 and L5 neurons of WT controls.

PL-BLA vs PL			
		Syngap1$^{+/+}$	*Syngap1*$^{+/-}$
Mean Length	PL-BLA	29.24 μm	28.67 μm
	PL L2/3	31.55 μm	29.05 μm
	PL L5	33.14 μm	31.06 μm
Min Length	PL-BLA	26.80 μm	26.81 μm
	PL L2/3	30.59 μm	28.36 μm
	PL L5	30.52 μm	30.29 μm
Max Length	PL-BLA	30.86 μm	29.84 μm
	PL L2/3	32.39 μm	30.95 μm
	PL L5	33.66 μm	32.43 μm
Range	PL-BLA	4.05 μm	3.02 μm
	PL L2/3	1.80 μm	2.59 μm
	PL L5	3.13 μm	2.13 μm

Table 4.6: Comparison of AIS lengths in PL-BLA projecting cells and whole-population PL cells

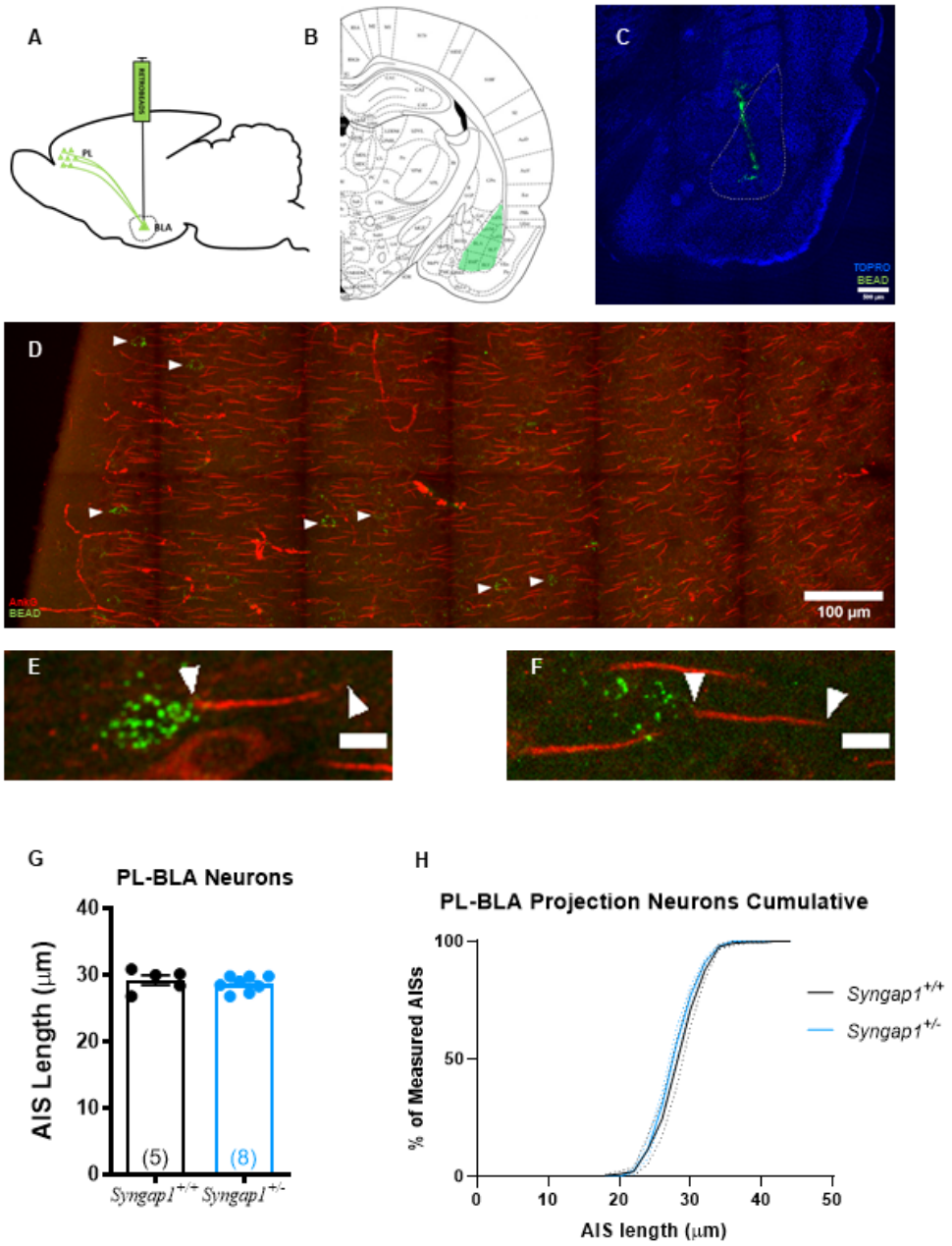

Figure 4.11: AIS lengths in PL-BLA projecting neurons of *Syngap1*$^{+/+}$ and *Syngap1*$^{+/-}$ rats (A) Schematic showing the retrograde labelling strategy (B) Schematic of a coronoal section of the rat brain at AP = -3.00, DV = $\pm$5.2 with the green region highlighting the BLA targeted by the stereotaxic injection (C) Example image of injection site targetting the BLA (outlined in white dotted line). Beads contain a 488 fluorophore, counterstained with TOPRO (D) Representative column stack of the PL used for analysis with white arrows identifying successfully labelled cells. (E-F) Representative single AISs with arrows representing the proximal and distal ends of *Syngap1*$^{+/+}$ (E) and *Syngap1*$^{+/-}$ (F) rats. Scale bar=10 μm. (G, H) No change in average AIS length (*Syngap1*$^{+/+}$= 29.24 $\pm$ 0.73 n=5, *Syngap1*$^{+/-}$= 28.67 $\pm$ 0.41 n=8 animals) or cumulative distribution of AIS lengths was observed in *Syngap1*$^{+/-}$ rats compared to controls

4.3 Discussion

The chief hypothesis tested in this chapter is that reduction in SynGAP alters *in vivo* morphological plasticity of the AIS. Specifically, analysis and comparison of genotype specific changes in AIS morphology over development was undertaken in neurons of the mPFC PL and the BLA. However, *Syngap1* haploinsufficiency did not alter age-dependent changes to AIS length in neurons of the LA, BA and PL L5, but showed a modest difference in age-dependent changes in AIS lengths of PL L2/3 neurons.

Subsequently, adaptation of AIS length following a cued fear conditioning (FC) associative-learning paradigm was analysed.The main results from this analysis revleaved that haploinsufficiency of SynGAP's GAP domain is sufficient to drive exaggerated fear recall behaviour, which in-turn is correlated with a reduction in AIS length, and haploinsufficiency of the full-length protein and the GAP domain differentially alter AIS lengths post FC in PL L2/3 and L5.

Finally, cell-type specific alterations in AIS length between reciprocal mPFC-BLA projection neurons was undertaken but no genotype specific alterations in mean or distribution of AIS lengths was observed in either sub-population.

4.3.1 Analysis of AIS lengths at different ages

Evidence of developmentally regulated plasticity of AIS length *in vivo*, with the consequent fine-tuning of neuronal firing, have been seen on the time-scale of days (Kuba et al., 2015), weeks (Gutzmann et al., 2014) and months (Cruz et al., 2009). Here, I examined AIS length over the course of normal development in adult (P90-120) animals of *Syngap1* haploinsufficiency and compared the results across genotypes to those obtained in juvenile (P28-32) animals described in chapter 3, with 4-6 week age difference between the animals. Reduction in SynGAP levels results in an exaggerated freezing response on re-call of fear memory, formed in a cued fear conditioning (FC) paradigm, with little to no extinction (ranging from 10.28-11.54% $\pm$ 6.20-8.59%) of this response. The prefrontal- amygdala circuitry is crucial for the appropriate formation and expression of fear and anxiety-related memories. Therefore, analysis was focused

on neurons of the PL and the BLA, which are known to alter their excitability in response to FC-induced learning.

Comparison of AIS lengths between juvenile and adult rats revealed two key findings. First, the distribution of AIS lengths in WT animals at P90-120 in all regions examined show a significant shift in AIS lengths towards longer lengths, without any statistically significant increase in mean length in neurons of PL L2/3, L5 and the BA and with statistically significant increase in the LA. Maturation of neuronal circuits with age results from altered synaptic and cellular excitability with corresponding elongation in AIS length in the rodent cortex (Gutzmann et al., 2014). The results from WT animals thus imply that in juvenile animals there is greater variability in AIS lengths due to differential maturation states of the neurons, while in adult animals neuronal maturity, and AIS lengths, are more homogenous. Similar to the alteration seen in WT animals, *Syngap1*$^{+/-}$ rats also show a shift in the cumulative distribution of AIS lengths towards longer lengths in adult animals in all brain regions examined with the exception of neurons in PL L2/3. Neurons of the PL have afferent projections to multiple targets, including the hippocampus, BLA, the medial-basal forebrain, the midline thalamus and the monoaminergic nuclei of the brain-stem (Hoover and Vertes, 2007; Song and Moyer, 2018). Depending on their projection target, neurons exhibit differential excitability, which may be accompanied by differences in AIS lengths (Senn et al., 2014; Yamashita et al., 2018). Thus, the failure of PL L2/3 neurons of *Syngap1*$^{+/-}$ rats to show elongation with age similar to those observed in PL L5, BA and LA could be attributed to altered cellular activity and AIS lengths of a sub-population of neurons projecting to a specific target. The argument of different sub-populations of neurons showing differential AIS length can also be extended to explain the high degree of variability observed in both the average and cumulative AIS length distribution of neurons in the BA across ages and genotypes. Similar to the mPFC, pyramidal cells the BA show afferent projections to multiple brain-regions with neurons differentially controlling behaviour and cellular excitability depending on the projection target (Verwer et al., 1996; Mcdonald et al., 1996; Arruda-Carvalho et al., 2017). Given that plasticity of AIS length is known to be dependent on altered synaptic stimuli (Kuba et al., 2015), the converse argument that AIS length of a neuron will be differentially altered depending on site of origin of efferent projections is equally valid. Further, a study by Beyeler et al. (2018) shows that anatomical organisation of the BLA affects cellular function such that pyramidal neurons express different intrinsic excitability depending on its location along the anterior-posterior axis of the BLA. Although the sections containing the

BLA chosen for AIS analysis were matched by hippocampal size, this matching was visually estimated allowing for errors. Therefore, another explanation for the increased variability in AIS lengths measured from neurons in the BA could be neuron location along the AP axis.

AIS analysis within a specific sub-population

The experimental and analytical design of described above occludes the identification of sub-population specific changes. Given the importance of reciprocal PL-BLA projections in fear memory formation (Arruda-Carvalho and Clem, 2015) and the exaggerated recall of fear memory upon reduction of SynGAP, I performed within subject examination of AIS lengths in PL neurons projecting to the BLA and vice-versa. Results showed no significant alterations in AIS length in either sub-population examined in *Syngap1*$^{+/-}$ rats compared to wildtype controls; indicating that AIS lengths - and its mediated cellular excitability - are unaltered in these neuronal sub-populations and do not underlie the exaggerated fear-memory recall phenotype seen in this preclinical model of *Syngap1* haploinsufficiency.

However, one technical reason for a lack of genotype specific alterations in AIS length in PL-BLA projection neurons might be bleed-through between the channels in which the different beads were imaged (fig.S7). The experiment was designed such that AIS lengths from both PL-BLA neurons and BLA-mPFC neurons could be analysed within the same subject, reducing inter-animal variability between sub-populations. Briefly, the contra-lateral hemisphere of the PL analysed for AIS lengths was injected with the 'red' bead while the ipsilateral BLA was injected with the 'green' bead. PL cortices of both hemispheres show extensive connectivity (Vertes, 2004), therefore the presence of beads of both colours in the images PL section was expected. Furthermore, neurons of the PL have previously been shown to project to more than one target region (McGarry and Carter, 2017), therefore the presence of double labelled 'yellow' cells in the analysed sections was also expected. However, the high degree of spatial overlap between fluorescent beads was suggestive of a technical issue (fig.S7B). To circumvent this complication, I applied stringent filter-settings during image acquisition to minimise channel bleed-through and restricted analysis of AIS lengths to only neurons show single-labelling with 'green' beads. A resulting caveat of this decision was that, in order to reach the minimum required AIS lengths to perform statistical analysis, neurons used for AIS analysis were pooled

across different cortical layers and along a wider rostro-caudal axis than used for any of the other modes of analysis. Previous studies reporting differences in cellular activity of this sub-population have restricted analysis to L5 neurons as pyramidal neurons from different cortical layers have different electrical properties (Song and Moyer, 2018). A biological explanation of the high-degree of spatial overlap seen in the doube-labelled cells could be bead sequestration. Within the BA to mPFC sub-population, there was no evidence of double-labelled cells. Lastly, while differences in the rostro-caudal axis of the injection site could result in labelling of different sub-populations of projection neurons, injection volumes was kept deliberately small and neurons from only those animals where the brain region of interest was successfully targeted by injection were included in the final analysis (see appendix fig. S5, S6).

AIS length mediation is only one mode of control of neuronal excitability. Particularly, alterations in learning and memory are associated with alterations in synaptic plasticity (Sehgal et al., 2013). Reduction in SynGAP levels is associated with synaptic plasticity impairments along with altered dendritic spine dynamics (Carlisle et al., 2008; Clement et al., 2012; Aceti et al., 2015; Araki et al., 2015). Therefore, other factors that might underlie the altered fear memory in the *Syngap1*$^{+/-}$ rat is AIS-independent alterations in cellular excitability and synaptic plasticity including alterations in number, density and function of voltage-gated ion channels and neurotransmitter receptors at dendritic spines and cell soma, number of functional synapses and altered pre-synaptic release probability. Electrophysiological characterisation of these cells should be undertaken to gain a better understanding of the underlying cellular and synaptic alterations.

4.3.2 Activity dependent changes to AIS length upon loss of SynGAP

In vivo experience-dependent plasticity of AIS morphology have been established through studies of sensory deprivation (Kuba et al., 2015; Gutzmann et al., 2014; Schlüter et al., 2017). Further, preliminary data shows elongation of AIS length in BA-PL projection neurons in adult wildtype mice 24 hours post fear conditioning (personal correspondence A L̈(u)thi). Whether these changes in AIS-length are accompanied by alterations in cellular excitability are not yet known. Given that we know BA-PL projection neurons show no alterations in AIS length in *Syngap1*$^{+/-}$ rats and that these rats show exaggerated fear-memory recall, I hypothesized that

following fear-conditioning, BA-PL projection neurons of *Syngap1*$^{+/-}$ rats would show altered experience dependent alteration in AIS length compared to CS only controls and wildtype animals subjected to FC. However, due to limitations of protocol severity set by the UKBA Home Office in the project license under which these experiments were performed, I analysed alterations in AIS length in whole population PL L2/3, L5 and BLA neurons. Specifically, both surgeries for stereotaxic injection of retrobeads and fear-conditioning are classified as protocols of 'moderate' severity. On the project license under which these experiments were performed each animal could only be subjected to one moderate procedure, therefore to perform both retrobead injections and fear conditioning on the same animal would have resulted in being in breach of the license. To avoid being in breach a new project license application was made to allow for two moderate procedures to be undertaken on the same animal, however license approval was pending at the time these experiments were undertaken. Thus, both retrobead injection and fear conditioning experiments were conducted on different cohorts of animals.

Post FC, both *Syngap1*$^{+/-}$ and *Syngap1*$^{+/\Delta Gap}$ rat models of *SYNGAP1*-ID show exagerrated recall of fear memory. Despite this similarity in behaviour, distinct alterations in AIS lengths were observed in these animals post FC. *Syngap*$^{+/-}$ rats show a significant shift in the cumulative distribution of AIS lengths measured in PL L2/3 neurons towards shorter lengths. This shift is reminiscent of the trend of shorter AIS length observed in PL L2/3 neurons of adult *Syngap*$^{+/-}$ animals (in comparison to WT age-matched controls) not subjected to fear conditioning (table.4.1). While, *Syngap1*$^{+/\Delta Gap}$ rats show increased average AIS lengths with a shift in cumulative distribution towards longer AIS lengths in neurons of PL L5 (when compared to WT and CS only controls). Suggesting that haploinsufficiency of the GAP domain and the full length protein might cause alterations in cellular excitability in a cell-type/ brain-region specific manner despite exhibiting similar behavioural abnormalities. This idea is further supported by correlational analysis run between the % freezing exhibited by an animal during recall and the AIS length of neurons in the various sub-regions analysed. *Syngap1*$^{+/\Delta Gap}$ FC rats showed a strong negative correlation of AIS length with % freezing exhibited by the during recall while *Syngap1*$^{+/-}$ FC rats showed a significant, negative correlation between % freezing exhibited during recall and AIS lengths measured in neurons of PL L2/3. Of note is the high percentage of freezing seen in *Syngap1*$^{+/-}$ and *Syngap1*$^{+/\Delta Gap}$ CS Only animals towards the end of the recall protocol (CS 8-12). While it was evident during analysis of behaviour that the animals had fallen asleep, the time spent immobile still fulfilled the criteria set for a 'freezing' response, and

thus the data was not discarded.

Interestingly, the data presented here shows that the plasticity of AIS length observed in wildtype mouse basal amygdala following fear conditioning is not recapitulated in WT rats. The evident reason for this lack of recapitulation is that their AIS analysis was conducted in BA-PL projection neurons whereas my analysis was conducted at the whole population level. However, species specific differences, as is seen in chapter 5, and difference in fear-conditioning protocol (auditory vs visual cue) could influence AIS length alteration in these neurons. Notably, unpublished work from the laboratory shows that *Syngap1*$^{+/-}$ rats subjected to an auditory cued fear conditioning paradigm exhibit reduced, and not exaggerated, levels of freezing during recall of fear memory.

The work under-taken in this chapter is part of an on-going project with additional experiments underway. Specifically, analysis of AIS lengths in the PL and the BLA and their sub-populations of adult *Syngap1*$^{+/\Delta Gap}$ rats, the effect of fear-conditioning and extinction on the AIS lengths of PL-BLA and BLA-mPFC projecting neurons and neurons of the infralimibic cortex of *Syngap1*$^{+/\Delta Gap}$ and *Syngap1*$^{+/-}$ rats are being carried out.

The data presented here provides the first evidence of *Syngap1* haploinsufficiency causing differential experience-dependent alterations in AIS-morphology. The similarities in results from assessment of fear memory recall in *Syngap1*$^{+/\Delta Gap}$ and *Syngap1*$^{+/-}$ rats implies that haploinsufficiency of GAP domain function is sufficient to cause an exaggerated recall phenotype. Given that the neural circuits underlying fear memory formation in rodents also underlie, to a degree, the development of threat and aggression related behaviours in humans (for review see Arruda-Carvalho et al. (2017)), GAP domain haploinsufficiency may underlie the increased aggression and threat-like behaviours exhibited by individuals with *SYNGAP1*-ID (Krepischi et al., 2010; Klitten et al., 2011; Parker et al., 2015; Vlaskamp et al., 2019). Further, it presents evidence of cell-type specific alteration of this AIS length plasticity depending on the nature of the protein haploinsufficiency, suggesting different underlying biological mechanisms in these disorders. Lastly, it is the first study to show age-dependent increase in AIS length in the basal and lateral nucleus of the amygdala. Electrophysiological characterisation will need to be undertaken to establish the altered cellular excitability of these neurons.

Chapter 5

Convergence of AIS pathology across models of monogenic forms of ASD/ID

5.1 Introduction

Identification of low frequency *de novo* mutations and candidate gene loci in patients with developmental disorders such as ASD/ID using exome sequencing and genome-wide association studies (GWAS) have led to the prediction of hundreds of risk loci underlying sporadic cases of disease (Iossifov et al., 2012; Devlin et al., 2012; O ' Roak et al., 2012; Sanders et al., 2012; Hormozdiari et al., 2015). This genetic heterogeneity notwithstanding, there is evidence that candidate genes cluster into distinct subsets based on biological function and protein-protein interaction (O'Roak et al., 2012; Allen et al., 2013; Gulsuner et al., 2013; Mitra et al., 2013; Parikshak et al., 2013; Willsey et al., 2013). These clusters include genes encoding regulators of transcription (*MECP2, FOXP1*) (Amir et al., 1999; Iossifov et al., 2014), chromatin modification (*CHD8, ARID1B*) (De Rubeis et al., 2014; Sanders et al., 2015)), translation (*FMR1, SYNGAP1, PTEN*) (Osterweil et al., 2010; Barnes et al., 2015; Hopkins et al., 2014; Myers et al., 1998), proteasome mediated degradation (*UBE3A*) (Kishino et al., 1997; Louros and Osterweil, 2016), synapse formation and maintenance (*SHANK3, NLGN3, 4, NRX1, CNTNAP2*) (De Rubeis et al., 2018).

Furthermore, a common feature of many of these mutations includes altered cellular and circuit excitability, either as a result of excitation/inhibition (E/I) imbalance or impaired homoeostasis (Rubenstein and Merzenich, 2003; Gogolla et al., 2010; Nelson and Valakh, 2015; Bourgeron, 2015). E/I imbalance in ASD have been reported both as a consequence of increased excitation, particularly the number of glutamatergic synapses in mouse models of *Syngap1* haploinsufficiency (Clement et al., 2012; Ozkan et al., 2014; Aceti et al., 2015) and *Neurofibromatosis-1* (Cui et al., 2008), as well as diminished GABA-ergic inhibition in mouse models of FXS (Gibson et al., 2008) and Rett syndrome (Dani et al., 2005; Durand et al., 2012). Altered cellular excitability may subsequently lead to long-term changes in synaptic efficacy, manifesting as impaired or exaggerated LTP and LTD. Indeed, evidence of this is found in multiple animal models of ASD. Exaggerated mGluR-LTD is found in the *Fmr1* KO mouse model of FXS (Huber et al., 2002), *Syngap1* het mouse model of *SYNGAP1*-ID (Barnes et al., 2015) and *Ube3a* KO mouse model of Angelman's syndrome (hui Jiang et al., 1998). Impaired LTD is found in mouse models of tuberous sclerosis complex (*Tsc2* het) (Auerbach et al., 2011), *NLGN3* associated non-syndromic ID (*Nlgn3* KO) (Baudouin et al., 2012) and Cowden syndrome (*Pten* KO) (Sperow et al., 2012). LTP is found to be impaired in models of FXS (Zhao et al., 2005; Xu et al., 2012), *BRAF* and *PTPN11* models of Noonan syndrome (Lee et al., 2014), NF1 (Silva et al., 1997) and *SYNGAP1*-haploinsufficiency (Komiyama et al., 2002; Ozkan et al., 2014)) while LTP is enhanced in the *HRAS* model of Costello syndrome (Manabe et al., 2000).

The observed alterations in excitability and synaptic plasticity do not occur throughout the brain, but rather appear to be circuit specific (Varghese et al., 2017). Brain regions particularly affected include the prefrontal cortex, sensory cortices, the dorsal hippocampus and the amygdala Varghese et al. (2017). Volumetric analysis showing increased size of the dorsolateral PFC and amygdala have been consistently reported in ASD diagnosed children aged 2-5 years (Carper and Courchesne, 2005; Courchesne et al., 2011; Carper et al., 2002; Hazlett et al., 2012; Schumann et al., 2009; Sparks et al., 2002)) while a reduction in the number of parvalbumin-positive chandelier interneurons is reported in the medial PFC (Hashemi et al., 2017; Ariza et al., 2018). In the visual cortex of individuals with ASD reduced GABAergic inhibition, with preserved glutamatergic activity, is found resulting in weakened functions such as binocular rivalry (Robertson et al., 2013, 2016; Freyberg et al., 2015). In the hippocampus, decreased neuronal cell size and dendritic complexity have been reported with increased cell density in individuals with ASD (Raymond et al., 1995). This increased cell density is specifically of

calbindin-immunoreactive interneurons of the dentate gyrus whereas the CA1 and CA3 sub regions of the hippocampus show increased density of parvalbumin-immunoreactive interneurons (Lawrence et al., 2010). Anatomical studies in the amygdala have been less consistent with some studies reporting decreased size with increased neuronal density in the medial, central, and cortical amygdalar nuclei (Bauman and Kemper, 2005) while others have reported significant reductions in neuron numbers in all amygdalar nuclei in adults with ASD (Morgan et al., 2014). Neuronal changes in specific amygdalo-sensory input pathways may account for these discrepancies (Rausch et al., 2016).

As alterations in AIS length have previously been linked to altered cellular excitability as well as ASD/ ID (Kaphzan et al., 2011; Kloth et al., 2017), particularly in the *Fmr1*$^{-/y}$ mouse model of Fragile-X syndrome (Booker et al., 2019), in this chapter I analysed AIS lengths in multiple brain regions including the mPFC, S1BF, V1, CA1, CA3, BA and LA, across 5 monogenic mutations that are either known to cause syndromic or non-syndromic ASD/ ID or have been ranked 'high-confidence, causative' genes by the SFARI autism gene database (https://gene.sfari.org/database/human-gene/). These models include *Fmr1*$^{-/y}$, *Nlgn3*$^{-/y}$, *Nrx1*$^{+/-}$, *Cntnap2*$^{+/-}$ and *Pten*$^{+/-}$. The aim of this chapter is two-fold: First, to inspect if altered AIS lengths is a common feature of the above stated models that show altered cellular excitability and second to see if reported AIS alterations in the *Fmr1* KO mouse translate to our rat model. Presented below is a brief introduction to each model followed by the results from the undertaken AIS analysis.

5.2 *Fragile-X Mental Retardation 1*

The most commonly inherited form of intellectual disability affecting 1:4,000-6,000 men and 1:6,000-11,00 women is Fragile-X Syndrome (De Vries et al., 1997; Coffee et al., 2009). First described as a novel form of ID showing X-linked segregation, FXS results from an expansion of a CGG trinucleotide repeat at the 5' UTR of the fragile-X mental retardation 1 gene (*FMR1*) at Xq27.3 (Martin and Bell, 1943). The presence of >200 repeats causes hypermethylation of the gene promoter (Naumann et al., 2009; Oberlé et al., 1991) resulting in transcriptional silencing and loss of expression of the fragile-x mental retardation protein (FMRP) (Wilmar Saldarriaga, Flora Tassone, Laura Yuriko González-Teshima, Jose Vicente Forero-Forero, Sebastián Ayala-Zapata, 2014). FMRP is an RNA binding protein, regulating RNA stability, subcellular transport and acts as a translation repressor of neural mRNAs that code for proteins involved in synapse development and activity (Weiler et al., 1997; Antar et al., 2004; Bassell and Warren, 2008; Chen et al., 2003; Darnell et al., 2011). FXS is associated with a wide range of cognitive, behavioural and physical symptoms including ASD (50-66% of males and 20% of females, (Lewis et al., 2006; Wang et al., 2010; Abbeduto et al., 2014)), anxiety (86.2% of males and 76.9% of females, (Cordeiro et al., 2011)), seizures (45% in adolescents and 24% in adults >20 years (Cowley et al., 2016; Sabaratnam et al., 2001)), abnormal sensory processing resulting in hypersensitivities (Fagiolini and Leblanc, 2011) and attention disorders (Royall et al., 2002).

EEG and fMRI studies in individuals with FXS indicate brain-region specific imbalances in neuronal excitation. Castrén et al. (2003) found increased event-related potentials, implying enhanced excitability, in the auditory cortex of children with FXS while other studies have found decreased activation in the prefrontal cortex (Holsen et al., 2008) and fusiform gyrus (Dalton et al., 2008) of adolescents with FXS. Still other studies have uncovered enlargement and sensitisation of the hippocampus (Kates et al., 1997) and the amygdala in adolescent males with FXS (Watson et al., 2008; Gothelf et al., 2008). Adults with FXS show enhanced theta oscillations at the scalp, an indicator of abnormal information transfer between brain regions as well as an imbalance in excitatory and inhibitory neuronal circuit activity (Van der Molen and Van der Molen, 2013; Van Der Molen et al., 2014).

Generation of the *Fmr1*$^{-/y}$ (KO) mouse has been key to the investigation of FXS pathophysiology, as it phenocopies the human disorder (Bakker et al., 1994) and has helped gain multiple insights into the aberrant cellular processes underlying this syndrome. A defining feature of FXS is ID accompanied with reduced cognitive ability (for review see Ciaccio et al. (2017)). The predominant cellular mechanism underlying cognition and memory is synaptic plasticity, the ability of a synapse to modulate its strength in an activity-dependent manner (Hebb, 1949). In FXS, deficits in cognition and accompanying deficits in synaptic plasticity have most extensively been studied in the hippocampus. *Fmr1*$^{-/y}$ mice show impairments in hippocampal associated spatial and short-term memory tasks including novel object recognition (Bhattacharya and Klann, 2012; King and Jope, 2013), reversal morris water maze (Gandhi et al., 2014) and Y-maze (Bhattacharya and Klann, 2012; Lim et al., 2014). In the CA1 of the hippocampus, long-term depression, a long-lasting decrease in synaptic strength, can be mediated by activation of group 1 metabotropic glutamate receptors (mGluR) either chemically or electrically and via NMDA receptor activation (Daoudal and Debanne, 2003). In the mouse model of FXS mGluR-LTD, but not NMDAR-LTD, in hippocampal CA1 region results in enhanced synaptic depression compared to wildtype controls (Godfraind et al., 1996; Paradee et al., 1999; Huber et al., 2002; Hou et al., 2006). However, no change in intrinsic membrane properties have been observed in these cells.

FMRP is expressed early in both human and murine development (Agulhon et al., 1999; Todd et al., 2003) with its loss resulting in altered critical-period plasticity in several sensory cortices. This is highlighted in the somatosensory (S1), auditory and visual (V1) cortices (Harlow et al., 2010; Dölen et al., 2007; Kim et al., 2013). In the S1, the critical period of NMDAR-dependent LTP at the thalamocortical afferents onto layer 4 (L4) spiny stellate cells occurs early in the first post-natal week (Crair and Malenka, 1995). In *Fmr1*$^{-/y}$ mice, this critical period is delayed until the second postnatal week (Harlow et al., 2010) concomitant with increased input resistance and neuronal hyper-excitability of these cells (Gibson et al., 2008). Following the closure of the L4-LTP critical period and typically during the second postnatal week, ascending connections from L4 to L2/3 pyramidal neurons develop (Weiler et al., 2008). *Fmr1*$^{-/y}$ mice show reduced connection probability at this stage of development (Bureau et al., 2008). However, both these changes in the S1 of *Fmr1* KO mice appear to be transient, normalising to WT levels by postnatal week 4, suggesting a delayed maturation of this cortical circuit (Bureau et al., 2008). However, increased sensitivity and neuronal excitability in the S1

in response to sensory stimuli was observed beyond the 4 week age point (Zhang et al., 2014).

The primary visual cortex also shows altered plasticity upon loss of FMRP. Juvenile *Fmr1*$^{-/y}$ mice exhibit loss of LTP in L5 pyramidal cells of V1 (Wilson and Cox, 2007). This loss of LTP may contribute to the 'hyperplastic' state of the V1 observed in *Fmr1*$^{-/y}$ mice. Typically, 3 days of monocular deprivation at postnatal day (P) 28 in wildtype mice results in depression of deprived eye responses and potentiation of non-deprived eye responses in the binocular region of V1 (Frenkel and Bear, 2004). In the case of *Fmr1* KO mice, an immediate potentiation of non-deprived eye responses is observed (Dölen et al., 2007) resulting in a 'hyperplastic' state. Imaging studies in adult *Fmr1*$^{-/y}$ mice revealed anatomical hyperconnectivity within the V1 with disproportionately low connectivity between the V1 and other neocortical circuits, suggesting that this hyperplastic state observed in the V1 at P28 persists into adulthood (Haberl et al., 2015).

In addition to sensory cortices, integrative cortices also show alterations in synaptic plasticity and cellular excitability in FXS. Of particular interest in FXS in the PFC, as individuals with FXS present with deficits in PFC-associated behaviours including attention, inhibitory control and cognitive flexibility (Royall et al., 2002). Similar to the patients, *Fmr1* KO mice exhibit impaired performance in PFC-mediated tasks including acquisition of visuo-spatial discrimination task (Krueger et al., 2011) and extinction of an instrumental learning task (Sidorov et al., 2014). Accompanying these behavioural deficits is abnormal synaptic plasticity, particularly deficits in LTP, in several subregions of the PFC including the anterior cingulate cortex (ACC), medial PFC (mPFC) and piriform cortex (Zhao et al., 2005; Meredith et al., 2007; Wang et al., 2008).

Other behavioural anomalies noted in *Fmr1*$^{-/y}$ mice include deficits in amygdalar dependent tasks including certain social behaviours, anxiety and fear conditioning (McNaughton et al., 2008; Paradee et al., 1999; Spencer et al., 2008). Impaired fear learning in *Fmr1* KO mice (Paradee et al., 1999) is accompanied by deficits in group1 mGluR mediated LTP at thalamic inputs to the LA (Suvrathan et al., 2010; Zhao et al., 2005), a nucleus of the amygdalar complex which forms the first node of appropriate fear memory acquisition (Romanski and LeDoux, 1992; Tsvetkov et al., 2002). Following acquisition, the basal amygdalar nucleus serves in the storage and expression of fear memory (Gale et al., 2004; Anglada-Figueroa and Quirk,

2005). Inhibitory signalling at the BA is impaired in *Fmr1*$^{-/y}$ mice, which could also contribute to the deficits observed in amygdala-mediated behaviours (Olmos-Serrano et al., 2010, 2011; Kratovac and Corbin, 2013; Martin et al., 2014; Vislay et al., 2013).

Booker et al. (2019) have found that despite the lack of altered membrane properties in pyramidal cells of the CA1 in *Fmr1*$^{-/y}$ mice, these cells show increased firing. This increased firing is accompanied by an increase in length of the axon initial segment. Given that the AIS has previously been shown to regulate cellular excitability, that cellular deficits found in the *Fmr1*$^{-/y}$ mouse are conserved in another *Fmr1*$^{-/y}$ rat model of FXS (Till et al., 2015; Asiminas et al., 2019) and a decrease in AIS length is observed in prelimbic PFC cells that project to the BLA in adult *Fmr1*$^{-/y}$ rats (Jackson, 2016), here I investigate if any AIS alterations are found in various brain regions in juvenile rats in a novel rat model of FXS.

5.2.1 Results

As mentioned above, synaptic and cellular deficits have been observed in the medial PFC, the primary somatosensory cortex S1 and the primary visual cortex V1 in the *Fmr1*$^{-/y}$ mice. Here, I assess alterations in AIS length upon loss of FMRP in these brain regions using a novel rat model of FXS (fig. 2.1, Asiminas et al. (2019)).

In the prelimbic mPFC, average AIS lengths and the cumulative distribution of AIS lengths were comparable between genotypes in L2/3 (fig.5.1B, B' *Fmr1*$^{+/y}$= 25.92 μm $\pm$ 0.51 μm n=6, *Fmr1*$^{-/y}$= 27.08 μm $\pm$ 0.75 μm n=6 animals). However, in layer 5, the average length was significantly increased (fig.5.1D *Fmr1*$^{+/y}$= 25.80 μm $\pm$ 0.60 μm n=6, *Fmr1*$^{-/y}$= 28.84 μm $\pm$ 1.10 μm n=6 animals, p=0.001) with the cumulative AIS length distribution showing a shift towards longer AIS lengths in *Fmr1*$^{-/y}$ rats compared to wildtypes (fig.5.1D').

Similar to the mPFC, no change in average AIS length or cumulative distribution of AIS lengths was seen between genotypes in S1 L2/3 (fig.5.1F, F' *Fmr1*$^{+/y}$= 29.29 μm $\pm$ 0.47 μm n=6, *Fmr1*$^{-/y}$= 29.50 μm $\pm$ 0.35 μm n=6 animals) whereas a significantly increased average length (fig.5.1J *Fmr1*$^{+/y}$= 28.80 μm $\pm$ 0.39 μm n=6, *Fmr1*$^{-/y}$= 31.39 μm $\pm$ 0.59 μm n=6 animals, p= 0.010) with a shift towards longer AIS lengths in cumulative distribution (Fig.5.1J')

was observed in S1 L5 cell of *Fmr1*$^{-/y}$ rats compared to controls. Given that cellular excitability changes have also been noted in L4 of the S1 in *Fmr1* KO mice, I also examined AIS lengths in this layer but found no changes in either average or cumulative distribution of AIS lengths in our KO rats compared to controls (fig.5.1H,H' *Fmr1*$^{+/y}$= 22.92 μm $\pm$ 0.48 μm n=6, *Fmr1*$^{-/y}$= 21.62 μm $\pm$ 0.81 μm n=6 animals).

Unlike results from the other two cortical regions, no changes were observed in average length or cumulative AIS length distribution in cells of either L2/3 or L5 of the visual cortex (V1 L2/3 fig.5.1L, L' *Fmr1*$^{+/y}$= 27.44 μm $\pm$ 0.80μm n=6, *Fmr1*$^{-/y}$= 27.77 μm $\pm$ 0.64 μm n=6 animals; V1 L5 fig.5.1N, N' *Fmr1*$^{+/y}$= 31.63 μm $\pm$ 0.51 μm n=6, *Fmr1*$^{-/y}$= 31.98 μm $\pm$ 0.55 μm n=6 animals).

The elongated AIS and its mediated alterations in cellular excitability phenotype of the *Fmr1*$^{-/y}$ mouse was observed in the CA1 sub-region of the dorsal hippocampus. Here, I inspected both the CA1 as well as the CA3 sub-region of the hippocampus as the CA3 projects extensively to the CA1 (Hannula and Duff, 2017). Contrary to results obtained in the mouse, I saw no alterations in average AIS length and cumulative AIS length distributions in the *Fmr1*$^{-/y}$ rat compared to controls (fig.5.2B, B' *Fmr1*$^{+/y}$= 30.76 μm $\pm$ 0.55 μm n=6, *Fmr1*$^{-/y}$= 30.90 $\pm$ 0.69 μm n=5 animals). While surprising, the data fits well with the electrophysiological characterisation of the CA1 in this rat model as no changes in cellular firing or intrinsic membrane properties have been observed in the CA1 pyramidal cells at this age (P28-32) (Jackson, 2016). Similar to the CA1, no changes were seen between genotypes in the average or cumulative distribution of AIS lengths in the CA3 (fig.5.2D, D' *Fmr1*$^{+/y}$= 37.45 μm $\pm$ 0.54 μm n=6, *Fmr1*$^{-/y}$= 37.13 μm $\pm$ 0.76 μm n=5 animals).

Previous characterisation of cellular excitability in the LA and BA of juvenile *Fmr1*$^{-/y}$ rats revealed no changes in either firing properties or membrane properties in pyramidal cells of the LA (Jackson, 2016). However, pyramidal cells of the BA were hyperexcitable showing increased firing with increased input resistance (Jackson, 2016). In agreement with these results, I found no change in the average or cumulative distribution of AIS lengths in the LA of juvenile *Fmr1*$^{-/y}$ rats compared to wildtype controls (fig.5.2F, F' *Fmr1*$^{+/y}$= 22.09 μm $\pm$ 1.11 μm n=6, *Fmr1*$^{-/y}$= 22.12 μm $\pm$ 0.70 μm n=5 animals). I did, however, observe a significant increase in average AIS length with a shift in cumulative distribution towards longer AIS lengths in neurons

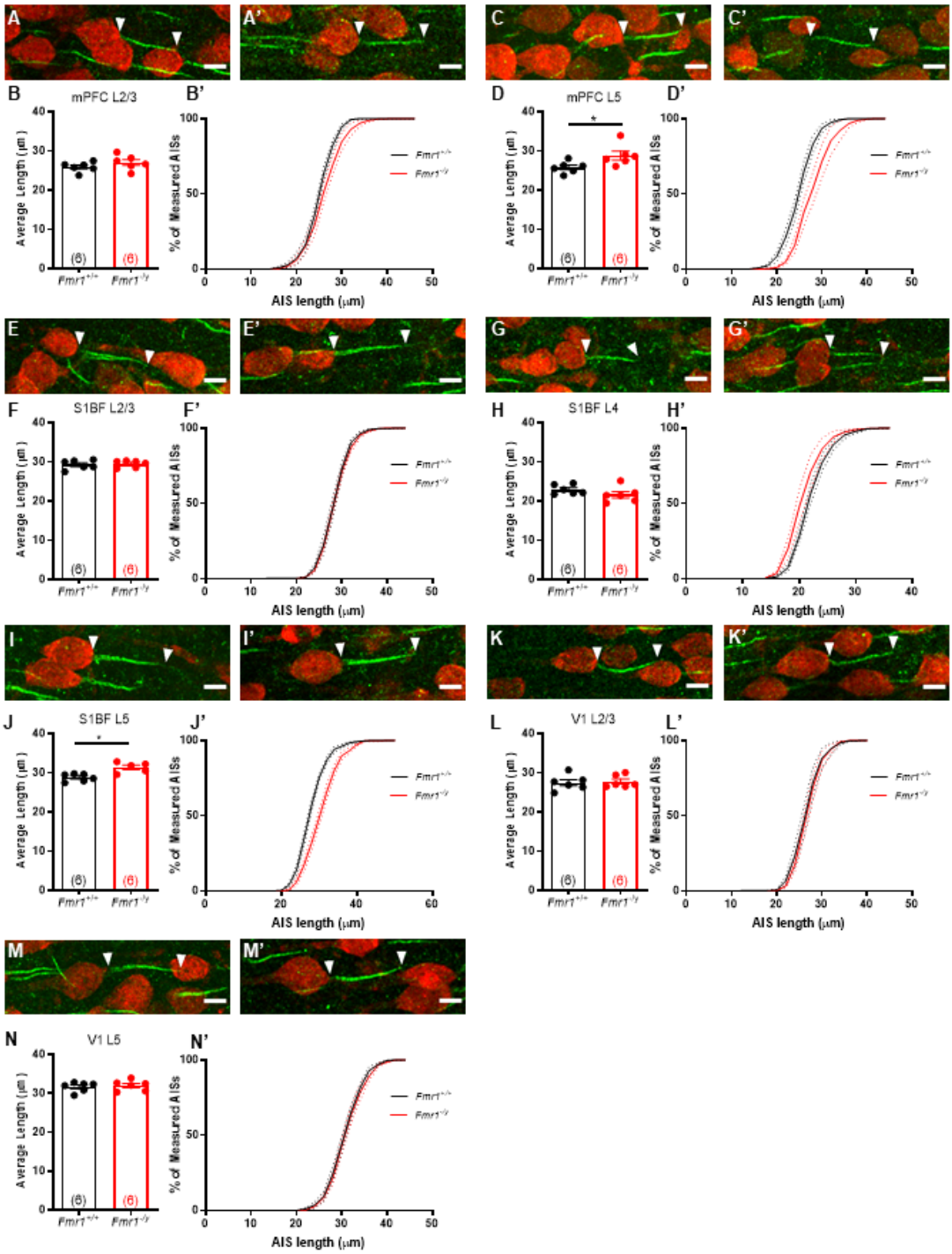

Figure 5.1: AIS lengths in cortical regions of *Fmr1*$^{-/y}$ rats (A-A', C-C', E-E', G-G', I-I',K-K',M-M') Representative single AIS from *Fmr1*$^{+/y}$ and *Fmr1*$^{-/y}$ rats respectively from the PL (L2/3 A-A', L5 C-C'), S1 (L2/3 E-E', L4 G-G', L5 I-I') and V1 (L2/3 K-K', L5 M-M'). No change in avg AIS length or cumulative distribution of AIS lengths was observed in PL L2/3 (B-B'), S1 L2/3 (F, F'), S1 L4(H-H'), V1 L2/3 (L-L') and V1 L5 (N-N') of *Fmr1*$^{-/y}$ rats compared to controls. AIS lengths were found increased in *Fmr1*$^{-/y}$ rats in PL L5 (D-D', p= 0.001) and S1 L5 (J-J', p= 0.010) compared to controls.

of the basal amygdala (BA) (fig.5.2H, H' $Fmr1^{+/y}$= 34.20 μm $\pm$ 1.08 μm n=6, $Fmr1^{-/y}$= 36.16 μm $\pm$ 0.40 μm n=5 animals, p=0.046).

Overall, the data indicates that loss of FMRP results in elongation of AIS lengths in the 'output' layers of the brain regions analysed including L5 of the PL and S1BF and the BA (Hoover and Vertes, 2007; Krettek and Price, 1977; Denardo et al., 2015). This increased AIS length maybe responsible for the increased cellular excitability observed in atleast 2 of these brain-regions (Jackson, 2016) and may be one of the underlying mechanisms of circuit hyperexcitability that has been noted in pre-clinical models of this disorder (Contractor et al., 2015). Further, the data suggest species specific differences in AIS length adaptation upon loss of FMRP as the AIS phenotype observed in the CA1 of the mouse model of FXS did not translate to our rat-model.

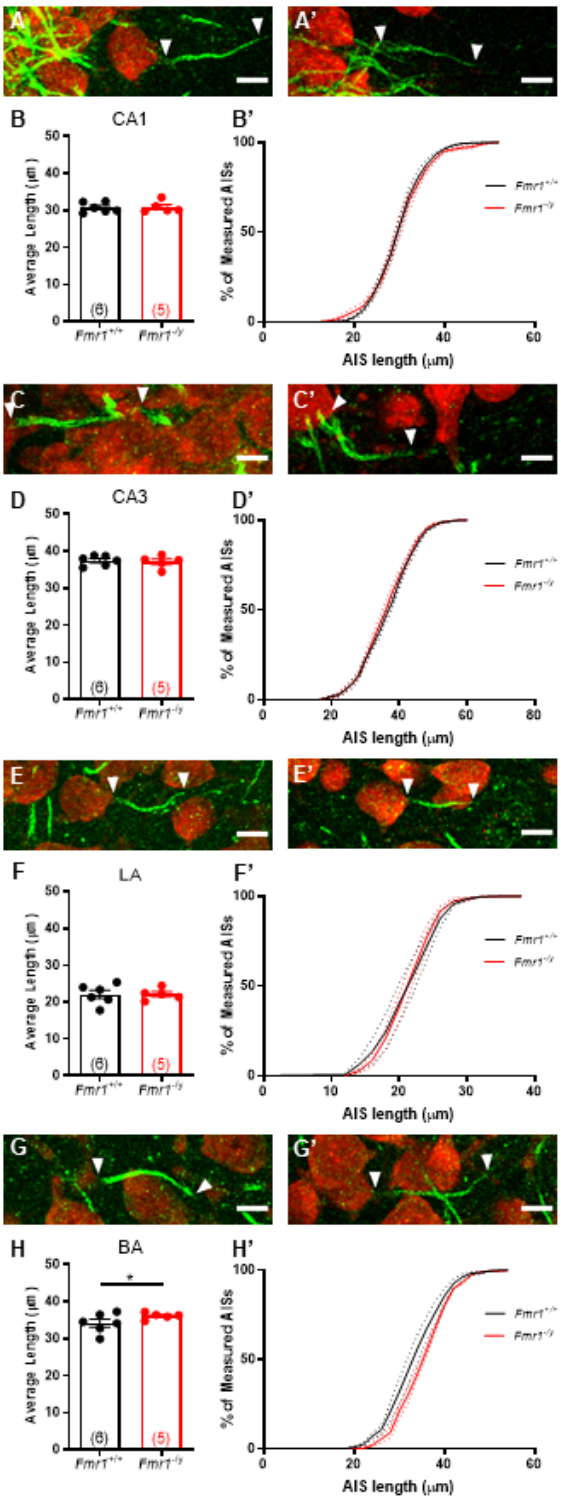

Figure 5.2: AIS lengths in sub-cortical regions of *Fmr1*$^{-/y}$ rats (A-A', C-C', E-E', G-G') Representative single AIS from *Fmr1*$^{+/y}$ and *Fmr1*$^{-/y}$ rats respectively from the hippocampus (CA1 A-A', CA3 C-C') and the BLA (LA E-E', BA G-G'). No change between *Fmr1*$^{-/y}$ and *Fmr1*$^{+/y}$ rats in avg AIS length or cumulative distribution of AIS lengths was observed in the CA1 (B-B'), CA3 (D, D') or the LA (F-F'). AIS lengths were found increased in *Fmr1*$^{-/y}$ rats in the BA (H-H', p= 0.046) compared to controls.

5.3 *Neuroligin 3*

Neuroligins are family of post-synaptic cell adhesion molecules (CAMs), that bind to the pre-synaptic neurexins (Ichtchenko et al., 1996; Song et al., 1999) to form a complex that triggers synapse formation, axon specialisation (Scheiffele et al., 2000) and influences post-synaptic differentiation (Rao et al., 2000). In the human genome, 5 genes (*NLGN1-4, 4Y*) encode this family of CAMs (Jamain et al., 2003) of which mutations in *NLGN3*, located at chromosomal locus Xq13, and those in *NLGN4*, located at Xp22.3, have been associated with Asperger's syndrome, ID and ASD (Jamain et al., 2003; Laumonnier et al., 2004; Levy et al., 2011; Sanders et al., 2011; Yuen et al., 2017). Neuroligin proteins are composed of a large extracellular neurexin-binding non-catalytic acetylcholinesterase homology domain (EF-hand domain) (Tsigelny et al., 2000), a transmembrane domain and a short cytoplasmic tail that contains a PDZ binding domain. This PDZ binding domain enables association of neuroligins with PSD-95, a key post-synaptic scaffolding molecule (Irie et al., 1997). Neuroligins are composed of multiple isoforms that show distinct localisation and alterations of synaptic function. Neuroligin 1 is found exclusively at excitatory glutamatergic synapses (Song et al., 1999), neuroligin 2 is found exclusively at GABAergic inhibitory synapses (Varoqueaux et al., 2004; Graf et al., 2004) while neuroligin 3 is found at both (Budreck and Scheiffele, 2007) and neuroligin 4 is found at glutamatergic and glycinergic synapses (Graf et al., 2004; Hoon et al., 2011). In line with this differential isoform localisation, *in vitro* over-expression of neuroligin 1 results in enhanced excitatory postsynaptic transmissions, that of neuroligin 2 enhances inhibitory postsynaptic transmissions (Levinsoni et al., 2005) while over-expression of neuroligin 3 also results in increased inhibitory transmission (Etherton et al., 2011).

NLGN3, is a category 1 'high confidence' gene thought to be causative for non-syndromic ID (SFARI database). A R451C mutation in *NLGN3* was first identified in a pair of Swedish brothers presenting with Asperger's syndrome and typical autism (Jamain et al., 2003). This mutation, found to be maternally inherited, impairs proper protein folding in the EF-hand domain required for binding to pre-synaptic neurexins (Nguyen and Südhof, 1997) and reduces surface neuroligin 3 expression due to increased retention in the endoplasmic reticulum (Comoletti et al., 2004; De Jaco et al., 2010; Ulbrich et al., 2016). In addition to this point mutation, large-scale sequencing and GWAS studies have found *de novo* copy number variations res-

ulting in a premature stop codon and complete loss of neuroligin 3 protein to be linked with autism (Levy et al., 2011; Sanders et al., 2011; Yuen et al., 2017). Clinical presentation of *NLGN3* associated NSID is highly variable, ranging from severe non-verbal autistic disorder to specific language impairment, Aspergers syndrome and Tourette's syndrome (Persico and Napolioni, 2013). Controversially, multiple studies have found no association between mutations in *NLGN3/4* and autism (Ylisaukko-oja et al., 2005; Gauthier et al., 2005; Wermter et al., 2008; Liu et al., 2013; Vincent et al., 2004; Xu et al., 2014). However, these studies were performed in high-functioning autistic individuals whereas mutations in *NLGN3/4* have typically been associated with low-functioning cases. A further resolution to this controversy is offered from findings in animal studies which show that manifestation of ASD-like symptoms upon introduction of the human NL3 R451C mutation is dependent on the background strain of the animal (Jaramillo et al., 2014, 2018), suggesting that these mutations might be more debilitating in some populations than other.

The functional consequence of pathological mutations in *NLGN3* have been explored in two mouse models. The first is a gain of function (knock-in) NL3 R451C mutation, resulting in a 90% loss of neuroligin 3 from the whole mouse brain (Tabuchi et al., 2007), that was identified by Jamain et al. (2003) and the second is a full protein knock out that mimics *NLGN3* CNV mutations linked with autism (Sanders et al., 2011).

Behavioural analysis of independently generated NL3 R451C mice have shown discrepancies in results obtained from social and spatial learning tasks. Tabuchi et al. (2007), using a 3-chamber sociability task, found impaired social interaction with enhanced spatial learning in a reversal morris water maze in NL3 R451C mice compared to wildtypes. On the other hand, Chadman et al. (2008) found no difference between the NL3 R451C and wildtype mice in either a juvenile reciprocal social interaction task, an adult social approach task or enhanced learning in a reversal Morris water maze. These differences in behaviour were later uncovered to be due to the differing background strains on which the mutations were generated. The background mouse strain in the paper by Tabuchi et al. (2007) was a hybrid C57BL6/J/129S2/SvPasCrl while the strain used in the Chadman et al. (2008) study was a pure C57BL6/J. Findings from Tabuchi et al. (2007) were replicated when the NL3 R451C mutation was generated on in mice with 129S2/SvPasCrl background strain (Jaramillo et al., 2014) but not when the mutation was generated on the C57BL6/J (Jaramillo et al., 2018), supporting the results obtained in Chadman

et al. (2008) study. Additional minor differences have also been noted between the NL3 R451C and *Nlgn3* knock-out (KO) mice, particularly with respect to locomotion and olfaction. *Nlgn3* KO mice show increased locomotion in open field, elevated plus maze and locomotion box test with reduced olfaction (Radyushkin et al., 2009) and olfactory discrimination (Bariselli et al., 2018) while no such alterations are noted in the NL3 R451C mice (Chadman et al., 2008; Jaramillo et al., 2018). *NLgn3* KO mice also showed decreased overall brain volume, which was not found in the NL R451C mice (Radyushkin et al., 2009).

Consistent findings across NL3 R451C and *Nlgn3* KO mice include reduced sensitivity to acoustic stimuli, as measured by reduced acoustic startle response to high-decibel tones without any irregularities in sensorimotor gating (Chadman et al., 2008; Radyushkin et al., 2009), reduced ultra-sonic vocalisations upon female approach (Chadman et al., 2008; Radyushkin et al., 2009; Fischer and Hammerschmidt, 2011; Kalbassi et al., 2017), a feature that is reminiscent of human pathology of reduced linguistic abilities (Persico and Napolioni, 2013), and improved motor co-ordination when measured using an accelerating rotarod (Chadman et al., 2008; Rothwell et al., 2014) compared to wildtype controls. Rothwell et al. (2014), argued that this enhanced performance on the rotarod is a proxy for heightened acquisition of repetitive behaviours, a feature that forms part of the core diagnostic criteria for ASDs (ICD-10). The same study found that selective knock-down of neuroligin 3 from dopamine receptor-1 (D1) expressing medium spiny neurons in the nucleus accumbens of wild-type mice increases inhibition onto these cells and is sufficient to recapitulate the enhanced rotarod performance exhibited by the NL3 R451C and *Nlgn3* KO mice (Rothwell et al., 2014). Another common manifestation of ASD-like repetitive behaviours in mice is exaggerated grooming. Selective knock-down of neuroligin-3 using siRNA in the dorsal striatum of wildtype mice results in increased grooming behaviour (Lee et al., 2018). Another core ASD-diagnosis criterion is impaired social communication and sociability preference. While neither NL3 R451C mice nor *Nlgn3* KO mice show impairments in sociability, both show a markedly reduced preference for social novelty (Radyushkin et al., 2009; Bariselli et al., 2018; Cao et al., 2018). Further, selective knockdown of neuroligin 3 from dopaminergic neurons of the ventral tegmental area in wildtype mice, causing inhibition of neuronal activity, mimics the phenotype of *Nlgn3* KO mice resulting in a loss social novelty preference in wildtype animals (Bariselli et al., 2018). This data supports the altered E/I balance hypothesis of ASD (Rubenstein and Merzenich, 2003; Nelson and Valakh, 2015) and suggests a shift towards increased inhibition upon loss of neuroligin 3. This

increased inhibition hypothesis is supported by additional studies. Notably, L2/3 pyramidal neurons of the somatosensory barrel cortex of P13-16 NL3 R451C mice showed 50% increased frequency of miniature inhibitory synaptic events (Tabuchi et al., 2007). In the same cells an independent study found accelerated spine tunrover of PSD-95 affiliated excitatory synapses but not gephyrin-associated inhibitory synapses suggesting that abnormal functioning of neuroligin 3 at excitatory synapses may drive reduced excitation (Isshiki et al., 2014). Recordings from the CA3 sub-region of the hippocampus of P4-9 NL3 R451C mice showed increased frequency of $GABA_A$, and not glutamate, mediated giant depolarising potentials along with increased frequency of miniature $GABA_A$-mediated postsynaptic currents (mGPSC) starting at P4 until adulthood (Pizzarelli and Cherubini, 2013). Given that in the first post-natal week the effects of $GABA_A$ are depolarising and excitatory and the increased mGPSCs show reduced attenuation upon application of the $GABA_A$ antagonist TPMPA, this may indicate that the R451C mutation alters presynaptic $GABA_A$ release. This could perhaps account for the increased inhibition observed at later time-points in NL3 R451C mice. Lastly, EEG inspection of sleep/wake cycle in NL3 R451C mice show increased power of delta oscillations during non rapid-eye movement (NREM) sleep (Liu et al., 2017). Delta oscillations are generated by the thalamocortical network (McCormick and Bal, 1997) and regulated by GABA inhibitory transmission (Kopp et al., 2004), with administration of GABA agonist diazepam resulting in decreased delta oscillations, therefore the gain-of-function R451C mutation might result in decreased delta power due to increased GABA-ergic transmission. In the primary visual cortex of NL3 R451C mice, an increase in GAD-65 positive GABA-ergic interneuron number is observed, suggesting increased inhibition in this brain region as well (Verma et al., 2019).

This increased inhibition, however, was found to be circuit specific. While the S1 L2/3 cells showed increased inhibition, CA1 cells of P13-16 NL3 R451C mice showed altered excitation with about ~1.5 fold increase in frequency of AMPAR-mediated excitatory synaptic transmission, a ~2 fold increase in NMDAR-mediate LTP and greater dendritic branching (Etherton et al., 2011). However, EEG studies showed a reduction in hippocampal mediated theta oscillations, which are suppressed due to increased GABA-ergic transmission (Liu et al., 2017). These differences may arise from both differences in age of experimental animals as well as different wake/sleep states of these animals. Gamma and theta oscillations in the mPFC are key in modulating social behaviours. In the mPFC of NL3 R451C mice, a reduction in gamma oscillations is observed along with reduced excitability of fast-spiking parvalbumin-immunoreactive

interneurons, suggesting increased excitation in this brain region as opposed to increased inhibition (Cao et al., 2018). Lastly, synaptic plasticity deficits are also observed in upon loss of neuroligin 3, particularly impaired LTD in the dorsal striatum (Martella et al., 2018) and impaired mGluR1 mediated LTD, which was reversed upon re-expression of neuroligin 3, in the cerebellum (Baudouin et al., 2012).

Given the synaptic and excitability deficits observed in the *Nlgn3* mutant mice, particularly in the sensory cortices and convergent pathway of mGluR mediated LTD deficits similar to the *Fmr1*$^{-/y}$ mice, I analysed AIS lengths in multiple brain regions in a loss of function knock-out rat model of *Nlgn3* (*Nlgn3*$^{-/y}$).

5.3.1 Results

In juvenile (P28-32) rats modelling *NLGN3*-NSID, and similar to the analyses performed in the rat models of *SYNGAP1*-ID (chapter 3) and FXS (above), I examined changes in AIS lengths in three cortical regions including the mPFC PL, the S1 barrel cortex and the visual cortex. No changes in average AIS length or cumulative distribution of AIS lengths was observed in either L2/3 (fig.5.3B, B' *Nlgn3*$^{+/y}$= 29.28 μm $\pm$ 0.92 μm n=6, *Nlgn3*$^{-/y}$= 29.10 μm $\pm$ 1.03 μm n=6 animals) or L5 (fig.5.3D, D' *Nlgn3*$^{+/y}$= 29.88 μm $\pm$ 1.35 μm n=6, *Nlgn3*$^{-/y}$= 29.22 μm $\pm$ 1.25 μm n=6 animals) of the mPFC PL of the *Nlgn3*$^{-/y}$ rats compared to wild-type, aged-matched, littermate controls. This finding is consistent with unpublished results from electrophysiological recordings in our laboratory which show no changes in intrinsic cellular excitability or firing properties in PL L5 pyramidal cells from P26-32 *Nlgn3*$^{-/y}$ rats compared to wildtype controls.

Reduced sensitivity to sensory stimuli and the increased inhibitory transmission observed in L2/3 cells of the S1 of *Nlgn3* KO mice could be a result of altered intrinsic excitability of these cells. However, no changes in intrinsic membrane properties or firing properties of these neurons were observed in NL3 R451C mice or *Nlgn3* KO mice (Tabuchi et al., 2007; Etherton et al., 2011). Consistent with these findings, no change in average or cumulative distribution of AIS lengths was observed in L2/3, L4 or L5 neurons of *Nlgn3*$^{-/y}$ rats compared to controls (L2/3 fig.5.3F, F' *Nlgn3*$^{+/y}$= 28.38 μm $\pm$ 0.15 μm n=6, *Nlgn3*$^{-/y}$= 27.32 $\pm$ 0.58 n=6 animals; L4 fig.5.3H, H' *Nlgn3*$^{+/y}$= 25.01 μm $\pm$ μm 0.81 n=6, *Nlgn3*$^{-/y}$= 23.29 μm $\pm$ 0.66 μm n=6

animals; L5 fig.5.3J, J' *Nlgn3*$^{+/y}$= 29.43 μm $\pm$ 0.36 μm n=6, *Nlgn3*$^{-/y}$= 29.56 μm $\pm$ 0.26 μm n=6 animals).

Similar to the other two cortical regions studied, no changes were observed in average or cumulative distribution of AIS lengths in L2/3 or L5 of the visual cortex of *Nlgn3*$^{-/y}$ rats compared to wildtype littermate controls (L2/3 fig.5.3L, L' *Nlgn3*$^{+/y}$= 25.28 μm $\pm$ 0.04 μm n=2, *Nlgn3*$^{-/y}$= 26.64 μm $\pm$ 1.07 μm n=2 animals; L5 fig.5.3N, N' *Nlgn3*$^{+/y}$= 29.01 μm $\pm$ 1.19 μm n=2, *Nlgn3*$^{-/y}$= 29.62 μm $\pm$ 1.17 μm n=2 animals). However, due to the low *n* in these experiments, conclusions are preliminary.

In the NL3 R451C mice, altered synaptic plasticity is observed in pyramidal cells of CA1 and CA3 regions of the hippocampus (Etherton et al., 2011; Pizzarelli and Cherubini, 2013). While altered plasticity does not always imply altered intrinsic excitability of the neuron, this maybe a contributing factor. Further, given the evidence of convergent cellular physiology between mouse models of FXS and *NLGN3*-NSID (Baudouin et al., 2012), the increased AIS length in the CA1 sub-region in the mouse model of FXS, and impairments in hippocampal-dependent spatial memory in mouse models of *NLGN3* -NSID, here I analysed AIS length in the CA1 and CA3 sub-regions of the dorsal hippocampus. In our rat model of *Nlgn3*$^{-/y}$, no genotype specific changes in average AIS length or cumulative distribution of AIS lengths is observed in either the CA1 or the CA3 of the *Nlgn3*$^{-/y}$ compared to controls (CA1 fig.5.4B, B' *Nlgn3*$^{+/y}$= 35.76 μm $\pm$ 1.40 μm n=6, *Nlgn3*$^{-/y}$= 32.99 μm $\pm$ 1.31 μm n=6 animals; CA3 fig.5.4D, D' *Nlgn3*$^{+/y}$= 42.38 μm $\pm$ 2.54 μm n=6, *Nlgn3*$^{-/y}$= 40.00 μm $\pm$ 1.98 μm n=6 animals). The lack of change in AIS length in the CA1 is consistent with the lack of changes in cellular excitability found in electrophysiological recordings of age-matched *Nlgn3*$^{-/y}$ rats compared to wild-type littermate controls (N Anstey, unpublished).

Laslty, *Nlgn3* KO mice show reduced levels of anxiety in amygdala-dependent contextual and cued fear conditioning paradigms (Radyushkin et al., 2009). Additionally, in our *Nlgn3*$^{-/y}$ rat model, these animals also show preferential activation of a 'flight' over 'freeze' response strategy in a cued fear conditioning paradigm (N Anstey et al., unpublished), suggesting further amygdalar circuit dysfunction. Altered amygdalar function is further corroborated by findings of impaired LTP of thalamocotical inputs into the basolateral amygdala of juvenile *Nlgn3*$^{-/y}$ rats, similar to *Syngap1*$^{+/-}$ and *Fmr1*$^{-/y}$ rats (Toft, 2019). Given that AIS morphology-dependent

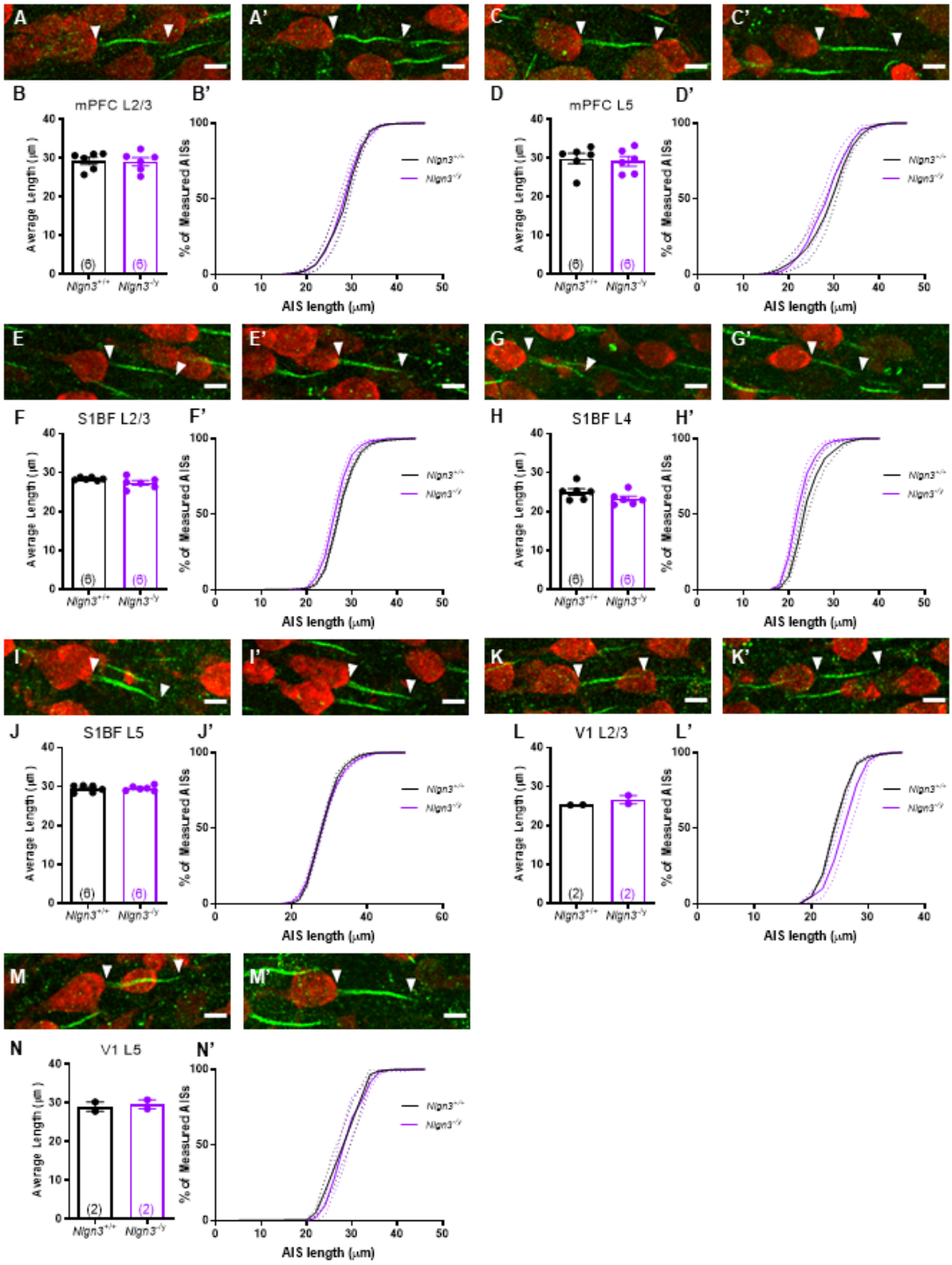

Figure 5.3: AIS lengths in cortical regions of *Nlgn3$^{-/y}$* rats(A-A', C-C', E-E', G-G', I-I',K-K',M-M') Representative single AIS from *Nlgn3$^{+/y}$* and *Nlgn3$^{-/y}$* rats respectively from the PL (L2/3 A-A', L5 C-C'), S1 (L2/3 E-E', L4 G-G', L5 I-I') and V1 (L2/3 K-K', L5 M-M'). No change in avg AIS length or cumulative distribution of AIS lengths was observed in PL L2/3 (B-B'), PL L5 (D-D'), S1 L2/3 (F, F'), S1 L4(H-H'), S1 L5 (J-J'), V1 L2/3 (L-L') and V1 L5 (N-N') of *Nlgn3$^{-/y}$* rats compared to controls.

alterations in cellular excitability might drive these plasticity changes, I analysed AIS lengths in the both the BA and LA neurons of juvenile *Nlgn3*$^{-/y}$ rats. No changes in either average length or cumulative distribution of lengths was found in P28 *Nlgn3*$^{-/y}$ rats compared to controls in either the lateral or the basal amygdala (LA fig.5.4F, F' *Nlgn3*$^{+/y}$= 26.65 μm $\pm$ 1.50 μm n=4, *Nlgn3*$^{-/y}$= 26.70 μm $\pm$ 1.31 μm n=4 animals; BA fig.5.4H, H' *Nlgn3*$^{+/y}$= 35.50 μm $\pm$ 3.56 μm n=5, *Nlgn3*$^{-/y}$= 37.58 μm $\pm$ 2.46 μm n=5 animals).

Overall, the data suggests that in our model, loss of Nlgn3 results in no alterations in AIS length or intrinsic cellular physiology (N Anstey, upublished, Toft (2019)) in any of the brain regions studied but does result in AIS-independent alterations in synaptic plasticity in the BLA (Toft, 2019). This the lack of genotype specific modulation of AIS-length in *Nlgn3*$^{-/y}$ rats is consistent with the findings in the *Syngap1*$^{+/-}$ (see chapter 3) but differs from those obtained in the *Fmr1*$^{-/y}$ rats.

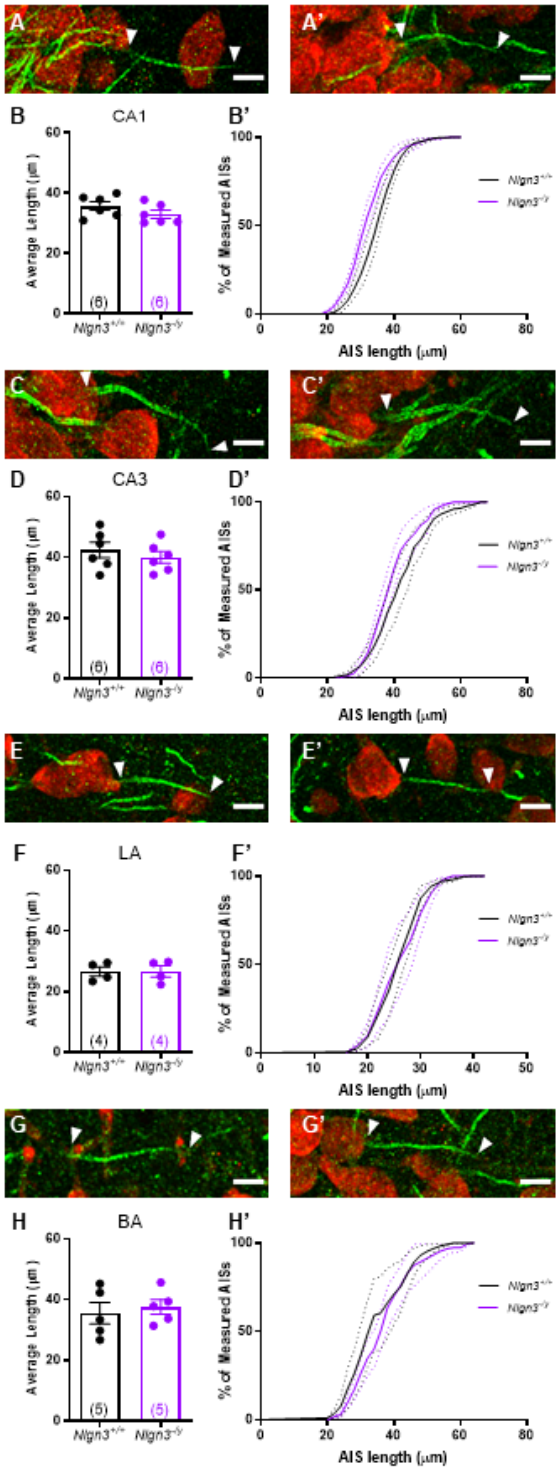

Figure 5.4: AIS lengths in sub-cortical regions of *Nlgn3*$^{-/y}$ rats (A-A', C-C', E-E', G-G') Representative single AIS from *Nlgn3*$^{+/y}$ and *Nlgn3*$^{-/y}$ rats respectively from the hippocampus (CA1 A-A', CA3 C-C') and the BLA (LA E-E', BA G-G'). No change between *Nlgn3*$^{-/y}$ and *Nlgn3*$^{+/y}$ rats in avg AIS length or cumulative distribution of AIS lengths was observed in the CA1 (B-B'), CA3 (D, D'), LA (F-F') or BA (H-H').

5.4 *Neurexin 1α*

Neurexins are the presynaptic binding partners of post-synaptic ligands including neurloligins (Ichtchenko et al., 1995; Graf et al., 2004), neurexophilin (Missler and Südhof, 1998) and leucine-rich repeat transmembrane neuronal proteins (LRRTMs) (Siddiqui et al., 2010). Encoded by the 1.1Mb long *NEUREXIN 1-3* (or *NRX1-3*) gene located on chromosome 2p16.3, neurexins were first identified in the rat brain as receptors for the black-widow venom α-latrotoxin (Ushkaryov et al., 1992). Neurexins have since been shown to act predominantly as cell adhesion molecules, influencing synapse formation and transmission through trans-synaptic association with post-synaptic ligands (Südhof, 2008; Reissner et al., 2013). Neurexins are also critically involved in Ca^{2+} dependent vesicular neurotransmitter release (Missler et al., 2003; Geppert et al., 1998; Kattenstroth et al., 2004; Reissner et al., 2013).

Arising from independent promoters, two major subclasses of neurexins exist: A highly evolutionarily conversed α-neurexin and a less conserved β-neurexin (Missler and Südhof, 1998). Both sub-classes share transmembrane C-terminal domains and cytoplasmic tails but differ critically in the composition of their extracellular N-terminal domain. α-Neurexin contains six LNS (Laminin A G domain/ Neurexin / Sex hormone globulin) repeats interspersed with epidermal-growth factor-like domains while the shorter β-neurexin only contains one LNS repeat (Missler and Südhof, 1998). In addition to the two major isoforms the presence of six alternative splice sites on *Nrx1-2* and five on *Nrx3* yield an extraordinary 4000 protein variants (Ullrich et al., 1995; Tabuchi and Südhof, 2002), impacting inter-molecular pairing affinities (Ichtchenko et al., 1995; Craig and Kang, 2007; Chih et al., 2006; Boucard et al., 2005; Graf et al., 2006).

Interest in *NRX1* as a gene important in neuropsychiatric disorders emerged in 2006 when a study by Friedman et al. (2006), using oligonucleotide microarray analysis, identified a deletion in 2p16.3 in a 7 year old boy with borderline-ID IQ of 74 and attention deficit disorder. Large-scale genome analysis studies and individual case reports alike have since identified mutations in *NRX1* and *NRX2* linked to ASD (Szatmari et al., 2007; Zahir et al., 2008; Marshall et al., 2008; Kim et al., 2008; Bucan et al., 2009; Ching et al., 2010; Pinto et al., 2010; Glessner et al., 2009; Gregor et al., 2011; Wiśniowiecka-Kowalnik et al., 2010; Harrison et al., 2011; Curran

et al., 2013; Schaaf et al., 2012; Imitola et al., 2014; Duong et al., 2012; Onay et al., 2016) and schizophrenia (Kirov et al., 2008; Vrijenhoek et al., 2008; Rujescu et al., 2009; Need et al., 2009; Gauthier et al., 2011; Levinson et al., 2011; Rees et al., 2014; Todarello et al., 2014; Li et al., 2016).

Most individuals with *NRX1* associated NDDs contained heterozygous exonic structural variation in α-Neurexin with only 11 patients, till date, presenting a bi-allelic loss of *NRX1* (Castronovo et al., 2019). Phenotypic presentations of individuals with *NRX1*-deletions is highly variable and includes moderate to severe intellectual disability (77-92%, (Dabell et al., 2013; Gregor et al., 2011; Béna et al., 2013)), ASD (43-70%; (Dabell et al., 2013; Gregor et al., 2011; Béna et al., 2013; Gonzalez-Mantilla et al., 2016; Al Shehhi et al., 2019)) developmental and speech delay (69%, (Ching et al., 2010; Sahoo et al., 2011; Curran et al., 2013; Brignell et al., 2018)), ADHD (9-41%, (Lowther et al., 2017; Schaaf et al., 2012)), epilepsy (14-53%, (Dabell et al., 2013; Harrison et al., 2011; Béna et al., 2013; Schaaf et al., 2012; Gonzalez-Mantilla et al., 2016)) and muscle hypotonia (38-47%, (Schaaf et al., 2012; Béna et al., 2013)). The putative effects of dysfunctional CAMs, such as NRXN1, on neural circuitry support pathophysiological 'two hit' hypothesis of neurodevelopmental disorders. In particular, the variability in clinical presentation associated with *NRXN1* deletions, ranging from unaffected carrier status to severe neurodevelopmental phenotypes, suggests that individual mutations in this gene may confer disease risk rather than play a causal role (Castronovo et al., 2019). Incomplete penetrance may be further be explained by secondary and independently segregating genetic risk factors, as supported by enhanced frequencies of additional pathogenic CNVs in cohorts of patients carrying NRXN1 deletions (Béna et al., 2013; Girirajan et al., 2013) or exposure to environmental factors (Bölte et al., 2019; Persico and Merelli, 2015).

Pre-clinical models to understand the biological mechanisms of *NRX1* deletions have used both null ($Nrx1^{-/-}$) (Missler et al., 2003; Dudanova et al., 2006; Etherton et al., 2009; Grayton et al., 2013; Esclassan et al., 2015; Twining et al., 2017) and heterozygous ($Nrx1^{+/-}$) (Laarakker et al., 2012; Grayton et al., 2013; Dachtler et al., 2015) mouse and rat models. (Missler et al., 2003) first generated the α-neurexin triple knock-out (KO) mice lacking Nrx 1α, 2α and 3α. This loss of α-neurexins was lethal, with triple KO animals showing marked difficulties in breathing and zero percent survival beyond post-natal day 1. However, gross brain anatomy in these triple KOs was found to be normal, with no evidence of defects in axonal path-finding, increased

apoptosis or altered distribution of synaptic proteins. Functionally; recordings from neocortical cultures, hippocampal cultures, acute brain stem slices and acute pituitary gland slices found a >50% deficit in spontaneous and evoked Ca^{2+}-triggered neurotransmitter release in adult double KOs (*Nrx1α*$^{-/-}$;*Nrx2α*$^{-/-}$) and newborn triple KOs (Missler et al., 2003; Dudanova et al., 2006). This reduction in neurotransmitter release was attributed to reduced numbers of functional Ca^{2+} channels, as absolute numbers of surface-expressed Ca^{2+} channels remained unaltered in both the double and triple KO animals (Missler et al., 2003; Dudanova et al., 2006).

Behavioural phenotyping of rat and mouse models of *Nrx1α* deletions have found stark differences between species, sexes and between heterozygous and homozygous models of *NRX1* associated ID (Etherton et al., 2009; Laarakker et al., 2012; Grayton et al., 2013; Dachtler et al., 2015; Esclassan et al., 2015). Behaviourally, *Nrx1*$^{-/-}$ male mice were found to show no deficits in the hippocampal-dependent Morris water maze spatial learning task (Etherton et al., 2009; Grayton et al., 2013), while *Nrx1*$^{+/-}$ male mice showed impaired hippocampal dependent long-term (24h interval) object discrimination memory (Laarakker et al., 2012). This deficit in object discrimination memory, however, was not reproduced in later studies in the same model (Dachtler et al., 2015). In a rat model of *NRX1*-ID ,*Nrx1*$^{-/-}$ rats show impaired performance in a hippocmapal-dependent spatial discrimination task with impairment being more pronounced in *Nrx1*$^{-/-}$ females (Esclassan et al., 2015). Similar to the mouse model of FXS, *Nrx1*$^{-/-}$ mice also display sensorimotor gating abnormalities as shown by decreased pre-pulse inhibition (PPI) with an exaggerated startle response (Etherton et al., 2009) whereas *Nrx1*$^{+/-}$ mice (Dachtler et al., 2015) and *Nrx1*$^{-/-}$ rats display no change in PPI, despite an exaggerated startle response in the rats (Esclassan et al., 2015). Contradictory results are also seen in measures of repetitive grooming behaviour with studies finding both increased (Etherton et al., 2009) and no alteration in grooming in *Nrx1*$^{-/-}$ (Grayton et al., 2013) and *Nrx1*$^{+/-}$ (Dachtler et al., 2015) male mice. Another behavioural discrepancy within *Nrx1*$^{-/-}$ mice is seen in locomotor activity. Where Etherton et al. (2009) and Dachtler et al. (2015) found no alterations in locomotor behaviour in *Nrx1*$^{-/-}$ and *Nrx1*$^{+/-}$ mice, studies by Laarakker et al. (2012) and (Esclassan et al., 2015) found hyperactivity of *Nrx1*$^{-/-}$ mice and rats, while still other studies found reduced locomotor activity in *Nrx1*$^{-/-}$ mice (Grayton et al., 2013). Anxiety-related disorders are a common co-morbidity in individuals with ASD. Inspection of anxiety-like behaviours in the *Nrx1*$^{-/-}$ and *Nrx1*$^{+/-}$ mice also yielded conflicting results with Etherton et al. (2009) and Dachtler et al. (2015) finding no change in anxiety-like behaviour in *Nrx1*$^{-/-}$ and *Nrx1*$^{+/-}$ mice in tasks such

as the elevated plus maze (EPM), forced swim test and tail suspension test while Grayton et al. (2013) found elevated anxiety in *Nrx1*$^{-/-}$ mice using EPM and light/dark box task. *Nrx1*$^{-/-}$ rats showed no alteration in innate anxiety upon examination using EPM (Twining et al., 2017). The most consistent behavioural finding in the pre-clinical *NRX1* models, however, is the lack of deficits in sociability in *Nrx1*$^{-/-}$ and *Nrx1*$^{+/-}$ mice and rats (Etherton et al., 2009; Grayton et al., 2013; Dachtler et al., 2015; Esclassan et al., 2015), though some studies observe a weaker discrimination of social novelty in *Nrx1*$^{+/-}$ mice (Dachtler et al., 2015) and increased preference for sociability in *Nrx1*$^{-/-}$ male mice (Grayton et al., 2013).

Further, independent studies have shown impairments in various aspects of cognition. Notably, Dachtler et al. (2015) found that in a passive avoidance task, female *Nrxn1*$\alpha^{+/-}$ mice showed an impairment in cognition, traversing back to the box where they received an aversive stimuli faster than wildtype controls. While Esclassan et al. (2015), found impairments in associative learning (instrumental conditioning) and attention (impaired latent inhibition) and Twining et al. (2017) found impairments in social-cued fear conditioning in *Nrx1*$^{-/-}$ rats.

Underlying behavioural and cognitive abnormalities are alterations in intrinsic cellular excitability and synaptic plasticity (Daoudal and Debanne, 2003). Therefore, in order to understand the biological mechanisms of impaired behaviour observed in the various models of *NRX1* associated ASD/ID, here I have analysed differences in the length of the axon initial segment, a neuronal compartment known to regulate cellular excitability via alterations in its length with these alterations being further shown to underlie excitability alterations in other mouse models of ASD/ID (Kaphzan et al., 2011; Leterrier, 2018; Booker et al., 2019). As majority of *NRX1*-mutations linked with ASD/ID are heterozygous, AIS lengths in various behaviourally relevant brain regions were examined in a *Nrx1*α heterozygous rat model (*Nrx1*$^{-/-}$).

5.4.1 Results

Previously, *Nrx1*$^{-/-}$ rats exhibited severe impairments in the acquisition of an mPFC-dependent (Ostlund and Balleine, 2005) associative learning operant task (Esclassan et al., 2015), showing little evidence of learning after 10 days of training. Intrinsic cellular excitability of neurons in the PL region of the mPFC in rodents have been shown to alter following training in associ-

ative learning tasks (Hayton et al., 2011). Therefore, one underlying mechanism of impaired acquisition in the *Nrx1*$^{-/-}$ rats, might be the inability to alter the intrinsic excitability of the PL neurons. Given that the AIS is known to regulate its length and alter cellular excitability in an activity-dependent manner (for review see Kuba (2012)), I hypothesized that in our rat model of *NRX1*-associated ASD/ID, the AIS length in PL L2/3 and L5 neurons would be altered compared to control animals. Upon examination, no alterations in average AIS length or cumulative distribution of AIS lengths was observed in either PL L2/3 or L5 neurons of *Nrx1*$^{+/-}$ rats compared to wildtype, littermate controls at P28-32 (L2/3 fig.5.5B, B' *Nrx1*$^{+/+}$= 29.07 μm $\pm$ 0.71 μm n=8, *Nrx1*$^{+/-}$= 28.69 μm $\pm$ 0.70 μm n=8 animals; L5 fig.5.5D, D' *Nrx1*$^{+/+}$= 30.02 μm $\pm$ 1.22 μm n=8, *Nrx1*$^{+/-}$= 29.67 μm $\pm$ 1.13 μm n=8 animals).

Similar to preclinical models of FXS (Contractor et al., 2015), *NLGN3*-ID (Tabuchi et al., 2007) and *SYNGAP1*-ID (Guo et al., 2009), *Nrx1*$^{-/-}$ rats also show disrupted sensory perception (Esclassan et al., 2015). As altered cellular excitability is shown to underlie disrupted sensory processing in models of ASD (Robertson and Baron-Cohen, 2017), I analysed AIS length changes in two sensory cortices, the somatosensory barrel cortex as well as the visual cortex, in the *Nrx1*$^{+/-}$ rats. No changes in average AIS length or cumulative distribution of AIS lengths in found in either L2/3, L4 or L5 of the of the S1 barrel cortex in these animals compared to wildtype controls (L2/3 fig.5.5F, F' *Nrx1*$^{+/+}$= 29.99 $\pm$ 0.37 n=6, *Nrx1*$^{+/-}$= 29.98 μm $\pm$ 0.62 μm n=6 animals; L4 fig.5.5H,H' *Nrx1*$^{+/+}$= 22.65 μm $\pm$ 0.48 μm n=6, *Nrx1*$^{+/-}$= 23.07 $\pm$ 0.29 n=6 animals; L5 fig.5.5J,J' *Nrx1*$^{+/+}$= 29.20 μm $\pm$ 0.38 μm n=6, *Nrx1*$^{+/-}$= 28.74 μm $\pm$ 0.57 μm n=6 animals). Similar to the barrel cortex, no changes were observed in either average AIS length or cumulative distribution of AIS lengths in L2/3 and L5 of the primary visual cortex in *Nrx1*$^{+/-}$ juvenile rats compared to controls (L2/3 fig.5.5L, L' *Nrx1*$^{+/+}$= 26.72 μm $\pm$ 4.06 μm n=2, *Nrx1*$^{+/-}$= 25.52 μm $\pm$ 1.04 μm n=3 animals; L5 fig.5.5N, N' *Nrx1*$^{+/+}$= 29.34 μm $\pm$ 3.74 μm n=2, *Nrx1*$^{+/-}$= 28.91 μm $\pm$ 1.72 μm n=3 animals). However, due to the low *n* in these experiments, conclusions are preliminary.

Further, *Nrx1*$^{-/-}$ rats showed impairments in hippocampal-dependent spatial navigation tasks, including spatial discrimination and reversal and rewarded alternation T-maze, and disruption in the CA1-dependent (Puga et al., 2007) latent inhibition task, where pre-exposure to a stimulus inhibits subsequent associations with that stimulus (Esclassan et al., 2015). Electrophysiologically, *Nrx1*$^{-/-}$ mice show decreased frequency of miniature excitatory post-synaptic currents

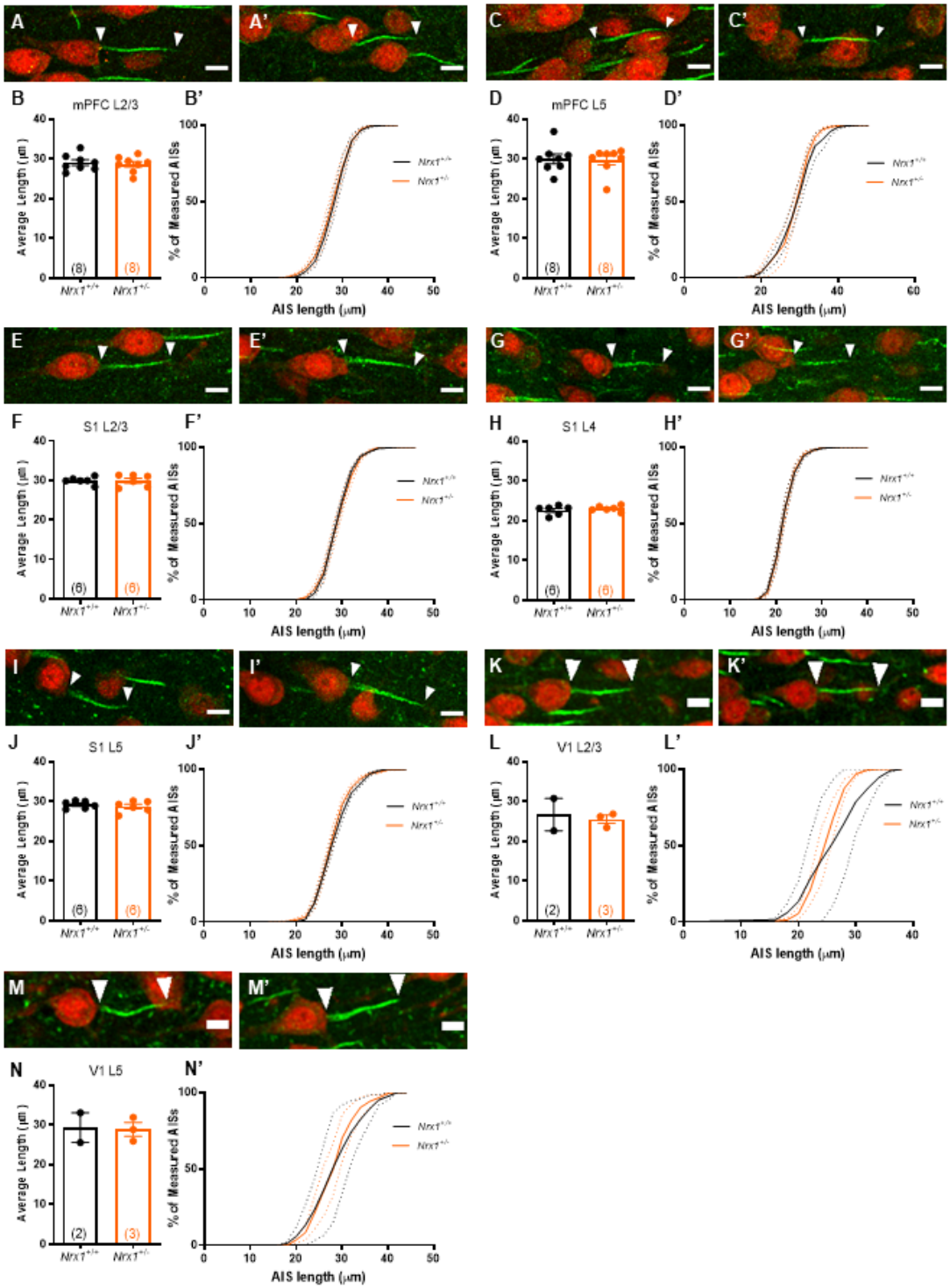

Figure 5.5: AIS lengths in cortical regions of *Nrx1*$^{+/-}$ rats (A-A', C-C', E-E', G-G', I-I',K-K',M-M') Representative single AIS from *Nrx1*$^{+/+}$ and *Nrx1*$^{+/-}$ rats respectively from the PL (L2/3 A-A', L5 C-C'), S1 (L2/3 E-E', L4 G-G', L5 I-I') and V1 (L2/3 K-K', L5 M-M'). No change in avg AIS length or cumulative distribution of AIS lengths was observed in PL L2/3 (B-B'), PL L5 (D-D'), S1 L2/3 (F, F'), S1 L4(H-H'), S1 L5 (J-J'), V1 L2/3 (L-L') and V1 L5 (N-N') of *Nrx1*$^{+/-}$ rats compared to controls.

(EPSCs) and input-output relation of evoked potentials in the CA1 (Etherton et al., 2009). Although mEPSCs are an action-potential independent measure of excitability, with altered resulting in a shift in the excitatory/inhibitory balance of individual CA1 pyramidal neurons to favor decreased excitatory input. The AIS is known homeostatically regulate its length and distance from cell soma to compensate for differences in input (Kuba et al., 2010; Gulledge and Bravo, 2016). However, no changes in average AIS length or cumulative distribution of AIS lengths was observed in either the CA1 or the CA3 or *Nrx1*$^{+/-}$ rats compared to controls (CA1 fig.5.6B, B' *Nrx1*$^{+/+}$= 34.84 μm $\pm$ 0.47 μm n=7, *Nrx1*$^{+/-}$= 35.19 μm $\pm$ 0.81 μm n=7 animals; CA3 fig.5.6D, D' *Nrx1*$^{+/+}$= 41.70 μm $\pm$ 0.55 μm n=7, *Nrx1*$^{+/-}$= 42.40 μm $\pm$ 1.30 μm n=7 animals).

Finally, Twining et al. (2017) found chemogenetically reversible deficits in a amygdala-dependent social cued fear conditioning paradigm in the *Nrx1*$^{-/-}$ rats. Accompanying this deficit was increased firing activity in neurons of the medial but not the lateral amygdala nucleus. In keeping with the lack of altered cellular firing in the LA of *Nrx1*$^{-/-}$ rats, no alterations in average AIS length or cumulative distribution of AIS lengths was observed in either the LA of *Nrx1*$^{+/-}$ rats compared to controls (fig.5.6F, F' *Nrx1*$^{+/+}$= 29.24 μm $\pm$ 0.76 μm n=8, *Nrx1*$^{+/-}$= 27.73 μm $\pm$ 0.53 μm n=7 animals). Further, as social-cued fear conditioning also involves the basal amygdala , I examined AIS lengths in neurons from this region as well but found no change in average legnth or cumulative distribution of AIS lengths in BA neurons of *Nrx1*$^{+/-}$ rats compared to controls (fig.5.6H, H' *Nrx1*$^{+/+}$= 41.76 μm $\pm$ 1.77 μm n=7, *Nrx1*$^{+/-}$= 38.94 μm $\pm$ 2.01 μm n=6 animals).

In keeping with results obtained from juvenile *Syngap1*$^{+/-}$ and *Nlgn3*$^{-/y}$ rats, heterozygosity of *Nrx1*, does not result in altered AIS lengths in any of the brain regions analysed here.

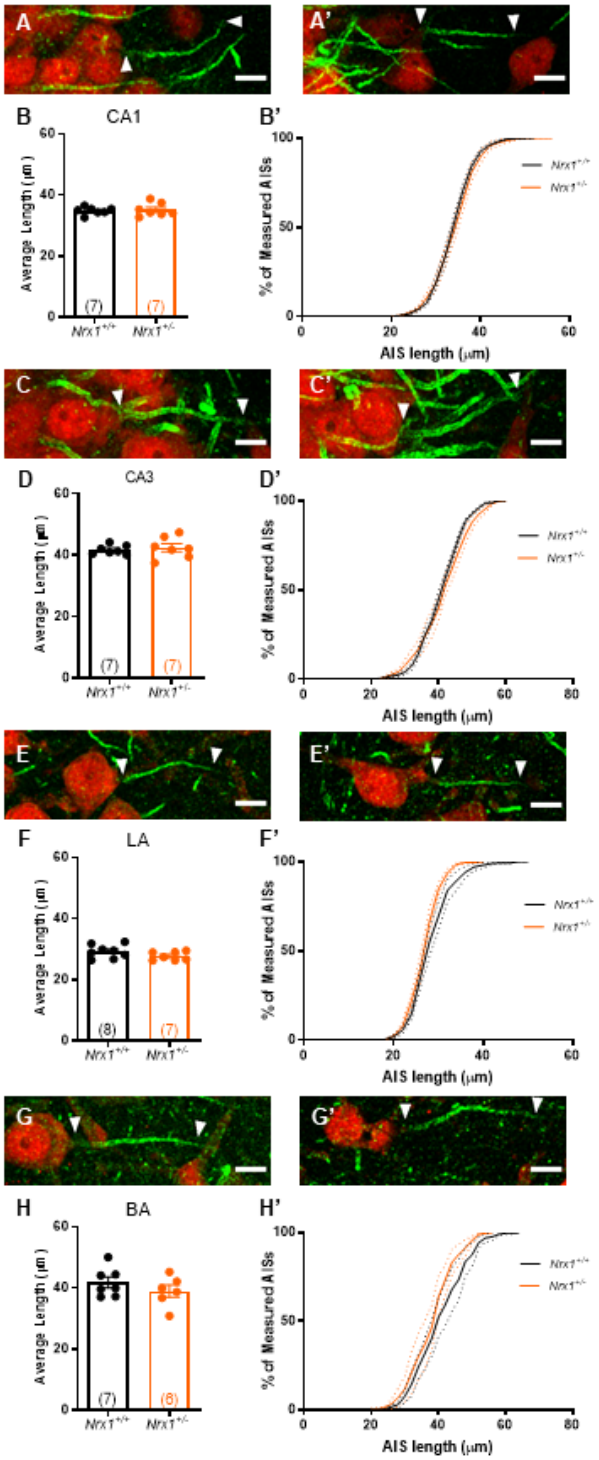

Figure 5.6: AIS lengths in sub-cortical regions of *Nrx1*$^{+/-}$ rats (A-A', C-C', E-E', G-G') Representative single AIS from *Nrx1*$^{+/+}$ and *Nrx1*$^{+/-}$ rats respectively from the hippocampus (CA1 A-A', CA3 C-C') and the BLA (LA E-E', BA G-G'). No change between *Nrx1*$^{+/-}$ and *Nrx1*$^{+/+}$ rats in avg AIS length or cumulative distribution of AIS lengths was observed in the CA1 (B-B'), CA3 (D, D'), LA (F-F') or BA (H-H').

5.5 *Contactin-associated protein-like 2 (Cntnap2)*

First identified in 1999, the *Contactin-associated protein-like 2* or *Cntnap2* gene is 2.3Mb long, located in chromosomal region 7q35 in humans (chromosome 6 in mice and rats), composed of 24 exons and encodes a transmembrane protein of the neurexin super-family of cell adhesion molecules (Poliak et al., 1999; Nakabayashi and Scherer, 2001). Functionally, Cntnap2 mediates K^+ channel clustering in mature complex peripheral neurons via a contactin-2/TAG-1 complex at the juxtaparanodes of myelinated axons (Poliak et al., 2003) and localisation of $K_v1.2$ channels in the distal axon initial segment of central pyramidal neurons (Rasband et al., 2002; Inda et al., 2006). In the developing brain, *Cntnap2* affects dendritic arborisation, spine development and stabilisation of newly formed synapses (Anderson et al., 2012).

CNTNAP2-related neuronal disorder was first reported by Verkerk et al. (2003) in a family carrying a heterozygous translocation at intron 8. Behavioural manifestations of this mutation included Gilles de la Tourette syndrome, ID and obsessive-compulsive disorder Verkerk et al. (2003)). In 2006, Strauss et al. (2006) reported a homozygous loss of function point-mutation in *CNTNAP2* in 13 pro-bands of old-order Amish descent presenting with cortical-dysplasia-focal epilepsy (CDFE), language regression, hyperactivity and intellectual disability. Temporal-lobe specimens from these individuals showed abnormal neuronal migration with reduced CNTNAP2 (or CASPR2) expression. Homozygous loss-of-function deletions in *CNTNAP2* have also been found in individuals with Pitt-Hopkins like ID (Zweier et al., 2009). Since then, heterozygous disruptions arising from gene dosage, rare mutations and common variation in *CNTNAP2* have been associated with various forms of NDDs including ID, ADHD, epilepsy and schizophrenia (Rodenas-Cuadrado et al., 2014). Currently, the SFARI Gene database classifies *CNTNAP2* as a 'strong-causative candidate' for syndromic ASD/ ID.

To date, pre-clinical studies on loss-of *Cntnap2* have focused on the homozygous loss-of-function mutation, despite most reported cases of *CNTNAP2* disruptions in humans being heterozygous in nature. *Cntnap2*$^{-/-}$ mice show deficits in the core ASD-like behaviour including repetitive stereotypy and social deficits as well as hyperactivity and seizures (Peñagarikano et al., 2011). Using a juvenile play test, Peñagarikano et al. (2011) show that *Cntnap2*$^{-/-}$ mice spend significantly less time interacting with a conspecific animal while showing increased

stereotyped behaviours like grooming and digging. Social deficits were also observed upon loss of Cntnap2, where *Cntnap2*$^{-/-}$ mice when places in a 3-chamber task showed no preference for sociability. Additionally, upon examination of nesting behaviour, which can act as an indicator or home-cage sociability, *Cntnap2*$^{-/-}$ mice showed decreased nesting (Peñagarikano et al., 2011). Sociability is known to be mediated by the mPFC (Yoon et al., 2018) and in *Cntnap2*$^{-/-}$ mice Selimbeyoglu et al. (2017) showed that optogenetically shifting the excitatory/inhibitory balance towards increased inhibition in the mPFC of these animals restores their preference for social novelty. The same study also found inherently different PV interneuron activity in the mPFC of *Cntnap2*$^{-/-}$ mice as, upon social interaction, PV interneuron activity showed no signs of increase, as was would be expected in wildtype animals (Selimbeyoglu et al., 2017). Further, *Cntnap2*$^{-/-}$ mice also show fewer PV interneurons in L4 of the somatosensory cortex (Vogt et al., 2018). Pyramidal cells of S1 L2/3, that receive feed-forward information from S1 L4 (Feldmeyer et al., 2013), show increased E/I conductance ratio in *Cntnap2*$^{-/-}$ mice (Antoine et al., 2019) while *in vivo* two-photon Ca^{2+} imaging showed asynchronous firing in S1 L2/3 cells of *Cntnap2*$^{-/-}$ mice compared to wildtypes (Peñagarikano et al., 2011). A reduction in PV interneurons was also observed in the hippocampus of *Cntnap2*$^{-/-}$ mice, accompanied by deficits in hippocampal dependent behavioural tasks (Peñagarikano et al., 2011) including reduced cognitive flexibility, with *Cntnap2*$^{-/-}$ mice failing to perform the reversal phase of the Morris water maze task and showing significantly reduced alternation in the spontaneous T-maze test (Peñagarikano et al., 2011). Lastly, elevated levels of social anxiety (Peñagarikano and Geschwind, 2012) are a common clinical feature in individuals with mutations in *CNTNAP2*. However, *Cntnap2*$^{-/-}$ mice show no elevation in anxiety-like behaviours in a light-dark box test (Peñagarikano and Geschwind, 2012).

This focus on the homozygous model is partly explained by the evidence of deleterious heterozygous mutations being identified in unaffected controls in studies (Strauss et al., 2006) as well as the general population (Bakkaloglu et al., 2008), lending weight to the argument that type of mutation and genetic background affects the translation of disruption into disorder. Given the above observed phenotypes, AIS length analysis in this chapter is focused on a heterozygous loss-of-function pre-clinical rat model of *Cntnap2* (*Cntnap2*$^{+/-}$) in the mPFC PL, S1BF, CA1, CA3, BLA and V1.

5.5.1 Results

In the mPFC, no change in average AIS length or cumulative distribution of AIS lengths was observed in either PL L2/3 or L5 of juvenile *Cntnap2*$^{+/-}$ rats compared to controls (L2/3 fig.5.7B, B' *Cntnap2*$^{+/+}$= 28.46 μm $\pm$ 0.69 μm n=5, *Cntnap2*$^{+/-}$= 30.03 μm $\pm$ 0.20 μm n=5 animals; L5 fig.5.7D, D' *Cntnap2*$^{+/+}$= 29.70 μm $\pm$ 0.47 μm n=5, *Cntnap2*$^{+/-}$= 31.39 μm $\pm$ 0.50 μm n=5 animals).

Given the altered excitability of neurons in the S1BF of *Cntnap2*$^{-/-}$ mice, I examined AIS lengths in various layers of the S1 in order to determine if alterations in AIS lengths could be a contributing factor to altered cellular excitability. No change in average AIS length or cumulative distribution of AIS lengths were observed in any of the superficial or deep layers of the S1BF in P28-35 *Cntnap2*$^{+/-}$ rats compared to littermate controls (fig.5.7F, F' S1 L2/3 *Cntnap2*$^{+/+}$= 29.03 μm $\pm$ 1.06 μm n=5, *Cntnap2*$^{+/-}$= 28.14 μm $\pm$ 0.44 μm n=5; H, H' S1 L4 *Cntnap2*$^{+/+}$= 23.19 μm $\pm$ 0.95 μm n=5, *Cntnap2*$^{+/-}$= 22.54 μm $\pm$ 0.25 μm n=5; J, J' S1 L5 *Cntnap2*$^{+/+}$= 29.62 μm $\pm$ 0.39 μm n=5, *Cntnap2*$^{+/-}$= 28.48 μm $\pm$ 0.76 μm n=5 animals). Further, AIS legnths were measured in primary visual cortex of *Cntnap2*$^{+/-}$ rats, to analyse if lengths were affected in another sensory region was altered. No difference in either average AIS length or cumulative distribution of AIS lengths was observed in either V1 L2/3 or L5 of juvenile *Cntnap2*$^{+/-}$ rats compared to controls (L2/3 fig.5.7L, L' *Cntnap2*$^{+/+}$= 26.87 μm $\pm$ 0.97 μm n=5, *Cntnap2*$^{+/-}$= 26.27 μm $\pm$ 0.89 μm n=5 animals; L5 fig.5.7N, N' *Cntnap2*$^{+/+}$= 31.05 μm $\pm$ 0.37 μm n=5, *Cntnap2*$^{+/-}$= 30.26 μm $\pm$ 0.47 μm n=5 animals).

Individuals with *CNTNAP2* mutations exhibit severe temporal lobe epilepsy and language impairments while *Cntnap2*$^{-/-}$ mice and rats exhibit spontaneous seizures (Peñagarikano et al., 2011; Thomas et al., 2017). Epileptiform activity is suggestive of increased network and cellular excitability (Tuchman et al., 2010; Samra et al., 2017) with alterations in AIS length and composition being implicated in temporal lobe epilepsy (Wimmer et al., 2010). Thus, here I examined AIS lengths in the CA1 and CA3 subregion of the hippocampus, where focal seizures originate (Scheffer et al., 2017). However, similar to results obtained in other brain regions, average and cumulative distribution of AIS lengths in both CA1 and CA3 were comparable across genotypes (fig.5.8B CA1 *Cntnap2*$^{+/+}$= 34.68 μm $\pm$ 1.32 μm n=4, *Cntnap2*$^{+/-}$= 35.17 μm $\pm$ 0.97 μm n=5; D CA3 *Cntnap2*$^{+/+}$= 42.02 μm $\pm$ 1.06 μm n=4, *Cntnap2*$^{+/-}$= 42.64 μm

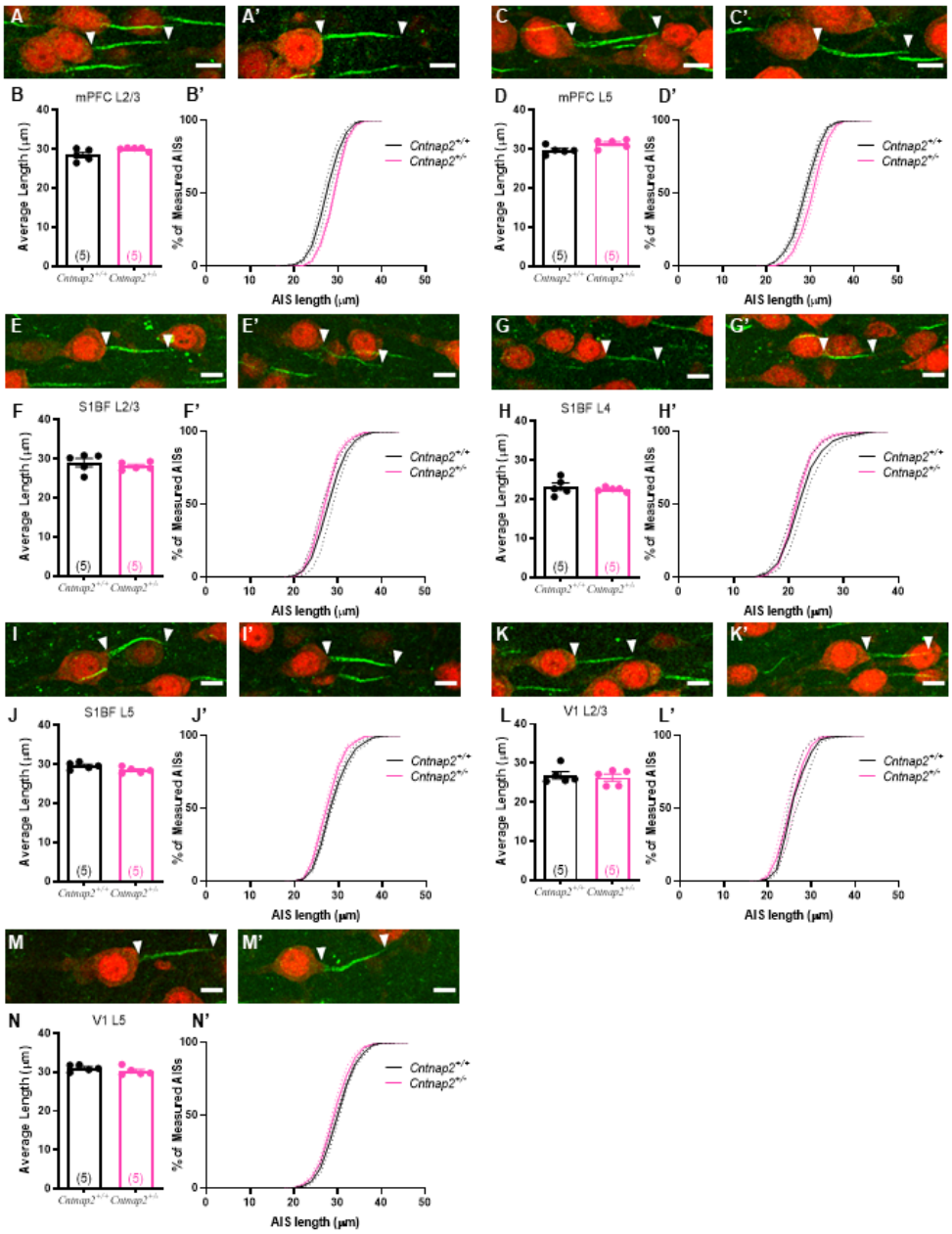

Figure 5.7: AIS lengths in cortical regions of *Cntnap2*$^{+/-}$ rats (A-A', C-C', E-E', G-G', I-I',K-K',M-M') Representative single AIS from *Cntnap2*$^{+/+}$ and *Cntnap2*$^{+/-}$ rats respectively from the PL (L2/3 A-A', L5 C-C'), S1 (L2/3 E-E', L4 G-G', L5 I-I') and V1 (L2/3 K-K', L5 M-M'). No change in avg AIS length or cumulative distribution of AIS lengths was observed in PL L2/3 (B-B'), PL L5 (D-D'), S1 L2/3 (F, F'), S1 L4(H-H'), S1 L5 (J-J'), V1 L2/3 (L-L') and V1 L5 (N-N') of *Cntnap2*$^{+/-}$ rats compared to controls.

$\pm$ 0.98 μm n=5 animals).

Although pre-clinical models of *CNTNAP2* associated ID donot present with over anxiety-deficits, in keeping with the comparison of looking at the basolateral amygdala in the other monogenic rat models of ASD/ID, I examined AIS lengths in the BLA of juvenile *Cntnap2*$^{+/-}$ rats. As expected, there were no genotype specific differences in either average AIS length or cumulative distribution of AIS lengths in either the LA or the BA (LA fig.5.8F, F' *Cntnap2*$^{+/+}$= 26.09 $\pm$ 0.65 n=4, *Cntnap2*$^{+/-}$= 26.07 μm $\pm$ 0.22 μm n=4 animals; BA fig.5.8H, H' *Cntnap2*$^{+/+}$= 37.01 μm $\pm$ 3.06 μm n=4, *Cntnap2*$^{+/-}$= 32.85 μm $\pm$ 3.05 μm n=5 animals).

Overall, the data here matches the findings from juvenile *Syngap1*$^{+/-}$, *Nlgn3*$^{-/y}$ and *Nrx1*$^{+/-}$ rats and suggests that reduction in Cntnap2/ Caspr2 levels does not affect AIS length in any of the brain regions analysed.

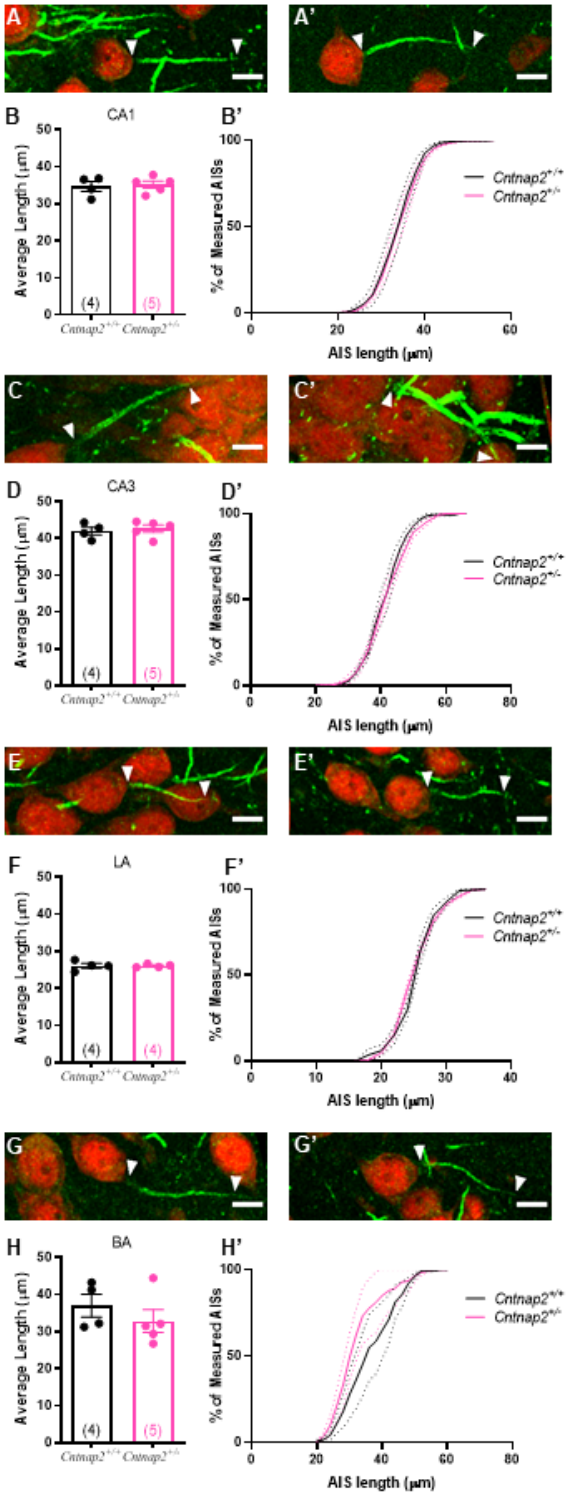

Figure 5.8: AIS lengths in sub-cortical regions of *Cntnap2*$^{+/-}$ rats (A-A', C-C', E-E', G-G') Representative single AIS from *Cntnap2*$^{+/+}$ and *Cntnap2*$^{+/-}$ rats respectively from the hippocampus (CA1 A-A', CA3 C-C') and the BLA (LA E-E', BA G-G'). No change between *Cntnap2*$^{+/-}$ and *Cntnap2*$^{+/+}$ rats in avg AIS length or cumulative distribution of AIS lengths was observed in the CA1 (B-B'), CA3 (D, D'), LA (F-F') or BA (H-H').

5.6 *Phosphatase and tensin homolog*

A canonical tumour suppressor, the phosphatase and tensin homolog (*PTEN*) gene maps to human chromosome 10q23.3 (Nelen et al., 1996; Feilotter et al., 1999) and was first identified as a Cowden syndrome and cancer susceptibility gene in 1996-7 (Nelen et al., 1996; Marsh et al., 1997b,a). Since then, multiple germline mutations in *PTEN* have been identified in individuals with Cowden's syndrome, Bannayan-Riley-Ruvalcaba syndrome and Proteus Syndrome (Zori et al., 1998; Goffin et al., 2001; Butler et al., 2005). Together, these mutations were dubbed PTEN hamartoma tumour syndromes (PHTS) (Mester et al., 2011). A characteristic of PHTS, reported to occur in as high as 94% in some studies (Mester et al., 2011), includes a greater than 2 standard deviation increase from mean in occipital-frontal circumference for given height, sex and ethnicity, or macrocephaly, a phenotype that is also commonly observed in individuals with autism spectrum disorder (Dementieva et al., 2005; Chaste et al., 2013).

The first case study of *PTEN* mutation with autism was reported by Goffin et al. (2001), in a proband with maternal diagnosis of Cowden syndrome. While the mother did not show altered social function or evidence of intellectual disability the child showed progressive macrocephaly with hallmark signs for ASD including severe speech delay, short attention span, lack of interest in social contacts and stereotyped behaviours like hand-flapping (Goffin et al., 2001). Following this initial case report, heterozygous germline mutations in *PTEN* associated with ASD and macrocephaly have been reported in over 11 studies (Butler et al., 2005; Buxbaum et al., 2007; Herman et al., 2007; Orrico et al., 2009; Varga et al., 2009; McBride et al., 2010; Klein et al., 2013; Hobert et al., 2014; Marchese et al., 2014). Other common co-morbidities present in these patients include intellectual disability Tan et al. (2011), delayed language development (Frazier et al., 2015), increased cortical white matter (Vanderver et al., 2014; Frazier et al., 2015), poor working memory (Frazier et al., 2015; Tilot et al., 2014, 2015) and increased seizure susceptibility with cortical dysplasia (Child and Cascino, 2013; Cheung et al., 2014; Elia et al., 2012; O'Rourke et al., 2012; Conti et al., 2012; Tilot et al., 2015).

PTEN encodes a phosphatase with four major domains: An N-terminal tail responsible for its nuclear versus cytoplasmic localisation and mediating binding of phosphatidylinositol4,5-bisphosphate (PIP_2) (Gil et al., 2006; Denning et al., 2007; Walker et al., 2004), the pro-

tein phosphatase catalytic core domain (Li et al., 1997), a membrane binding C2 domain and a PDZ-domain containing C-terminal tail (Li et al., 1997; Jurado et al., 2010). The PDZ-binding domain allows PTEN to bind to scaffolding proteins such as PSD-95, resulting in localisation at the post-synaptic density (Li et al., 1997; Jurado et al., 2010). In its capacity as a phosphatase, PTEN hydrolyses phosphatidylinositol (3,4,5)-trisphosphate (PIP_3) to phosphatidylinositol4,5-bisphosphate (PIP_2) thus antagonising the phosphatidylinositol 3-phosphate kinase (PI3K)/protein kinase B (PKB/AKT) / mammalian target of rapamycin (mTOR) pathway (Li et al., 1997; Maehama and Dixon, 1998; Worby and Dixon, 2014). Through these downstream signalling cascades PTEN modulates cellular proliferation, differentiation and death during development (Kwon et al., 2006; Stiles et al., 2004) and in adults (Gregorian et al., 2009; Amiri et al., 2012; Chow et al., 2009). The PI3K/AKT/mTOR pathway is of particular interest within the ASD community as another model of ASD, tuberous sclerosis, results from mutations in genes encoding the tuberous sclerosis complex, an inhibitor of the mTOR pathway (Inoki et al., 2002).

Full knock-down of *Pten* is embryonic lethal, therefore various conditional knock-out lines have been created to study the underlying biological changes occurring upon reduction in PTEN levels (Kwon et al., 2001; Backman et al., 2001; Kwon et al., 2006; Kazdoba et al., 2012; Lugo et al., 2014; Amiri et al., 2012). Loss of ~50% of PTEN protein results in various cytoarchitectural alterations particularly hyperproliferation of neuronal precursor cells (Kazdoba et al., 2012), defective migration and cortical lamination (Kwon et al., 2001; Backman et al., 2001; Wen et al., 2013) and neuronal hypertrophy resulting in macrocephaly (Kwon et al., 2001, 2006; Rademacher and Eickholt, 2019). However, given the focus on AIS in this thesis, I summarize here the ASD-like behavioural phenotypes, synaptic and intrinsic cellular excitability deficits observed in various mouse models of *Pten* haploinsufficiency.

Altered social behaviours and communication form one half of the ASD diagnostic criteria. Selective loss of *Pten* from adult neuronal populations in the cerebral cortex and hippocampus (Kwon et al., 2006), neuronal precursor cells (Amiri et al., 2012) and granule neurons of the cerebellum and hippocampus (Lugo et al., 2014) results in reduced social behaviour with a loss of preference for sociability in *Pten* heterozygous mice, as measured using a three-chamber task. However, a knock-in germline mutant of *Pten*, resulting in increased cytoplasmic localisation of the protein, exhibits increased sociability (Tilot et al., 2014). Further, germline *Pten* knock-

down heterozygous (*Pten*$^{+/-}$) mice (Clipperton-Allen and Page, 2014) as well as mice in which *Pten* has selectively been knocked down from hippocampal dentate granule cells results in increased repetitive behaviours measured by marble burying and increased grooming (Lugo et al., 2014). Additional PTEN-ASD co-morbidities that are recapitulated in these mouse models include increased incidence of seizures (Backman et al., 2001) with lowered threshold for induction of audiogenic seizures (Kwon et al., 2006; Ogawa et al., 2007), increased sensitivity to acoustic stimuli with impaired sensorimotor gating (Kwon et al., 2006) and balance and gait abnormalities as measured using an accelerating rota-rod test (Tilot et al., 2014). There is also come evidence of impaired hippocampal dependent spatial memory, as *Pten+/-* mice with protein selectively knocked down from post-mitotic neurons of the hippocampus and cerebral cortex show increased latency with a slower learning curve to finding a platform in the Morris water maze (Kwon et al., 2006). Hyperactivity and anxiety-like behaviours upon loss of *Pten* appear to be specific to the conditional knock-out as some models show elevated anxiety with hyperactivity (Page et al., 2009; Clipperton-Allen and Page, 2014; Kwon et al., 2006) while others show reduced anxiety (Lugo et al., 2014).

Underlying these behaviours are various intrinsic excitability and synaptic plasticity changes (Daoudal and Debanne, 2003). In a model where *Pten* has been selectively knocked down from cells of the medial ganglionic eminence, the region where somatostatin-positive GABAergic interneuons arise, an increase in parvalbumin/somatostatin ratio with lowered E/I ratio and impaired social behaviours is found (Vogt et al., 2015). Conversely, *Pten* deletion from developing hippocampal excitatory neurons , but not those of the mature amygdala and auditory cortex Sperow et al. (2012); Haws et al. (2014); Xiong et al. (2012), causes cellular hyper-excitability as measured by increased numbers of synapses with an excess of excitatory inputs and increased frequency of mEPSCs (Sperow et al., 2012; Xiong et al., 2012; Williams et al., 2015; Pun et al., 2012; Skelton et al., 2019). Conditional single-copy deletion of PTEN increases expression of small-conductance calcium-activated potassium channels with a reduction in pyramidal cell excitability, evidenced by decreased frequency of action potential firing, lowered membrane resistance and increased after-hyperpolarisation (Garcia-Junco-Clemente et al., 2013). Synaptic plasticity alterations upon loss of PTEN, particularly LTP, are animal-age and brain region dependent. Neuron-specific deletion of PTEN enhances dentate gyrus granule cell theta burst-LTP in adult (8-12 week) mice, whereas it impairs theta burst-LTP in both the dentate gyrus and CA1 neurons of aged mice (20-30 weeks) (Takeuchi et al., 2013). Comparably, at CA3-CA1

synapses NMDAR-LTP in 8 week-old mice lacking PTEN is decreased (Sperow et al., 2012; Fraser et al., 2008) while mice at both ages show impaired NMDAR- and mGluR-LTD (Sperow et al., 2012; Takeuchi et al., 2013). Interestingly, pharmacological blockade of PTEN lipid phosphatase activity results in impaired NMDAR- but not mGluR-LTD or LTP (Jurado et al., 2010). Together, these results indicate developmental loss of *Pten* can result in altered cellular excitability and connectivity whereas selective loss in mature neurons results in altered synaptic plasticity (Rademacher and Eickholt, 2019).

Given this evidence of altered cellular excitability, particularly in the hippocampus, amygdala and auditory sensory cortex, and the presence of impairments in hippocampal, prefrontal cortex and sensory-behaviours here I have analysed AIS lengths in a rat model of *Pten* haploinsufficiency.

5.6.1 Results

While our laboratory has found a gross increase in brain size, with enlarged ventricles, in the $Pten^{+/-}$ rats (A Sharma, unpublished), no change in average AIS length or cumulative distribution of AIS lengths is observed in either L2/3 or L5 of the PL of juvenile (P28-32) $Pten^{+/-}$ rats compared to wildtype, littermate controls (L2/3 fig.5.9B, B' $Pten^{+/+}$= 29.00 μm $\pm$ 0.99 μm n=5, $Pten^{+/-}$= 28.91 μm $\pm$ 0.60 μm n=5 animals; L5 fig.5.9D, D' $Pten^{+/+}$= 29.32 μm $\pm$ 1.33 n=5, $Pten^{+/-}$= 30.14 $\pm$ 1.25 μm n=5 animals). Similarly, no change is observed in average or cumulative AIS lengths in L2/3, L4 or L5 of the somatosensory barrel cortex of $Pten^{+/-}$ rats compared to controls (L2/3 fig.5.9F, F' $Pten^{+/+}$= 26.76 $\pm$ 1.13 n=5, $Pten^{+/-}$= 27.35 μm $\pm$ 1.22 μm n=5 animals; L4 fig.5.9H, H' $Pten^{+/+}$= 22.21 μm $\pm$ 0.37 μm n=5, $Pten^{+/-}$= 22.37 μm $\pm$ 0.96 μm n=5 animals; L5 fig.5.9J, J' $Pten^{+/+}$= 28.62 μm $\pm$ 0.47 μm n=5, $Pten^{+/-}$= 30.10 μm $\pm$ 0.67 μm n=5 animals). Due to poor tissue quality of sections containing the primary visual cortex was severely degraded and could not be collected.

The hippocampus is where majority of the excitability deficits in *Pten* heterozygous mouse models are observed. Here however, no statistically significant differences were seen in average AIS length or cumulative AIS lengths between $Pten^{+/-}$ and wildtype control animals in either the CA1 or the CA3 (CA1 fig.5.10B, B' $Pten^{+/+}$= 34.69 μm $\pm$ 1.43 μm n=4, $Pten^{+/-}$= 37.82 μm $\pm$

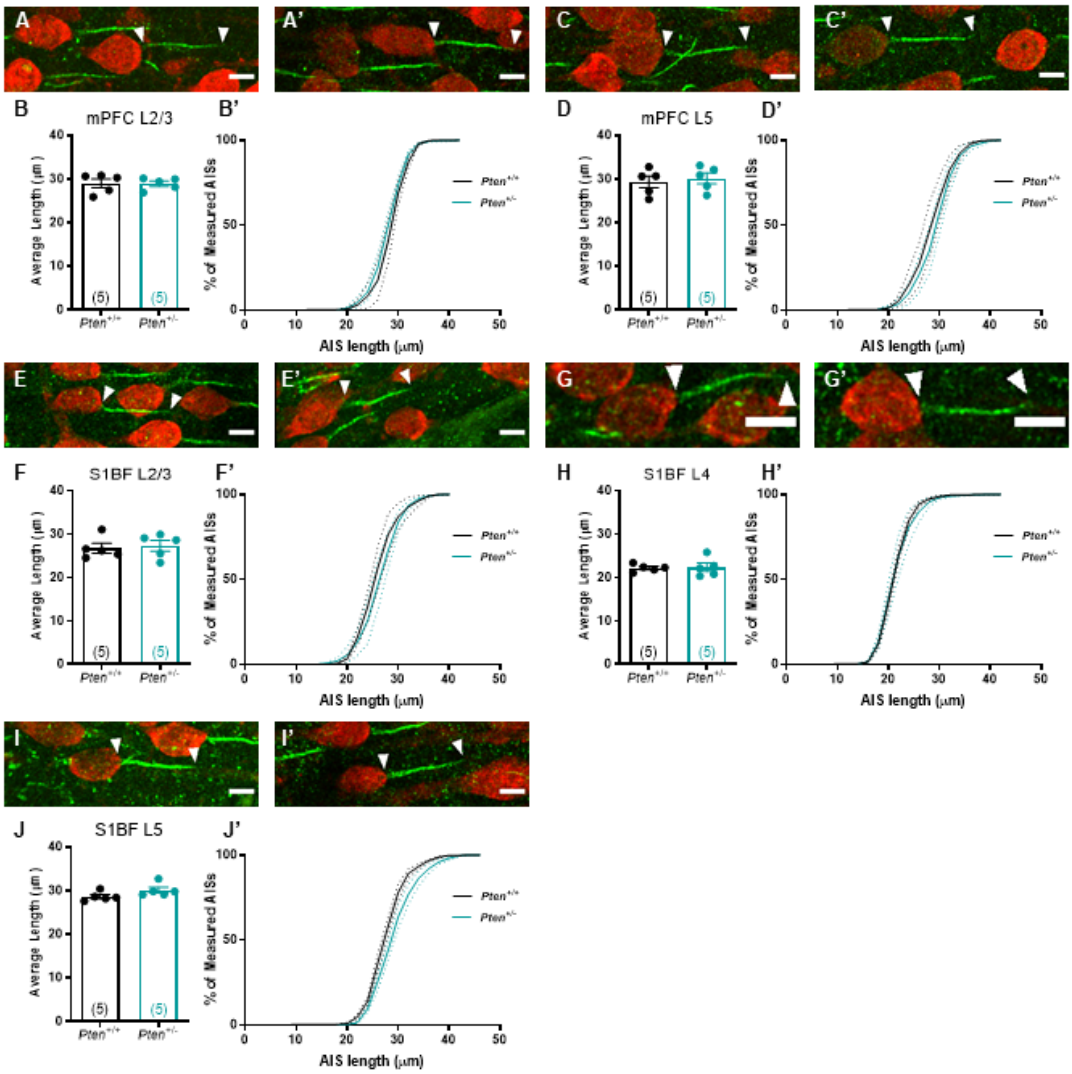

Figure 5.9: AIS lengths in cortical regions of *Pten*$^{+/-}$ rats (A-A', C-C', E-E', G-G', I-I') Representative single AIS from *Pten*$^{+/+}$ and *Pten*$^{+/-}$ rats respectively from the PL (L2/3 A-A', L5 C-C') and S1 (L2/3 E-E', L4 G-G', L5 I-I'). No change in average AIS length or cumulative distribution of AIS lengths was observed in PL L2/3 (B-B'), PL L5 (D-D'), S1 L2/3 (F, F'), S1 L4(H-H') or S1 L5 (J-J') of *Pten*$^{+/-}$ rats compared to controls.

0.89 μm n=3 animals; CA3 fig.5.10D, D' *Pten*$^{+/+}$= 40.69 μm $\pm$ 1.07 μm n=3, *Pten*$^{+/-}$= 46.91 μm $\pm$ 2.30 μm n=3 animals). Similarly, no alterations in average or cumulative distribution of AIS lengths was observed in either the LA or the BA of the *Pten*$^{+/-}$ animals compared to controls (LA fig.5.10F, F' *Pten*$^{+/+}$= 27.13 μm $\pm$ 0.50 μm n=5, *Pten*$^{+/-}$= 29.29 μm $\pm$ 1.14 μm n=3 animals; BA fig.5.10H, H' *Pten*$^{+/+}$= 40.20 μm $\pm$ 2.72 μm n=5, *Pten*$^{+/-}$= 34.52 μm $\pm$ 4.76 μm n=3 animals). Due poor tissue quality of the sections containing the CA1, CA3, BA and LA, the power of these experiments is low and the results are preliminary.

Overall, AIS length data from *Pten*$^{+/-}$ rats matched those obtained from *Syngap1*$^{+/-}$, *Nlgn3*$^{-/y}$, *Nrx1*$^{+/-}$ and *Cntnap2*$^{+/-}$ rats in that no genotype specific alterations were found in any brain region analysed.

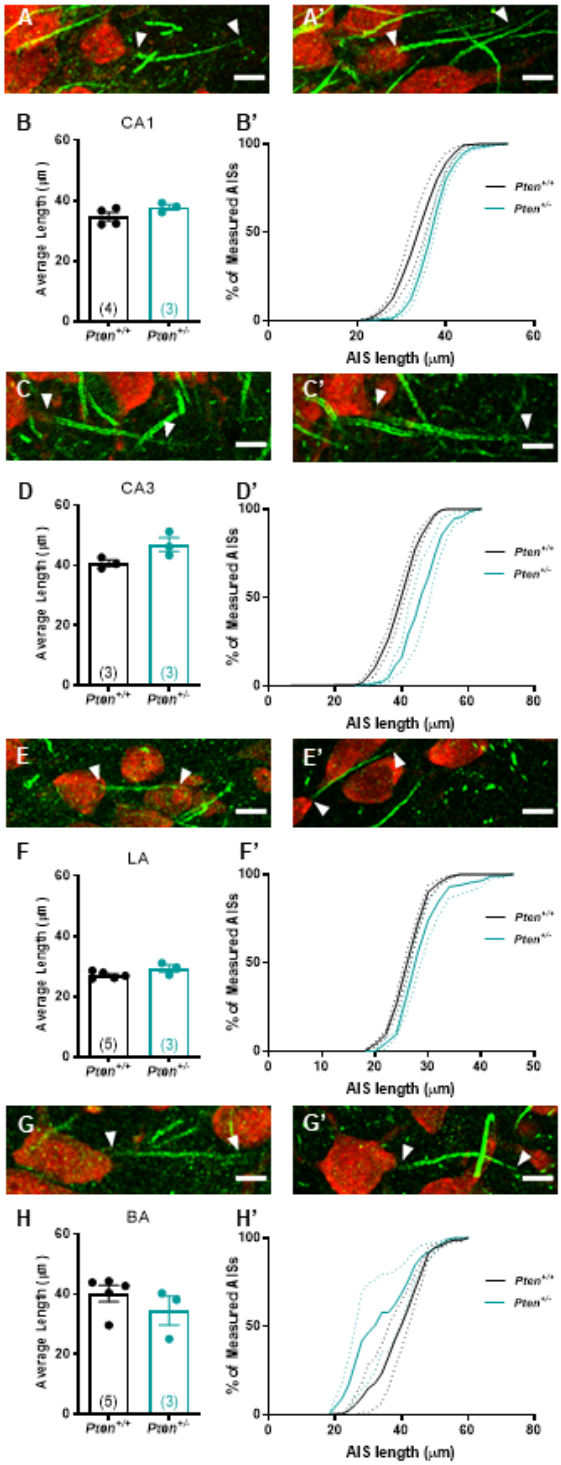

Figure 5.10: AIS lengths in sub-cortical regions of *Pten*$^{+/-}$ rats (A-A', C-C', E-E', G-G') Representative single AIS from *Pten*$^{+/+}$ and *Pten*$^{+/-}$ rats respectively from the hippocampus (CA1 A-A', CA3 C-C') and the BLA (LA E-E', BA G-G'). No change between *Pten*$^{+/-}$ and *Pten*$^{+/+}$ rats in avg AIS length or cumulative distribution of AIS lengths was observed in the CA1 (B-B'), CA3 (D, D'), LA (F-F') or BA (H-H').

5.7 Discussion

Alterations in cellular excitability have been noted in multiple models of ASD/ID (Contractor et al., 2015; Nelson and Valakh, 2015). However, variation in experimental design across studies in brain region, cell type, age of experimental animal and choice of physiological methods complicates the identification of common cellular, synaptic and circuit deficits in these models (Antoine et al., 2019). Given recent findings that AIS length is differentially regulated in models of ASD/ID (Kaphzan et al., 2011; Kloth et al., 2017; Booker et al., 2019), I hypothesized that alteration in AIS length may be a point of convergence in ASD/ID that underlies this altered cellular excitability. In comparison to electrophysiological techniques, such as patch-clamping, measuring differences in AIS lengths as a proxy measurement for difference in cellular excitability is more high-throughput; thus allowing for rapid analysis across multiple brain regions to select one for further investigation. Taking advantage of this high-throughput read-out, I conducted a systematic analysis of AIS lengths across six different brain regions in five novel monogenic rat models of ASD/ID. As ASD/ID is a developmental disorder and altered cellular excitability in preclinical models is shown to underlie sensory hypersensitivities in these models, the juvenile age (P28-35) of experimental animals was chosen to coincide with the critical period of experience-dependent plasticity of the visual cortex (De Villers-Sidani et al., 2008; Fagiolini and Leblanc, 2011).

Of the five rats models analysed in this chapter, and six in this thesis, genotype specific changes in AIS length at P28 was observed only in the PL L5, S1 L5 and BA of the *Fmr1*$^{-/y}$ rats with AIS lengths in all other brain regions and models being comparable to wildtype littermate controls. Thus suggesting that alterations in AIS length of pyramidal cells in the selected brain regions is not a node of convergence and does not contribute to the excitability pathophysiology observed in these models. However, this result does not preclude additional factors, such as altered circuit excitability, being a convergent node in the pathophysiology of these models.

5.7.1 Altered AIS length in *Fmr1*$^{-/y}$ rats

The only model to show genotype specific alterations in AIS length was the *Fmr1*$^{-/y}$ model of FXS, making it an interesting candidate for further study. Specifically, increased AIS lengths were noted in neurons of of PL L5, S1BF and the BA. Given that in the *Fmr1*$^{-/y}$ mouse model, increased AIS length in the CA1 is shown to underlie cellular hyperexcitability (Booker et al., 2019) and increased AIS length in the BA was coupled with increased cellular firing (Jackson, 2016), loss of FMRP results in AIS length mediated alterations in cellular excitability in a brain-region and layer-specific. All the layers shown to have increased AIS length are known to have long-range projections (Hoover and Vertes, 2007; Krettek and Price, 1977; Denardo et al., 2015), with local excitatory connectivity of these neurons being highly correlated with their long range targets (Brown and Hestrin, 2009). Of particular interest is the ~11% increased length in PL L5, as previous work in the laboratory has found that a ~20% reduction in AIS length in PL-BLA projection neurons of adult (>P60) *Fmr1*$^{-/y}$ rats accompanied by cellular hypoexcitability (see appendix figS1, Jackson (2016)). This would further suggest sub-population specific alterations in AIS length upon loss of FMRP or sub-population specific adaptation of AIS length during development in this model. PL-BLA projection neurons are imperative for the appropriate consolidation and retrieval of fear related memory (Arruda-Carvalho and Clem, 2015; Akers et al., 2012). Assessment of acquisition and recall of fear memory in rodents is performed using cued or contextual fear conditioning (Akers et al., 2012), a form of associative memory that is found to be impaired in the *Fmr1*$^{-/y}$ rats (see appendix fig.S2). In a visually cued-fear conditioning task, similar to the one used in chapter 4, *Fmr1*$^{-/y}$ rats show freezing rates comparable to WTs during the conditioning phase. 24 hours after conditioning, when recall of fear memory is assessed, *Fmr1*$^{-/y}$ rats showed markedly reduced freezing upon re-exposure to the exposed to the conditioned stimulus, indicating impaired formation of fear-associated memory. This behavioural phenotype is opposed to that observed in the *Syngap1*$^{+/-}$ and *Syngap1*$^{+/\Delta Gap}$ rats, where the animals showed an exaggerated freezing response during re-call of fear-memory (figs. 4.5B, 4.7B). Future experiments should assess if differential alterations in AIS lengths in PL-BLA projection neurons are observed between *Fmr1*$^{-/y}$, *Syngap1*$^{+/-}$ and *Syngap1*$^{+/\Delta Gap}$ rats post fear conditioning.

Overall, the data suggests that alterations in AIS length may be one of the underlying mechanisms of circuit hyperexcitability noted in pre-clinical models of FXS (Contractor et al.,

2015) with species specific differences, as the elongated AIS phenotype observed in the CA1 of the mouse model of FXS did not translate to our rat-model.

5.7.2 Additional factors underlying ASD pathophysiology

Additional factors known to be causative of ASD include altered chromatin function and impaired transcriptional control (Sullivan et al., 2019), perturbed synapse formation and function (Gilman et al., 2011; Krumm et al., 2014) and altered neuronal signalling pathways (Krumm et al., 2014; Pinto et al., 2014). Gene expression studies comparing post-mortem brains from individuals with ASD and matched unaffected controls highlight the role of impaired epigenetic/transcriptional regulation in ASD (for review see Sullivan et al. (2019); Quesnel-Vallières et al. (2019)). Given that alternative splicing occurs more frequently in the brain than in any other tissue (Melé et al., 2015) and abnormal patterns of RNA splicing and isoform usage have been identified in brains of individuals with ASD (Gandal et al., 2018), transcriptional dysregulation may have a particular impact on brain development and physiology. However, as protein products of none of the mutations studied in this chapter are known to affect transcriptional regulation or chromatin remodelling, disruptions in these processes is unlikely to be the causative pathophysiology these models. Further, although FMRP and PTEN are known to regulate various signalling pathways, all the mutations studied in this thesis occur in synaptic proteins. Therefore, a core convergent process likely to be causative of ASD in these models is perturbed synaptic development and functional maturation (Gilman et al., 2011).

The fundamental function of a neurons is the transformation of synaptic input, beyond a certain threshold, into output signals usually in the form of all-or-none reversal of membrane potential polarity and is defined as the excitability of a cell. This integration of synaptic input occurs in dendritic spines, the cell soma and the AIS, with the latter also being the site for AP initiation, which together determine this threshold for AP generation. Development of cellular excitability is a key regulator of neuronal networks, disruption of which results altered neural circuit activity and is implicated in various neurodevelopmental disorders (Rubenstein and Merzenich, 2003), with neuronal hyperexcitability being a proposed model for ASD/ID pathophysiology (Contractor et al., 2015). While the focus of this thesis has been on alteration of AIS morphology driven changes in cellular excitability, synaptogenesis and dendritic spine

dynamics including spine number, morphology and expression of voltage-gated ion channels play a key role in determining synpatic weight and efficiency, and regulating cellular excitability (Van Spronsen and Hoogenraad, 2010; Yuste, 2011). Within models of ASD, disruptions in synaptogenesis, synaptic pruning, spine-turnover and alterations in the expression or activity of ion channels at dendritic spines and cell soma and altered neurotransmitter release could all be contributing mechanisms for neuronal hyperexcitability. Alteration of intrinsic properties of neurons as a result of these perturbation can result in altered synaptic plasticity, exaggerated neuronal firing, abnormally high synchrony of neural networks, and exaggerated sensory-evoked activity. Thus investigation at multiple levels (i.e., molecular, synaptic, cellular, network) is necessary to determine both the pathophysiological effects of different genetic mutations and their resultant ASD phenotype.

5.7.3 Limitations in experimental design

Although the AIS length data from the rat models is fairly conclusive, some decisions of experimental design may contribute to the lack of alterations observed here. These include:

Age of experimental animals The 'ideal' age of the experimental animal depends on the question being investigated and is intrinsically linked to mutation and specific circuit/brain region being studied. Cells in different brain regions show differential excitability over development, depending on the developmental trajectory of the neuronal circuit of which it is a part (Tau and Peterson, 2010). Notably, in *Nlgn3*$^{-/y}$ mice altered cellular excitability in CA3 pyramidal neurons is observed from P4-9 and not at P14, while in *Pten*$^{+/-}$ mice alterations in cellular excitability of CA1 pyramidal cell only occur in animals aged 8 weeks and older. The decision to use juvenile animals for these experiments was chosen to coincide with developmental critical period of experience-dependent alterations in cellular excitability in most of the brain regions studied (De Villers-Sidani et al., 2008; Fagiolini and Leblanc, 2011; Ehrlich et al., 2012). Additionally, the study which found increased AIS length in the CA1 pyramidal neurons of *Fmr1*$^{-/y}$ mice as causative for cellular hyperexcitability was conducted in juvenile animals (P28-32). However, increased AIS length and cellular hyperexcitablity in CA1 pyramidal neurons of the mouse model of Angelman's syndrome was observed in adult (8-12 week) mice. Thus, while the age chosen for analysis was optimised for the brain regions being studied,

given the cellular excitability phenotypes observed analysis of AIS lengths at different ages and adaptation of AIS length with age might be more appropriate depending on the model.

Selection of brain regions A two tiered rationale was used to select the brain-regions where alterations in AIS were analysed. First, these brain regions were behaviourally relevant, with impairments in behavioural assessments involving these brain regions being observed in other pre-clinical models of the genetic mutations studied here. Second, cellular excitability and synaptic plasticity have been widely studied in these brain-regions in the context of neurodevelopmental disorders (for review see Takarae and Sweeney (2017)). However, most studies focus on characterisation of cellular deficits in a single brain-region, whereas I have chosen to perform within subject systematic analysis of AIS length across multiple brain-regions reported with altered excitability in autism (for review see Takarae and Sweeney (2017)). Consequently, brain-regions that have been disrupted in the individual models were excluded. For example, sociability deficits observed in *Nlgn3*$^{-/y}$ mice was shown to be dependent on dopaminergic neurons of the dorsal striatum (Lee et al., 2018), while social novelty deficits were found to be dependent on dopaminergic neurons of the ventral tegmental area (Bariselli et al., 2018).

Further, AIS analysis in this thesis was largely restricted to pyramidal cells. Höfflin et al. (2017) characterised AIS morphology and distance from soma in a variety of cortical cell types including excitatory pyramidal neurons and different sub-type of interneurons. Based on their classification, the AISs measured in this thesis belonged to excitatory pyramidal cells as all measured AISs were of somatic origin, with a minimally discernible gap between the AIS and the soma and followed near perpendicular trajectory to the cell soma. Inhibitory signalling in the BA of *Fmr1*$^{-/y}$ mice is impaired, as is the excitability of fast-spiking inter-neurons in the mPFC of *Nlgn3*$^{-/y}$ mice. Thus, literary evidence suggests future investigation of altered AIS lengths and excitability of interneurons in our rat models of ASD/ID and brain regions of interest might be of value.

Nature of mutations Genome-wide association studies published in parallel to the undertaking of this project found no association between mutations in some of the genes studied in this chapter and ASD. Notably, rare heterozygous mutations in *CNTNAP2* were not found to be substantially different between cohorts of psychiatric patients and the general control population (Murdoch et al., 2015; Toma et al., 2018). Congruent with these studies, behavioural

and electrophysiological studies performed by members of the lab found no genotype specific differences between *Cntnap2*$^{+/-}$ and control rats. Thus, the lack of alteration in AIS length observed in all brain regions in *Cntnap2*$^{+/-}$ is unsurprising. However, homozygous mutations in *CNTNAP2* are still associated with ASD (Poot, 2015), with pre-clinical models of *Cntnap2*$^{-/-}$ showing evidence of cellular hyperexcitability (Antoine et al., 2019). Given that Cntnap2/ Caspr2 is expressed at the AIS (Poliak et al., 1999; Nakabayashi and Scherer, 2001), alterations in AIS morphology should be analysed in a loss of function model.

Environmental factors External environmental factors such as home-cage enrichment, mixed genotype housing and maternal care have been shown to influence the expression of ASD-like behaviours. A 2017 study showed that the decision to co-house single or mixed genotype animals in the home cage critically influenced the development of behavioural phenotypes upon loss of Nlgn3. They found that mixed genotype housing of *Nlgn*$^{-/y}$ KO mice with wildtype littermates resulted in reduced vocalisation by the WTs and disrupted home-cage social hierarchies, measured using tests of dominance, compared to single-genotype housed animals, while re-expression of Nlgn3 specifically in PV-immuno reactive interneurons ameliorated these alterations (Kalbassi et al., 2017). Further, enrichment of the home-cage with objects that allow the animal to isolate itself into micro-environments and experience different textures or materials, such as presence of nesting materials and wooden blocks that engage fine-motor movement, are known to boost social interaction and mitigate anxiety like behaviours in laboratory rodents (Hutchinson et al., 2005). A third environmental factor that is known to influence stress levels, adaptive and problematic behaviours in individuals with ASD is maternal warmth and responsiveness (Greenberg et al., 2012; Robinson et al., 2016; Smith et al., 2016). While there is no current evidence of altered maternal care upon introduction of any of these mutations in rodents, anecdotal evidence of *Syngap1* heterozygous female mice being less attentive to pups has been reported (Biological and Vetrinary services, University of Edinburgh). The animals used in this study were mix genotype housed, both wildtype and heterozygous mutant females were used for mating and animals were kept in moderately enriched cages containing small wooden chewing blocks, nesting tissues and cardboard rolls. The above discussed environmental factors could therefore have played a role in the social and cognitive development in these animals, though the exact mechanisms of environmental enrichment on AIS length alterations is unknown.

5.8 Conclusion

The results detailed in this chapter, cause me to reject my hypothesis that alterations in AIS length would be a point of convergence in ASD/ID, underlying observed alterations in cellular excitability. In doing so, my results do validate the null hypothesis. Moving forward, results from both mouse and rat studies will help us gain a more complete understanding of the biological mechanisms underlying human pathology of these disorders.

Chapter 6

Concluding Remarks

6.1 Summary of results

Characterisation of AIS lengths in juvenile models of ASD/ID. The data presented in this thesis here provides the first systematic characterisation of AIS lengths across behaviourally relevant brain regions in juvenile rat models of monogenic forms of ASD/ID. This undertaking revealed a baseline increase in AIS length, indicative of increased cellular excitability (Kuba et al., 2014), in layer 5 of the prelimbic and somatosensory barrel cortices and the basal amygdala in the *Fmr1* knock-out model of Fragile-X syndrome (FXS). However, no difference in AIS length was observed in any of the brain regions in any of the other models, which included *Syngap1, Nlgn3, Nrx1, Cntnap2 and Pten* mediated ASD/ID (table 6.1).

Species specific differences in AIS deficits in models of Fragile-X Syndome. The results from the *Fmr1* model are of particular interest, as the findings are indicative of species specific differences in AIS length within the preclinical models of the same syndrome. In a mouse model of FXS, Booker et al. (2019) show that knock-out animals exhibit increased AIS length and cellular hyper-excitability in pyramidal cells of the CA1 sub-region of the dorsal hippocampus, but this increased is not observed in the prelimbic, visual or somatosensory barrel cortices. In my work, no increase in AIS length was observed in neurons of the CA1 regions in *Fmr1*$^{-/y}$ animals. Concurrent with these results, *ex vivo* intracellular recordings from the CA1 neurons in these

animals showed no alterations in cellular excitability (Jackson, 2016). Increased AIS length was, however, observed in the juvenile *Fmr1*$^{-/y}$ rats in pyramidal neurons of layer 5 pre-limbic medial prefrontal cortex (PL) and somatosensory barrel cortex (S1BF) as well as in principal neurons of the basal amygdala (BA). This increase in AIS length in the BA was accompanied by cellular hyper-excitability (Jackson, 2016) in these animals. Similar to the work performed in Jackson (2016), whole-cell patch clamp recordings should be undertaken to complement the present AIS study and characterise alterations in intrinsic cellular excitability of PL and S1BF L5 neurons in juvenile *Fmr1*$^{-/y}$ rats. Divergent phenotypes across pre-clinical models of the same neurodevelopmental disorder (NDD) have been widely reported (Eltokhi et al., 2018; Till et al., 2015; Homberg et al., 2016; Guo et al., 2020), including across models of Fragile-X Syndrome (Till et al., 2015). Given the rich interplay of genetic and environmental factors that affect the developmental trajectory of NDDs, an emerging theory argues for a move away from a single endophenotype model to more integrative 'poly-phenotype' models (Homberg et al., 2016). Using multiple model systems of the same disorder ranging from *in vitro* induced pluripotent patient stem cell lines to mouse and rat models will thus allow for better dissection of unique and shared biomarkers for each model system, working in conjunction to extend our understanding of disease pathophysiology. Recent unpublished work by Dr. Sam Booker (personal correspondence) bears testament to this, as CA1 neurons in adult *Fmr1*$^{-/y}$ rats show hyperexcitabliity despite no observed difference in cellular excitability in these neurons in juvenile animals. This result would argue for re-assessment of AIS lengths in the CA1 neurons in older animals, and assess if age-dependent plasticity of the AIS is impaired in this model of FXS.

Assessment of morphological plasticity of the AIS in models of *SYNGAP1*-ID. Further, this thesis aimed to characterise the morphological plasticity of the AIS and how this maybe perturbed in a rat model of *Syngap1* haploinsufficiency. This entailed analysis of age and experience dependent plasticity (table 6.2). This study is the first to show an show age-dependent increase in AIS length in the BA and lateral nucleus of the amygdala (LA) of wildtype rats. Secondly, in *Syngap1*$^{+/-}$ rats, age-dependent elongation of AIS length does not occur in cells of PL L2/3, while this process is unaffected in cells of PL L5, BA and LA. Furthermore, I provide evidence that the nature of SynGAP protein haploinsufficiency differentially affects AIS plasticity. Using a fear-conditioning paradigm to assess experience-dependent alterations in AIS length revealed that despite haploinsufficiency of the full-length or GTPase activating (GAP)

domain of SynGAP resulting in similarly exacerbated re-call of fear memory, only animals haploinsufficient for the GAP domain showed an increase AIS length post fear conditioning and only in PL L5 neurons. This difference in AIS modulation would suggest that *SYNGAP1*-ID patients with mutations resulting in loss of GAP domain activity may have distinct biological mechanisms underlying their pathology when compared to patients haploinsufficient for the full length protein.

		Model													
		Syngap1$^{+/\Delta Gap}$		*Syngap1*$^{+/-}$		*Fmr1*$^{-/y}$		*Nlgn3*$^{-/y}$		*Nrx1*$^{+/-}$		*Cntnap2*$^{+/-}$		*Pten*$^{+/-}$	
Brain Region		AIS Length	AP Firing	AIS Length	AP Firing	AIS Length	AP Firing	AIS Length	AP Firing	AIS Length	AP Firing	AIS Length	AP Firing	AIS Length	AP Firing
	PL L2/3	-	N/A	-	N/A	-	N/A	-	N/A	-	N/A	-	N/A	-	N/A
	PL L5	-	-	-	-	↑	N/A	-	-	-	-	-	N/A	-	N/A
	CA1	-	-	-	-	-	-	-	-	-	↓	-	N/A	-	N/A
	CA3	-	N/A	-	N/A		N/A	-	N/A	-	N/A	-	N/A	-	N/A
	LA	-	-	-	↑	-	-	-	↑	-	N/A	-	-	-	N/A
	BA	-	↓	-	-	↑	↑	-	↑	-	N/A	-	-	-	N/A
	S1BF L2/3	-	N/A	-	N/A	-	N/A	-	N/A	-	N/A	-	N/A	-	N/A
	S1BF L4	-	N/A	-	N/A	-	N/A	-	N/A	-	N/A	-	N/A	-	N/A
	S1BF L5	-	N/A	-	N/A	↑	N/A	-	N/A	-	N/A	-	N/A	-	N/A
	V1 L2/3	-	N/A	-	N/A	-	N/A	-	N/A	-	N/A	-	N/A	-	N/A
	V1 L5	-	N/A	-	N/A	-	N/A	-	N/A	-	N/A	-	N/A	-	N/A

Table 6.1: Summary table comparing genotype specific differences in juvenile animals (P28-32). AIS lengths across all 6 ASD/ID models and the corresponding electrophysiological results are summarized above. '↑' indicates an increase in length or intrinsic excitability, '↓' indicates a decrease in length or intrinsic excitability, '-' indicates no change in the animals containing the mutation compared to littermate wild-type controls. N/A indicates results are not available. Electrophysiological recordings performed by A. Toft, N. Anstey, A. Jackson, L. Mizen.

Plasticity of the AIS (average AIS length)

		Syngap1$^{+/+}$					*Syngap1*$^{+/-}$				
		P 28-35	P 90-120	Fear		Sub-pop	P28-35	P90-120	Fear		Sub-pop
				CS	CS+US				CS	CS+US	
Brain Region	PL L2/3	28.75 μm	31.55 μm	29.82 μm	30.00 μm	PL $\Longrightarrow$ BLA	28.73 μm	29.05 μm, *	27.95 μm	27.98 μm, *	PL $\Longrightarrow$ BLA
	PL L5	28.99 μm	33.14 μm, $\uparrow$	29.29 μm	29.41 μm	26.80 μm	28.73 μm	31.06 μm,$\uparrow$	29.26 μm	29.30 μm	26.81 μm
	LA	24.43 μm	29.13 μm, $\uparrow$	26.45 μm	26.38 μm	BLA $\Longrightarrow$ PL	23.71 μm	28.31 μm, $\uparrow$	25.40 μm	26.26 μm	BLA $\Longrightarrow$ PL
	BA	33.21 μm	40.07 μm, $\uparrow$	40.18 μm	37.17 μm	42.20 μm	30.94 μm	38.42 μm, $\uparrow$	36.64 μm	38.30 μm	40.99 μm

Table 6.2: Summary table showing AIS plasticity in a rat model of *Syngap1* haploinsufficiency Table shows the average AIS length at two developmental time points P28-35 (juveniles) and P90-120 (adults), post fear conditioning (FC) as well as in two distinct sub-populations: PL neurons that project to the BLA (PL $\Longrightarrow$ BLA) and BLA neurons that project to the PL (BLA $\Longrightarrow$ PL). '$\uparrow$' indicates significantly increased AIS length within the same genotype with age, '*' indicates significantly altered AIS length across genotypes. For statistics and complete results see chapter 4.

6.2 Translational implications for ASD/ID research: Convergence, divergence and homeostatic platicity

Across models for distinct genetic causes of ASD/ID, phenotypic convergence and divergence have been reported at cellular, molecular and behavioural levels. For example, elevated rates of *de novo* protein synthesis have been reported in mouse models of Fragile-X syndrome and *SYNGAP1* haploinsufficiency (Barnes et al., 2015) whereas decreased levels of protein synthesis have been observed in mouse models of Tuberous sclerosis complex (Auerbach et al., 2011). Similarly, metabotropic glutamate receptor (mGluR) mediated long-term depression is found to be exaggerated in models of Fragile-X syndrome and *SYNGAP1* haploinsufficiency (Barnes et al., 2015) whereas mGluR mediated long-term potentiation is disrupted in mouse models of Neuroligin 3 mediated non-syndromic ID (Baudouin et al., 2012). Such studies have resulted in the postulation of certain celluar and molecular process as 'nodes' of convergence across the various models, allowing for the focussing of drug discovery and other therapeutic approaches. Cellular hyper-excitability has widely been regarded as one such node (Contractor et al., 2015), and the work of this thesis has focused on determining if changes in AIS morphology maybe a direct pathophysiological consequences of the genetic mutations causing ASD/ID and under-pin the observed cellular hyper-excitability. However, the ASD phenotype is also comprised of pleiotropic compensatory changes in addition to direct pathophysiological effects (Nelson and Valakh, 2015; Contractor et al., 2015; Antoine et al., 2019). Examples of these compensatory changes can be found at the molecular level, where in a mouse model of Fragile-X syndrome shown to excessively translate mRNAs, some of these candidates corrected, rather than exacerbated, the pathological changes observed in FXS (Thomson et al., 2017). Another recent example in four mouse models of ASD/ID showed that increased neuronal activity and E/I conductance ratio served to homeostatically stabilize, rather than drive, network hyperexcitability (Antoine et al., 2019). The study proposes that ASD symptoms in these animals arises as a result of imperfect homeostasis, for example, the increased E/I ratio observed here impairs the ability of these cells to compensate for future strong inputs (Ramocki and Zoghbi, 2008; Antoine et al., 2019). However, delineating pathogenicity of these mutations on network activity from maladaptive homeostatic compensation is complicated by the activity-dependent plasticity of neuronal and network excitability (Nelson and Valakh, 2015). The focus thus far has been on understanding the biophysical changes in post-synaptic cellular and sub-cellular compartments

with alterations in pre-synaptic processes, such as altered rates of synaptic vesicle re-cycling (Bonnycastle, 2018) being overlooked. However, structural plasticity of the AIS, and its corresponding control of intrinsic cellular excitability, is homeostatically regulated and depends on incoming synaptic inputs (Kuba et al., 2006; Kole and Stuart, 2012). Therefore, perturbations in pre-synaptic processes coupled with a lack of alterations in AIS morphology could result in impaired homoeostasis and underlie the pathology in our models of ASD/ID.

6.3 Future Directions: Differential approaches to understanding AIS deficits in *SYNGAP1*-ID and Fragile-X Syndrome

Moving forward, experiments should focus on delineating the exact fear-experience induced morphological plasticity of the AIS and how these might be distinctly regulated in the present rat models of *Syngap1*-ID and FXS. The visual cued fear conditioning paradigm described in this thesis is an adaptation of the classical pavlovian associative memory paradigm (Pavlov, 1927) and as such composes of three distinct stages:

- **Acquisition and consolidation** of associative memory, wherein an initially neutral flashing light cue signals an aversive foot-shock and induces expression of fear-behaviours such as freezing
- **Re-call of fear memory** such that sole presentation of the cue induces the expression of fear behaviour
- **Extinction** of the acquired fear-behavioural response when the cue ceases to denote an aversive outcome

As shown in chapter 4, rat models of *Syngap1* haploinsufficiency exhibit no deficits in fear memory acquisition, displaying freeing levels comparable to their wild-type counterparts. However, these animals display exaggerated fear re-call with limited extinction, displaying sustained levels of freezing behaviour despite repetitive presentations of the cue unaccompanied by the aversive foot-shock stimulus. Similar to the *Syngap1*$^{+/-}$ animals, *Fmr1*$^{-/y}$ animals also show no deficits in conditioning, freezing to similar levels as the wild-type littermates. Unlike

the *Syngap1*$^{+/-}$ animals, the *Fmr1*$^{-/y}$ animals show decreased levels with rapid extinction of freezing behaviour when tested for fear-memory re-call. This diametrically opposite behavioural response within the same paradigm maybe suggestive of opposing deficits in cellular excitability within the same neural circuit. The pre-limbic cortex and basolateral amygdala reciprocal network is crucial for fear memory consolidation and re-call (Vidal-Gonzalez et al., 2006; Laviolette et al., 2005; Corcoran and Quirk, 2007). Additionally, preliminary data from the laboratory of Professor Andreas Lüthi has shown that in BA cells that project to the PL, AIS lengths increased following fear learning in wildtype mice. Therefore, investigation of alterations in intrinsic cellular excitability as well changes in AIS lengths post fear conditioning specifically in the BA to PL and PL to BLA projecting neurons in both the *Syngap1*$^{+/-}$ animals and the *Fmr1*$^{-/y}$ animals should be undertaken. However, experiments exploring AIS changes specifically in the PL-BLA, BLA-Pl circuit presents with some limitations due to the underlying assumption that the observed abnormal freezing behaviours occur as a consequence of perturbed memory consolidation and recall. In case of *Syngap1*$^{+/-}$ animals, the exaggerated freezing response might be a consequence of impaired extinction learning while in the *Fmr1*$^{-/y}$ animals the reduced freezing behaviour might be because the animals choose to express fear memory as a 'flight' rather than the classical 'freeze' response (Roelofs, 2017). In order to distinguish between these possibilities, a more methodical approach must be employed. For SynGAP haploinsufficient animals, an additional behaviour experimental day should be added to assess extinction re-call levels followed by investigation of AIS lengths in the infra-limbic (IL), rather than pre-limbic, cortex as the IL is crucial for fear extinction learning (Do-Monte et al., 2015). It would also be prudent to assess alterations in AIS length in the PL-BLA network of *Syngap1*$^{+/-}$ animals following conditioning with a more brief re-call protocol. For the *Fmr1*$^{-/y}$ animals, analysis of cellular excitability and AIS lengths could be undertaken in the central amygdala (CeA) and periaqueductal gray (PAG), as these brain regions lie downstream of the BLA-mPFC circuit and determine the expression of fear-induced behaviour as either 'fight', 'flight' or 'freeze' (Roelofs, 2017). Another possible underlying mechanism contributing to the altered fear-memory mediated behaviours in these models might disrupted 'engram' formation. Engrams are cell ensembles that serve as the neural substrate for storing and re-calling memories (Herry et al., 2008; Josselyn and Tonegawa, 2020) and are composed of the same sub-set of cells that are activated during memory formation and memory re-call. Engram cells are most easily identified by their expression of early gene markers, such as c-Fos and *Arc* mRNA (Kramer et al., 2018). Thus, an altogether non-circuit specific method to dissect the perturbed

cellular mechanisms in fear memory formation in our ASD/ID models would be use a viral tracing approach to record the intrinsic cellular properties and analyse AIS lengths specifically in the engram cells.

Finally, a fundamental question that arises from the assessment of AIS lengths and genotype specific differences in models of ASD/ID is 'What does the magnitude of change mean for the individual cell?' Would a 4 μm alteration in AIS length in a cell with baseline AIS length of 40 μm alter cell function to the same extent as a 4 μm alteration for a cell with baseline AIS length of 20μm? Given that AIS length is determined as a consequence of neuronal input, this question might best be answered using a computational model. In order to build the model, experimental data could be obtained by performing dye-fills, to assess dendritic architecture and spine density, when recording cellular intrinsic excitability with the cells being post-hoc stained for the AIS. This would allow for a more definite determination of the functional consequences of a 10 or 20% change in AIS length in our models, as well as answering the question if a lack of homeostatic alteration in AIS length might be driving cellular hyperexcitability.

Chapter 7

Appendix

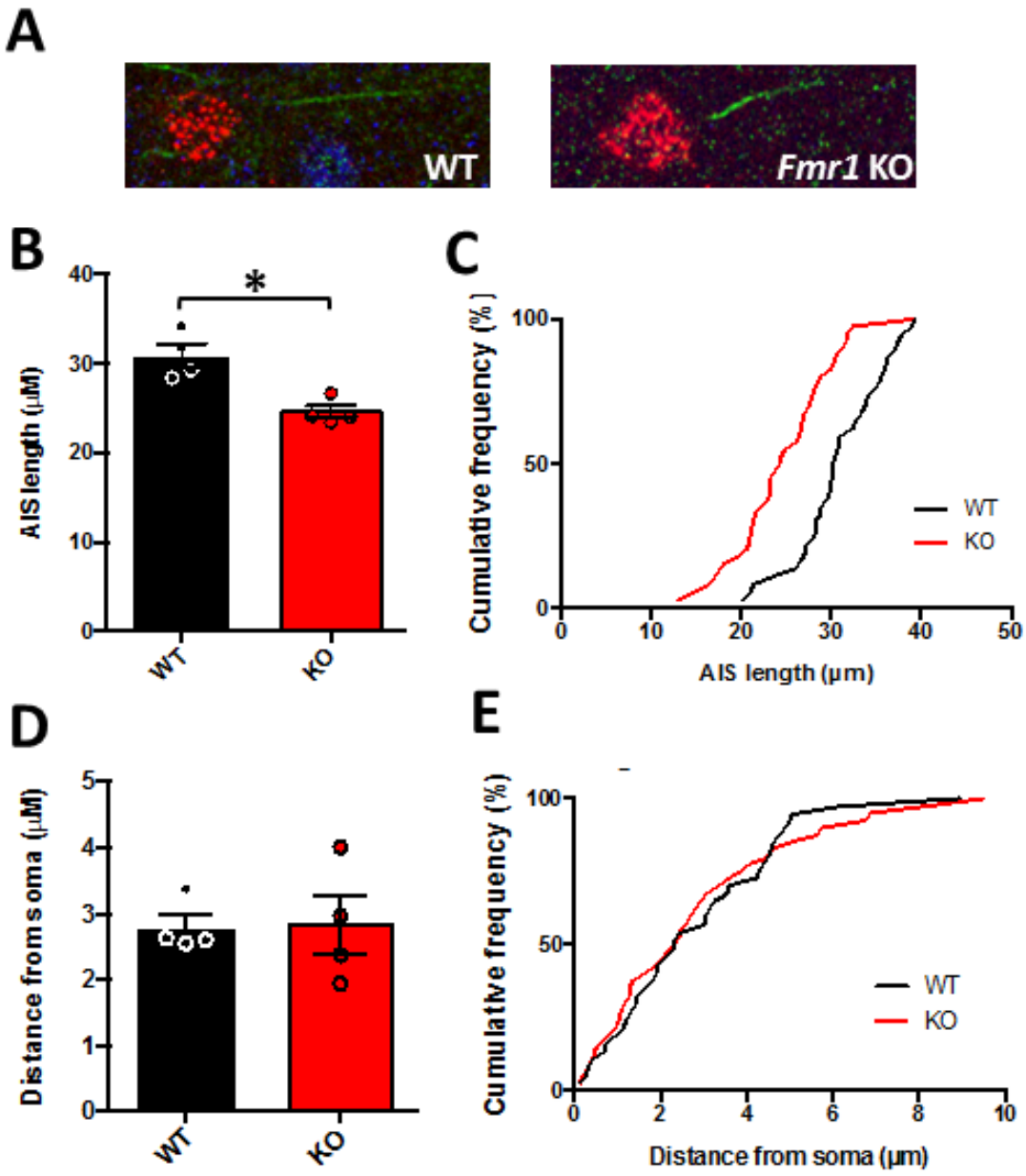

Figure S1: Axon initial segment is significantly shorter in adult *Fmr1* KO rat PL-BLA projection neurons These experiments were performed by Dr. Adam Jackson (Thesis: A Jackson 2016) (A) Confocal image of bead labelled soma showing immunocytochemistry for axon initial segment (AIS) specific Ankyrin-G (green) and NeuN (blue). (B) AIS length is significantly increased in Fmr1 KO rats (WT: 30.90 $\pm$ 1.30μm; n=4 animals; KO: 24.60 $\pm$ 0.72μm; n=4 animals; p=0.03) (C) Cumulative distribution of AIS length data. (D) No difference between genotypes was observed in AIS distance from soma (WT: 2.79 $\pm$ 0.20μm; n=4 animals; KO: 2.82 $\pm$ 0.45μm; n=4 animals; p=0.95). (E) Cumulative distribution of AIS distances from soma.

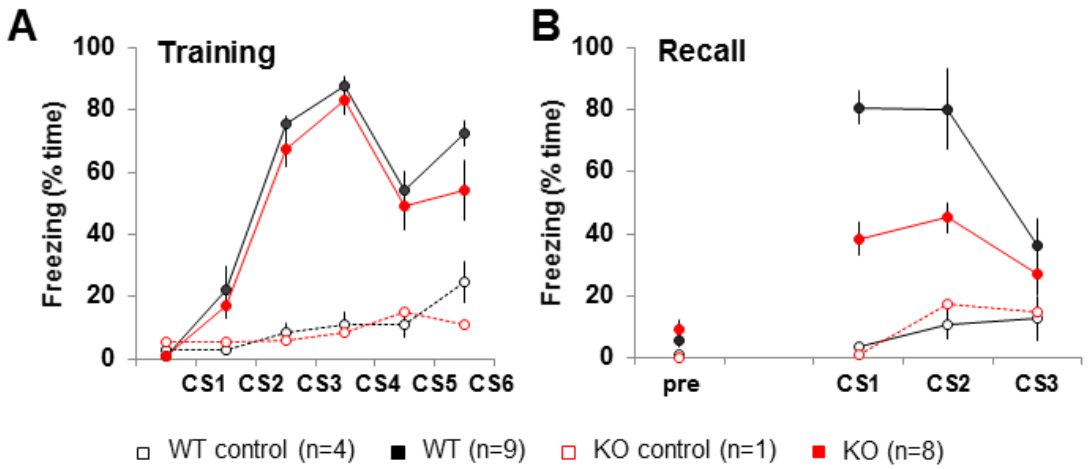

Figure S2: *Fmr1* KO rats show impaired fear recall These experiments were performed by Dr. Sally Till (A) Using the same visual-cued fear conditioning paradigm as outlined in chapter 2, both *Fmr1* KO and WT rats show comparable levels of fear memory acquisition on training/ conditioning as witnessed by increased %freezing compared to both WT and *Fmr1* KO control animals that were only presented with the CS without the aversive footshock (B) However, when testing recall *Fmr1* KO rats showed significantly reduced re-call. The re-call protocol used in this figure is different to the one used in this thesis such that animals in this figure were subjected to 3x2min CS presentations interleaved by 2 min ITI.

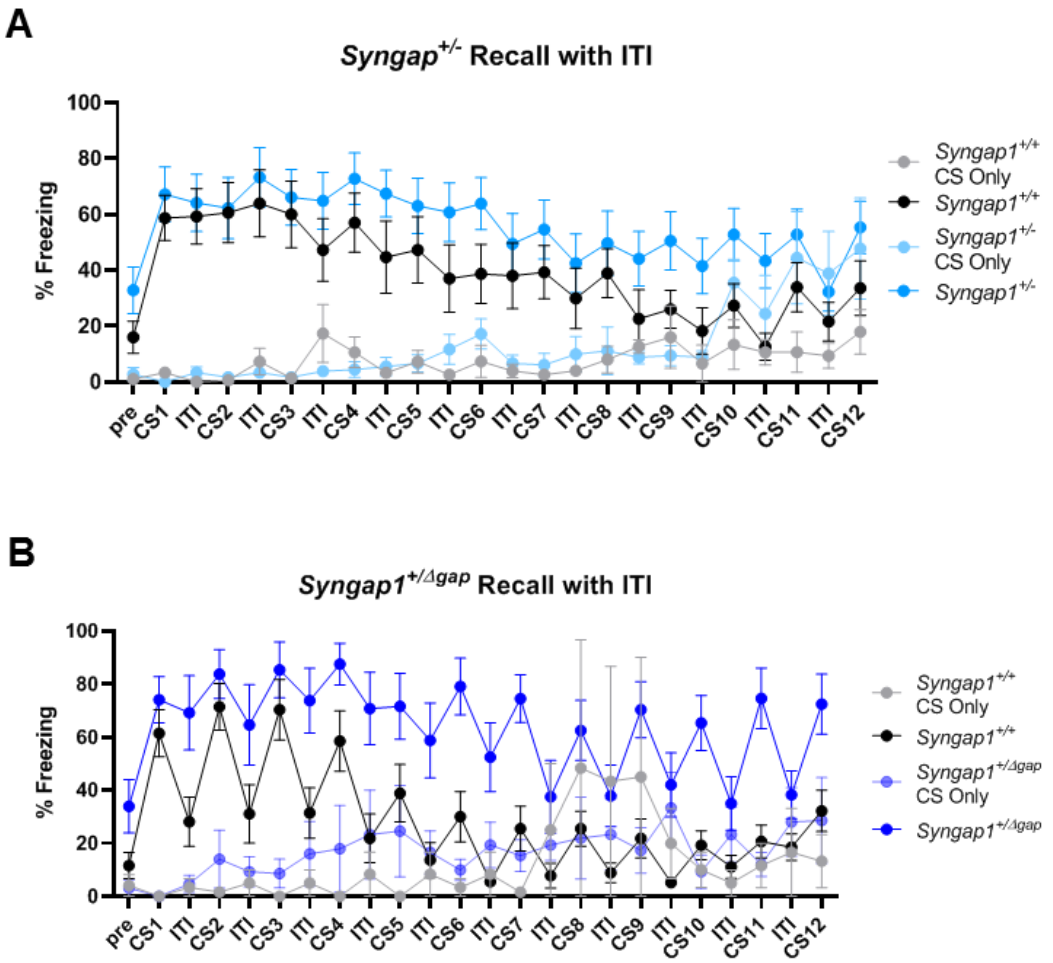

Figure S3: Fear re-call data with inter-trial interval in *Syngap1*$^{+/-}$ and *Syngap1*$^{+/\Delta Gap}$ rats (A) During re-call of fear memory both *Syngap1*$^{+/+}$ and *Syngap1*$^{+/-}$ show reduced modulation of freezing response during the 'light off' inter-trial intervals for the first 8 CS presentations, following which WT rats show greater modulation of fear response than *Syngap1*$^{+/-}$ rats (*Syngap1*$^{+/+}$ CS only n=5, *Syngap1*$^{+/+}$ FC n=11, *Syngap1*$^{+/-}$ CS only n=6, *Syngap1*$^{+/-}$ FC n=14) (B) Wildtype *Syngap1*$^{+/+}$ and *Syngap1*$^{+/\Delta Gap}$ show greater modulation of freezing response during ITIs than *Syngap1*$^{+/-}$ rats (*Syngap1*$^{+/+}$ CS only n=2, *Syngap1*$^{+/+}$ FC n=9, *Syngap1*$^{+/\Delta Gap}$ CS only n=5, textitSyngap1$^{+/\Delta Gap}$ FC n=8).

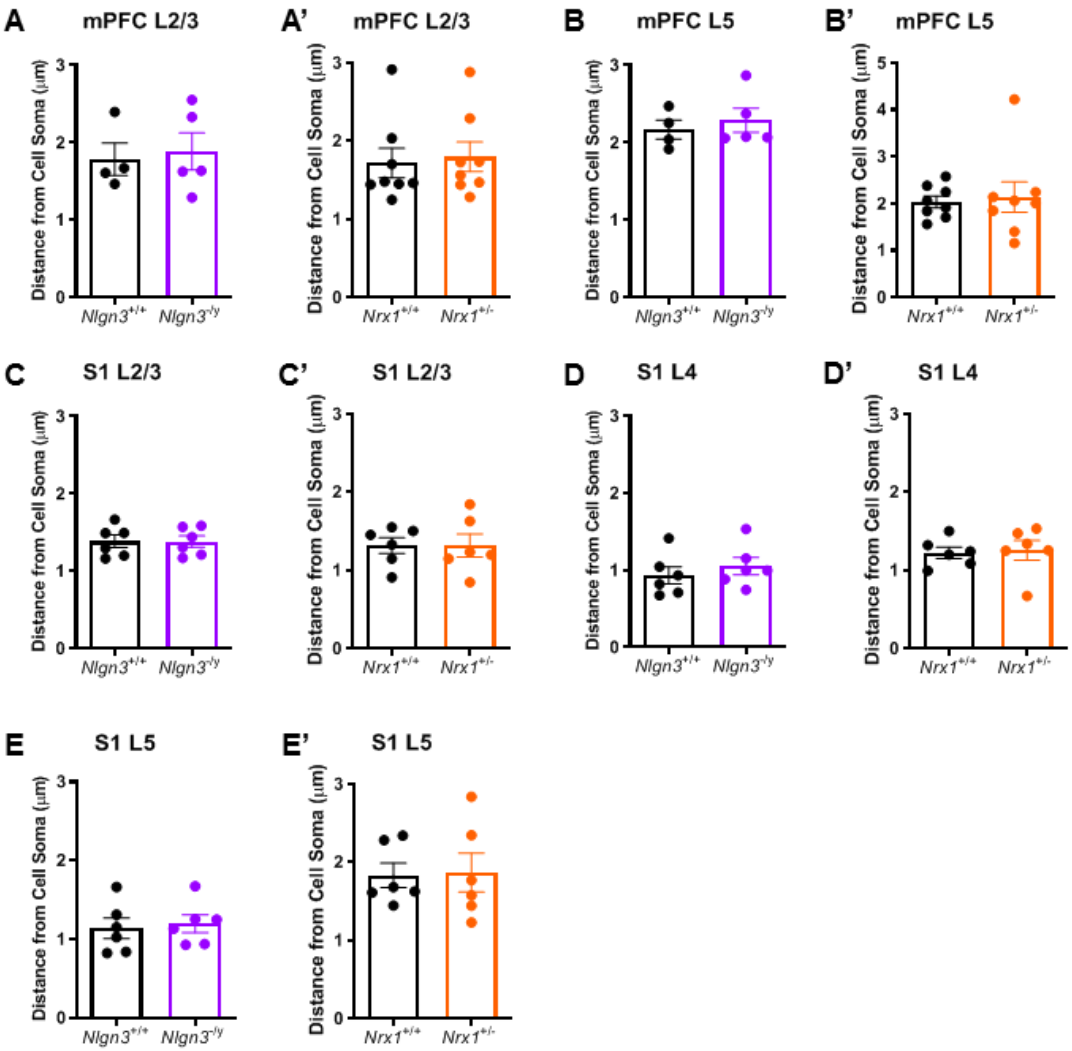

Figure S4: AIS Distance from cell soma measurements in *Nlgn3*$^{-/y}$ and *Nrx1*$^{+/-}$ rats No significant difference in distance from cell soma in mPFC L2/3 (A, A' *Nlgn3*$^{+/+}$ =1.787 ± 0.4156, N=4, *Nlgn3*$^{-/y}$= 1.888 ± 0.5305, N=5, *Nrx1*$^{+/+}$= 1.718 ± 0.5381, N=8, *Nrx1*$^{+/-}$= 1.800 ± 0.5319, N=8), L5 (B, B'*Nlgn3*$^{+/+}$= 2.171 ± 0.2439, N=4, *Nlgn3*$^{-/y}$= 2.290 ± 0.3499, N=5, *Nrx1*$^{+/+}$= 2.036 ± 0.3484, N=8, *Nrx1*$^{+/-}$= 2.135 ± 0.9229, N=8), S1 L2/3 (C, C'*Nlgn3*$^{+/+}$= 1.386 ± 0.1972, N=6, *Nlgn3*$^{-/y}$= 1.383 ± 0.1796, N=6, *Nrx1*$^{+/+}$= 1.316 ± 0.2464,, N=6, *Nrx1*$^{+/-}$= 1.317 ± 0.3588, N=6), S1 L4 (D, D'*Nlgn3*$^{+/+}$= 0.9332 ± 0.2735, N=6, *Nlgn3*$^{-/y}$= 1.052 ± 0.2726, N=6, *Nrx1*$^{+/+}$= 1.224 ± 0.1788, N=6, *Nrx1*$^{+/-}$= 1.255 ± 0.3075, N=6) and S1 L5 (E, E'*Nlgn3*$^{+/+}$= 1.136 ± 0.3181, N=6, *Nlgn3*$^{-/y}$= 1.197 ± 0.2735, N=6, *Nrx1*$^{+/+}$= 1.832 ± 0.3815, N=6, *Nrx1*$^{+/-}$= 1.867 ± 0.6089, N=6) in *Nlgn3*$^{-/y}$ and *Nrx1*$^{+/-}$ rats compared to wildtype littermate controls.

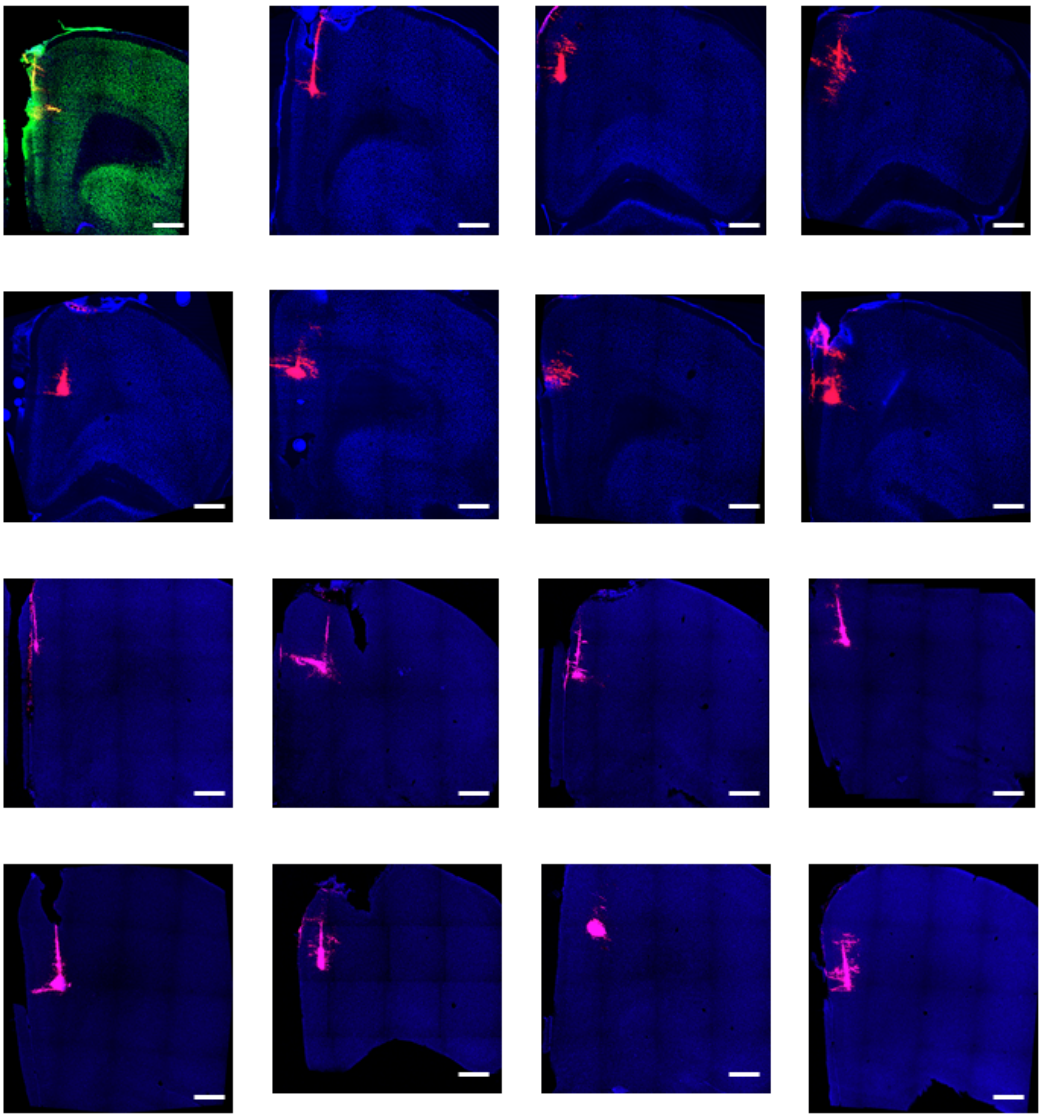

Figure S5: Injection sites into the mPFC This figure shows the retrobead injection sites into the mPFC from all the animals included in AIS analysis in chapter 4. Beads are shown in red and counter-stained with either NeuN (green) or TOPRO (blue) Scale bar= 500 μm.

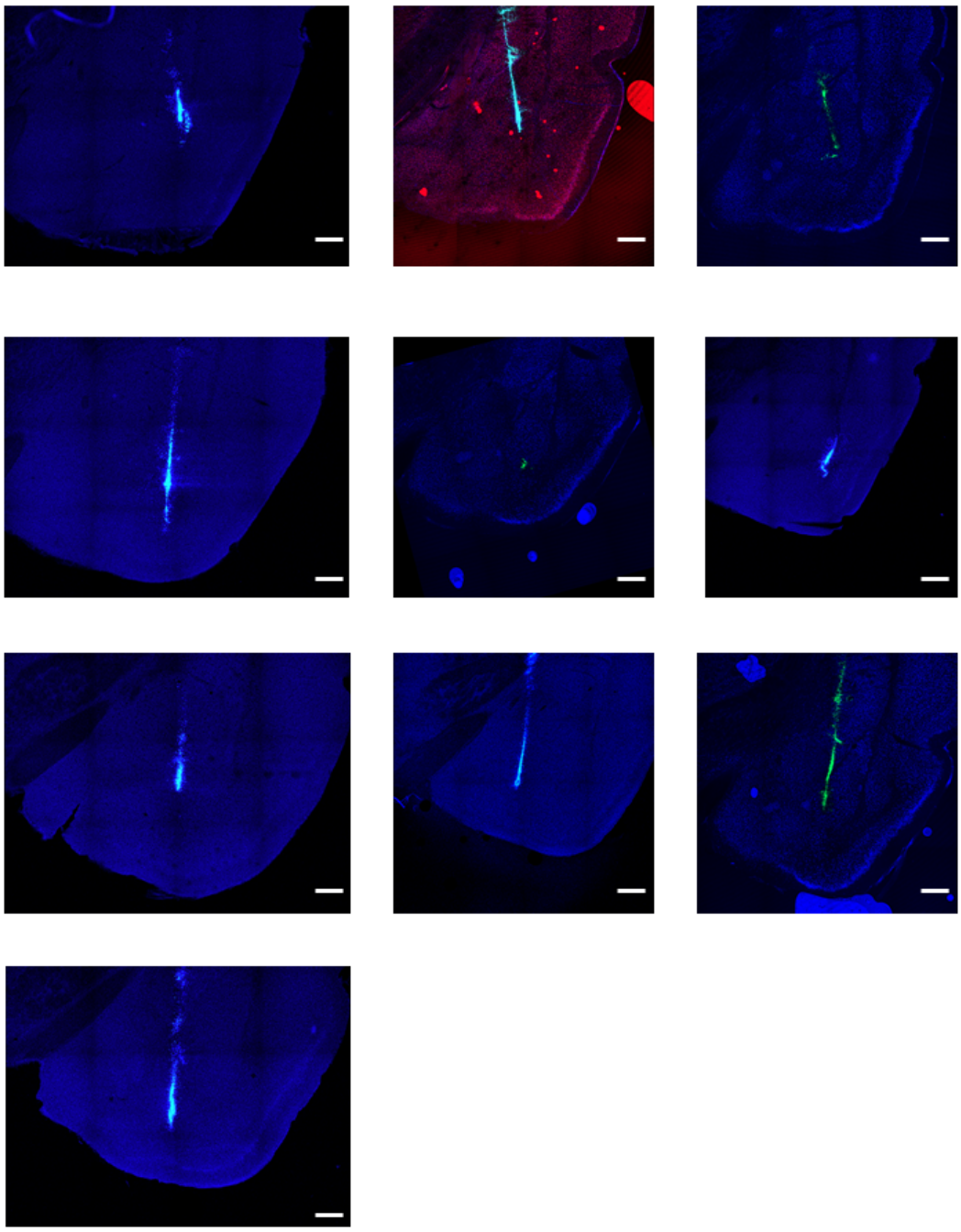

Figure S6: Injection sites into the BLA This figure shows the retrobead injection sites into the BLA from n-2 animals included in AIS analysis in chapter 4. 2 animals are not shown due to damage to the injection site during tissue handling. Beads are shown in green and counter-stained with either NeuN (red) or TOPRO (blue) Scale bar= 500 μm.

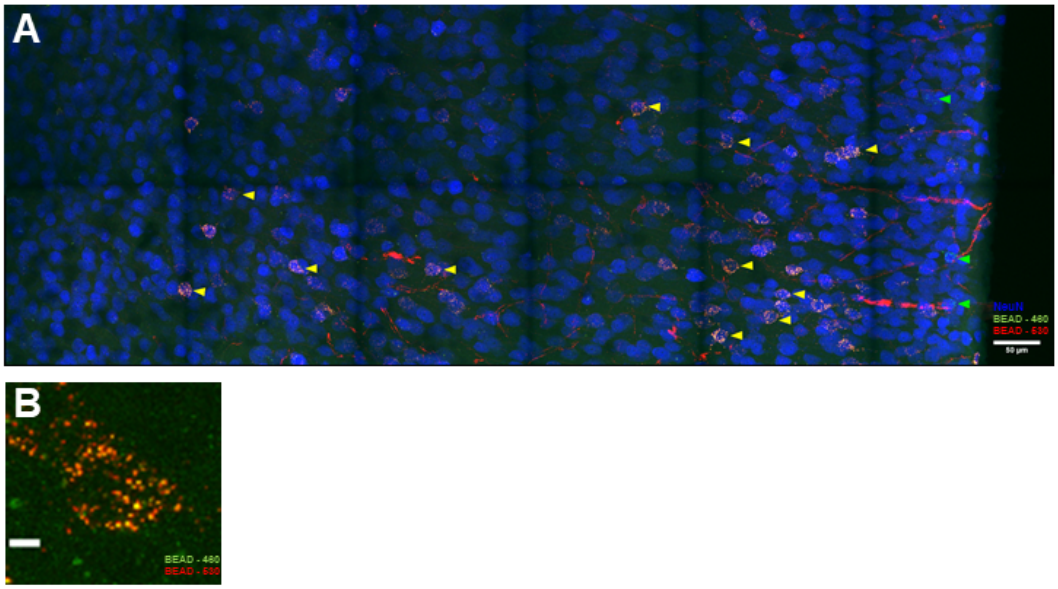

Figure S7: Three channel image showing overlap between retrobead expression in the mPFC (A) Representative image of the PL stack acquired showing the high degree of overlap between the red and green retrobeads, indicated using the yellow arrow. Some only green-bead expressing cells were also see, indicated by the green arrow, and these were the ones measured in chapter 4. Slices were counter-stained with NeuN pseudo-coloured in blue Scale bar = 50 μm. (B) Magnified image of a single 'yellow' cell showing the overlap between red and green beads. Scale bar = 5 μm.

Bibliography

Abbeduto L, McDuffie A, Thurman AJ (2014) The fragile x syndrome-autism comorbidity: What do we really know? *Frontiers in Genetics* 5:355.

Aceti M, Creson TK, Vaissiere T, Rojas C, Huang WC, Wang YX, Petralia RS, Page DT, Miller CA, Rumbaugh G (2015) Syngap1 haploinsufficiency damages a postnatal critical period of pyramidal cell structural maturation linked to cortical circuit assembly. *Biological Psychiatry* 77:805–815.

Agulhon C, Blanchet P, Kobetz A, Marchant D, Faucon N, Sarda P, Moraine C, Sittler A, Biancalana V, Malafosse A, Abitbol M (1999) Expression of FMR1, FXR1, and FXR2 genes in human prenatal tissues. *Journal of Neuropathology and Experimental Neurology* 58:867–880.

Akers KG, Arruda-Carvalho M, Josselyn SA, Frankland PW (2012) Ontogeny of contextual fear memory formation, specificity, and persistence in mice. *Learning and Memory* 19:598–604.

Akhter S, Hussain AH, Shefa J, Kundu GK, Rahman F, Biswas A (2018) Prevalence of Autism Spectrum Disorder (ASD) among the children aged 18-36 months in a rural community of Bangladesh: A cross sectional study [version 1; referees: 1 approved, 2 approved with reservations]. *F1000Research* 7.

Al Shehhi M, Forman EB, Fitzgerald JE, McInerney V, Krawczyk J, Shen S, Betts DR, Ardle LM, Gorman KM, King MD, Green A, Gallagher L, Lynch SA (2019) NRXN1 deletion syndrome; phenotypic and penetrance data from 34 families. *European Journal of Medical Genetics* 62:204–209.

Allen AS, Berkovic SF, Cossette P, Delanty N, Dlugos D, Eichler EE, Epstein MP, Glauser T, Goldstein DB, Han Y, Heinzen EL, Hitomi Y, Howell KB, Johnson MR, Kuzniecky R, Lowenstein DH, Lu YF, Madou MR, Marson AG, Mefford HC, Esmaeeli Nieh S, O'Brien TJ, Ottman R, Petrovski S, Poduri A, Ruzzo EK, Scheffer IE, Sherr EH, Yuskaitis CJ, Abou-Khalil B, Alldredge BK, Bautista JF, Boro A, Cascino GD, Consalvo D, Crumrine P, Devinsky O, Fiol M, Fountain NB, French J, Friedman D, Geller EB, Glynn S, Haut SR, Hayward J, Helmers SL, Joshi S, Kanner A, Kirsch HE, Knowlton RC, Kossoff EH, Kuperman R, McGuire SM, Motika PV, Novotny EJ, Paolicchi JM, Parent JM, Park K, Shellhaas RA, Shih JJ, Singh R, Sirven J, Smith MC, Sullivan J, Lin Thio L, Venkat A, Vining EP, Von Allmen GK, Weisenberg JL, Widdess-Walsh P, Winawer MR (2013) De novo mutations in epileptic encephalopathies. *Nature* 501:217–221.

Amir RE, Van Den Veyver IB, Wan M, Tran CQ, Francke U, Zoghbi HY (1999) Rett syndrome is caused by mutations in X-linked MECP2, encoding methyl- CpG-binding protein 2. *Nature Genetics* 23:185–188.

Amiri A, Cho W, Zhou J, Birnbaum SG, Sinton CM, McKay RM, Parada LF (2012) Pten deletion in adult hippocampal neural stem/progenitor cells causes cellular abnormalities and alters neurogenesis. *Journal of Neuroscience* 32:5880–5890.

Anderson GR, Galfin T, Xu W, Aoto J, Malenka RC, Südhof TC (2012) Candidate autism gene screen identifies critical role for cell-adhesion molecule CASPR2 in dendritic arborization and spine development. *Proceedings of the National Academy of Sciences of the United States of America* 109:18120–18125.

Anglada-Figueroa D, Quirk GJ (2005) Lesions of the basal amygdala block expression of conditioned fear but not extinction. *Journal of Neuroscience* 25:9680–9685.

Ango F, Di Cristo G, Higashiyama H, Bennett V, Wu P, Huang ZJ (2004) Ankyrin-based subcellular gradient of neurofascin, an immunoglobulin family protein, directs GABAergic innervation at Purkinje axon initial segment. *Cell* 119:257–272.

Antar LN, Afroz R, Dictenberg JB, Carroll RC, Bassell GJ (2004) Metabotropic Glutamate Receptor Activation Regulates Fragile X Mental Retardation Protein and Fmr1 mRNA Localization Differentially in Dendrites and at Synapses. *Journal of Neuroscience* 24:2648–2655.

Antoine MW, Langberg T, Schnepel P, Feldman DE (2019) Increased Excitation-Inhibition Ratio Stabilizes Synapse and Circuit Excitability in Four Autism Mouse Models. *Neuron* 101:648–661.e4.

Araki Y, Zeng M, Zhang M, Huganir RL (2015) Rapid Dispersion of SynGAP from Synaptic Spines Triggers AMPA Receptor Insertion and Spine Enlargement during LTP. *Neuron* 85:173–189.

Ariza J, Rogers H, Hashemi E, Noctor SC, Martínez-Cerdeño V (2018) The Number of Chandelier and Basket Cells Are Differentially Decreased in Prefrontal Cortex in Autism. *Cerebral Cortex* 28:411–420.

Arruda-Carvalho M, Clem RL (2015) Prefrontal-amygdala fear networks come into focus. *Frontiers in Systems Neuroscience* 9.

Arruda-Carvalho M, Wu WC, Cummings KA, Clem RL (2017) Optogenetic examination of prefrontal-amygdala synaptic development. *Journal of Neuroscience* 37:2976–2985.

Asadi S (2018) SYNGAP1-Related Intellectual Disability Syndrome. *Archives in Neurology & Neuroscience* 1.

Asiminas A, Jackson AD, Louros SR, Till SM, Spano T, Dando O, Bear MF, Chattarji S, Hardingham GE, Osterweil EK, Wyllie DJ, Wood ER, Kind PC (2019) Sustained correction of associative learning deficits after brief, early treatment in a rat model of Fragile X Syndrome. *Science Translational Medicine* 11.

Assaf M, Jagannathan K, Calhoun VD, Miller L, Stevens MC, Sahl R, O'Boyle JG, Schultz RT, Pearlson GD (2010) Abnormal functional connectivity of default mode sub-networks in autism spectrum disorder patients. *NeuroImage* 53:247–256.

Auerbach BD, Osterweil EK, Bear MF (2011) Mutations causing syndromic autism define an axis of synaptic pathophysiology. *Nature* 480:63–68.

Backman SA, Stambolic V, Suzuki A, Haight J, Elia A, Pretorius J, Tsao MS, Shannon P, Bolon B, Ivy GO, Mak TW (2001) Deletion of Pten in mouse brain causes seizures, ataxia and defects in soma size resembling Lhermitte-Duclos disease. *Nature Genetics* 29:396–403.

Bacon SJ, Headlam aJ, Gabbott PL, Smith aD (1996) Amygdala input to medial prefrontal cortex (mPFC) in the rat: alight and electron microscope study. *Brain. Res.* 720:211–219.

Bakkaloglu B, O'Roak BJ, Louvi A, Gupta AR, Abelson JF, Morgan TM, Chawarska K, Klin A, Ercan-Sencicek AG, Stillman AA, Tanriover G, Abrahams BS, Duvall JA, Robbins EM, Geschwind DH, Biederer T, Gunel M, Lifton RP, State MW (2008) Molecular Cytogenetic Analysis and Resequencing of Contactin Associated Protein-Like 2 in Autism Spectrum Disorders. *American Journal of Human Genetics* 82:165–173.

Bakker CE, Verheij C, Willemsen R, van der Helm R, Oerlemans F, Vermey M, Bygrave A, Hoogeveen AT, Oostra BA, Reyniers E, De Boule K, D'Hooge R, Cras P, van Velzen D, Nagels G, Martin JJ, De Deyn PP, Darby JK, Willems PJ (1994) Fmr1 knockout mice: A model to study fragile X mental retardation. *Cell* 78:23–33.

Balasanyan V, Watanabe K, Dempsey WP, Lewis TL, Trinh LA, Arnold DB (2017) Structure and Function of an Actin-Based Filter in the Proximal Axon. *Cell Reports* 21:2696–2705.

Bariselli S, Hörnberg H, Prévost-Solié C, Musardo S, Hatstatt-Burklé L, Scheiffele P, Bellone C (2018) Role of VTA dopamine neurons and neuroligin 3 in sociability traits related to nonfamiliar conspecific interaction. *Nature Communications* 9.

Barnes AP, Polleux F (2009) Establishment of Axon-Dendrite Polarity in Developing Neurons. *Annual Review of Neuroscience* 32:347–381.

Barnes SA, Wijetunge LS, Jackson AD, Katsanevaki D, Osterweil EK, Komiyama NH, Grant SGN, Bear MF, Nagerl UV, Kind PC, Wyllie DJA (2015) Convergence of Hippocampal Pathophysiology in Syngap+/- and Fmr1-/y Mice. *Journal of Neuroscience* 35:15073–15081.

Barnett MW, Watson RF, Vitalis T, Porter K, Komiyama NH, Stoney PN, Gillingwater TH, Grant SG, Kind PC (2006) Synaptic Ras GTPase activating protein regulates pattern formation in the trigeminal system of mice. *Journal of Neuroscience* 26:1355–1365.

Barttfeld P, Wicker B, Cukier S, Navarta S, Lew S, Leiguarda R, Sigman M (2012) State-dependent changes of connectivity patterns and functional brain network topology in autism spectrum disorder. *Neuropsychologia* .

Barttfeld P, Wicker B, Cukier S, Navarta S, Lew S, Sigman M (2011) A big-world network in ASD: Dynamical connectivity analysis reflects a deficit in long-range connections and an excess of short-range connections. *Neuropsychologia* 49:254–263.

Bassell GJ, Warren ST (2008) Fragile X Syndrome: Loss of Local mRNA Regulation Alters Synaptic Development and Function.

Baudouin SJ, Gaudias J, Gerharz S, Hatstatt L, Zhou K, Punnakkal P, Tanaka KF, Spooren W, Hen R, De Zeeuw CI, Vogt K, Scheiffele P (2012) Shared synaptic pathophysiology in syndromic and nonsyndromic rodent models of autism. *Science* 338:128–132.

Bauman ML, Kemper TL (2005) Neuroanatomic observations of the brain in autism: A review and future directions.

Baxter AJ, Brugha TS, Erskine HE, Scheurer RW, Vos T, Scott JG (2015) The epidemiology and global burden of autism spectrum disorders. *Psychological Medicine* 45:601–613.

Belford GR, Killackey HP (1979) The development of vibrissae representation in subcortical trigeminal centers of the neonatal rat. *Journal of Comparative Neurology* 188:63–74.

Belmonte MK, Allen G, Beckel-Mitchener A, Boulanger LM, Carper RA, Webb SJ (2004) Autism and abnormal development of brain connectivity In *Journal of Neuroscience*, Vol. 24, pp. 9228–9231.

Belzung C, Lemoine M (2011) Criteria of validity for animal models of psychiatric disorders: focus on anxiety disorders and depression. *Biology of Mood & Anxiety Disorders* 1.

Béna F, Bruno DL, Eriksson M, van Ravenswaaij-Arts C, Stark Z, Dijkhuizen T, Gerkes E, Gimelli S, Ganesamoorthy D, Thuresson AC, Labalme A, Till M, Bilan F, Pasquier L, Kitzis A, Dubourgm C, Rossi M, Bottani A, Gagnebin M, Sanlaville D, Gilbert-Dussardier B, Guipponi M, van Haeringen A, Kriek M, Ruivenkamp C, Antonarakis SE, Anderlid BM, Slater HR, Schoumans J (2013) Molecular and clinical characterization of 25 individuals with exonic deletions of NRXN1 and comprehensive review of the literature. *American Journal of Medical Genetics, Part B: Neuropsychiatric Genetics* 162:388–403.

Bender KJ, Ford CP, Trussell LO (2010) Dopaminergic Modulation of Axon Initial Segment Calcium Channels Regulates Action Potential Initiation. *Neuron* 68:500–511.

Bender KJ, Trussell LO (2009) Axon initial segment Ca2+ channels influence action potential generation and timing. *Neuron* 61:259–271.

Benned-Jensen T, Christensen RK, Denti F, Perrier JF, Rasmussen HB, Olesen SP (2016) Live imaging of kv7.2/7.3 cell surface dynamics at the axon initial segment: High steady-state stability and calpain-dependent excitotoxic downregulation revealed. *Journal of Neuroscience* 36:2261–2266.

Bennett V (1992) Ankyrins. Adaptors between diverse plasma membrane proteins and the cytoplasm.

Bennett V, Baines AJ (2001) Spectrin and ankyrin-based pathways: Metazoan inventions for integrating cells into tissues.

Berkovic SF, Heron SE, Giordano L, Marini C, Guerrini R, Kaplan RE, Gambardella A, Steinlein OK, Grinton BE, Dean JT, Bordo L, Hodgson BL, Yamamoto T, Mulley JC, Zara F, Scheffer IE (2004) Benign Familial Neonatal-Infantile Seizures: Characterization of a New Sodium Channelopathy. *Annals of Neurology* 55:550–557.

Berryer MH, Chattopadhyaya B, Xing P, Riebe I, Bosoi C, Sanon N, Antoine-Bertrand J, Lévesque M, Avoli M, Hamdan FF, Carmant L, Lamarche-Vane N, Lacaille JC, Michaud JL, Di Cristo G (2016) Decrease of SYNGAP1 in GABAergic cells impairs inhibitory synapse connectivity, synaptic inhibition and cognitive function. *Nature Communications* 7.

Berryer MH, Hamdan FF, Klitten LL, Møller RS, Carmant L, Schwartzentruber J, Patry L, Dobrzeniecka S, Rochefort D, Neugnot-Cerioli M, Lacaille JC, Niu Z, Eng CM, Yang Y, Palardy S, Belhumeur C, Rouleau GA, Tommerup N, Immken L, Beauchamp MH, Patel

GS, Majewski J, Tarnopolsky MA, Scheffzek K, Hjalgrim H, Michaud JL, Di Cristo G (2013) Mutations in SYNGAP1 Cause Intellectual Disability, Autism, and a Specific Form of Epilepsy by Inducing Haploinsufficiency. *Human Mutation* 34:385–394.

Besag FM (2018) Epilepsy in patients with autism: Links, risks and treatment challenges.

Beyeler A, Chang CJ, Silvestre M, Lévêque C, Namburi P, Wildes CP, Tye KM (2018) Organization of Valence-Encoding and Projection-Defined Neurons in the Basolateral Amygdala. *Cell Reports* 22:905–918.

Bhattacharya A, Klann E (2012) Fragile X Syndrome Therapeutics S(C)TEP through the Developmental Window.

Bi C, Wu J, Jiang T, Liu Q, Cai W, Yu P, Cai T, Zhao M, Jiang YH, Sun ZS (2012) Mutations of ANK3 identified by exome sequencing are associated with Autism susceptibility. *Human Mutation* 33:1635–1638.

Binder EB, Nemeroff CB (2010) The CRF system, stress, depression and anxietyinsights from human genetic studies.

Blanchard RJ, Griebel G, Henrie JA, Blanchard DC (1997) Differentiation of anxiolytic and panicolytic drugs by effects on rat and mouse defense test batteries In *Neuroscience and Biobehavioral Reviews*, Vol. 21, pp. 783–789.

Blumenfeld H, Lampert A, Klein JP, Mission J, Chen MC, Rivera M, Dib-Hajj S, Brennan AR, Hains BC, Waxman SG (2009) Role of hippocampal sodium channel Nav1.6 in kindling epileptogenesis. *Epilepsia* 50:44–55.

Boiko T, Van Wart A, CaldWell JH, Levinson SR, Trimmer JS, Matthews G (2003) Functional specialization of the axon initial segment by isoform-specific sodium channel targeting. *Journal of Neuroscience* 23:2306–2313.

Bolivar VJ, Walters SR, Phoenix JL (2007) Assessing autism-like behavior in mice: Variations in social interactions among inbred strains. *Behavioural Brain Research* 176:21–26.

Bolós M, Terreros-Roncal J, Perea JR, Pallas-Bazarra N, Ávila J, Llorens-Martín M (2019) Maturation dynamics of the axon initial segment (AIS) of newborn dentate granule cells in young adult C57BL/6J mice. *Journal of Neuroscience* 39:1605–1620.

Bölte S, Girdler S, Marschik PB (2019) The contribution of environmental exposure to the etiology of autism spectrum disorder.

Bonnycastle K (2018) Synaptic Vesicle Recycling in Preclinical Models of Intellectual Disability , Autism Spectrum Disorder , and Epilepsy Katherine Bonnycastle Doctor of Philosophy The University of Edinburgh Ph.D. diss.

Booker SA, Simões de Oliveira L, Anstey N, Kozic Z, Dando OR, Jackson AD, Baxter PS, Isom LL, Sherman DL, Hardingham GE, Brophy PJ, Wyllie DJA, Kind PC (2019) Increased bidirectional cellular homeostasis in a mouse model of Fragile X Syndrome. *in review* .

Boucard AA, Chubykin AA, Comoletti D, Taylor P, Südhof TC (2005) A splice code for trans-synaptic cell adhesion mediated by binding of neuroligin 1 to α- and β-neurexins. *Neuron* 48:229–236.

Bourgeron T (2015) From the genetic architecture to synaptic plasticity in autism spectrum disorder.

Bouton ME (2004) Context and behavioral processes in extinction.

Brackenbury WJ, Calhoun JD, Chen C, Miyazaki H, Nukina N, Oyama F, Ranscht B, Isom LL (2010) Functional reciprocity between Na+ channel Nav1.6 and β1 subunits in the coordinated regulation of excitability and neurite outgrowth. *Proceedings of the National Academy of Sciences of the United States of America* 107:2283–2288.

Braff DL, Geyer MA, Swerdlow NR (2001) Human studies of prepulse inhibition of startle: Normal subjects, patient groups, and pharmacological studies.

Brignell A, St John M, Boys A, Bruce A, Dinale C, Pigdon L, Hildebrand MS, Amor DJ, Morgan AT (2018) Characterization of speech and language phenotype in children with NRXN1 deletions. *American Journal of Medical Genetics, Part B: Neuropsychiatric Genetics* 177:700–708.

Brito GNO, Brito LSO (1990) Septohippocampal system and the prelimbic sector of frontal cortex: A neuropsychological battery analysis in the rat. *Behavioural Brain Research* 36:127–146.

Brown DA, Adams PR (1980) Muscarinic suppression of a novel voltage-sensitive K+ current in a vertebrate neurone [18].

Brown SP, Hestrin S (2009) Intracortical circuits of pyramidal neurons reflect their long-range axonal targets. *Nature* 457:1133–1136.

Browne DL, Gancher ST, Nutt JG, Brunt ER, Smith EA, Kramer P, Litt M (1994) Episodic ataxia/myokymia syndrome is associated with point mutations in the human potassium channel gene, KCNA1. *Nature Genetics* 8:136–140.

Bucan M, Abrahams BS, Wang K, Glessner JT, Herman EI, Sonnenblick LI, Alvarez Retuerto AI, Imielinski M, Hadley D, Bradfield JP, Kim C, Gidaya NB, Lindquist I, Hutman T, Sigman M, Kustanovich V, Lajonchere CM, Singleton A, Kim J, Wassink TH, McMahon WM, Owley T, Sweeney JA, Coon H, Nurnberger JI, Li M, Cantor RM, Minshew NJ, Sutcliffe JS, Cook EH, Dawson G, Buxbaum JD, Grant SF, Schellenberg GD, Geschwind DH, Hakonarson H (2009) Genome-wide analyses of exonic copy number variants in a family-based study point to novel autism susceptibility genes. *PLoS Genetics* 5:e1000536.

Budreck EC, Scheiffele P (2007) Neuroligin-3 is a neuronal adhesion protein at GABAergic and glutamatergic synapses. *European Journal of Neuroscience* 26:1738–1748.

Bureau I, Shepherd GM, Svoboda K (2008) Circuit and plasticity defects in the developing somatosensory cortex of Fmr1 knock-out mice. *Journal of Neuroscience* 28:5178–5188.

Burgdorf J, Moskal JR, Brudzynski SM, Panksepp J (2013) Rats selectively bred for low levels of play-induced 50kHz vocalizations as a model for Autism Spectrum Disorders: A role for NMDA receptors. *Behavioural Brain Research* 251:18–24.

Burghy CA, Stodola DE, Ruttle PL, Molloy EK, Armstrong JM, Oler JA, Fox ME, Hayes AS, Kalin NH, Essex MJ, Davidson RJ, Birn RM (2012) Developmental pathways to amygdala-prefrontal function and internalizing symptoms in adolescence. *Nature Neuroscience* 15:1736–1741.

Burgos-Robles A, Kimchi EY, Izadmehr EM, Porzenheim MJ, Ramos-Guasp WA, Nieh EH, Felix-Ortiz AC, Namburi P, Leppla CA, Presbrey KN, Anandalingam KK, Pagan-Rivera PA, Anahtar M, Beyeler A, Tye KM (2017) Amygdala inputs to prefrontal cortex guide behavior amid conflicting cues of reward and punishment. *Nature Neuroscience* 20:824–835.

Bussey TJ, Padain TL, Skillings EA, Winters BD, Morton AJ, Saksida LM (2008) The touchscreen cognitive testing method for rodents: How to get the best out of your rat. *Learning and Memory* 15:516–523.

Butler MG, Dazouki MJ, Zhou XP, Talebizadeh Z, Brown M, Takahashi TN, Miles JH, Wang CH, Stratton R, Pilarski R, Eng C (2005) Subset of individuals with autism spectrum disorders and extreme macrocephaly associated with germline PTEN tumour suppressor gene mutations. *Journal of Medical Genetics* 42:318–321.

Buxbaum JD, Cai G, Chaste P, Nygren G, Goldsmith J, Reichert J, Anckarsäter H, Rastam M, Smith CJ, Silverman JM, Hollander E, Leboyer M, Gillberg C, Verloes A, Betancur C (2007) Mutation screening of the PTEN gene in patients with autism spectrum disorders and macrocephaly. *American Journal of Medical Genetics, Part B: Neuropsychiatric Genetics* 144:484–491.

Callewaert G, Eilers J, Konnerth A (1996) Axonal calcium entry during fast 'sodium' action potentials in rat cerebellar Purkinje neurones. *Journal of Physiology* 495:641–647.

Cao W, Lin S, qiang Xia Q, lan Du Y, Yang Q, ying Zhang M, qing Lu Y, Xu J, min Duan S, Xia J, Feng G, Xu J, hong Luo J (2018) Gamma Oscillation Dysfunction in mPFC Leads to Social Deficits in Neuroligin 3 R451C Knockin Mice. *Neuron* 97:1253–1260.e7.

Carlisle HJ, Manzerra P, Marcora E, Kennedy MB (2008) SynGAP regulates steady-state and activity-dependent phosphorylation of cofilin. *Journal of Neuroscience* 28:13673–13683.

Carper RA, Courchesne E (2005) Localized enlargement of the frontal cortex in early autism. *Biological Psychiatry* 57:126–133.

Carper RA, Moses P, Tigue ZD, Courchesne E (2002) Cerebral lobes in autism: Early hyperplasia and abnormal age effects. *NeuroImage* 16:1038–1051.

Carvill GL, Heavin SB, Yendle SC, McMahon JM, O'Roak BJ, Cook J, Khan A, Dorschner MO, Weaver M, Calvert S, Malone S, Wallace G, Stanley T, Bye AM, Bleasel A, Howell KB, Kivity S, Mackay MT, Rodriguez-Casero V, Webster R, Korczyn A, Afawi Z, Zelnick N, Lerman-Sagie T, Lev D, Møller RS, Gill D, Andrade DM, Freeman JL, Sadleir LG, Shendure J, Berkovic SF, Scheffer IE, Mefford HC (2013) Targeted resequencing in epileptic encephalopathies identifies de novo mutations in CHD2 and SYNGAP1. *Nature Genetics* 45:825–830.

Castelli F (2002) Autism, Asperger syndrome and brain mechanisms for the attribution of mental states to animated shapes. *Brain* 125:1839–1849.

Castrén M, Pääkkönen A, Tarkka IM, Ryynänen M, Partanen J (2003) Augmentation of auditory N1 in children with fragile X syndrome. *Brain Topography* 15:165–171.

Castronovo P, Baccarin M, Ricciardello A, Picinelli C, Tomaiuolo P, Cucinotta F, Frittoli M, Lintas C, Sacco R, Persico AM (2019) Phenotypic spectrum of NRXN1 mono- and bi-allelic deficiency: A systematic review.

Catterall WA (2000) From ionic currents to molecular mechanisms: The structure and function of voltage-gated sodium channels.

Chadman KK, Gong S, Scattoni ML, Boltuck SE, Gandhy SU, Heintz N, Crawley JN (2008) Minimal aberrant behavioral phenotypes of neuroligin-3 R451C knockin mice. *Autism Research* 1:147–158.

Chand AN, Galliano E, Chesters RA, Grubb MS (2015) A distinct subtype of dopaminergic interneuron displays inverted structural plasticity at the axon initial segment. *Journal of Neuroscience* 35:1573–1590.

Chang CH, Knapska E, Orsini CA, Rabinak CA, Zimmerman JM, Maren S (2009) Fear extinction in rodents.

Chaste P, Klei L, Sanders SJ, Murtha MT, Hus V, Lowe JK, Willsey AJ, Moreno-De-Luca D, Yu TW, Fombonne E, Geschwind D, Grice DE, Ledbetter DH, Lord C, Mane SM, Lese Martin C, Martin DM, Morrow EM, Walsh CA, Sutcliffe JS, State MW, Devlin B, Cook EH, Kim SJ (2013) Adjusting head circumference for covariates in autism: Clinical correlates of a highly heritable continuous trait. *Biological Psychiatry* 74:576–584.

Chelly J, Khelfaoui M, Francis F, Chérif B, Bienvenu T (2006) Genetics and pathophysiology of mental retardation.

Chen HJ, Rojas-Soto M, Oguni A, Kennedy MB (1998) A synaptic Ras-GTPase activating protein (p135 SynGAP) inhibited by CaM kinase II. *Neuron* 20:895–904.

Chen Y, Lu J, Pan H, Zhang Y, Wu H, Xu K, Liu X, Jiang Y, Bao X, Yao Z, Ding K, Lo WH, Qiang B, Chan P, Shen Y, Wu X (2003) Association between genetic variation of CACNA1H and childhood absence epilepsy. *Annals of Neurology* 54:239–243.

Chen-Bee CH, Zhou Y, Jacobs NS, Lim B, Frostig RD (2012) Whisker array functional representation in rat barrel cortex: transcendence of one-to-one topography and its underlying mechanism. *Frontiers in neural circuits* 6:93.

Cheung KM, Lam CW, Chan YK, Siu WK, Yong L (2014) Atypical focal cortical dysplasia in a patient with Cowden syndrome. *Hong Kong Medical Journal* 20:165–167.

Chih B, Gollan L, Scheiffele P (2006) Alternative Splicing Controls Selective Trans-Synaptic Interactions of the Neuroligin-Neurexin Complex. *Neuron* 51:171–178.

Child ND, Cascino GD (2013) Mystery case: Cowden syndrome presenting with partial epilepsy related to focal cortical dysplasia.

Ching MS, Shen Y, Tan WH, Jeste SS, Morrow EM, Chen X, Mukaddes NM, Yoo SY, Hanson E, Hundley R, Austin C, Becker RE, Berry GT, Driscoll K, Engle EC, Friedman S, Gusella JF, Hisama FM, Irons MB, Lafiosca T, LeClair E, Miller DT, Neessen M, Picker JD, Rappaport L, Rooney CM, Sarco DP, Stoler JM, Walsh CA, Wolff RR, Zhang T, Nasir RH, Wu BL, Children's Hospital Boston Genotype Phenotype Study Group (2010) Deletions of NRXN1 (neurexin-1) predispose to a wide spectrum of developmental disorders. *American Journal of Medical Genetics Part B: Neuropsychiatric Genetics* 153B:n/a–n/a.

Chiurazzi P, Pirozzi F (2016) Advances in understanding - genetic basis of intellectual disability. *F1000Research* 5.

Choleris E, Galea LA, Sohrabji F, Frick KM (2018) Sex differences in the brain: Implications for behavioral and biomedical research.

Chow DK, Groszer M, Pribadi M, Machniki M, Carmichael ST, Liu X, Trachtenberg JT (2009) Laminar and compartmental regulation of dendritic growth in mature cortex. *Nature Neuroscience* 12:116–118.

Chung HJ, Jan YN, Jan LY (2006) Polarized axonal surface expression of neuronal KCNQ channels is mediated by multiple signals in the KCNQ2 and KCNQ3 C-terminal domains. *Proceedings of the National Academy of Sciences of the United States of America* 103:8870–8875.

Ciaccio C, Fontana L, Milani D, Tabano S, Miozzo M, Esposito S (2017) Fragile X syndrome: a review of clinical and molecular diagnoses.

Clement JP, Aceti M, Creson TK, Ozkan ED, Shi Y, Reish NJ, Almonte AG, Miller BH, Wiltgen BJ, Miller CA, Xu X, Rumbaugh G (2012) Pathogenic SYNGAP1 mutations impair cognitive development by disrupting maturation of dendritic spine synapses. *Cell* 151:709–23.

Clement JP, Ozkan ED, Aceti M, Miller CA, Rumbaugh G (2013) SYNGAP1 links the maturation rate of excitatory synapses to the duration of critical-period synaptic plasticity. *Journal of Neuroscience* 33:10447–10452.

Clipperton-Allen AE, Page DT (2014) Pten haploinsufficient mice show broad brain overgrowth but selective impairments in autism-relevant behavioral tests. *Human Molecular Genetics* 23:3490–3505.

Coffee B, Keith K, Albizua I, Malone T, Mowrey J, Sherman SL, Warren ST (2009) Incidence of Fragile X Syndrome by Newborn Screening for Methylated FMR1 DNA. *American Journal of Human Genetics* 85:503–514.

Cohen GB, Ren R, Baltimore D (1995) Modular binding domains in signal transduction proteins.

Comoletti D, De Jaco A, Jennings LL, Flynn RE, Gaietta G, Tsigelny I, Ellisman MH, Taylor P (2004) The Arg451Cys-neuroligin-3 mutation associated with autism reveals a defect in protein processing. *Journal of Neuroscience* 24:4889–4893.

Conti S, Condò M, Posar A, Mari F, Resta N, Renieri A, Neri I, Patrizi A, Parmeggiani A (2012) Phosphatase and Tensin Homolog (PTEN) gene mutations and autism: Literature review and a case report of a patient with cowden syndrome, autistic disorder, and epilepsy. *Journal of Child Neurology* 27:392–397.

Contractor A, Klyachko VA, Portera-Cailliau C (2015) Altered Neuronal and Circuit Excitability in Fragile X Syndrome. *Neuron* 87:699–715.

Cooper SA, Smiley E, Jackson A, Finlayson J, Allan L, Mantry D, Morrison J (2009) Adults with intellectual disabilities: Prevalence, incidence and remission of aggressive behaviour and related factors. *Journal of Intellectual Disability Research* 53:217–232.

Corcoran KA, Quirk GJ (2007) Activity in prelimbic cortex is necessary for the expression of learned, but not innate, fears. *Journal of Neuroscience* 27:840–844.

Cordeiro L, Ballinger E, Hagerman R, Hessl D (2011) Clinical assessment of DSM-IV anxiety disorders in fragile X syndrome: prevalence and characterization. *Journal of Neurodevelopmental Disorders* 3:57–67.

Costa-Mattioli M, Monteggia LM (2013) mTOR complexes in neurodevelopmental and neuropsychiatric disorders.

Cotel F, Exley R, Cragg SJ, Perrier JF (2013) Serotonin spillover onto the axon initial segment of motoneurons induces central fatigue by inhibiting action potential initiation. *Proceedings of the National Academy of Sciences of the United States of America* 110:4774–4779.

Courchesne E, Jane Webb S, Schumann CM (2011) From Toddlers to Adults: The Changing Landscape of the Brain in Autism In *Autism Spectrum Disorders*, pp. 611–631. Oxford University Press.

Cowley B, Kirjanen S, Partanen J, Castrén ML (2016) Epileptic electroencephalography profile associates with attention problems in children with fragile X syndrome: Review and case series.

Craig AM, Kang Y (2007) Neurexin-neuroligin signaling in synapse development.

Crair MC, Malenka RC (1995) A critical period for long-term potentiation at thalamocortical synapses. *Nature* 375:325–328.

Crawley JN, Olschowka JA, Diz DI, Jacobowitz DM (1985) Behavioral investigation of the coexistence of substance P, corticotropin releasing factor, and acetylcholinesterase in lateral dorsal tegmental neurons projecting to the medial frontal cortex of the rat. *Peptides* 6:891–901.

Cruz DA, Lovallo EM, Stockton S, Rasband M, Lewis DA (2009) Postnatal development of synaptic structure proteins in pyramidal neuron axon initial segments in monkey prefrontal cortex. *Journal of Comparative Neurology* 514:353–367.

Cui Y, Costa RM, Murphy GG, Elgersma Y, Zhu Y, Gutmann DH, Parada LF, Mody I, Silva AJ (2008) Neurofibromin Regulation of ERK Signaling Modulates GABA Release and Learning. *Cell* 135:549–560.

Curran S, Ahn JW, Grayton H, Collier DA, Ogilvie CM (2013) NRXN1 deletions identified by array comparative genome hybridisation in a clinical case series – further understanding of the relevance of NRXN1 to neurodevelopmental disorders. *Journal of Molecular Psychiatry* 1:4.

Dabell MP, Rosenfeld JA, Bader P, Escobar LF, El-Khechen D, Vallee SE, Dinulos MBP, Curry C, Fisher J, Tervo R, Hannibal MC, Siefkas K, Wyatt PR, Hughes L, Smith R, Ellingwood S, Lacassie Y, Stroud T, Farrell SA, Sanchez-Lara PA, Randolph LM, Niyazov D, Stevens CA, Schoonveld C, Skidmore D, Mackay S, Miles JH, Moodley M, Huillet A, Neill NJ, Ellison JW, Ballif BC, Shaffer LG (2013) Investigation of NRXN1 deletions: Clinical and molecular characterization. *American Journal of Medical Genetics, Part A* 161:717–731.

Dachtler J, Ivorra JL, Rowland TE, Lever C, John Rodgers R, Clapcote SJ (2015) Heterozygous deletion of α-neurexin I or α-neurexin II results in behaviors relevant to autism and schizophrenia. *Behavioral Neuroscience* 129:765–776.

Dalton KM, Holsen L, Abbeduto L, Davidson RJ (2008) Brain function and gaze fixation during facial-emotion processing in fragile X and autism. *Autism Research* 1:231–239.

Dani VS, Chang Q, Maffei A, Turrigiano GG, Jaenisch R, Nelson SB (2005) Reduced cortical activity due to a shift in the balance between excitation and inhibition in a mouse model of Rett Syndrome. *Proceedings of the National Academy of Sciences of the United States of America* 102:12560–12565.

Daoudal G, Debanne D (2003) Long-Term Plasticity of Intrinsic Excitability: Learning Rules and Mechanisms.

Darnell JC, Van Driesche SJ, Zhang C, Hung KYS, Mele A, Fraser CE, Stone EF, Chen C, Fak JJ, Chi SW, Licatalosi DD, Richter JD, Darnell RB (2011) FMRP stalls ribosomal translocation on mRNAs linked to synaptic function and autism. *Cell* 146:247–261.

Davis M, Whalen PJ (2001) The amygdala: Vigilance and emotion.

Davis M (2006) Neural systems involved in fear and anxiety measured with fear-potentiated startle. *American Psychologist* 61:741–756.

De Jaco A, Lin MZ, Dubi N, Comoletti D, Miller MT, Camp S, Ellisman M, Butko MT, Tsien RY, Taylor P (2010) Neuroligin trafficking deficiencies arising from mutations in the α/β-hydrolase fold protein family. *Journal of Biological Chemistry* 285:28674–28682.

De La Torre-Ubieta L, Won H, Stein JL, Geschwind DH (2016) Advancing the understanding of autism disease mechanisms through genetics.

De Ligt J, Willemsen MH, Van Bon BW, Kleefstra T, Yntema HG, Kroes T, Vulto-van Silfhout AT, Koolen DA, De Vries P, Gilissen C, Del Rosario M, Hoischen A, Scheffer H, De Vries BB, Brunner HG, Veltman JA, Vissers LE (2012) Diagnostic exome sequencing in persons with severe intellectual disability. *New England Journal of Medicine* 367:1921–1929.

De Rubeis S, He X, Goldberg AP, Poultney CS, Samocha K, Cicek AE, Kou Y, Liu L, Fromer M, Walker S, Singh T, Klei L, Kosmicki J, Fu SC, Aleksic B, Biscaldi M, Bolton PF, Brownfeld JM, Cai J, Campbell NG, Carracedo A, Chahrour MH, Chiocchetti AG, Coon H, Crawford EL, Crooks L, Curran SR, Dawson G, Duketis E, Fernandez BA, Gallagher L, Geller E, Guter SJ, Hill RS, Ionita-Laza I, Gonzalez PJ, Kilpinen H, Klauck SM, Kolevzon A, Lee I, Lei J, Lehtimäki T, Lin CF, Ma'ayan A, Marshall CR, McInnes AL, Neale B, Owen MJ, Ozaki N, Parellada M, Parr JR, Purcell S, Puura K, Rajagopalan D, Rehnström K, Reichenberg A, Sabo A, Sachse M, Sanders SJ, Schafer C, Schulte-Rüther M, Skuse D, Stevens C, Szatmari P, Tammimies K, Valladares O, Voran A, Wang LS, Weiss LA, Willsey AJ, Yu TW, Yuen RK, Cook EH, Freitag CM, Gill M, Hultman CM, Lehner T, Palotie A, Schellenberg GD, Sklar P, State MW, Sutcliffe JS, Walsh CA, Scherer SW, Zwick ME, Barrett JC, Cutler DJ, Roeder K, Devlin B, Daly MJ, Buxbaum JD (2014) Synaptic, transcriptional and chromatin genes disrupted in autism. *Nature* 515:209–215.

De Rubeis S, Siper PM, Durkin A, Weissman J, Muratet F, Halpern D, Trelles MDP, Frank Y, Lozano R, Wang AT, Holder JL, Betancur C, Buxbaum JD, Kolevzon A (2018) Delineation of the genetic and clinical spectrum of Phelan-McDermid syndrome caused by SHANK3 point mutations. *Molecular Autism* 9.

De Villers-Sidani E, Simpson KL, Lu YF, Lin RC, Merzenich MM (2008) Manipulating critical period closure across different sectors of the primary auditory cortex. *Nature Neuroscience* 11:957–965.

De Vries BB, Van Den Ouweland AM, Mohkamsing S, Duivenvoorden HJ, Mol E, Gelsema K, Van Rijn M, Halley DJ, Sandkuijl LA, Oostra BA, Tibben A, Niermeijer MF (1997) Screening and diagnosis for the fragile X syndrome among the mentally retarded: An epidemiological and psychological survey. *American Journal of Human Genetics* 61:660–667.

Deacon RM, Rawlins JNP (2006) T-maze alternation in the rodent. *Nature Protocols* 1:7–12.

Deal AL, Erickson KJ, Shiers SI, Burman MA (2016) Limbic system development underlies the emergence of classical fear conditioning during the third and fourth weeks of life in the rat. *Behavioral Neuroscience* 130:212–230.

Debanne D (2009) Plasticity of neuronal excitability in vivo.

Del Puerto A, Fronzaroli-Molinieres L, Perez-Alvarez MJ, Giraud P, Carlier E, Wandosell F, Debanne D, Garrido JJ (2015) ATP-P2X7 Receptor Modulates Axon Initial Segment Composition and Function in Physiological Conditions and Brain Injury. *Cerebral Cortex* 25:2282–2294.

Delatour B, Gisquet-Verrier P (1997) Functional dissociations between prelimbic and anterior cingulate parts of the medial prefrontal cortex in the rat In *Annual Meeting of the Society for Neuroscience*.

Delatour B, Gisquet-Verrier P (1996) Prelimbic cortex specific lesions disrupt delayed-variable response tasks in the rat. *Behavioral Neuroscience* 110:1282–1298.

Delatour B, Gisquet-Verrier P (1999) Lesions of the prelimbic-infralimbic cortices in rats do not disrupt response selection processes but induce delay-dependent deficits: Evidence for a role in working memory? *Behavioral Neuroscience* 113:941–955.

Delatour B, Gisquet-Verrier P (2000) Functional role of rat prelimbic-infralimbic cortices in spatial memory: Evidence for their involvement in attention and behavioural flexibility. *Behavioural Brain Research* 109:113–128.

Delattre V, La Mendola D, Meystre J, Markram H, Markram K (2013) Nlgn4 knockout induces network hypo-excitability in juvenile mouse somatosensory cortex in vitro. *Scientific Reports* 3.

Dembrow NC, Chitwood RA, Johnston D (2010) Projection-specific neuromodulation of medial prefrontal cortex neurons. *Journal of Neuroscience* 30:16922–16937.

Dementieva YA, Vance DD, Donnelly SL, Elston LA, Wolpert CM, Ravan SA, Delong GR, Abramson RK, Wright HH, Cuccaro ML (2005) Accelerated head growth in early development of individuals with autism. *Pediatric Neurology* 32:102–108.

Denardo LA, Berns DS, Deloach K, Luo L (2015) Connectivity of mouse somatosensory and prefrontal cortex examined with trans-synaptic tracing. *Nature Neuroscience* 18:1687–1697.

Denning G, Jean-Joseph B, Prince C, Durden DL, Vogt PK (2007) A short N-terminal sequence of PTEN controls cytoplasmic localization and is required for suppression of cell growth. *Oncogene* 26:3930–3940.

D'Este E, Kamin D, Balzarotti F, Hell SW (2017) Ultrastructural anatomy of nodes of Ranvier in the peripheral nervous system as revealed by STED microscopy. *Proceedings of the National Academy of Sciences of the United States of America* 114:E191–E199.

D'Este E, Kamin D, Göttfert F, El-Hady A, Hell SW (2015) STED Nanoscopy Reveals the Ubiquity of Subcortical Cytoskeleton Periodicity in Living Neurons. *Cell Reports* 10:1246–1251.

Devlin B, Boone BE, Levy SE, Lihm J, Buxbaum JD, Wu Y, Lewis L, Han Y, Boerwinkle E, Gibbs RA, Fromer M, Shakir K, Fennell T, Garimella K, Banks E, Poplin R, Gabriel S, De Pristo M, Sunyaev S, Daly MJ (2012) Patterns and rates of exonic de novo mutations in autism spectrum disorders.

Dieckmann F, Giovis C, Offergeld J (2015) The Life Expectancy of People with Intellectual Disabilities in Germany. *Journal of Applied Research in Intellectual Disabilities* 28:373–382.

Do-Monte FH, Manzano-Nieves G, Quiñones-Laracuente K, Ramos-Medina L, Quirk GJ (2015) Revisiting the role of infralimbic cortex in fear extinction with optogenetics. *Journal of Neuroscience* 35:3607–3615.

Dodson PD, Barker MC, Forsythe ID (2002) Two heteromeric Kv1 potassium channels differentially regulate action potential firing. *Journal of Neuroscience* 22:6953–6961.

Dölen G, Osterweil E, Rao BS, Smith GB, Auerbach BD, Chattarji S, Bear MF (2007) Correction of Fragile X Syndrome in Mice. *Neuron* 56:955–962.

Dudanova I, Sedej S, Ahmad M, Masius H, Sargsyan V, Zhang W, Riedel D, Angenstein F, Schild D, Rupnik M, Missler M (2006) Important contribution of α-neurexins to Ca2+-triggered exocytosis of secretory granules. *Journal of Neuroscience* 26:10599–10613.

Duflocq A, Chareyre F, Giovannini M, Couraud F, Davenne M (2011) Characterization of the axon initial segment (AIS) of motor neurons and identification of a para-AIS and a juxtapara-AIS, organized by protein 4.1B. *BMC Biology* 9.

Duflocq A, Le Bras B, Bullier E, Couraud F, Davenne M (2008) Nav1.1 is predominantly expressed in nodes of Ranvier and axon initial segments. *Molecular and Cellular Neuroscience* 39:180–192.

Dunn AJ, Swiergiel AH (2008) Effects of acute and chronic stressors and CRF in rat and mouse tests for depression In *Annals of the New York Academy of Sciences*, Vol. 1148, pp. 118–126. Blackwell Publishing Inc.

Duong L, Klitten LL, Møller RS, Ingason A, Jakobsen KD, Skjødt C, Didriksen M, Hjalgrim H, Werge T, Tommerup N (2012) Mutations in NRXN1 in a family multiply affected with brain disorders: NRXN1 mutations and brain disorders. *American Journal of Medical Genetics, Part B: Neuropsychiatric Genetics* 159 B:354–358.

Durand S, Patrizi A, Quast KB, Hachigian L, Pavlyuk R, Saxena A, Carninci P, Hensch TK, Fagiolini M (2012) NMDA Receptor Regulation Prevents Regression of Visual Cortical Function in the Absence of Mecp2. *Neuron* 76:1078–1090.

Dzhashiashvili Y, Zhang Y, Galinska J, Lam I, Grumet M, Salzer JL (2007) Nodes of Ranvier and axon initial segments are ankyrin G-dependent domains that assemble by distinct mechanisms. *Journal of Cell Biology* 177:857–870.

Ehrlich DE, Ryan SJ, Rainnie DG (2012) Postnatal development of electrophysiological properties of principal neurons in the rat basolateral amygdala. *Journal of Physiology* 590:4819–4838.

Elia M, Amato C, Bottitta M, Grillo L, Calabrese G, Esposito M, Carotenuto M (2012) An atypical patient with Cowden syndrome and PTEN gene mutation presenting with cortical malformation and focal epilepsy. *Brain and Development* 34:873–876.

Ellenbroek B, Youn J (2016) Rodent models in neuroscience research: Is it a rat race? *DMM Disease Models and Mechanisms* 9:1079–1087.

Eltokhi A, Rappold G, Sprengel R (2018) Distinct Phenotypes of Shank2 Mouse Models Reflect Neuropsychiatric Spectrum Disorders of Human Patients With SHANK2 Variants.

Emerson E, Baines S (2011) Health inequalities and people with learning disabilities in the UK. *Tizard Learning Disability Review* 16:42–48.

Engineer CT, Centanni TM, Im KW, Rahebi KC, Buell EP, Kilgard MP (2014) Degraded speech sound processing in a rat model of fragile X syndrome. *Brain Research* 1564:72–84.

Esclassan F, Francois J, Phillips KG, Loomis S, Gilmour G (2015) Phenotypic characterization of nonsocial behavioral impairment in neurexin 1α knockout rats. *Behavioral Neuroscience* 129:74–85.

Espinosa JS, Stryker MP (2012) Development and Plasticity of the Primary Visual Cortex.

Etherton M, Földy C, Sharma M, Tabuchi K, Liu X, Shamloo M (2011) Differentially Alters Hippocampal and Cortical Synaptic Function. *Pnas* 108.

Etherton MR, Blaiss CA, Powell CM, Südhof TC (2009) Mouse neurexin-1α deletion causes correlated electrophysiological and behavioral changes consistent with cognitive impairments. *Proceedings of the National Academy of Sciences of the United States of America* 106:17998–18003.

Evans MD, Dumitrescu AS, Kruijssen DL, Taylor SE, Grubb MS (2015) Rapid Modulation of Axon Initial Segment Length Influences Repetitive Spike Firing. *Cell Reports* 13:1233–1245.

Evans MD, Sammons RP, Lebron S, Dumitrescu AS, Watkins TBK, Uebele VN, Renger JJ, Grubb MS (2013) Calcineurin signaling mediates activity-dependent relocation of the Axon Initial segment. *Journal of Neuroscience* 33:6950–6963.

Fagiolini M, Leblanc JJ (2011) Autism: A critical period disorder?

Fagiolini M, Pizzorusso T, Porciatti V, Cenni M, Maffei L (1997) Transplant of Schwann cells allows normal development of the visual cortex of dark-reared rats. *European Journal of Neuroscience* 9:102–112.

Farías GG, Guardia CM, Britt DJ, Guo X, Bonifacino JS (2015) Sorting of Dendritic and Axonal Vesicles at the Pre-axonal Exclusion Zone. *Cell Reports* 13:1221–1232.

Feilotter HE, Coulon V, McVeigh JL, Boag AH, Dorion-Bonnet F, Duboué B, Latham WC, Eng C, Mulligan LM, Longy M (1999) Analysis of the 10q23 chromosomal region and the PTEN gene in human sporadic breast carcinoma. *British Journal of Cancer* 79:718–723.

Feldmeyer D, Brecht M, Helmchen F, Petersen CC, Poulet JF, Staiger JF, Luhmann HJ, Schwarz C (2013) Barrel cortex function.

Feng Z, Chen X, Zeng M, Zhang M (2019) Phase separation as a mechanism for assembling dynamic postsynaptic density signalling complexes.

Ferreira MA, O'Donovan MC, Meng YA, Jones IR, Ruderfer DM, Jones L, Fan J, Kirov G, Perlis RH, Green EK, Smoller JW, Grozeva D, Stone J, Nikolov I, Chambert K, Hamshere ML, Nimgaonkar VL, Moskvina V, Thase ME, Caesar S, Sachs GS, Franklin J, Gordon-Smith K, Ardlie KG, Gabriel SB, Fraser C, Blumenstiel B, Defelice M, Breen G, Gill M, Morris DW, Elkin A, Muir WJ, McGhee KA, Williamson R, MacIntyre DJ, MacLean AW, St Clair D, Robinson M, Van Beck M, Pereira AC, Kandaswamy R, McQuillin A, Collier DA, Bass NJ, Young AH, Lawrence J, Nicol Ferrier I, Anjorin A, Farmer A, Curtis D, Scolnick EM, McGuffin P, Daly MJ, Corvin AP, Holmans PA, Blackwood DH, Gurling HM, Owen MJ, Purcell SM, Sklar P, Craddock N (2008) Collaborative genome-wide association analysis supports a role for ANK3 and CACNA1C in bipolar disorder. *Nature Genetics* 40:1056–1058.

Firth HV, Wright CF (2011) The Deciphering Developmental Disorders (DDD) study.

Fischer J, Hammerschmidt K (2011) Ultrasonic vocalizations in mouse models for speech and socio-cognitive disorders: Insights into the evolution of vocal communication.

Fisher RS, Acevedo C, Arzimanoglou A, Bogacz A, Cross JH, Elger CE, Engel J, Forsgren L, French JA, Glynn M, Hesdorffer DC, Lee BI, Mathern GW, Moshé SL, Perucca E, Scheffer IE, Tomson T, Watanabe M, Wiebe S (2014) ILAE Official Report: A practical clinical definition of epilepsy. *Epilepsia* 55:475–482.

Fitzgerald TW, Gerety SS, Jones WD, Van Kogelenberg M, King DA, McRae J, Morley KI, Parthiban V, Al-Turki S, Ambridge K, Barrett DM, Bayzetinova T, Clayton S, Coomber EL, Gribble S, Jones P, Krishnappa N, Mason LE, Middleton A, Miller R, Prigmore E, Rajan D, Sifrim A, Tivey AR, Ahmed M, Akawi N, Andrews R, Anjum U, Archer H, Armstrong R, Balasubramanian M, Banerjee R, Baralle D, Batstone P, Baty D, Bennett C, Berg J, Bernhard B, Bevan AP, Blair E, Blyth M, Bohanna D, Bourdon L, Bourn D, Brady A, Bragin E, Brewer C, Brueton L, Brunstrom K, Bumpstead SJ, Bunyan DJ, Burn J, Burton J, Canham N, Castle B, Chandler K, Clasper S, Clayton-Smith J, Cole T, Collins A, Collinson MN, Connell F, Cooper N, Cox H, Cresswell L, Cross G, Crow Y, D'Alessandro M, Dabir T, Davidson R, Davies S, Dean J, Deshpande C, Devlin G, Dixit A, Dominiczak A, Donnelly C, Donnelly D, Douglas A, Duncan A, Eason J, Edkins S, Ellard S, Ellis P, Elmslie F, Evans K, Everest S, Fendick T, Fisher R, Flinter F, Foulds N, Fryer A, Fu B, Gardiner C, Gaunt L, Ghali N, Gibbons R, Gomes Pereira SL, Goodship J, Goudie D, Gray E, Greene P, Greenhalgh L, Harrison L, Hawkins R, Hellens S, Henderson A, Hobson E, Holden S, Holder S, Hollingsworth G, Homfray T, Humphreys M, Hurst J, Ingram S, Irving M, Jarvis J, Jenkins L, Johnson D, Jones D, Jones E, Josifova D, Joss S, Kaemba B, Kazembe S, Kerr B, Kini U, Kinning E, Kirby G, Kirk C, Kivuva E, Kraus A, Kumar D, Lachlan K, Lam W, Lampe A, Langman C, Lees M, Lim D, Lowther G, Lynch SA, Magee A, Maher E, Mansour S, Marks K, Martin K, Maye U, McCann E, McConnell V, McEntagart M, McGowan R, McKay K, McKee S, McMullan DJ, McNerlan S, Mehta S, Metcalfe K, Miles E, Mohammed S, Montgomery T, Moore D, Morgan S, Morris A, Morton J, Mugalaasi H, Murday V, Nevitt L, Newbury-Ecob R, Norman A, O'Shea R, Ogilvie C, Park S, Parker MJ, Patel C, Paterson J, Payne S, Phipps J, Pilz DT, Porteous D, Pratt N, Prescott K, Price S, Pridham A, Procter A, Purnell H, Ragge N, Rankin J, Raymond L, Rice D, Robert L, Roberts E, Roberts G, Roberts J, Roberts P, Ross A, Rosser E, Saggar A, Samant S, Sandford R, Sarkar A, Schweiger S, Scott C, Scott R, Selby A, Seller A, Sequeira C, Shannon N, Sharif S, Shaw-Smith C, Shearing E, Shears D, Simonic I, Simpkin D, Singzon R, Skitt Z, Smith A, Smith B, Smith K, Smithson S, Sneddon L, Splitt M, Squires M, Stewart F, Stewart H, Suri M, Sutton V, Swaminathan GJ, Sweeney E, Tatton-Brown K, Taylor C, Taylor R, Tein M, Temple IK, Thomson J, Tolmie J, Torokwa A, Treacy B, Turner C, Turnpenny P, Tysoe C, Vandersteen A,

Vasudevan P, Vogt J, Wakeling E, Walker D, Waters J, Weber A, Wellesley D, Whiteford M, Widaa S, Wilcox S, Williams D, Williams N, Woods G, Wragg C, Wright M, Yang F, Yau M, Carter NP, Parker M, Firth HV, FitzPatrick DR, Wright CF, Barrett JC, Hurles ME (2015) Large-scale discovery of novel genetic causes of developmental disorders.

Floresco SB, Seamans JK, Phillips AG (1997) Selective roles for hippocampal, prefrontal cortical, and ventral striatal circuits in radial-arm maze tasks with or without a delay. *Journal of Neuroscience* 17:1880–1890.

Forster L. G, Novick M. A, Scholl L. J, Watt J. M (2012) The Role of the Amygdala in Anxiety Disorders In *The Amygdala - A Discrete Multitasking Manager*. InTech.

Fraser MM, Bayazitov IT, Zakharenko SS, Baker SJ (2008) Phosphatase and tensin homolog, deleted on chromosome 10 deficiency in brain causes defects in synaptic structure, transmission and plasticity, and myelination abnormalities. *Neuroscience* 151:476–488.

Frazier TW, Embacher R, Tilot AK, Koenig K, Mester J, Eng C (2015) Molecular and phenotypic abnormalities in individuals with germline heterozygous PTEN mutations and autism. *Molecular Psychiatry* 20:1132–1138.

Frenkel MY, Bear MF (2004) How monocular deprivation shifts ocular dominance in visual cortex of young mice. *Neuron* 44:917–923.

Freyberg J, Robertson CE, Baron-Cohen S (2015) Reduced perceptual exclusivity during object and grating rivalry in autism. *Journal of Vision* 15.

Fried SI, Lasker ACW, Desai NJ, Eddington DK, Rizzo JF (2009) Axonal sodium-channel bands shape the response to electric stimulation in retinal ganglion cells. *Journal of Neurophysiology* 101:1972–1987.

Friedman JM, Baross Á, Delaney AD, Ally A, Arbour L, Asano J, Bailey DK, Barber S, Birch P, Brown-John M, Cao M, Chan S, Charest DL, Farnoud N, Fernandes N, Flibotte S, Go A, Gibson WT, Holt RA, Jones SJ, Kennedy GC, Krzywinski M, Langlois S, Li HI, McGillivray BC, Nayar T, Pugh TJ, Rajcan-Separovic E, Schein JE, Schnerch A, Siddiqui A, Van Allen MI, Wilson G, Yong SL, Zahir F, Eydoux P, Marra MA (2006) Oligonucleotide microarray analysis of genomic imbalance in children with mental retardation. *American Journal of Human Genetics* 79:500–513.

Frith U (2003) *Autism: Explaining the Enigma (2nd edition)* Blackwell; Oxford.

Funahashi R, Maruyama T, Yoshimura Y, Komatsu Y (2013) Silent synapses persist into adulthood in layer 2/3 pyramidal neurons of visual cortex in dark-reared mice. *Journal of Neurophysiology* 109:2064–2076.

Gabbott PL, Warner TA, Jays PR, Salway P, Busby SJ (2005) Prefrontal cortex in the rat: Projections to subcortical autonomic, motor, and limbic centers. *Journal of Comparative Neurology* 492:145–177.

Gale GD, Anagnostaras SG, Godsil BP, Mitchell S, Nozawa T, Sage JR, Wiltgen B, Fanselow MS (2004) Role of the Basolateral Amygdala in the Storage of Fear Memories across the Adult Lifetime of Rats. *Journal of Neuroscience* 24:3810–3815.

Galiano MR, Jha S, Ho TSY, Zhang C, Ogawa Y, Chang KJ, Stankewich MC, Mohler PJ, Rasband MN (2012) A distal axonal cytoskeleton forms an intra-axonal boundary that controls axon initial segment assembly. *Cell* 149:1125–1139.

Gandal MJ, Zhang P, Hadjimichael E, Walker RL, Chen C, Liu S, Won H, Van Bakel H, Varghese M, Wang Y, Shieh AW, Haney J, Parhami S, Belmont J, Kim M, Losada PM, Khan Z, Mleczko J, Xia Y, Dai R, Wang D, Yang YT, Xu M, Fish K, Hof PR, Warrell J, Fitzgerald D, White K, Jaffe AE, Peters MA, Gerstein M, Liu C, Iakoucheva LM, Pinto D, Geschwind DH (2018) Transcriptome-wide isoform-level dysregulation in ASD, schizophrenia, and bipolar disorder. *Science* 362.

Gandhi RM, Kogan CS, Messier C (2014) 2-Methyl-6-(phenylethynyl) pyridine (MPEP) reverses maze learning and PSD-95 deficits in Fmrl knock-out mice. *Frontiers in Cellular Neuroscience* 8.

Garcia-Junco-Clemente P, Chow DK, Tring E, Lazaro MT, Trachtenberg JT, Golshani P (2013) Overexpression of calcium-activated potassium channels underlies cortical dysfunction in a model of PTEN-associated autism. *Proceedings of the National Academy of Sciences of the United States of America* 110:18297–18302.

Gauthier J, Bonnel A, St-Onge J, Karemera L, Laurent S, Mottron L, Fombonne É, Joober R, Rouleau GA (2005) NLGN3/NLGN4 gene mutations are not responsible for autism in the Quebec population. *American Journal of Medical Genetics - Neuropsychiatric Genetics* 132 B:74–75.

Gauthier J, Siddiqui TJ, Huashan P, Yokomaku D, Hamdan FF, Champagne N, Lapointe M, Spiegelman D, Noreau A, Lafreniére F, Fathalli F, Joober R, Krebs MO, DeLisi LE, Mottron L, Fombonne É, Michaud JL, Drapeau P, Carbonetto S, Craig AM, Rouleau GA (2011) Truncating mutations in NRXN2 and NRXN1 in autism spectrum disorders and schizophrenia. *Human Genetics* 130:563–573.

Geppert M, Khvotchev M, Krasnoperov V, Goda Y, Missler M, Hammer RE, Ichtchenko K, Petrenko AG, Südhof TC (1998) Neurexin Iα is a major α-latrotoxin receptor that cooperates in α- latrotoxin action. *Journal of Biological Chemistry* 273:1705–1710.

Gibson JR, Bartley AF, Hays SA, Huber KM (2008) Imbalance of neocortical excitation and inhibition and altered UP states reflect network hyperexcitability in the mouse model of fragile X syndrome. *Journal of Neurophysiology* 100:2615–2626.

Gil A, Andrés-Pons A, Fernândez E, Valiente M, Torres J, Cervera J, Pulido R (2006) Nuclear localization of PTEN by a Ran-dependent mechanism enhances apoptosis: Involvement of an N-terminal nuclear localization domain and multiple nuclear exclusion motifs. *Molecular Biology of the Cell* 17:4002–4013.

Gilman SR, Iossifov I, Levy D, Ronemus M, Wigler M, Vitkup D (2011) Rare De Novo Variants Associated with Autism Implicate a Large Functional Network of Genes Involved in Formation and Function of Synapses. *Neuron* 70:898–907.

Girirajan S, Dennis MY, Baker C, Malig M, Coe BP, Campbell CD, Mark K, Vu TH, Alkan C, Cheng Z, Biesecker LG, Bernier R, Eichler EE (2013) Refinement and discovery of new hotspots of copy-number variation associated with autism spectrum disorder. *American Journal of Human Genetics* 92:221–237.

Gkogkas CG, Khoutorsky A, Ran I, Rampakakis E, Nevarko T, Weatherill DB, Vasuta C, Yee S, Truitt M, Dallaire P, Major F, Lasko P, Ruggero D, Nader K, Lacaille JC, Sonenberg N (2013) Autism-related deficits via dysregulated eIF4E-dependent translational control. *Nature* 493:371–377.

Glessner JT, Wang K, Cai G, Korvatska O, Kim CE, Wood S, Zhang H, Estes A, Brune CW, Bradfield JP, Imielinski M, Frackelton EC, Reichert J, Crawford EL, Munson J, Sleiman PMA, Chiavacci R, Annaiah K, Thomas K, Hou C, Glaberson W, Flory J, Otieno F, Garris M, Soorya L, Klei L, Piven J, Meyer KJ, Anagnostou E, Sakurai T, Game RM, Rudd DS, Zurawiecki D, McDougle CJ, Davis LK, Miller J, Posey DJ, Michaels S, Kolevzon A, Silverman JM, Bernier R, Levy SE, Schultz RT, Dawson G, Owley T, McMahon WM, Wassink TH, Sweeney JA, Nurnberger JI, Coon H, Sutcliffe JS, Minshew NJ, Grant SFA, Bucan M, Cook EH, Buxbaum JD, Devlin B, Schellenberg GD, Hakonarson H, Schellenberg GD, Hakonarson H (2009) Autism genome-wide copy number variation reveals ubiquitin and neuronal genes. *Nature* 459:569–73.

Godfraind JM, Reyniers E, De Boulle K, D'Hooge R, De Deyn PP, Bakker CE, Oostra BA, Kooy RF, Willems PJ (1996) Long-term potentiation in the hippocampus of fragile X knockout mice. *American Journal of Medical Genetics* 64:246–251.

Goffin A, Hoefsloot LH, Bosgoed E, Swillen A, Fryns JP (2001) PTEN mutation in a family with Cowden syndrome and autism. *American Journal of Medical Genetics - Neuropsychiatric Genetics* 105:521–524.

Gogolla N, Leblanc JJ, Quast KB, Südhof T, Fagiolini M, Hensch TK (2010) Common circuit defect of excitatory-inhibitory balance in mouse models of autism. *Journal of neurodevelopmental disorders* 1:172–181.

Goldberg EM, Clark BD, Zagha E, Nahmani M, Erisir A, Rudy B (2008) K+ Channels at the Axon Initial Segment Dampen Near-Threshold Excitability of Neocortical Fast-Spiking GABAergic Interneurons. *Neuron* 58:387–400.

Gonzalez-Mantilla AJ, Moreno-De-Luca A, Ledbetter DH, Martin CL (2016) A cross-disorder method to identify novel candidate genes for developmental brain disorders.

Gordon NS, Burke S, Akil H, Watson SJ, Panksepp J (2003) Socially-induced brain 'fertilization': play promotes brain derived neurotrophic factor transcription in the amygdala and dorsolateral frontal cortex in juvenile rats. *Neuroscience letters* 341:17–20.

Gothelf D, Furfaro JA, Hoeft F, Eckert MA, Hall SS, O'Hara R, Erba HW, Ringel J, Hayashi KM, Patnaik S, Golianu B, Kraemer HC, Thompson PM, Piven J, Reiss AL (2008) Neuroanatomy of fragile X syndrome is associated with aberrant behavior and the fragile X mental retardation protein (FMRP). *Annals of Neurology* 63:40–51.

Graf ER, Kang Y, Hauner AM, Craig AM (2006) Structure function and splice site analysis of the synaptogenic activity of the neurexin-1β LNS domain. *Journal of Neuroscience* 26:4256–4265.

Graf ER, Zhang X, Jin SX, Linhoff MW, Craig AM (2004) Neurexins induce differentiation of GABA and glutamate postsynaptic specializations via neuroligins. *Cell* 119:1013–1026.

Grayton HM, Missler M, Collier DA, Fernandes C (2013) Altered Social Behaviours in Neurexin 1α Knockout Mice Resemble Core Symptoms in Neurodevelopmental Disorders. *PLoS ONE* 8.

Greenberg J, Seltzer M, Baker J, Smith L, Warren SF, Brady N, Hong J (2012) Family environment and behavior problems in children, adolescents, and adults with fragile x syndrome. *American Journal on Intellectual and Developmental Disabilities* 117:331–346.

Gregor A, Albrecht B, Bader I, Bijlsma EK, Ekici AB, Engels H, Hackmann K, Horn D, Hoyer J, Klapecki J, Kohlhase J, Maystadt I, Nagl S, Prott E, Tinschert S, Ullmann R, Wohlleber E, Woods G, Reis A, Rauch A, Zweier C (2011) Expanding the clinical spectrum associated with defects in CNTNAP2 and NRXN1. *BMC Medical Genetics* 12:106.

Gregorian C, Nakashima J, Dry SM, Nghiemphu PL, Smith KB, Ao Y, Dang J, Lawson G, Mellinghoff IK, Mischel PS, Phelps M, Parada LF, Liu X, Sofroniew MV, Eilber FC, Wu H (2009) PTEN dosage is essential for neurofibroma development and malignant transformation. *Proceedings of the National Academy of Sciences of the United States of America* 106:19479–19484.

Griebel G, Perrault G, Sanger DJ (1997) A comparative study of the effects of selective and non-selective 5- HT2 receptor subtype antagonists in rat and mouse models of anxiety. *Neuropharmacology* 36:793–802.

Grubb MS, Burrone J (2010) Activity-dependent relocation of the axon initial segment fine-tunes neuronal excitability. *Nature* 465:1070–1074.

Gulledge AT, Bravo JJ (2016) Neuron morphology influences axon initial segment plasticity. *eNeuro* 3:255–265.

Gulsuner S, Walsh T, Watts AC, Lee MK, Thornton AM, Casadei S, Rippey C, Shahin H, Nimgaonkar VL, Go RC, Savage RM, Swerdlow NR, Gur RE, Braff DL, King MC, McClellan JM (2013) Spatial and temporal mapping of de novo mutations in schizophrenia to a fetal prefrontal cortical network. *Cell* 154.

Gumy LF, Katrukha EA, Grigoriev I, Jaarsma D, Kapitein LC, Akhmanova A, Hoogenraad CC (2017) MAP2 Defines a Pre-axonal Filtering Zone to Regulate KIF1- versus KIF5-Dependent Cargo Transport in Sensory Neurons. *Neuron* 94:347–362.e7.

Guo D, Yang X, Shi L (2020) *Rho GTPase Regulators and Effectors in Autism Spectrum Disorders: Animal Models and Insights for Therapeutics*, Vol. 9.

Guo J, Ji Y, Ding Y, Jiang W, Sun Y, Lu B, Nagappan G (2016) BDNF pro-peptide regulates dendritic spines via caspase-3. *Cell Death and Disease* 7.

Guo X, Hamilton PJ, Reish NJ, Sweatt JD, Miller CA, Rumbaugh G (2009) Reduced expression of the NMDA receptor-interacting protein SynGAP causes behavioral abnormalities that model symptoms of schizophrenia. *Neuropsychopharmacology* 34:1659–1672.

Guo X, Farías GG, Mattera R, Bonifacino JS (2016) Rab5 and its effector FHF contribute to neuronal polarity through dynein-dependent retrieval of somatodendritic proteins from the axon. *Proceedings of the National Academy of Sciences of the United States of America* 113:E5318–E5327.

Guo Y, Su ZJ, Chen YK, Chai Z (2017) Brain-derived neurotrophic factor/neurotrophin 3 regulate axon initial segment location and affect neuronal excitability in cultured hippocampal neurons. *Journal of Neurochemistry* 142:260–271.

Gutzmann A, ErgÃ$\frac{1}{4}$l N, Grossmann R, Schultz C, Wahle P, Engelhardt M (2014) A period of structural plasticity at the axon initial segment in developing visual cortex. *Frontiers in Neuroanatomy* 8:1–13.

Haberl MG, Zerbi V, Veltien A, Ginger M, Heerschap A, Frick A (2015) Structural-functional connectivity deficits of neocortical circuits in the Fmr1-/y mouse model of autism. *Science Advances* 1.

Hamdan FF, Daoud H, Piton A, Gauthier J, Dobrzeniecka S, Krebs MO, Joober R, Lacaille JC, Nadeau A, Milunsky JM, Wang Z, Carmant L, Mottron L, Beauchamp MH, Rouleau GA, Michaud JL (2011) De novo syngap1 mutations in nonsyndromic intellectual disability and autism. *Biological Psychiatry* 69:898–901.

Hamdan FF, Pellerin S, Carmant L, D'Anjou G, Michaud JL, Gauthier J, Spiegelman D, Noreau A, Yang Y, Dobrzeniecka RNS, Côté M, Marineau C, Lafrenière RG, Rouleau GA, Drapeau P, Lacaille JC, Perreault-Linck E, Mottron L, Fombonne É, Joober R, Addington AM, Rapoport JL, Delisi LE, Krebs MO, Mouaffak F (2009) Mutations in SYNGAPL in autosomai nonsyndromic mental retardation. *New England Journal of Medicine* 360:599–605.

Hannula DE, Duff MC (2017) *The Hippocampus from Cells to Systems: Structure, Connectivity, and Functional Contributions to Memory and Flexible Cognition* Springer International Publishing.

Harlow EG, Till SM, Russell TA, Wijetunge LS, Kind P, Contractor A (2010) Critical Period Plasticity Is Disrupted in the Barrel Cortex of Fmr1 Knockout Mice. *Neuron* 65:385–398.

Harper C (2014) Diagnostic and statistical manual of mental disorders In *A Companion to Criminal Justice, Mental Health & Risk*. American Psychological Association.

Harrington AJ, Raissi A, Rajkovich K, Berto S, Kumar J, Molinaro G, Raduazzo J, Guo Y, Loerwald K, Konopka G, Huber KM, Cowan CW (2016) MEF2C regulates cortical inhibitory and excitatory synapses and behaviors relevant to neurodevelopmental disorders. *eLife* 5.

Harrison V, Connell L, Hayesmoore J, McParland J, Pike MG, Blair E (2011) Compound heterozygous deletion of NRXN1 causing severe developmental delay with early onset epilepsy in two sisters. *American Journal of Medical Genetics, Part A* 155:2826–2831.

Hashemi E, Ariza J, Rogers H, Noctor SC, Martínez-Cerdeño V (2017) The Number of Parvalbumin-Expressing Interneurons Is Decreased in the Medial Prefrontal Cortex in Autism. *Cerebral cortex (New York, N.Y. : 1991)* 27:1931–1943.

Haws ME, Jaramillo TC, Espinosa F, Widman AJ, Stuber GD, Sparta DR, Tye KM, Russo SJ, Parada LF, Stavarache M, Kaplitt M, Bonci A, Powell CM (2014) PTEN knockdown alters dendritic spine/protrusion morphology, not density. *Journal of Comparative Neurology* 522:1171–1190.

Hayton SJ, Olmstead MC, Dumont ÉC (2011) Shift in the intrinsic excitability of medial prefrontal cortex neurons following training in impulse control and cued-responding tasks. *PLoS ONE* 6:e23885.

Hazlett HC, Poe MD, Lightbody AA, Styner M, MacFall JR, Reiss AL, Piven J (2012) Trajectories of early brain volume development in fragile X syndrome and autism. *Journal of the American Academy of Child and Adolescent Psychiatry* 51:921–933.

He M, Jenkins P, Bennett V (2012) Cysteine 70 of ankyrin-G is S-palmitoylated and is required for function of ankyrin-G in membrane domain assembly. *Journal of Biological Chemistry* 287:43995–44005.

Hebb DO (1949) Organization of behavior. *Journal of Clinical Psychology* 6:335.

Hedstrom KL, Ogawa Y, Rasband MN (2008) AnkyrinG is required for maintenance of the axon initial segment and neuronal polarity. *Journal of Cell Biology* 183:635–640.

Heinen K, Bosman LW, Spijker S, Van Pelt J, Smit AB, Voorn P, Baker RE, Brussaard AB (2004) Gabaa receptor maturation in relation to eye opening in the rat visual cortex. *Neuroscience* 124:161–171.

Herman GE, Butter E, Enrile B, Pastore M, Prior TW, Sommer A (2007) Increasing knowledge of PTEN germline mutations: Two additional patients with autism and macrocephaly. *American Journal of Medical Genetics, Part A* 143:589–593.

Heron SE, Khosravani H, Varela D, Bladen C, Williams TC, Newman MR, Scheffer IE, Berkovic SF, Mulley JC, Zamponi GW (2007) Extended spectrum of idiopathic generalized epilepsies associated with CACNA1H functional variants. *Annals of Neurology* 62:560–568.

Heron SE, Phillips HA, Mulley JC, Mazarib A, Neufeld MY, Berkovic SF, Scheffer IE (2004) Genetic Variation of CACNA1H in Idiopathic Generalized Epilepsy [1].

Herry C, Ciocchi S, Senn V, Demmou L, Müller C, Lüthi A (2008) Switching on and off fear by distinct neuronal circuits. *Nature* 454:600–606.

Herry C, Johansen JP (2014) Encoding of fear learning and memory in distributed neuronal circuits. *Nature Neuroscience* 17:1644–1654.

Hinman JD, Rasband MN, Carmichael ST (2013) Remodeling of the axon initial segment after focal cortical and white matter stroke. *Stroke* 44:182–189.

Hobert JA, Embacher R, Mester JL, Frazier TW, Eng C (2014) Biochemical screening and PTEN mutation analysis in individuals with autism spectrum disorders and macrocephaly. *European Journal of Human Genetics* 22:273–276.

Hodges J (1995) Memory, Amnesia and the Hippocampal System. *Journal of Neurology, Neurosurgery & Psychiatry* 58:128–128.

Höfflin F, Jack A, Riedel C, Mack-Bucher J, Roos J, Corcelli C, Schultz C, Wahle P, Engelhardt M (2017) Heterogeneity of the axon initial segment in interneurons and pyramidal cells of rodent visual cortex. *Frontiers in Cellular Neuroscience* 11.

Hoischen A, Krumm N, Eichler EE (2014) Prioritization of neurodevelopmental disease genes by discovery of new mutations.

Holsen LM, Dalton KM, Johnstone T, Davidson RJ (2008) Prefrontal social cognition network dysfunction underlying face encoding and social anxiety in fragile X syndrome. *NeuroImage* 43:592–604.

Homberg JR, Kyzar EJ, Nguyen M, Norton WH, Pittman J, Poudel MK, Gaikwad S, Nakamura S, Koshiba M, Yamanouchi H, Scattoni ML, Ullman JF, Diamond DM, Kaluyeva AA, Parker MO, Klimenko VM, Apryatin SA, Brown RE, Song C, Gainetdinov RR, Gottesman II, Kalueff AV (2016) Understanding autism and other neurodevelopmental disorders through experimental translational neurobehavioral models.

Hoon M, Soykan T, Falkenburger B, Hammer M, Patrizi A, Schmidt KF, Sassoè-Pognetto M, Löwel S, Moser T, Taschenberger H, Brose N, Varoqueaux F (2011) Neuroligin-4 is localized to glycinergic postsynapses and regulates inhibition in the retina. *Proceedings of the National Academy of Sciences of the United States of America* 108:3053–3058.

Hoover WB, Vertes RP (2007) Anatomical analysis of afferent projections to the medial prefrontal cortex in the rat. *Brain Structure and Function* 212:149–179.

Hopkins BD, Hodakoski C, Barrows D, Mense SM, Parsons RE (2014) PTEN function: The long and the short of it.

Hormozdiari F, Penn O, Borenstein E, Eichler EE (2015) The discovery of integrated gene networks for autism and related disorders. *Genome Research* 25:142–154.

Horschitz S, Matthäus F, Groß A, Rosner J, Galach M, Greffrath W, Treede RD, Utikal J, Schloss P, Meyer-Lindenberg A (2015) Impact of preconditioning with retinoic acid during early development on morphological and functional characteristics of human induced pluripotent stem cell-derived neurons. *Stem Cell Research* 15:30–41.

Hou L, Antion MD, Hu D, Spencer CM, Paylor R, Klann E (2006) Dynamic Translational and Proteasomal Regulation of Fragile X Mental Retardation Protein Controls mGluR-Dependent Long-Term Depression. *Neuron* 51:441–454.

Hu W, Tian C, Li T, Yang M, Hou H, Shu Y (2009) Distinct contributions of Nav1.6 and Nav1.2 in action potential initiation and backpropagation. *Nature Neuroscience* 12:996–1002.

Huber KM, Gallagher SM, Warren ST, Bear MF (2002) Altered synaptic plasticity in a mouse model of fragile X mental retardation. *Proceedings of the National Academy of Sciences of the United States of America* 99:7746–7750.

hui Jiang Y, Armstrong D, Albrecht U, Atkins CM, Noebels JL, Eichele G, Sweatt JD, Beaudet AL (1998) Mutation of the Angelman ubiquitin ligase in mice causes increased cytoplasmic p53 and deficits of contextual learning and long-term potentiation. *Neuron* 21:799–811.

Hutchinson E, Avery A, VandeWoude S (2005) Environmental enrichment for laboratory rodents.

Ichtchenko K, Hata Y, Nguyen T, Ullrich B, Missler M, Moomaw C, Südhof TC (1995) Neuroligin 1: A splice site-specific ligand for β-neurexins.

Ichtchenko K, Nguyen T, Südhof TC (1996) Structures, alternative splicing, and neurexin binding of multiple neuroligins. *Journal of Biological Chemistry* 271:2676–2682.

Imitola J, Walleigh D, Anderson CE, Jethva R, Carvalho KS, Legido A, Khurana DS (2014) Fraternal twins with autism, severe cognitive deficit, and epilepsy: Diagnostic role of chromosomal microarray analysis. *Seminars in Pediatric Neurology* 21:167–171.

Inda MC, DeFelipe J, Muñoz A (2006) Voltage-gated ion channels in the axon initial segment of human cortical pyramidal cells and their relationship with chandelier cells. *Proceedings of the National Academy of Sciences of the United States of America* 103:2920–2925.

Inoki K, Li Y, Zhu T, Wu J, Guan KL (2002) TSC2 is phosphorylated and inhibited by Akt and suppresses mTOR signalling. *Nature Cell Biology* 4:648–657.

Iossifov I, O'Roak BJ, Sanders SJ, Ronemus M, Krumm N, Levy D, Stessman HA, Witherspoon KT, Vives L, Patterson KE, Smith JD, Paeper B, Nickerson DA, Dea J, Dong S, Gonzalez LE, Mandell JD, Mane SM, Murtha MT, Sullivan CA, Walker MF, Waqar Z, Wei L, Willsey AJ, Yamrom B, Lee YH, Grabowska E, Dalkic E, Wang Z, Marks S, Andrews P, Leotta A, Kendall J, Hakker I, Rosenbaum J, Ma B, Rodgers L, Troge J, Narzisi G, Yoon S, Schatz MC, Ye K, McCombie WR, Shendure J, Eichler EE, State MW, Wigler M (2014) The contribution of de novo coding mutations to autism spectrum disorder. *Nature* 515:216–221.

Iossifov I, Ronemus M, Levy D, Wang Z, Hakker I, Rosenbaum J, Yamrom B, ha Lee Y, Narzisi G, Leotta A, Kendall J, Grabowska E, Ma B, Marks S, Rodgers L, Stepansky A, Troge J, Andrews P, Bekritsky M, Pradhan K, Ghiban E, Kramer M, Parla J, Demeter R, Fulton LL, Fulton RS, Magrini VJ, Ye K, Darnell JC, Darnell RB, Mardis ER, Wilson RK, Schatz MC, McCombie RW, Wigler M (2012) De Novo Gene Disruptions in Children on the Autistic Spectrum. *Neuron* 74:285–299.

Iqbal Z, Vandeweyer G, Van der voet M, Waryah AM, Zahoor MY, Besseling JA, Roca LT, Vulto-van silfhout AT, Nijhof B, Kramer JM, Van der Aa N, Ansar M, Peeters H, Helsmoortel C, Gilissen C, Vissers LE, Veltman JA, De brouwer AP, Frank kooy R, Riazuddin S, Schenck A, Van bokhoven H, Rooms L (2013) Homozygous and heterozygous disruptions of ANK3: At the crossroads of neurodevelopmental and psychiatric disorders. *Human Molecular Genetics* 22:1960–1970.

Irie M, Hata Y, Takeuchi M, Ichtchenko K, Toyoda A, Hirao K, Takai Y, Rosahl TW, Südhof TC (1997) Binding of neuroligins to PSD-95. *Science* 277:1511–1515.

Isshiki M, Tanaka S, Kuriu T, Tabuchi K, Takumi T, Okabe S (2014) Enhanced synapse remodelling as a common phenotype in mouse models of autism. *Nature Communications* 5.

Jackson A (2016) Cellular and synaptic pathophysiology in a rat model of Fragile X syndrome Ph.D. diss., University of Edinburgh.

Jamain S, Quach H, Betancur C, Råstam M, Colineaux C, Gillberg C, Soderstrom H, Giros B, Leboyer M, Gillberg C, Bourgeron T, Nydén A, Philippe A, Cohen D, Chabane N, Mouren-Siméoni MC, Brice A, Sponheim E, Spurkland I, Skjeldal OH, Coleman M, Pearl PL, Cohen IL, Tsiouris J, Zappella M, Menchetti G, Pompella A, Aschauer H, Van Maldergem L (2003) Mutations of the X-linked genes encoding neuroligins NLGN3 and NLGN4 are associated with autism. *Nature Genetics* 34:27–29.

Jamann N, Jordan M, Engelhardt M (2018) Activity-dependent axonal plasticity in sensory systems.

Jamur MC, Oliver C (2010) Permeabilization of cell membranes. *Methods in molecular biology (Clifton, N.J.)* 588:63–66.

Janssen AF, Tas RP, Van Bergeijk P, Oost R, Hoogenraad CC, Kapitein LC (2017) Myosin-V induces cargo immobilization and clustering at the axon initial segment. *Frontiers in Cellular Neuroscience* 11.

Jaramillo TC, Escamilla CO, Liu S, Peca L, Birnbaum SG, Powell CM (2018) Genetic background effects in Neuroligin-3 mutant mice: Minimal behavioral abnormalities on C57 background. *Autism Research* 11:234–244.

Jaramillo TC, Liu S, Pettersen A, Birnbaum SG, Powell CM (2014) Autism-Related Neuroligin-3 Mutation Alters Social Behavior and Spatial Learning. *Autism Research* 7:264–272.

Jenkins PM, Kim N, Jones SL, Tseng WC, Svitkina TM, Yin HH, Bennett V (2015) Giant ankyrin-G: A critical innovation in vertebrate evolution of fast and integrated neuronal signaling. *Proceedings of the National Academy of Sciences of the United States of America* 112:957–964.

Jenkins SM, Bennett V (2001) Ankyrin-G coordinates assembly of the spectrin-based membrane skeleton, voltage-gated sodium channels, and L1 CAMs at Purkinje neuron initial segments. *Journal of Cell Biology* 155:739–745.

Jentsch TJ (2000) Neuronal KCNQ potassium channels: Physislogy and role in disease. *Nature Reviews Neuroscience* 1:21–30.

Jeyabalan N, Clement JP (2016) SYNGAP1: Mind the Gap. *Frontiers in Cellular Neuroscience* 10.

Jimenez-Gomez A, Niu S, Andujar-Perez F, McQuade EA, Balasa A, Huss D, Coorg R, Quach M, Vinson S, Risen S, Holder JL (2019) Phenotypic characterization of individuals with SYNGAP1 pathogenic variants reveals a potential correlation between posterior dominant rhythm and developmental progression. *Journal of Neurodevelopmental Disorders* 11.

Jonckers E, van Audekerke J, de Visscher G, van der Linden A, Verhoye M (2011) Functional connectivity fMRI of the rodent brain: Comparison of functional connectivity networks in rat and mouse. *PLoS ONE* 6.

Jones SL, Svitkina TM (2016) Axon Initial Segment Cytoskeleton: Architecture, Development, and Role in Neuron Polarity.

JoséGarrido J, Giraud P, Carlier E, Fernandes F, Moussif A, Fache MP, Debanne D, Dargent B (2003) A targeting motif involved in sodium channel clustering at the axonal initial segment. *Science* 300:2091–2094.

Josselyn SA, Tonegawa S (2020) Memory engrams: Recalling the past and imagining the future. *Science* 367.

Jung YH, Shin JE, Lee YI, Jang JH, Jo HJ, Choi SH (2018) Altered amygdala resting-state functional connectivity and hemispheric asymmetry in patients with social anxiety disorder. *Frontiers in Psychiatry* 9.

Jurado S, Benoist M, Lario A, Knafo S, Petrok CN, Esteban JA (2010) PTEN is recruited to the postsynaptic terminal for NMDA receptor-dependent long-term depression. *EMBO Journal* 29:2827–2840.

Kalbassi S, Bachmann SO, Cross E, Roberton VH, Baudouin SJ (2017) Male and female mice lacking neuroligin-3 modify the behavior of their wild-type littermates. *eNeuro* 4.

Kalume F, Yu FH, Westenbroek RE, Scheuer T, Catterall WA (2007) Reduced sodium current in Purkinje neurons from Nav1.1 mutant mice: Implications for ataxia in severe myoclonic epilepsy in infancy. *Journal of Neuroscience* 27:11065–11074.

Kaphzan H, Buffington SA, Jung JI, Rasband MN, Klann E (2011) Alterations in intrinsic membrane properties and the axon initial segment in a mouse model of Angelman syndrome. *Journal of Neuroscience* 31:17637–17648.

Kates WR, Abrams MT, Kaufmann WE, Breiter SN, Reiss AL (1997) Reliability and validity of MRI measurement of the amygdala and hippocampus in children with fragile X syndrome. *Psychiatry Research - Neuroimaging* 75:31–48.

Katsanevaki D (2017) Cortical circuit and behavioural pathophysiology in rodent models of SYNGAP1 haploinsufficiency Ph.D. diss., University of Edinburgh.

Kattenstroth G, Tantalaki E, Südhof TC, Gottmann K, Missler M (2004) Postsynaptic N-methyl-D-aspartate receptor function requires α-neurexins. *Proceedings of the National Academy of Sciences of the United States of America* 101:2607–2612.

Kaufman L, Ayub M, Vincent JB (2010) The genetic basis of non-syndromic intellectual disability: A review. *Journal of Neurodevelopmental Disorders* 2:182–209.

Kawakubo Y, Kuwabara H, Watanabe KI, Minowa M, Someya T, Minowa I, Kono T, Nishida H, Sugiyama T, Kato N, Kasai K (2009) Impaired prefrontal hemodynamic maturationin autism and unaffected siblings. *PLoS ONE* 4:e6881.

Kazdoba TM, Sunnen CN, Crowell B, Lee GH, Anderson AE, D'Arcangelo G (2012) Development and characterization of NEX-Pten, a novel forebrain excitatory neuron-specific knockout mouse. *Developmental Neuroscience* 34:198–209.

Kerns CM, Kendall PC (2012) The Presentation and Classification of Anxiety in Autism Spectrum Disorder. *Clinical Psychology: Science and Practice* 19:323–347.

Kesner RP (2007) A behavioral analysis of dentate gyrus function.

Khosravani H, Altier C, Simms B, Hamming KS, Snutchll TP, Mezeyova J, McRory JE, Zamponi GW (2004) Gating Effects of Mutations in the Cav3.2 T-type Calcium Channel Associated with Childhood Absence Epilepsy. *Journal of Biological Chemistry* 279:9681–9684.

Khosravani H, Bladen C, Parker DB, Snutch TP, McRory JE, Zamponi GW (2005) Effects of Cav3.2 channel mutations linked to idiopathic generalized epilepsy. *Annals of Neurology* 57:745–749.

Kim HG, Kishikawa S, Higgins AW, Seong IS, Donovan DJ, Shen Y, Lally E, Weiss LA, Najm J, Kutsche K, Descartes M, Holt L, Braddock S, Troxell R, Kaplan L, Volkmar F, Klin A, Tsatsanis K, Harris D, Noens I, Pauls D, Daly MJ, Macdonald ME, Morton CC, Quade BJ, Gusella JF (2008) Disruption of neurexin 1 associated with autism spectrum disorder. *The American Journal of Human Genetics* 82:199–207.

Kim H, Gibboni R, Kirkhart C, Bao S (2013) Impaired critical period plasticity in primary auditory cortex of fragile x model mice. *Journal of Neuroscience* 33:15686–15692.

Kim JH, Lee HK, Takamiya K, Huganir RL (2003) The role of synaptic GTPase-activating protein in neuronal development and synaptic plasticity. *Journal of Neuroscience* 23:1119–1124.

Kim JH, Liao D, Lau LF, Huganir RL (1998) SynGAP: A synaptic RasGAP that associates with the PSD-95/SAP90 protein family. *Neuron* 20:683–691.

King MK, Jope RS (2013) Lithium treatment alleviates impaired cognition in a mouse model of fragile X syndrome. *Genes, Brain and Behavior* 12:723–731.

Kirov G, Gumus D, Chen W, Norton N, Georgieva L, Sari M, O'Donovan MC, Erdogan F, Owen MJ, Ropers HH, Ullmann R (2008) Comparative genome hybridization suggests a role for NRXN1 and APBA2 in schizophrenia. *Human Molecular Genetics* 17:458–465.

Kishino T, Lalande M, Wagstaff J (1997) UBE3A/E6-AP mutations cause Angelman syndrome. *Nature Genetics* 15:70–73.

Klavir O, Prigge M, Sarel A, Paz R, Yizhar O (2017) Manipulating fear associations via optogenetic modulation of amygdala inputs to prefrontal cortex. *Nature Neuroscience* 20:836–844.

Klein S, Sharifi-Hannauer P, Martinez-Agosto JA (2013) Macrocephaly as a clinical indicator of genetic subtypes in autism. *Autism Research* 6:51–56.

Klinman E, Tokito M, Holzbaur EL (2017) CDK5-dependent activation of dynein in the axon initial segment regulates polarized cargo transport in neurons. *Traffic* 18:808–824.

Klitten LL, Møller RS, Nikanorova M, Silahtaroglu A, Hjalgrim H, Tommerup N (2011) A balanced translocation disrupts SYNGAP1 in a patient with intellectual disability, speech impairment, and epilepsy with myoclonic absences (EMA). *Epilepsia* 52.

Kloth K, Denecke J, Hempel M, Johannsen J, Strom TM, Kubisch C, Lessel D (2017) First de novo ANK3 nonsense mutation in a boy with intellectual disability, speech impairment and autistic features. *European Journal of Medical Genetics* 60:494–498.

Knuesel I, Elliott A, Chen HJ, Mansuy IM, Kennedy MB (2005) A role for synGAP in regulating neuronal apoptosis. *European Journal of Neuroscience* 21:611–621.

Ko KW, Rasband MN, Meseguer V, Kramer RH, Golding NL (2016) Serotonin modulates spike probability in the axon initial segment through HCN channels. *Nature Neuroscience* 19:823–834.

Kobayashi T, Storrie B, Simons K, Dotti CG (1992) A functional barrier to movement of lipids in polarized neurons. *Nature* 359:647–650.

Kole MHP, Letzkus JJ, Stuart GJ (2007) Axon Initial Segment Kv1 Channels Control Axonal Action Potential Waveform and Synaptic Efficacy. *Neuron* 55:633–647.

Kole MHP, Stuart GJ (2012) Signal Processing in the Axon Initial Segment. *Neuron* 73:235–247.

Komada M, Soriano P (2002) βIV-spectrin regulates sodium channel clustering through ankyrin-G at axon initial segments and nodes of Ranvier. *Journal of Cell Biology* 156:337–348.

Komiyama NH, Watabe AM, Carlisle HJ, Porter K, Charlesworth P, Monti J, Strathdee DJC, O'Carroll CM, Martin SJ, Morris RGM, O'Dell TJ, Grant SGN (2002) SynGAP regulates ERK/MAPK signaling, synaptic plasticity, and learning in the complex with postsynaptic density 95 and NMDA receptor. *The Journal of neuroscience : the official journal of the Society for Neuroscience* 22:9721–9732.

Konstandi M, Johnson E, Lang MA, Malamas M, Marselos M (2000) Noradrenaline, dopamine, serotonin: Different effects of psychological stress on brain biogenic amines in mice and rats. *Pharmacological Research* 41:341–346.

Kopp C, Rudolph U, Löw K, Tobler I (2004) Modulation of rhythmic brain activity by diazepam: GABAA receptor subtype and state specificity. *Proceedings of the National Academy of Sciences of the United States of America* 101:3674–3679.

Kordeli E, Lambert S, Bennett V (1995) Ankyrin(G). A new ankyrin gene with neural-specific isoforms localized at the axonal initial segment and node of Ranvier. *Journal of Biological Chemistry* 270:2352–2359.

Kramer EE, Steadman PE, Epp JR, Frankland PW, Josselyn SA (2018) Assessing Individual Neuronal Activity Across the Intact Brain: Using Hybridization Chain Reaction (HCR) to Detect Arc mRNA Localized to the Nucleus in Volumes of Cleared Brain Tissue. *Current Protocols in Neuroscience* 84:e49.

Krapivinsky G, Medina I, Krapivinsky L, Gapon S, Clapham DE (2004) SynGAP-MUPP1-CaMKII synaptic complexes regulate p38 MAP kinase activity and NMDA receptor- dependent synaptic AMPA receptor potentiation. *Neuron* 43:563–574.

Kratovac S, Corbin JG (2013) Developmental changes in expression of inhibitory neuronal proteins in the Fragile X Syndrome mouse basolateral amygdala. *Brain Research* 1537:69–78.

Krepischi ACV, Rosenberg C, Costa SS, Crolla JA, Huang S, Vianna-Morgante AM (2010) A novel de novo microdeletion spanning the SYNGAP1 gene on the short arm of chromosome 6 associated with mental retardation.

Krettek JE, Price JL (1977) The cortical projections of the mediodorsal nucleus and adjacent thalamic nuclei in the rat. *Journal of Comparative Neurology* 171:157–191.

Kriebel M, Metzger J, Trinks S, Chugh D, Harvey RJ, Harvey K, Volkmer H (2011) The cell adhesion molecule neurofascin stabilizes axo-axonic GABAergic terminals at the axon initial segment. *Journal of Biological Chemistry* 286:24385–24393.

Krueger DD, Osterweil EK, Chen SP, Tye LD, Bear MF (2011) Cognitive dysfunction and prefrontal synaptic abnormalities in a mouse model of fragile X syndrome. *Proceedings of the National Academy of Sciences of the United States of America* 108:2587–2592.

Krumm N, O'Roak BJ, Shendure J, Eichler EE (2014) A de novo convergence of autism genetics and molecular neuroscience.

Kuba H (2012) Structural tuning and plasticity of the axon initial segment in auditory neurons. *Journal of Physiology* 590:5571–5579.

Kuba H, Adachi R, Ohmori H (2014) Activity-dependent and activity-independent development of the axon initial segment. *Journal of Neuroscience* 34:3443–3453.

Kuba H, Ishii TM, Ohmori H (2006) Axonal site of spike initiation enhances auditory coincidence detection. *Nature* 444:1069–1072.

Kuba H, Ohmori H (2009) Roles of axonal sodium channels in precise auditory time coding at nucleus magnocellularis of the chick. *Journal of Physiology* 587:87–100.

Kuba H, Oichi Y, Ohmori H (2010) Presynaptic activity regulates Na+ channel distribution at the axon initial segment. *Nature* 465:1075–1078.

Kuba H, Yamada R, Ishiguro G, Adachi R (2015) Redistribution of Kv1 and Kv7 enhances neuronal excitability during structural axon initial segment plasticity. *Nature Communications* 6.

Kuijpers M, van de Willige D, Freal A, Chazeau A, Franker MA, Hofenk J, Rodrigues RJ, Kapitein LC, Akhmanova A, Jaarsma D, Hoogenraad CC (2016) Dynein Regulator NDEL1 Controls Polarized Cargo Transport at the Axon Initial Segment. *Neuron* 89:461–471.

Kummer KK, Hofhansel L, Barwitz CM, Schardl A, Prast JM, Salti A, El Rawas R, Zernig G (2014) Differences in social interaction- vs. cocaine reward in mouse vs. rat. *Frontiers in Behavioral Neuroscience* 8:1–7.

Kwon CH, Luikart BW, Powell CM, Zhou J, Matheny SA, Zhang W, Li Y, Baker SJ, Parada LF (2006) Pten Regulates Neuronal Arborization and Social Interaction in Mice. *Neuron* 50:377–388.

Kwon CH, Zhu X, Zhang J, Knoop LL, Tharp R, Smeyne RJ, Eberhart CG, Burger PC, Baker SJ (2001) Pten regulates neuronal soma size: A mouse model of Lhermitte-Duclos disease. *Nature Genetics* 29:404–411.

Laarakker MC, Reinders NR, Bruining H, Ophoff RA, Kas MJ (2012) Sex-dependent novelty response in neurexin-1α mutant mice. *PLoS ONE* 7.

Lambert S, Bennett V (1993) From anemia to cerebellar dysfunction: A review of the ankyrin gene family. *European Journal of Biochemistry* 211:1–6.

Langille JJ, Brown RE (2018) The synaptic theory of memory: A historical survey and reconciliation of recent opposition. *Frontiers in Systems Neuroscience* 12.

Langston RF, Ainge JA, Couey JJ, Canto CB, Bjerknes TL, Witter MP, Moser EI, Moser MB (2010) Development of the spatial representation system in the rat. *Science* 328:1576–1580.

Larm JA, Shen PJ, Gundlach AL (2003) Differential galanin receptor-1 and galanin expression by 5-HT neurons in dorsal raphé nucleus of rat and mouse: Evidence for species-dependent modulation of serotonin transmission. *European Journal of Neuroscience* 17:481–493.

LaSalle JM, Reiter LT, Chamberlain SJ (2015) Epigenetic regulation of UBE3A and roles in human neurodevelopmental disorders.

Laumonnier F, Bonnet-Brilhault F, Gomot M, Blanc R, David A, Moizard MP, Raynaud M, Ronce N, Lemonnier E, Calvas P, Laudier B, Chelly J, Fryns JP, Ropers HH, Hamel BC, Andres C, Barthélémy C, Moraine C, Briault S (2004) X-Linked Mental Retardation and Autism Are Associated with a Mutation in the NLGN4 Gene, a Member of the Neuroligin Family. *American Journal of Human Genetics* 74:552–557.

Lautz JD, Gniffke EP, Brown EA, Immendorf KB, Mendel RD, Smith SE (2019) Activity-dependent changes in synaptic protein complex composition are consistent in different detergents despite differential solubility. *Scientific Reports* 9.

Laviolette SR, Lipski WJ, Grace AA (2005) A subpopulation of neurons in the medial prefrontal cortex encodes emotional learning with burst and frequency codes through a dopamine D 4 receptor-dependent basolateral amygdala input. *Journal of Neuroscience* 25:6066–6075.

Lawrence YA, Kemper TL, Bauman ML, Blatt GJ (2010) Parvalbumin-, calbindin-, and calretinin-immunoreactive hippocampal interneuron density in autism. *Acta Neurologica Scandinavica* 121:99–108.

Le Bras B, Fréal A, Czarnecki A, Legendre P, Bullier E, Komada M, Brophy PJ, Davenne M, Couraud F (2014) In vivo assembly of the axon initial segment in motor neurons. *Brain Structure and Function* 219:1433–1450.

LeDoux JE, Cicchetti P, Xagoraris A, Romanski LM (1990) The lateral amygdaloid nucleus: Sensory interface of the amygdala in fear conditioning. *Journal of Neuroscience* 10:1062–1069.

Lee E, Lee J, Kim E (2017) Excitation/Inhibition Imbalance in Animal Models of Autism Spectrum Disorders.

Lee YS, Ehninger D, Zhou M, Oh JY, Kang M, Kwak C, Ryu HH, Butz D, Araki T, Cai Y, Balaji J, Sano Y, I Nam C, Kim HK, Kaang BK, Burger C, Neel BG, Silva AJ (2014) Mechanism and treatment for learning and memory deficits in mouse models of Noonan syndrome. *Nature Neuroscience* 17:1736–1743.

Lee Y, Kim H, Han PL (2018) Striatal Inhibition of MeCP2 or TSC1 Produces Sociability Deficits and Repetitive Behaviors. *Experimental Neurobiology* 27:539.

Leitner Y (2014) The co-occurrence of autism and attention deficit hyperactivity disorder in children - What do we know? *Frontiers in Human Neuroscience* 8.

León-Espinosa G, Antón-Fernández A, Tapia-González S, DeFelipe J, Muñoz A (2018) Modifications of the axon initial segment during the hibernation of the Syrian hamster. *Brain Structure and Function* 223:4307–4321.

Leterrier C (2018) The axon initial segment: An updated viewpoint. *Journal of Neuroscience* 38:2135–2145.

Leterrier C, Dargent B (2014) No Pasaran! Role of the axon initial segment in the regulation of protein transport and the maintenance of axonal identity.

Leterrier C, Potier J, Caillol G, Debarnot C, Rueda Boroni F, Dargent B (2015) Nanoscale Architecture of the Axon Initial Segment Reveals an Organized and Robust Scaffold. *Cell Reports* 13:2781–2793.

Leterrier C, Vacher H, Fache MP, D'Ortoli SA, Castets F, Autillo-Touat A, Dargent B (2011) End-binding proteins EB3 and EB1 link microtubules to ankyrin G in the axon initial segment. *Proceedings of the National Academy of Sciences of the United States of America* 108:8826–8831.

Leussis MP, Madison JM, Petryshen TL (2012) Ankyrin 3: genetic association with bipolar disorder and relevance to disease pathophysiology. *Biology of Mood & Anxiety Disorders* 2:18.

Levinson DF, Duan J, Oh S, Wang K, Sanders AR, Shi J, Zhang N, Mowry BJ, Olincy A, Amin F, Cloninger CR, Silverman JM, Buccola NG, Byerley WF, Black DW, Kendler KS, Freedman R, Dudbridge F, Pe'er I, Hakonarson H, Bergen SE, Fanous AH, Holmans PA, Gejman PV (2011) Copy number variants in schizophrenia: Confirmation of five previous finding sand new evidence for 3q29 microdeletions and VIPR2 duplications. *American Journal of Psychiatry* 168:302–316.

Levinsoni JN, Chéry N, Huang K, Wong TP, Gerrow K, Kang R, Prange O, Wang YT, El-Husseini A (2005) Neuroligins mediate excitatory and inhibitory synapse formation: Involvement of PSD-95 and neueexin-1β in neuroligin-induced synaptic specificity. *Journal of Biological Chemistry* 280:17312–17319.

Levy D, Ronemus M, Yamrom B, ha Lee Y, Leotta A, Kendall J, Marks S, Lakshmi B, Pai D, Ye K, Buja A, Krieger A, Yoon S, Troge J, Rodgers L, Iossifov I, Wigler M (2011) Rare De Novo and Transmitted Copy-Number Variation in Autistic Spectrum Disorders. *Neuron* 70:886–897.

Lewis DA, Hashimoto T, Volk DW (2005) Cortical inhibitory neurons and schizophrenia.

Lewis P, Abbeduto L, Murphy M, Richmond E, Giles N, Bruno L, Schroeder S (2006) Cognitive, language and social-cognitive skills of individuals with fragile X syndrome with and without autism. *Journal of Intellectual Disability Research* 50:532–545.

Lewis TL, Mao T, Svoboda K, Arnold DB (2009) Myosin-dependent targeting of transmembrane proteins to neuronal dendrites. *Nature Neuroscience* 12:568–576.

Li J, Yen C, Liaw D, Podsypanina K, Bose S, Wang SI, Puc J, Miliaresis C, Rodgers L, McCombie R, Bigner SH, Giovanella BC, Ittmann M, Tycko B, Hibshoosh H, Wigler MH, Parsons R (1997) PTEN, a putative protein tyrosine phosphatase gene mutated in human brain, breast, and prostate cancer. *Science* 275:1943–1947.

Li W, Okano A, Tian QB, Nakayama K, Furihata T, Nawa H, Suzuki T (2001) Characterization of a Novel synGAP Isoform, synGAP-β. *Journal of Biological Chemistry* 276:21417–21424.

Li Z, Chen J, Xu Y, Yi Q, Ji W, Wang P, Shen J, Song Z, Wang M, Yang P, Wang Q, Feng G, Liu B, Sun W, Xu Q, Li B, He L, He G, Li W, Wen Z, Liu K, Huang F, Zhou J, Ji J, Li X, Shi Y (2016) Genome-wide Analysis of the Role of Copy Number Variation in Schizophrenia Risk in Chinese. *Biological Psychiatry* 80:331–337.

Liang J, Xu W, Hsu YT, Yee A, Chen L, Südhof T (2015) Conditional knockout of Nlgn2 in the adult medial prefrontal cortex (mPFC) induces delayed loss of inhibitory synapses.

Lim CS, Hoang ET, Viar KE, Stornetta RL, Scott MM, Zhu JJ (2014) Pharmacological rescue of Ras signaling, GluA1-dependent synaptic plasticity, and learning deficits in a fragile X model. *Genes and Development* 28:273–289.

Lipp HP, Wolfer DP (1998) Genetically modified mice and cognition. *Current Opinion in Neurobiology* 8:272–280.

Lister RG (1987) The use of a plus-maze to measure anxiety in the mouse. *Psychopharmacology* 92:180–185.

Liu JJ, Grace KP, Horner RL, Cortez MA, Shao Y, Jia Z (2017) Neuroligin 3 R451C mutation alters electroencephalography spectral activity in an animal model of autism spectrum disorders. *Molecular Brain* 10.

Liu Y, Du Y, Liu W, Yang C, Liu Y, Wang H, Gong X (2013) Lack of Association between NLGN3, NLGN4, SHANK2 and SHANK3 Gene Variants and Autism Spectrum Disorder in a Chinese Population. *PLoS ONE* 8.

Lorincz A, Nusser Z (2008) Cell-type-dependent molecular composition of the axon initial segment. *Journal of Neuroscience* 28:14329–14340.

Louros SR, Osterweil EK (2016) Perturbed proteostasis in autism spectrum disorders.

Lowther C, Speevak M, Armour CM, Goh ES, Graham GE, Li C, Zeesman S, Nowaczyk MJ, Schultz LA, Morra A, Nicolson R, Bikangaga P, Samdup D, Zaazou M, Boyd K, Jung JH, Siu V, Rajguru M, Goobie S, Tarnopolsky MA, Prasad C, Dick PT, Hussain AS, Walinga M, Reijenga RG, Gazzellone M, Lionel AC, Marshall CR, Scherer SW, Stavropoulos DJ, Mccready E, Bassett AS (2017) Molecular characterization of NRXN1 deletions from 19,263 clinical microarray cases identifies exons important for neurodevelopmental disease expression. *Genetics in Medicine* 19:53–61.

Lugo JN, Smith GD, Arbuckle EP, White J, Holley AJ, Floruta CM, Ahmed N, Gomez MC, Okonkwo O (2014) Deletion of PTEN produces autism-like behavioral deficits and alterations in synaptic proteins. *Frontiers in Molecular Neuroscience* 7.

Maehama T, Dixon JE (1998) The tumor suppressor, PTEN/MMAC1, dephosphorylates the lipid second messenger, phosphatidylinositol 3,4,5-trisphosphate. *Journal of Biological Chemistry* 273:13375–13378.

Manabe T, Aiba A, Yamada A, Ichise T, Sakagami H, Kondo H, Katsuki M (2000) Regulation of long-term potentiation by H-Ras through NMDA receptor phosphorylation. *Journal of Neuroscience* 20:2504–2511.

Mao W, Watanabe T, Cho S, Frost JL, Truong T, Zhao X, Futai K (2015) Shank1 regulates excitatory synaptic transmission in mouse hippocampal parvalbumin-expressing inhibitory interneurons. *European Journal of Neuroscience* 41:1025–1035.

Marchand AR, Luck D, DiScala G (2003) Evaluation of an improved automated analysis of freezing behaviour in rats and its use in trace fear conditioning. *Journal of Neuroscience Methods* 126:145–153.

Marchese M, Conti V, Valvo G, Moro F, Muratori F, Tancredi R, Santorelli FM, Guerrini R, Sicca F (2014) Autism-epilepsy phenotype with macrocephaly suggests PTEN, but not GLIALCAM, genetic screening. *BMC Medical Genetics* 15.

Marco EJ, Hinkley LB, Hill SS, Nagarajan SS (2011) Sensory processing in autism: A review of neurophysiologic findings. *Pediatric Research* 69:48–54.

Maren S, De Oca B, Fanselow MS (1994) Sex differences in hippocampal long-term potentiation (LTP) and Pavlovian fear conditioning in rats: positive correlation between LTP and contextual learning. *Brain Research* 661:25–34.

Marik SA, Yamahachi H, McManus JN, Szabo G, Gilbert CD (2010) Axonal dynamics of excitatory and inhibitory neurons in somatosensory cortex. *PLoS Biology* 8:e1000395.

Markram K, Rinaldi T, Mendola DL, Sandi C, Markram H (2008) Abnormal fear conditioning and amygdala processing in an animal model of autism. *Neuropsychopharmacology* 33:901–912.

Marsh DJ, Zheng Z, Zedenius J, Kremer H, Padberg GW, Larsson C, Longy M, Eng C (1997a) Differential loss of heterozygosity in the region of the Cowden locus within 10q22-23 in follicular thyroid adenomas and carcinomas. *Cancer Research* 57:500–503.

Marsh DJ, Zheng Z, Zedenius J, Kremer H, Padberg GW, Larsson C, Longy M, Eng C (1997b) Germline mutations of the PTEN gene in Cowden disease, an inherited breast and thyroid cancer syndrome. *Cancer Research* 57:500–503.

Marshall CR, Noor A, Vincent JB, Lionel AC, Feuk L, Skaug J, Shago M, Moessner R, Pinto D, Ren Y, Thiruvahindrapduram B, Fiebig A, Schreiber S, Friedman J, Ketelaars CE, Vos YJ, Ficicioglu C, Kirkpatrick S, Nicolson R, Sloman L, Summers A, Gibbons CA, Teebi A, Chitayat D, Weksberg R, Thompson A, Vardy C, Crosbie V, Luscombe S, Baatjes R, Zwaigenbaum L, Roberts W, Fernandez B, Szatmari P, Scherer SW (2008) Structural Variation of Chromosomes in Autism Spectrum Disorder. *American Journal of Human Genetics* 82:477–488.

Martella G, Meringolo M, Trobiani L, De Jaco A, Pisani A, Bonsi P (2018) The neurobiological bases of autism spectrum disorders: the R451C-neuroligin 3 mutation hampers the expression of long-term synaptic depression in the dorsal striatum. *European Journal of Neuroscience* 47:701–708.

Martin BS, Corbin JG, Huntsman MM (2014) Deficient tonic GABAergic conductance and synaptic balance in the fragile X syndrome amygdala. *Journal of Neurophysiology* 112:890–902.

Martin JP, Bell J (1943) A PEDIGREE OF MENTAL DEFECT SHOWING SEX-LINKAGE. *Journal of Neurology, Neurosurgery & Psychiatry* 6:154–157.

Martin MS, Tang B, Papale LA, Yu FH, Catterall WA, Escayg A (2007) The voltage-gated sodium channel Scn8a is a genetic modifier of severe myoclonic epilepsy of infancy. *Human Molecular Genetics* 16:2892–2899.

Martinello K, Huang Z, Lujan R, Tran B, Watanabe M, Cooper EC, Brown DA, Shah MM (2015) Cholinergic afferent stimulation induces axonal function plasticity in adult hippocampal granule cells. *Neuron* 85:346–363.

Mathey EK, Derfuss T, Storch MK, Williams KR, Hales K, Woolley DR, Al-Hayani A, Davies SN, Rasband MN, Olsson T, Moldenhauer A, Velhin S, Hohlfeld R, Meinl E, Linington C (2007) Neurofascin as a novel target for autoantibody-mediated axonal injury. *Journal of Experimental Medicine* 204:2363–2372.

Mayford M, Mansuy IM, Muller RU, Kandel ER (1997) Memory and behavior: A second generation of genetically modified mice.

McBride KL, Varga EA, Pastore MT, Prior TW, Manickam K, Atkin JF, Herman GE (2010) Confirmation study of PTEN mutations among individuals with autism or developmental delays/mental retardation and macrocephaly. *Autism Research* 3:137–141.

McCormick DA, Bal T (1997) SLEEP AND AROUSAL: Thalamocortical Mechanisms. *Annual Review of Neuroscience* 20:185–215.

Mcdonald AJ, Mascagni F, Guo L (1996) Projections of the medial and lateral prefrontal cortices to the amygdala: A Phaseolus vulgaris leucoagglutinin study in the rat. *Neuroscience* 71:55–75.

McGarry LM, Carter AG (2017) Prefrontal Cortex Drives Distinct Projection Neurons in the Basolateral Amygdala. *Cell Reports* 21:1426–1433.

McKinney WT, Bunney WE (1969) Animal Model of Depression: I. Review of Evidence: Implications for Research. *Archives of General Psychiatry* 21:240–248.

McLaren J, Bryson SE (1987) Review of recent epidemiological studies of mental retardation: Prevalence, associated disorders, and etiology.

McMahon AC, Barnett MW, O'Leary TS, Stoney PN, Collins MO, Papadia S, Choudhary JS, Komiyama NH, Grant SGN, Hardingham GE, Wyllie DJA, Kind PC (2012) SynGAP isoforms exert opposing effects on synaptic strength. *Nat Commun* 3:900.

McNaughton CH, Moon J, Strawderman MS, Maclean KN, Evans J, Strupp BJ (2008) Evidence for Social Anxiety and Impaired Social Cognition in a Mouse Model of Fragile X Syndrome. *Behavioral Neuroscience* 122:293–300.

Melé M, Ferreira PG, Reverter F, DeLuca DS, Monlong J, Sammeth M, Young TR, Goldmann JM, Pervouchine DD, Sullivan TJ, Johnson R, Segrè AV, Djebali S, Niarchou A, Wright FA, Lappalainen T, Calvo M, Getz G, Dermitzakis ET, Ardlie KG, Guigó R (2015) The human transcriptome across tissues and individuals. *Science* 348:660–665.

Meredith RM, Holmgren CD, Weidum M, Burnashev N, Mansvelder HD (2007) Increased Threshold for Spike-Timing-Dependent Plasticity Is Caused by Unreliable Calcium Signaling in Mice Lacking Fragile X Gene Fmr1. *Neuron* 54:627–638.

Mester JL, Tilot AK, Rybicki LA, Frazier TW, Eng C (2011) Analysis of prevalence and degree of macrocephaly in patients with germline PTEN mutations and of brain weight in Pten knock-in murine model. *European Journal of Human Genetics* 19:763–768.

Miceli F, Soldovieri MV, Lugli L, Bellini G, Ambrosino P, Migliore M, del Giudice EM, Ferrari F, Pascotto A, Taglialatela M (2009) Neutralization of a unique, negatively-charged residue in the voltage sensor of KV7.2 subunits in a sporadic case of benign familial neonatal seizures. *Neurobiology of Disease* 34:501–510.

Michaelson SD, Ozkan ED, Aceti M, Maity S, Llamosas N, Weldon M, Mizrachi E, Vaissiere T, Gaffield MA, Christie JM, Holder JL, Miller CA, Rumbaugh G (2018) SYNGAP1 heterozygosity disrupts sensory processing by reducing touch-related activity within somatosensory cortex circuits. *Nature Neuroscience* 21.

Mignot C, von Stülpnage C, Nava C, Ville D, Sanlaville D, Lesca G, Rastetter A, Gachet B, Marie Y, Korenke GC, Borggraefe I, Hoffmann-Zacharska D, Szczepanik E, Rudzka-Dybala M, Yiş U, Çağlayan H, Isapof A, Marey I, Panagiotakaki E, Korff C, Rossier E, Riess A, Beck-Woedl S, Rauch A, Zweier C, Hoyer J, Reis A, Mironov M, Bobylova M, Mukhin K, Hernandez-Hernandez L, Maher B, Sisodiya S, Kuhn M, Glaeser D, Wechuysen S, Myers CT, Mefford HC, Hörtnagel K, Biskup S, Lemke JR, Héron D, Kluger G, Depienne C, Craiu D, De Jonghe P, Helbig I, Guerrini R, Lehesjoki AE, Marini C, Muhle H, Møller RS, Neubauer B, Pal D, Selmer K, Stephani U, Sterbova K, Striano P, Talvik T, von Spiczak S (2016) Genetic and neurodevelopmental spectrum of SYNGAP1-associated intellectual disability and epilepsy. *Journal of Medical Genetics* 53:511–522.

Miller EK (2000) The prefontral cortex and cognitive control. *Nature Reviews Neuroscience* 1:59–65.

Misane I, Razani H, Wang FH, Jansson A, Fuxe K, Ogren SO (1998) Intraventricular galanin modulates a 5-HT(1A) receptor-mediated behavioural response in the rat. *European Journal of Neuroscience* 10:1230–1240.

Missler M, Südhof TC (1998) Neurexins: Three genes and 1001 products. *Trends in Genetics* 14:20–26.

Missler M, Zhang W, Rohlmann A, Kattenstroth G, Hammer RE, Gottmann K, Südhof TC (2003) α-neurexins couple Ca 2+ channels to synaptic vesicle exocytosis. *Nature* 423:939–948.

Mitra K, Carvunis AR, Ramesh SK, Ideker T (2013) Integrative approaches for finding modular structure in biological networks.

Mizen LAM (2017) Characteristics of Cellular and Synaptic Function in Rodent Forebrain Neurons with Altered SynGAP Expression Ph.D. diss., The University of Edinburgh.

Moon IS, Sakagami H, Nakayama J, Suzuki T (2008) Differential distribution of synGAPα1 and synGAPβ isoforms in rat neurons. *Brain Research* 1241:62–75.

Morales B, Choi SY, Kirkwood A (2002) Dark rearing alters the development of GABAergic transmission in visual cortex. *Journal of Neuroscience* 22:8084–8090.

Morgan JT, Barger N, Amaral DG, Schumann CM (2014) Stereological study of amygdala glial populations in adolescents and adults with autism spectrum disorder. *PLoS ONE* 9.

Moseley RL, Ypma RJ, Holt RJ, Floris D, Chura LR, Spencer MD, Baron-Cohen S, Suckling J, Bullmore E, Rubinov M (2015) Whole-brain functional hypoconnectivity as an endophenotype of autism in adolescents. *NeuroImage: Clinical* 9:140–152.

Muhia M, Feldon J, Knuesel I, Yee BK (2009) Appetitively Motivated Instrumental Learning in SynGAP Heterozygous Knockout Mice. *Behavioral Neuroscience* 123:1114–1128.

Muhia M, Willadt S, Yee BK, Feldon J, Paterna JC, Schwendener S, Vogt K, Kennedy MB, Knuesel I (2012) Molecular and behavioral changes associated with adult hippocampus-specific SynGAP1 knockout. *Learning and Memory* 19:268–281.

Muhia M, Yee BK, Feldon J, Markopoulos F, Knuesel I (2010) Disruption of hippocampus-regulated behavioural and cognitive processes by heterozygous constitutive deletion of SynGAP. *European Journal of Neuroscience* 31:529–543.

Murdoch JD, Gupta AR, Sanders SJ, Walker MF, Keaney J, Fernandez TV, Murtha MT, Anyanwu S, Ober GT, Raubeson MJ, DiLullo NM, Villa N, Waqar Z, Sullivan C, Gonzalez L, Willsey AJ, Choe SY, Neale BM, Daly MJ, State MW (2015) No Evidence for Association of Autism with Rare Heterozygous Point Mutations in Contactin-Associated Protein-Like 2 (CNTNAP2), or in Other Contactin-Associated Proteins or Contactins. *PLoS Genetics* 11:1–15.

Myers MP, Pass I, Batty IH, Van Der Kaay J, Stolarov JP, Hemmings BA, Wigler MH, Downes CP, Tonks NK (1998) The lipid phosphatase activity of PTEN is critical for its tumor supressor function. *Proceedings of the National Academy of Sciences of the United States of America* 95:13513–13518.

Nabavi S, Fox R, Proulx CD, Lin JY, Tsien RY, Malinow R (2014) Engineering a memory with LTD and LTP. *Nature* 511:348–352.

Nadler JJ, Moy SS, Dold G, Trang D, Simmons N, Perez A, Young NB, Barbaro RP, Piven J, Magnuson TR, Crawley JN (2004) Automated apparatus for quantitation of social approach behaviors in mice. *Genes, Brain and Behavior* 3:303–314.

Nakabayashi K, Scherer SW (2001) The human contactin-associated protein-like 2 gene (CNTNAP2) spans over 2 Mb of DNA at chromosome 7q35. *Genomics* 73:108–112.

Nakada C, Ritchie K, Oba Y, Nakamura M, Hotta Y, Iino R, Kasai RS, Yamaguchi K, Fujiwara T, Kusumi A (2003) Accumulation of anchored proteins forms membrane diffusion barriers during neuronal polarization. *Nature Cell Biology* 5:626–632.

Nakata T, Hirokawa N (2003) Microtubules provide directional cues for polarized axonal transport through interaction with kinesin motor head. *Journal of Cell Biology* 162:1045–1055.

Naumann A, Hochstein N, Weber S, Fanning E, Doerfler W (2009) A Distinct DNA-Methylation Boundary in the 5′- Upstream Sequence of the FMR1 Promoter Binds Nuclear Proteins and Is Lost in Fragile X Syndrome. *American Journal of Human Genetics* 85:606–616.

Need AC, Ge D, Weale ME, Maia J, Feng S, Heinzen EL, Shianna KV, Yoon W, Kasperavičiute D, Gennarelli M, Strittmatter WJ, Bonvicini C, Rossi G, Jayathilake K, Cola PA, McEvoy

JP, Keefe RS, Fisher EM, St. Jean PL, Giegling I, Hartmann AM, Möller HJ, Ruppert A, Fraser G, Crombie C, Middleton LT, St. Clair D, Roses AD, Muglia P, Francks C, Rujescu D, Meltzer HY, Goldstein DB (2009) A genome-wide investigation of SNPs and CNVs in schizophrenia. *PLoS Genetics* 5.

Nelen MR, Padberg GW, Peeters EA, Lin AY, Van Den Helm B, Frants RR, Coulon V, Goldstein AM, Van Reen MM, Easton DF, Eeles RA, Hodgson S, Mulvihill JJ, Murday VA, Tucker MA, Mariman EC, Starink TM, Ponder BA, Ropers HH, Kremer H, Longy M, Eng C (1996) Localization of the gene for Cowden disease to chromosome 10q22-23. *Nature Genetics* 13:114–116.

Nelson AD, Jenkins PM (2017) Axonal membranes and their domains: Assembly and function of the axon initial segment and node of Ranvier.

Nelson SB, Valakh V (2015) Excitatory/Inhibitory Balance and Circuit Homeostasis in Autism Spectrum Disorders.

Nguyen T, Südhof TC (1997) Binding properties of neuroligin 1 and neurexin 1β reveal function as heterophilic cell adhesion molecules. *Journal of Biological Chemistry* 272:26032–26039.

Nirschl JJ, Ghiretti AE, Holzbaur EL (2017) The impact of cytoskeletal organization on the local regulation of neuronal transport.

Nowak LG, Bullier J (1997) The Timing of Information Transfer in the Visual System In *Extrastriate Cortex in Primates*, pp. 205–241. Springer, Boston, MA.

Nozari M, Suzuki T, Rosa MG, Yamakawa K, Atapour N (2017) The impact of early environmental interventions on structural plasticity of the axon initial segment in neocortex. *Developmental Psychobiology* 59:39–47.

O ' Roak BJ, Vives L, Girirajan S, Karakoc E, Krumm N, Coe BP, Levy R, Ko A, Lee C, Smith JD, Turner EH, Stanaway IB, Vernot B, Malig M, Baker C, Akey JM, Borenstein E, Rieder MJ, Nickerson DA, Bernier R, Shendure J, Eichler EE (2012) Sporadic autism exomes reveal a highly interconnected protein network of de novo mutations. *Nature* 485:246–250.

Oberlander JG, Woolley CS (2016) 17β-estradiol acutely potentiates glutamatergic synaptic transmission in the hippocampus through distinct mechanisms in males and females. *Journal of Neuroscience* 36:2677–2690.

Oberlé I, Rousseau F, Heitz D, Kretz C, Devys D, Hanauer A, Boué J, Bertheas MF, Mandel JL (1991) Instability of a 550-base pair DNA segment and abnormal methylation in fragile X syndrome. *Science* 252:1097–1102.

Ogawa S, Kwon CH, Zhou J, Koovakkattu D, Parada LF, Sinton CM (2007) A seizure-prone phenotype is associated with altered free-running rhythm in Pten mutant mice. *Brain Research* 1168:112–123.

Ogawa Y, Horresh I, Trimmer JS, Bredt DS, Peles E, Rasband MN (2008) Postsynaptic density-93 clusters Kv1 channels at axon initial segments independently of Caspr2. *Journal of Neuroscience* 28:5731–5739.

Ogiwara I, Ito K, Sawaishi Y, Osaka H, Mazaki E, Inoue I, Montal M, Hashikawa T, Shike T, Fujiwara T, Inoue Y, Kaneda M, Yamakawa K (2009) De novo mutations of voltage-gated sodium channel αiI gene SCN2A in intractable epilepsies. *Neurology* 73:1046–1053.

Ogiwara I, Miyamoto H, Morita N, Atapour N, Mazaki E, Inoue I, Takeuchi T, Itohara S, Yanagawa Y, Obata K, Furuichi T, Hensch TK, Yamakawa K (2007) Nav1.1 localizes to axons of parvalbumin-positive inhibitory interneurons: A circuit basis for epileptic seizures in mice carrying an Scn1a gene mutation. *Journal of Neuroscience* 27:5903–5914.

Oh JS, Manzerra P, Kennedy MB (2004) Regulation of the Neuron-specific Ras GTPase-activating Protein, synGAP, by Ca 2+ /Calmodulin-dependent Protein Kinase II. *Journal of Biological Chemistry* 279:17980–17988.

Olmos-Serrano JL, Corbin JG, Burns MP (2011) The GABA A receptor agonist THIP ameliorates specific behavioral deficits in the mouse model of fragile X syndrome.

Olmos-Serrano JL, Paluszkiewicz SM, Martin BS, Kaufmann WE, Corbin JG, Huntsman MM (2010) Defective GABAergic neurotransmission and pharmacological rescue of neuronal hyperexcitability in the amygdala in a mouse model of fragile X syndrome. *Journal of Neuroscience* 30:9929–9938.

Onay H, Kacamak D, Kavasoglu AN, Akgun B, Yalcinli M, Kose S, Ozbaran B (2016) Mutation analysis of the NRXN1 gene in autism spectrum disorders. *Balkan Journal of Medical Genetics* 19:17–22.

Opazo P, Choquet D (2011) A three-step model for the synaptic recruitment of AMPA receptors.

O'Roak BJ, Stessman HA, Boyle EA, Witherspoon KT, Martin B, Lee C, Vives L, Baker C, Hiatt JB, Nickerson DA, Bernier R, Shendure J, Eichler EE (2014) Recurrent de novo mutations implicate novel genes underlying simplex autism risk. *Nature Communications* 5.

O'Roak BJ, Vives L, Fu W, Egertson JD, Stanaway IB, Phelps IG, Carvill G, Kumar A, Lee C, Ankenman K, Munson J, Hiatt JB, Turner EH, Levy R, O'Day DR, Krumm N, Coe BP, Martin BK, Borenstein E, Nickerson DA, Mefford HC, Doherty D, Akey JM, Bernier R, Eichler EE, Shendure J (2012) Multiplex targeted sequencing identifies recurrently mutated genes in autism spectrum disorders. *Science* 338:1619–1622.

O'Rourke DJ, Twomey E, Lynch SA, King MD (2012) Cortical dysplasia associated with the PTEN mutation in Bannayan-Riley-Ruvalcaba syndrome: A rare finding. *Clinical Dysmorphology* 21:91–92.

Orrico A, Galli L, Buoni S, Orsi A, Vonella G, Sorrentino V (2009) Novel PTEN mutations in neurodevelopmental disorders and macrocephaly. *Clinical Genetics* 75:195–198.

Osterweil EK, Krueger DD, Reinhold K, Bear MF (2010) Hypersensitivity to mGluR5 and ERK1/2 leads to excessive protein synthesis in the hippocampus of a mouse model of fragile X syndrome. *The Journal of neuroscience : the official journal of the Society for Neuroscience* 30:15616–27.

Ostlund SB, Balleine BW (2005) Lesions of medial prefrontal cortex disrupt the acquisition but not the expression of goal-directed learning. *The Journal of neuroscience : the official journal of the Society for Neuroscience* 25:7763–70.

Ozkan ED, Creson TK, Kramár EA, Rojas C, Seese RR, Babyan AH, Shi Y, Lucero R, Xu X, Noebels JL, Miller CA, Lynch G, Rumbaugh G (2014) Reduced cognition in Syngap1 mutants is caused by isolated damage within developing forebrain excitatory neurons. *Neuron* 82:1317–1333.

Page DT, Kuti OJ, Prestia C, Sur M (2009) Haploinsufficiency for Pten and Serotonin transporter cooperatively influences brain size and social behavior. *Proceedings of the National Academy of Sciences of the United States of America* 106:1989–1994.

Palay SL, Sotelo C, Peters A, Orkand PM (1968) The axon hillock and the initial segment. *The Journal of cell biology* 38:193–201.

Palsson EM, Popoff M, Thelestam M, O'Neill LAJ (2000) Divergent roles for Ras and Rap in the activation of p38 mitogen- activated protein kinase by interleukin-1. *Journal of Biological Chemistry* 275:7818–7825.

Pan Z, Kao T, Horvath Z, Lemos J, Sul JY, Cranstoun SD, Bennett V, Scherer SS, Cooper EC (2006) A common ankyrin-G-based mechanism retains KCNQ and Na V channels at electrically active domains of the axon. *Journal of Neuroscience* 26:2599–2613.

Panksepp J (1981) The ontogeny of play in rats. *Developmental Psychobiology* 14:327–332.

Paradee W, Melikian HE, Rasmussen DL, Kenneson A, Conn PJ, Warren ST (1999) Fragile X mouse: Strain effects of knockout phenotype and evidence suggesting deficient amygdala function. *Neuroscience* 94:185–192.

Paré D, Gaudreau H (1996) Projection cells and interneurons of the lateral and basolateral amygdala: Distinct firing patterns and differential relation to theta and delta rhythms in conscious cats. *Journal of Neuroscience* 16:3334–3350.

Parikshak NN, Luo R, Zhang A, Won H, Lowe JK, Chandran V, Horvath S, Geschwind DH (2013) Integrative functional genomic analyses implicate specific molecular pathways and circuits in autism. *Cell* 155:1008.

Parker CC, Chen H, Flagel SB, Geurts AM, Richards JB, Robinson TE, Solberg Woods LC, Palmer AA (2014) Rats are the smart choice: Rationale for a renewed focus on rats in behavioral genetics.

Parker MJ, Fryer AE, Shears DJ, Lachlan KL, Mckee SA, Magee AC, Mohammed S, Vasudevan PC, Park SM, Benoit V, Lederer D, Maystadt I, Study D, Fitzpatrick DR (2015) De novo, heterozygous, loss-of-function mutations in SYNGAP1 cause a syndromic form of intellectual disability. *American Journal of Medical Genetics, Part A* 167:2231–2237.

Parks TN, Rubel EW (1975) Organization and development of brain stem auditory nuclei of the chicken: Organization of projections from N. magnocellularis to N. laminaris. *Journal of Comparative Neurology* 164:435–448.

Patino GA, Claes LR, Lopez-Santiago LF, Slat EA, Dondeti RS, Chen C, O'Malley HA, Gray CB, Miyazaki H, Nukina N, Oyama F, De Jonghe P, Isom LL (2009) A functional null mutation of SCN1B in a patient with Dravet syndrome. *Journal of Neuroscience* 29:10764–10778.

Patja K, Mölsä P, Iivanainen M (2001) Cause-specific mortality of people with intellectual disability in a population-based, 35-year follow-up study. *Journal of Intellectual Disability Research* 45:30–40.

Paul M, Pinto YM, Schunkert H, Ganten D, Bohm M (1994) Activation of the Renin-Angiotensin System in Heart Failure and Hypertrophy–Studies in Human Hearts and Transgenic Rats. *European Heart Journal* 15:63–67.

Pavlov IP (1927) Conditioned reflexes: An investigation of the physiological activity of the cerebral cortex. *Annals of neurosciences* 17:430, xv, 430–xv.

Paxinos G, Watson C (2007) *The rat brain in stereotaxic coordinates* Academic Press Inc., 6 edition.

Peier AM (2000) (Over)correction of FMR1 deficiency with YAC transgenics: behavioral and physical features. *Human Molecular Genetics* 9:1145–1159.

Pena V, Hothorn M, Eberth A, Kaschau N, Parret A, Gremer L, Bonneau F, Ahmadian MR, Scheffzek K (2008) The C2 domain of SynGAP is essential for stimulation of the Rap GTPase reaction. *EMBO Reports* 9:350–355.

Peñagarikano O, Abrahams BS, Herman EI, Winden KD, Gdalyahu A, Dong H, Sonnenblick LI, Gruver R, Almajano J, Bragin A, Golshani P, Trachtenberg JT, Peles E, Geschwind DH (2011) Absence of CNTNAP2 leads to epilepsy, neuronal migration abnormalities, and core autism-related deficits. *Cell* 147:235–246.

Peñagarikano O, Geschwind DH (2012) What does CNTNAP2 reveal about autism spectrum disorder?

Persico AM, Merelli S (2015) Environmental factors and autism spectrum disorder. *Key Issues in Mental Health* 180:113–134.

Persico AM, Napolioni V (2013) Autism genetics. *Behavioural Brain Research* 251:95–112.

Peters A, Proskauer CC, Kaiserman-Abramof IR (1968) The small pyramidal neuron of the rat cerebral cortex. The axon hillock and initial segment. *The Journal of cell biology* 39:604–619.

Petersen AV, Cotel F, Perrier JF (2017) Plasticity of the Axon Initial Segment: Fast and Slow Processes with Multiple Functional Roles. *Neuroscientist* 23:364–373.

Petersen CC (2007) The functional organization of the barrel cortex.

Pinto D, Delaby E, Merico D, Barbosa M, Merikangas A, Klei L, Thiruvahindrapuram B, Xu X, Ziman R, Wang Z, Vorstman JA, Thompson A, Regan R, Pilorge M, Pellecchia G, Pagnamenta AT, Oliveira B, Marshall CR, Magalhaes TR, Lowe JK, Howe JL, Griswold AJ, Gilbert J, Duketis E, Dombroski BA, De Jonge MV, Cuccaro M, Crawford EL, Correia CT, Conroy J, Conceição IC, Chiocchetti AG, Casey JP, Cai G, Cabrol C, Bolshakova N, Bacchelli E, Anney R, Gallinger S, Cotterchio M, Casey G, Zwaigenbaum L, Wittemeyer K, Wing K, Wallace S, Van Engeland H, Tryfon A, Thomson S, Soorya L, Rogé B, Roberts W, Poustka F, Mouga S, Minshew N, McInnes LA, McGrew SG, Lord C, Leboyer M, Le Couteur AS, Kolevzon A, Jiménez González P, Jacob S, Holt R, Guter S, Green J, Green A, Gillberg C, Fernandez BA, Duque F, Delorme R, Dawson G, Chaste P, Café C, Brennan S, Bourgeron T, Bolton PF, Bölte S, Bernier R, Baird G, Bailey AJ, Anagnostou E, Almeida J, Wijsman EM, Vieland VJ, Vicente AM, Schellenberg GD, Pericak-Vance M, Paterson AD, Parr JR, Oliveira G, Nurnberger JI, Monaco AP, Maestrini E, Klauck SM, Hakonarson H, Haines JL, Geschwind DH, Freitag CM, Folstein SE, Ennis S, Coon H, Battaglia A, Szatmari P, Sutcliffe JS, Hallmayer J, Gill M, Cook EH, Buxbaum JD, Devlin B, Gallagher L, Betancur C, Scherer SW (2014) Convergence of genes and cellular pathways dysregulated in autism spectrum disorders. *American Journal of Human Genetics* 94:677–694.

Pinto D, Pagnamenta AT, Klei L, Anney R, Merico D, Regan R, Conroy J, Magalhaes TR, Correia C, Abrahams BS, Almeida J, Bacchelli E, Bader GD, Bailey AJ, Baird G, Battaglia A, Berney T, Bolshakova N, Bolte S, Bolton PF, Bourgeron T, Brennan S, Brian J, Bryson SE, Carson AR, Casallo G, Casey J, Chung BHY, Cochrane L, Corsello C, Crawford EL, Crossett A, Cytrynbaum C, Dawson G, de Jonge M, Delorme R, Drmic I, Duketis E, Duque F, Estes A, Farrar P, Fernandez BA, Folstein SE, Fombonne E, Freitag CM, Gilbert J, Gillberg C, Glessner JT, Goldberg J, Green A, Green J, Guter SJ, Hakonarson H, Heron EA, Hill M, Holt R, Howe JL, Hughes G, Hus V, Igliozzi R, Kim C, Klauck SM, Kolevzon A, Korvatska O, Kustanovich V, Lajonchere CM, Lamb JA, Laskawiec M, Leboyer M, Le Couteur A, Leventhal BL, Lionel AC, Liu XQ, Lord C, Lotspeich L, Lund SC, Maestrini E, Mahoney W, Mantoulan C, Marshall CR, McConachie H, McDougle CJ, McGrath J, McMahon WM, Merikangas A, Migita O, Minshew NJ, Mirza GK, Munson J, Nelson SF, Noakes C, Noor A, Nygren G, Oliveira G, Papanikolaou K, Parr JR, Parrini B, Paton T, Pickles A, Pilorge M, Piven J, Ponting CP, Posey DJ, Poustka A, Poustka F, Prasad A, Ragoussis J, Renshaw K, Rickaby J, Roberts W, Roeder K, Roge B, Rutter ML, Bierut LJ, Rice JP, Salt J, Sansom K, Sato D, Segurado R, Sequeira AF, Senman L, Shah N, Sheffield VC, Soorya L, Sousa I, Stein O, Sykes N, Stoppioni V, Strawbridge C, Tancredi R, Tansey K, Thiruvahindrapduram B, Thompson AP, Thomson S, Tryfon A, Tsiantis J, Van Engeland H, Vincent JB, Volkmar F, Wallace S, Wang K, Wang Z, Wassink TH, Webber C, Weksberg R, Wing K, Wittemeyer K, Wood S, Wu J, Yaspan BL, Zurawiecki D, Zwaigenbaum L, Buxbaum JD, Cantor RM, Cook EH, Coon H, Cuccaro ML, Devlin B, Ennis S, Gallagher L, Geschwind DH, Gill M, Haines JL, Hallmayer J, Miller J, Monaco AP, Nurnberger Jr JI, Paterson AD, Pericak-Vance MA, Schellenberg GD, Szatmari P, Vicente AM, Vieland VJ, Wijsman EM, Scherer SW, Sutcliffe JS, Betancur C (2010) Functional impact of global rare copy number variation in autism spectrum disorders. *Nature* 466:368–372.

Pizzarelli R, Cherubini E (2013) Developmental regulation of GABAergic signalling in the hippocampus of neuroligin 3 R451C knock-in mice: An animal model of Autism. *Frontiers in Cellular Neuroscience* 7:85.

Poliak S, Gollan L, Martinez R, Custer A, Einheber S, Salzer JL, Trimmer JS, Shrager P, Peles E (1999) Caspr2, a new member of the Neurexin superfamily, is localized at the juxtaparanodes of myelinated axons and associates with K+ channels. *Neuron* 24:1037–1047.

Poliak S, Salomon D, Elhanany H, Sabanay H, Kiernan B, Pevny L, Stewart CL, Xu X, Chiu SY, Shrager P, Furley AJ, Peles E (2003) Juxtaparanodal clustering of Shaker-like K+ channels in myelinated axons depends on Caspr2 and TAG-1. *Journal of Cell Biology* 162:1149–1160.

Polli FE, Wright CI, Milad MR, Dickerson BC, Vangel M, Barton JJ, Rauch SL, Manoach DS (2009) Hemispheric differences in amygdala contributions to response monitoring. *NeuroReport* 20:398–402.

Poot M (2015) Connecting the CNTNAP2 networks with neurodevelopmental disorders.

Porter K, Komiyama NH, Vitalis T, Kind PC, Grant SGN (2005) Differential expression of two NMDA receptor interacting proteins, PSD-95 and SynGAP during mouse development. *European Journal of Neuroscience* 21:351–362.

Prchalova D, Havlovicova M, Sterbova K, Stranecky V, Hancarova M, Sedlacek Z (2017) Analysis of 31-year-old patient with SYNGAP1 gene defect points to importance of variants in broader splice regions and reveals developmental trajectory of SYNGAP1-associated phenotype: Case report. *BMC Medical Genetics* 18.

Puga F, Barrett DW, Bastida CC, Gonzalez-Lima F (2007) Functional networks underlying latent inhibition learning in the mouse brain. *NeuroImage* 38:171–183.

Pun RY, Rolle IJ, LaSarge CL, Hosford BE, Rosen JM, Uhl JD, Schmeltzer SN, Faulkner C, Bronson SL, Murphy BL, Richards DA, Holland KD, Danzer SC (2012) Excessive Activation of mTOR in Postnatally Generated Granule Cells Is Sufficient to Cause Epilepsy. *Neuron* 75:1022–1034.

Quesnel-Vallières M, Weatheritt RJ, Cordes SP, Blencowe BJ (2019) Autism spectrum disorder: insights into convergent mechanisms from transcriptomics.

Rademacher S, Eickholt BJ (2019) PTEN in Autism and Neurodevelopmental Disorders. *Cold Spring Harbor Perspectives in Medicine* p. a036780.

Radivojevic M, Franke F, Altermatt M, Müller J, Hierlemann A, Bakkum DJ (2017) Tracking individual action potentials throughout mammalian axonal arbors. *eLife* 6.

Radyushkin K, Hammerschmidt K, Boretius S, Varoqueaux F, El-Kordi A, Ronnenberg A, Winter D, Frahm J, Fischer J, Brose N, Ehrenreich H (2009) Neuroligin-3-deficient mice: Model of a monogenic heritable form of autism with an olfactory deficit. *Genes, Brain and Behavior* 8:416–425.

Ragozzino ME, Adams S, Kesner RP (1998) "Differential involvement of the dorsal anterior cingulate and prelimbic-infralimbic areas of the rodent prefrontal cortex in spatial working memory": Correction to Ragozzino et al. (1998). *Behavioral Neuroscience* 112:747–747.

Ramocki MB, Zoghbi HY (2008) Failure of neuronal homeostasis results in common neuropsychiatric phenotypes.

Randrup A, Munkvad I (1974) Pharmacology and physiology of stereotyped behavior. *Journal of Psychiatric Research* 11:1–10.

Rao A, Harms KJ, Craig AM (2000) Neuroligation: Building synapses around the neurexin-neuroligin link.

Rasband MN (2010) The axon initial segment and the maintenance of neuronal polarity. *Nature Reviews Neuroscience* 11:552–562.

Rasband MN, Park EW, Zhen D, Arbuckle MI, Poliak S, Peles E, Grant SG, Trimmer JS (2002) Clustering of neuronal potassium channels is independent of their interaction with PSD-95. *Journal of Cell Biology* 159:663–672.

Rauch A, Wieczorek D, Graf E, Wieland T, Endele S, Schwarzmayr T, Albrecht B, Bartholdi D, Beygo J, Di Donato N, Dufke A, Cremer K, Hempel M, Horn D, Hoyer J, Joset P, Röpke A, Moog U, Riess A, Thiel CT, Tzschach A, Wiesener A, Wohlleber E, Zweier C, Ekici AB, Zink AM, Rump A, Meisinger C, Grallert H, Sticht H, Schenck A, Engels H, Rappold G, Schröck E, Wieacker P, Riess O, Meitinger T, Reis A, Strom TM (2012) Range of genetic mutations associated with severe non-syndromic sporadic intellectual disability: An exome sequencing study. *The Lancet* 380:1674–1682.

Rausch A, Zhang W, Haak KV, Mennes M, Hermans EJ, Van Oort E, Van Wingen G, Beckmann CF, Buitelaar JK, Groen WB (2016) Altered functional connectivity of the amygdaloid input nuclei in adolescents and young adults with autism spectrum disorder: A resting state fMRI study. *Molecular Autism* 7.

Raymond GV, Bauman ML, Kemper TL (1995) Hippocampus in autism: a Golgi analysis. *Acta Neuropathologica* 91:117–119.

Rebsam A, Seif I, Gaspar P (2002) Refinement of thalamocortical arbors and emergence of barrel domains in the primary somatosensory cortex: A study of normal and monoamine oxidase A knock-out mice. *Journal of Neuroscience* 22:8541–8552.

Redin C, Gérard B, Lauer J, Herenger Y, Muller J, Quartier A, Masurel-Paulet A, Willems M, Lesca G, El-Chehadeh S, Gras SL, Vicaire S, Philipps M, Dumas M, Geoffroy V, Feger C, Haumesser N, Alembik Y, Barth M, Bonneau D, Colin E, Dollfus H, Doray B, Delrue MA, Drouin-Garraud V, Flori E, Fradin M, Francannet C, Goldenberg A, Lumbroso S, Mathieu-Dramard M, Martin-Coignard D, Lacombe D, Morin G, Polge A, Sukno S, Thauvin-Robinet C, Thevenon J, Doco-Fenzy M, Genevieve D, Sarda P, Edery P, Isidor B, Jost B, Olivier-Faivre L, Mandel JL, Piton A (2014) Efficient strategy for the molecular diagnosis of intellectual disability using targeted high-throughput sequencing. *Journal of Medical Genetics* 51:724–736.

Rees E, Walters JT, Georgieva L, Isles AR, Chambert KD, Richards AL, Mahoney-Davies G, Legge SE, Moran JL, McCarroll SA, O'Donovan MC, Owen MJ, Kirov G (2014) Analysis of copy number variations at 15 schizophrenia-associated loci. *British Journal of Psychiatry* 204:108–114.

Reissner C, Runkel F, Missler M (2013) Neurexins. *Genome biology* 14:213.

Reyes A (2001) Influence of Dendritic Conductances on the Input-Output Properties of Neurons. *Annual Review of Neuroscience* 24:653–675.

Ribak CE (1985) Axon terminals of GABAergic chandelier cells are lost at epileptic foci. *Brain Research* 326:251–260.

Rinaldi T, Perrodin C, Markram H (2008) Hyper-connectivity and hyper-plasticity in the medial prefrontal cortex in the valproic acid animal model of autism. *Frontiers in Neural Circuits* 2.

Robertson CE, Baron-Cohen S (2017) Sensory perception in autism.

Robertson CE, Kravitz DJ, Freyberg J, Baron-Cohen S, Baker CI (2013) Slower Rate of binocular rivalry in autism. *Journal of Neuroscience* 33:16983–16991.

Robertson CE, Ratai EM, Kanwisher N (2016) Reduced GABAergic Action in the Autistic Brain. *Current Biology* 26:80–85.

Robinson AN, Roberts JE, Brady NC, McQuillin SD, Warren SF (2016) Physiological correlates of maternal responsivity in mothers of preschoolers with fragile X syndrome. *American Journal on Intellectual and Developmental Disabilities* 121:111–120.

Rodenas-Cuadrado P, Ho J, Vernes SC (2014) Shining a light on CNTNAP2: Complex functions to complex disorders.

Roelofs K (2017) Freeze for action: Neurobiological mechanisms in animal and human freezing.

Romanski LM, LeDoux JE (1992) Equipotentiality of thalamo-amygdala and thalamo-cortico-amygdala circuits in auditory fear conditioning. *Journal of Neuroscience* 12:4501–4509.

Rothwell PE, Fuccillo MV, Maxeiner S, Hayton SJ, Gokce O, Lim BK, Fowler SC, Malenka RC, Südhof TC (2014) Autism-associated neuroligin-3 mutations commonly impair striatal circuits to boost repetitive behaviors. *Cell* 158:198–212.

Royall DR, Lauterbach EC, Cummings JL, Reeve A, Rummans TA, Kaufer DI, LaFrance WC, Coffey CE (2002) Executive control function: A review of its promise and challenges for clinical research - A report from the Committee on Research of the American Neuropsychiatric Association.

Rubenstein JL, Merzenich MM (2003) Model of autism: Increased ratio of excitation/inhibition in key neural systems. *Genes, Brain and Behavior* 2:255–267.

Rudy JW (1993) Contextual Conditioning and Auditory Cue Conditioning Dissociate During Development. *Behavioral Neuroscience* 107:887–891.

Rujescu D, Ingason A, Cichon S, Pietiläinen OP, Barnes MR, Toulopoulou T, Picchioni M, Vassos E, Ettinger U, Bramon E, Murray R, Ruggeri M, Tosato S, Bonetto C, Steinberg S, Sigurdsson E, Sigmundsson T, Petursson H, Gylfason A, Olason PI, Hardarsson G, Jonsdottir GA, Gustafsson O, Fossdal R, Giegling I, Möller HJ, Hartmann AM, Hoffmann P, Crombie C, Fraser G, Walker N, Lonnqvist J, Suvisaari J, Tuulio-Henriksson A, Djurovic S, Melle I, Andreassen OA, Hansen T, Werge T, Kiemeney LA, Franke B, Veltman J, Buizer-Voskamp JE, Sabatti C, Ophoff RA, Rietschel M, Nöthen MM, Stefansson K, Peltonen L, St Clair D, Stefansson H, Collier DA, Kahn RS, Linszen D, von Os J, Wiersma D, Bruggeman R, Cahn W, de Haan L, Krabbendam L, Myin-Germeys I (2009) Disruption of the neurexin 1 gene is associated with schizophrenia. *Human Molecular Genetics* 18:988–996.

Rumbaugh G, Adams JP, Kim JH, Huganir RL (2006) SynGAP regulates synaptic strength and mitogen-activated protein kinases in cultured neurons. *Proceedings of the National Academy of Sciences of the United States of America* 103:4344–4351.

S. Fanselow M (1984) What is conditioned fear? *Trends in Neurosciences* 7:460–462.

Sabaratnam M, Vroegop PG, Gangadharan SK (2001) Epilepsy and EEG findings in 18 males with fragile X syndrome. *Seizure* 10:60–63.

Saha R, Shrivastava K, Jing L, Schayek R, Maroun M, Kriebel M, Volkmer H, Richter-Levin G (2018) Perturbation of GABAergic synapses at the axon initial segment of basolateral amygdala induces trans-regional metaplasticity at the medial prefrontal cortex. *Cerebral Cortex* 28:395–410.

Sahoo T, Theisen A, Rosenfeld JA, Lamb AN, Ravnan JB, Schultz RA, Torchia BS, Neill N, Casci I, Bejjani BA, Shaffer LG (2011) Copy number variants of schizophrenia susceptibility loci are associated with a spectrum of speech and developmental delays and behavior problems. *Genetics in Medicine* 13:868–880.

Samadi SA, McConkey R (2011) Autism in Developing Countries: Lessons from Iran. *Autism Research and Treatment* 2011:1–11.

Samra NM, Abdel Ghaffar HM, El Awady HA, Soltan MR, Moktader RMA (2017) Epilepsy and EEG Findings in Children with Autism Spectrum Disorders. *Autism-Open Access* 07.

Sanders SJ, Ercan-Sencicek AG, Hus V, Luo R, Murtha MT, Moreno-De-Luca D, Chu SH, Moreau MP, Gupta AR, Thomson SA, Mason CE, Bilguvar K, Celestino-Soper PB, Choi M, Crawford EL, Davis L, Davis Wright NR, Dhodapkar RM, DiCola M, DiLullo NM,

Fernandez TV, Fielding-Singh V, Fishman DO, Frahm S, Garagaloyan R, Goh GS, Kammela S, Klei L, Lowe JK, Lund SC, McGrew AD, Meyer KA, Moffat WJ, Murdoch JD, O'Roak BJ, Ober GT, Pottenger RS, Raubeson MJ, Song Y, Wang Q, Yaspan BL, Yu TW, Yurkiewicz IR, Beaudet AL, Cantor RM, Curland M, Grice DE, Günel M, Lifton RP, Mane SM, Martin DM, Shaw CA, Sheldon M, Tischfield JA, Walsh CA, Morrow EM, Ledbetter DH, Fombonne E, Lord C, Martin CL, Brooks AI, Sutcliffe JS, Cook EH, Geschwind D, Roeder K, Devlin B, State MW (2011) Multiple Recurrent De Novo CNVs, Including Duplications of the 7q11.23 Williams Syndrome Region, Are Strongly Associated with Autism. *Neuron* 70:863–885.

Sanders SJ, He X, Willsey AJ, Ercan-Sencicek AG, Samocha KE, Cicek AE, Murtha MT, Bal VH, Bishop SL, Dong S, Goldberg AP, Jinlu C, Keaney JF, Klei L, Mandell JD, Moreno-De-Luca D, Poultney CS, Robinson EB, Smith L, Solli-Nowlan T, Su MY, Teran NA, Walker MF, Werling DM, Beaudet AL, Cantor RM, Fombonne E, Geschwind DH, Grice DE, Lord C, Lowe JK, Mane SM, Martin DM, Morrow EM, Talkowski ME, Sutcliffe JS, Walsh CA, Yu TW, Ledbetter DH, Martin CL, Cook EH, Buxbaum JD, Daly MJ, Devlin B, Roeder K, State MW (2015) Insights into Autism Spectrum Disorder Genomic Architecture and Biology from 71 Risk Loci. *Neuron* 87:1215–1233.

Sanders SJ, Murtha MT, Gupta AR, Murdoch JD, Raubeson MJ, Willsey AJ, Ercan-Sencicek AG, Di Lullo NM, Parikshak NN, Stein JL, Walker MF, Ober GT, Teran NA, Song Y, El-Fishawy P, Murtha RC, Choi M, Overton JD, Bjornson RD, Carriero NJ, Meyer KA, Bilguvar K, Mane SM, Š estan N, Lifton RP, Günel M, Roeder K, Geschwind DH, Devlin B, State MW (2012) De novo mutations revealed by whole-exome sequencing are strongly associated with autism. *Nature* 485:237–241.

Sato N, Tan L, Tate K, Okada M (2015) Rats demonstrate helping behavior toward a soaked conspecific. *Animal Cognition* 18:1039–1047.

Schaaf CP, Boone PM, Sampath S, Williams C, Bader PI, Mueller JM, Shchelochkov OA, Brown CW, Crawford HP, Phalen JA, Tartaglia NR, Evans P, Campbell WM, Chun-Hui Tsai A, Parsley L, Grayson SW, Scheuerle A, Luzzi CD, Thomas SK, Eng PA, Kang SHL, Patel A, Stankiewicz P, Cheung SW (2012) Phenotypic spectrum and genotype-phenotype correlations of NRXN1 exon deletions. *European Journal of Human Genetics* 20:1240–1247.

Schafer DP, Jha S, Liu F, Akella T, McCullough LD, Rasband MN (2009) Disruption of the axon initial segment cytoskeleton is a new mechanism for neuronal injury. *Journal of Neuroscience* 29:13242–13254.

Scheffer IE, Berkovic S, Capovilla G, Connolly MB, French J, Guilhoto L, Hirsch E, Jain S, Mathern GW, Moshé SL, Nordli DR, Perucca E, Tomson T, Wiebe S, Zhang YH, Zuberi SM (2017) ILAE classification of the epilepsies: Position paper of the ILAE Commission for Classification and Terminology. *Epilepsia* 58:512–521.

Scheffer IE, Harkin LA, Grinton BE, Dibbens LM, Turner SJ, Zielinski MA, Xu R, Jackson G, Adams J, Connellan M, Petrou S, Wellard RM, Briellmann RS, Wallace RH, Mulley JC, Berkovic SF (2007) Temporal lobe epilepsy and GEFS+ phenotypes associated with SCN1B mutations. *Brain* 130:100–109.

Scheffer IE, Zhang YH, Jansen FE, Dibbens L (2009) Dravet syndrome or genetic (generalized) epilepsy with febrile seizures plus?

Scheiffele P, Fan J, Choih J, Fetter R, Serafini T (2000) Neuroligin expressed in nonneuronal cells triggers presynaptic development in contacting axons. *Cell* 101:657–669.

Schlüter A, Del Turco D, Deller T, Gutzmann A, Schultz C, Engelhardt M (2017) Structural plasticity of synaptopodin in the axon initial segment during visual cortex development. *Cerebral Cortex* 27:4662–4675.

Schmid-Holmes S, Drickamer LC, Robinson AS, Gillie LL (2001) Burrows and Burrow-Cleaning Behavior of House Mice (Mus musculus domesticus). *The American Midland Naturalist* 146:53–62.

Schultz C, König HG, Del Turco D, Politi C, Eckert GP, Ghebremedhin E, Prehn JH, Kögel D, Deller T (2006) Coincident enrichment of phosphorylated IκBα, activated IKK, and phosphorylated p65 in the axon initial segment of neurons. *Molecular and Cellular Neuroscience* 33:68–80.

Schumann CM, Barnes CC, Lord C, Courchesne E (2009) Amygdala Enlargement in Toddlers with Autism Related to Severity of Social and Communication Impairments. *Biological Psychiatry* 66:942–949.

Seamans JK, Floresco SB, Phillips AG (1995) Functional Differences Between the Prelimbic and Anterior Cingulate Regions of the Rat Prefrontal Cortex. *Behavioral Neuroscience* 109:1063–1073.

Sehgal M, Song C, Ehlers VL, Moyer JR (2013) Learning to learn - Intrinsic plasticity as a metaplasticity mechanism for memory formation. *Neurobiology of Learning and Memory* 105:186–199.

Selimbeyoglu A, Kim CK, Inoue M, Lee SY, Hong AS, Kauvar I, Ramakrishnan C, Fenno LE, Davidson TJ, Wright M, Deisseroth K (2017) Modulation of prefrontal cortex excitation/inhibition balance rescues social behavior in CNTNAP2-deficient mice. *Science Translational Medicine* 9.

Selleck RA, Zhang W, Samberg HD, Padival M, Rosenkranz JA (2018) Limited prefrontal cortical regulation over the basolateral amygdala in adolescent rats. *Scientific Reports* 8.

Senn V, Wolff SBE, Herry C, Grenier F, Ehrlich I, Gründemann J, Fadok JP, Müller C, Letzkus JJ, Lüthi A (2014) Long-range connectivity defines behavioral specificity of amygdala neurons. *Neuron* 81:428–437.

Shechner T, Hong M, Britton JC, Pine DS, Fox NA (2014) Fear conditioning and extinction across development: Evidence from human studies and animal models.

Shevell M, Ashwal S, Donley D, Flint J, Gingold M, Hirtz D, Majnemer A, Noetzel M, Sheth RD (2003) Practice parameter: Evaluation of the child with global developmental delay: Report of the quality standards subcommittee of the American Academy of Neurology and The Practice Committee of the Child Neurology Society. *Neurology* 60:367–380.

Siddiqui TJ, Pancaroglu R, Kang Y, Rooyakkers A, Craig AM (2010) LRRTMs and neuroligins bind neurexins with a differential code to cooperate in glutamate synapse development. *Journal of Neuroscience* 30:7495–7506.

Sidorov MS, Krueger DD, Taylor M, Gisin E, Osterweil EK, Bear MF (2014) Extinction of an instrumental response: A cognitive behavioral assay in Fmr1 knockout mice. *Genes, Brain and Behavior* 13:451–458.

Siglin JC, Baker WH (2001) Laboratory animal management In *Handbook of Toxicology, Second Edition*, pp. 1–68. National Academies Press (US).

Silva AJ, Frankland PW, Marowitz Z, Friedman E, Lazlo G, Cioffi D, Jacks T, Bourtchuladze R (1997) A mouse model for the learning and memory deficits associated with neurofibromatosis type I. *Nature Genetics* 15:281–284.

Simon P, Dupuis R, Costentin J (1994) Thigmotaxis as an index of anxiety in mice. Influence of dopaminergic transmissions. *Behavioural Brain Research* 61:59–64.

Siviy SM, Panksepp J (2011) In search of the neurobiological substrates for social playfulness in mammalian brains.

Skelton PD, Frazel PW, Lee D, Suh H, Luikart BW (2019) Pten loss results in inappropriate excitatory connectivity. *Molecular Psychiatry* 24:1627–1640.

Smith LE, Hong J, Greenberg JS, Mailick MR (2016) Change in the Behavioral Phenotype of Adolescents and Adults with FXS: Role of the Family Environment. *Journal of Autism and Developmental Disorders* 46:1824–1833.

Song C, Ehlers VL, Moyer JR (2015) Trace fear conditioning differentially modulates intrinsic excitability of medial prefrontal cortex–basolateral complex of amygdala projection neurons in infralimbic and prelimbic cortices. *Journal of Neuroscience* 35:13511–13524.

Song C, Moyer JR (2018) Layer- and subregion-specific differences in the neurophysiological properties of rat medial prefrontal cortex pyramidal neurons. *Journal of Neurophysiology* 119:177–191.

Song HA, Wang D, Chen G, Li Y, Luo J, Duan S, ming Poo M (2009) A Selective Filter for Cytoplasmic Transport at the Axon Initial Segment. *Cell* 136:1148–1160.

Song JY, Ichtchenko K, Südhof TC, Brose N (1999) Neuroligin 1 is a postsynaptic cell-adhesion molecule of excitatory synapses. *Proceedings of the National Academy of Sciences of the United States of America* 96:1100–1105.

Sparks BF, Friedman SD, Shaw DW, Aylward EH, Echelard D, Artru AA, Maravilla KR, Giedd JN, Munson J, Dawson G, Dager SR (2002) Brain structural abnormalities in young children with autism spectrum disorder. *Neurology* 59:184–192.

Spencer CM, Graham DF, Yuva-Paylor LA, Nelson DL, Paylor R (2008) Social Behavior in Fmr1 Knockout Mice Carrying a Human FMR1 Transgene. *Behavioral Neuroscience* 122:710–715.

Sperow M, Berry RB, Bayazitov IT, Zhu G, Baker SJ, Zakharenko SS (2012) PTEN regulates synaptic plasticity independently of its effect on neuronal morphology and migration. *J Physiol* 590:777–792.

Stiles B, Groszer M, Wang S, Jiao J, Wu H (2004) PTENless means more.

Strauss KA, Puffenberger EG, Huentelman MJ, Gottlieb S, Dobrin SE, Parod JM, Stephan DA, Morton DH (2006) Recessive symptomatic focal epilepsy and mutant contactin-associated protein-like 2. *New England Journal of Medicine* 354:1370–1377.

Südhof TC (2008) Neuroligins and neurexins link synaptic function to cognitive disease. *Nature* 455:903–911.

Sullivan JM, De Rubeis S, Schaefer A (2019) Convergence of spectrums: neuronal gene network states in autism spectrum disorder.

Sun T, Song Z, Tian Y, Tian W, Zhu C, Ji G, Luo Y, Chen S, Wang L, Mao Y, Xie W, Zhong H, Zhao F, Luo MH, Tao W, Wang H, Li J, Li J, Zhou J, Wang K, Zhang Z (2019) Basolateral amygdala input to the medial prefrontal cortex controls obsessive-compulsive disorder-like checking behavior. *Proceedings of the National Academy of Sciences* 116:3799–3804.

Suvrathan A, Hoeffer CA, Wong H, Klann E, Chattarji S (2010) Characterization and reversal of synaptic defects in the amygdala in a mouse model of fragile X syndrome. *Proceedings of the National Academy of Sciences of the United States of America* 107:11591–11596.

Szatmari P, Paterson AD, Zwaigenbaum L, Roberts W, Brian J, Liu XQ, Vincent JB, Skaug JL, Thompson AP, Senman L, Feuk L, Qian C, Bryson SE, Jones MB, Marshall CR, Scherer SW, Vieland VJ, Bartlett C, Mangin LV, Goedken R, Segre A, Pericak-Vance MA, Cuccaro ML, Gilbert JR, Wright HH, Abramson RK, Betancur C, Bourgeron T, Gillberg C, Leboyer M, Buxbaum JD, Davis KL, Hollander E, Silverman JM, Hallmayer J, Lotspeich L, Sutcliffe JS, Haines JL, Folstein SE, Piven J, Wassink TH, Sheffield V, Geschwind DH, Bucan M, Brown WT, Cantor RM, Constantino JN, Gilliam TC, Herbert M, LaJonchere C, Ledbetter DH, Lese-Martin C, Miller J, Nelson S, Samango-Sprouse CA, Spence S, State M, Tanzi RE, Coon H, Dawson G, Devlin B, Estes A, Flodman P, Klei L, McMahon WM, Minshew N, Munson J, Korvatska E, Rodier PM, Schellenberg GD, Smith M, Spence MA, Stodgell C, Tepper PG, Wijsman EM, Yu CE, Rogé B, Mantoulan C, Wittemeyer K, Poustka A, Felder B, Klauck SM, Schuster C, Poustka F, Bölte S, Feineis-Matthews S, Herbrecht E, Schmötzer G, Tsiantis J, Papanikolaou K, Maestrini E, Bacchelli E, Blasi F, Carone S, Toma C, Van Engeland H, De Jonge M, Kemner C, Koop F, Langemeijer M, Hijimans C, Staal WG, Baird G, Bolton PF, Rutter ML, Weisblatt E, Green J, Aldred C, Wilkinson JA, Pickles A, Le Couteur A, Berney T, McConachie H, Bailey AJ, Francis K, Honeyman G, Hutchinson A, Parr JR, Wallace S, Monaco AP, Barnby G, Kobayashi K, Lamb JA, Sousa I, Sykes N, Cook EH, Guter SJ, Leventhal BL, Salt J, Lord C, Corsello C, Hus V, Weeks DE, Volkmar F, Tauber M, Fombonne E, Shih A (2007) Mapping autism risk loci using genetic linkage and chromosomal rearrangements. *Nature Genetics* 39:319–328.

Tabuchi K, Blundell J, Etherton MR, Hammer RE, Liu X, Powell CM, Südhof TC (2007) A neuroligin-3 mutation implicated in autism increases inhibitory synaptic transmission in mice. *Science* 318:71–76.

Tabuchi K, Südhof TC (2002) Structure and evolution of neurexin genes: Insight into the mechanism of alternative splicing. *Genomics* 79:849–859.

Takarae Y, Sweeney J (2017) Neural hyperexcitability in autism spectrum disorders. *Brain Sciences* 7.

Takeuchi K, Gertner MJ, Zhou J, Parada LF, Bennett MV, Zukin RS (2013) Dysregulation of synaptic plasticity precedes appearance of morphological defects in a Pten conditional knockout mouse model of autism. *Proceedings of the National Academy of Sciences of the United States of America* 110:4738–4743.

Tan MH, Mester J, Peterson C, Yang Y, Chen JL, Rybicki LA, Milas K, Pederson H, Remzi B, Orloff MS, Eng C (2011) A clinical scoring system for selection of patients for pten mutation testing is proposed on the basis of a prospective study of 3042 probands. *American Journal of Human Genetics* 88:42–56.

Tau GZ, Peterson BS (2010) Normal development of brain circuits.

Taurog JD, Maika SD, Satumtira N, Dorris ML, McLean IL, Yanagisawa H, Sayad A, Stagg AJ, Fox GM, O'Brien AL, Rehman M, Zhou M, Weiner AL, Splawski JB, Richardson JA, Hammer RE (1999) Inflammatory disease in HLA-B27 transgenic rats.

Testa-Silva G, Loebel A, Giugliano M, De Kock CP, Mansvelder HD, Meredith RM (2012) Hyperconnectivity and slow synapses during early development of medial prefrontal cortex in a mouse model for mental retardation and Autism. *Cerebral Cortex* 22:1333–1342.

Thomas AM, Schwartz MD, Saxe MD, Kilduff TS (2017) Cntnap2 knockout rats and mice exhibit epileptiform activity and abnormal sleep-wake physiology. *Sleep* 40.

Thomson SR, Seo SS, Barnes SA, Louros SR, Muscas M, Dando O, Kirby C, Wyllie DJ, Hardingham GE, Kind PC, Osterweil EK (2017) Cell-Type-Specific Translation Profiling Reveals a Novel Strategy for Treating Fragile X Syndrome. *Neuron* 95:550–563.e5.

Till SM, Asiminas A, Jackson AD, Katsanevaki D, Barnes SA, Osterweil EK, Bear MF, Chattarji S, Wood ER, Wyllie DJ, Kind PC (2015) Conserved hippocampal cellular pathophysiology but distinct behavioural deficits in a new rat model of FXS. *Human Molecular Genetics* 24:5977–5984.

Tilot AK, Frazier TW, Eng C (2015) Balancing Proliferation and Connectivity in PTEN-associated Autism Spectrum Disorder.

Tilot AK, Gaugler MK, Yu Q, Romigh T, Yu W, Miller RH, Frazier TW, Eng C (2014) Germline disruption of Pten localization causes enhanced sex-dependent social motivation and increased glial production. *Human Molecular Genetics* 23:3212–3227.

Todarello G, Feng N, Kolachana BS, Li C, Vakkalanka R, Bertolino A, Weinberger DR, Straub RE (2014) Incomplete penetrance of NRXN1 deletions in families with schizophrenia. *Schizophrenia Research* 155:1–7.

Todd PK, Mack KJ, Malter JS (2003) The fragile X mental retardation protein is required for type-I metabotropic glutamate receptor-dependent translation of PSD-95. *Proceedings of the National Academy of Sciences of the United States of America* 100:14374–14378.

Toft AKH (2019) Impact of two autism related genes on amygdala physiology Ph.D. diss., The University of Edinburgh.

Toma C, Pierce KD, Shaw AD, Heath A, Mitchell PB, Schofield PR, Fullerton JM (2018) Comprehensive cross-disorder analyses of CNTNAP2 suggest it is unlikely to be a primary risk gene for psychiatric disorders. *PLoS Genetics* 14:1–21.

Tsigelny I, Shindyalov IN, Bourne PE, Sudhof TC, Taylor P (2000) Common EF-hand motifs in cholinesterases and neuroligins suggest a role for Ca2+ binding in cell surface associations. *Protein Sci.* 9:180.

Tsvetkov E, Carlezon WA, Benes FM, Kandel ER, Bolshakov VY (2002) Fear conditioning occludes LTP-induced presynaptic enhancement of synaptic transmission in the cortical pathway to the lateral amygdala. *Neuron* 34:289–300.

Tuchman R, Cuccaro M, Alessandri M (2010) Autism and epilepsy: Historical perspective.

Twining RC, Vantrease JE, Love S, Padival M, Rosenkranz JA (2017) An intra-amygdala circuit specifically regulates social fear learning. *Nature Neuroscience* 20:459–469.

Tyrer F, Smith LK, Mcgrother CW (2007) Mortality in adults with moderate to profound intellectual disability: A population-based study. *Journal of Intellectual Disability Research* 51:520–527.

Ulbrich L, Favaloro FL, Trobiani L, Marchetti V, Patel V, Pascucci T, Comoletti D, Marciniak SJ, De Jaco A (2016) Autism-associated R451C mutation in neuroligin3 leads to activation of the unfolded protein response in a PC12 Tet-On inducible system. *Biochemical Journal* 473:423–434.

Ullrich B, Ushkaryov YA, Südhof TC (1995) Cartography of neurexins: More than 1000 isoforms generated by alternative splicing and expressed in distinct subsets of neurons. *Neuron* 14:497–507.

Ushkaryov Y, Petrenko A, Geppert M, Sudhof T (1992) Neurexins: synaptic cell surface proteins related to the alpha-latrotoxin receptor and laminin. *Science* 257:50–56.

Van Beuningen SF, Will L, Harterink M, Chazeau A, Van Battum EY, Frias CP, Franker MA, Katrukha EA, Stucchi R, Vocking K, Antunes AT, Slenders L, Doulkeridou S, Sillevis Smitt P, Altelaar AF, Post JA, Akhmanova A, Pasterkamp RJ, Kapitein LC, de Graaff E, Hoogenraad CC (2015) TRIM46 Controls Neuronal Polarity and Axon Specification by Driving the Formation of Parallel Microtubule Arrays. *Neuron* 88:1208–1226.

Van Der Molen MJ, Stam CJ, Van Der Molen MW (2014) Resting-state EEG oscillatory dynamics in fragile X syndrome: Abnormal functional connectivity and brain network organization. *PLoS ONE* 9.

Van der Molen MJ, Van der Molen MW (2013) Reduced alpha and exaggerated theta power during the resting-state EEG in fragile X syndrome. *Biological Psychology* 92:216–219.

Van Spronsen M, Hoogenraad CC (2010) Synapse pathology in psychiatric and neurologic disease.

Van Wart A, Trimmer JS, Matthews G (2007) Polarized distribution of ion channels within microdomains of the axon initial segment. *Journal of Comparative Neurology* 500:339–352.

Van zegeren K (1979) Variation in aggressiveness and the regulation of numbers in house mouse populations. *Netherlands Journal of Zoology* 30:635–770.

Vanderver A, Tonduti D, Kahn I, Schmidt J, Medne L, Vento J, Chapman KA, Lanpher B, Pearl P, Gropman A, Lourenco C, Bamforth JS, Sharpe C, Pineda M, Schallner J, Bodamer O, Orcesi S, Oberstein SA, Sistermans EA, Yntema HG, Bonnemann C, Waldman AT, Van Der Knaap MS (2014) Characteristic brain magnetic resonance imaging pattern in patients with macrocephaly and PTEN mutations. *American Journal of Medical Genetics, Part A* 164:627–633.

Van'T Veer A, Yano JM, Carroll FI, Cohen BM, Carlezon WA (2012) Corticotropin-releasing factor (CRF)-induced disruption of attention in rats is blocked by the κ-opioid receptor antagonist JDTic. *Neuropsychopharmacology* 37:2809–2816.

Varga EA, Pastore M, Prior T, Herman GE, McBride KL (2009) The prevalence of PTEN mutations in a clinical pediatric cohort with autism spectrum disorders, developmental delay, and macrocephaly. *Genetics in Medicine* 11:111–117.

Varghese M, Keshav N, Jacot-Descombes S, Warda T, Wicinski B, Dickstein DL, Harony-Nicolas H, De Rubeis S, Drapeau E, Buxbaum JD, Hof PR (2017) Autism spectrum disorder: neuropathology and animal models. *Acta Neuropathologica* 134:537–566.

Varoqueaux F, Jamain S, Brose N (2004) Neuroligin 2 is exclusively localized to inhibitory synapses. *European Journal of Cell Biology* 83:449–456.

Vassilopoulos S, Gibaud S, Jimenez A, Caillol G, Leterrier C (2019) Ultrastructure of the axonal periodic scaffold reveals a braid-like organization of actin rings. *bioRxiv* p. 636217.

Vazquez LE, Chen HJ, Sokolova I, Knuesel I, Kennedy MB (2004) SynGAP regulates spine formation. *Journal of Neuroscience* 24:8862–8872.

Verkerk AJ, Mathews CA, Joosse M, Eussen BH, Heutink P, Oostra BA (2003) CNTNAP2 is disrupted in a family with Gilles de la Tourette syndrome and obsessive compulsive disorder. *Genomics* 82:1–9.

Verma V, Paul A, Amrapali Vishwanath A, Vaidya B, Clement JP (2019) Understanding intellectual disability and autism spectrum disorders from common mouse models: synapses to behaviour. *Open biology* 9:180265.

Vertes RP (2004) Differential Projections of the Infralimbic and Prelimbic Cortex in the Rat. *Synapse* 51:32–58.

Verwer RW, Van Vulpen EH, Van Uum JF (1996) Postnatal development of amygdaloid projections to the prefrontal cortex in the rat studied with retrograde and anterograde tracers. *Journal of Comparative Neurology* 376:75–96.

Vidal-Gonzalez I, Vidal-Gonzalez B, Rauch SL, Quirk GJ (2006) Microstimulation reveals opposing influences of prelimbic and infralimbic cortex on the expression of conditioned fear. *Learning and Memory* 13:728–733.

Vincent JB, Kolozsvari D, Roberts WS, Bolton PF, Gurling HM, Scherer SW (2004) Mutation screening of X-chromosomal neuroligin genes: No mutations in 196 autism probands. *American Journal of Medical Genetics* 129B:82–84.

Vislay RL, Martin BS, Olmos-Serrano JL, Kratovac S, Nelson DL, Corbin JG, Huntsman MM (2013) Homeostatic responses fail to correct defective amygdala inhibitory circuit maturation in fragile X syndrome. *Journal of Neuroscience* 33:7548–7558.

Vitko I, Chen Y, Arias JM, Shen Y, Wu XR, Perez-Reyes E (2005) Functional characterization and neuronal modeling of the effects of childhood absence epilepsy variants of CACNA1H, a T-type calcium channel. *Journal of Neuroscience* 25:4844–4855.

Vlaskamp DR, Shaw BJ, Burgess R, Mei D, Montomoli M, Xie H, Myers CT, Bennett MF, Xiangwei W, Williams D, Maas SM, Brooks AS, Mancini GM, Van De Laar IM, Van Hagen JM, Ware TL, Webster RI, Malone S, Berkovic SF, Kalnins RM, Sicca F, Korenke GC, Van Ravenswaaij-Arts CM, Hildebrand MS, Mefford HC, Jiang Y, Guerrini R, Scheffer IE (2019) SYNGAP1 encephalopathy: A distinctive generalized developmental and epileptic encephalopathy. *Neurology* 92:E96–E107.

Vogt D, Cho KK, Lee AT, Sohal VS, Rubenstein JL (2015) The Parvalbumin/Somatostatin Ratio Is Increased in Pten Mutant Mice and by Human PTEN ASD Alleles. *Cell Reports* 11:944–956.

Vogt D, Cho KK, Shelton SM, Paul A, Huang ZJ, Sohal VS, Rubenstein JL (2018) Mouse Cntnap2 and Human CNTNAP2 ASD Alleles Cell Autonomously Regulate PV + Cortical Interneurons. *Cerebral Cortex* 28:3868–3879.

Von Stülpnagel C, Funke C, Haberl C, Hörtnagel K, Jüngling J, Weber YG, Staudt M, Kluger G (2015) SYNGAP1 Mutation in Focal and Generalized Epilepsy: A Literature Overview and A Case Report with Special Aspects of the EEG.

Vrijenhoek T, Buizer-Voskamp JE, van der Stelt I, Strengman E, Genetic Risk and Outcome in Psychosis (GROUP) Consortium GR, in Psychosis (GROUP) O, Sabatti C, Geurts van Kessel A, Brunner HG, Ophoff RA, Veltman JA (2008) Recurrent CNVs Disrupt Three Candidate Genes in Schizophrenia Patients. *American Journal of Human Genetics* 83:504–510.

Walker SM, Leslie NR, Perera NM, Batty IH, Downes CP (2004) The tumour-suppressor function of PTEN requires an N-terminal lipid-binding motif. *Biochemical Journal* 379:301–307.

Walkup WG, Mastro TL, Schenker LT, Vielmetter J, Hu R, Iancu A, Reghunathan M, Bannon BD, Kennedy MB (2016) A model for regulation by syngap-α1 of binding of synaptic proteins to PDZ-domain 'slots' in the postsynaptic density. *eLife* 5.

Walkup WG, Sweredoski MJ, Graham RL, Hess S, Kennedy MB (2018) Phosphorylation of synaptic GTPase-activating protein (synGAP) by polo-like kinase (Plk2) alters the ratio of its GAP activity toward HRas, Rap1 and Rap2 GTPases. *Biochemical and Biophysical Research Communications* 503:1599–1604.

Walkup WG, Washburn L, Sweredoski MJ, Carlisle HJ, Graham RL, Hess S, Kennedy MB (2015) Phosphorylation of synaptic GTPase-activating protein (synGAP) by Ca2<inf>+</inf>/Calmodulin-dependent protein kinase II (CaMKII) and cyclin-dependent kinase 5 (CDK5) alters the ratio of its GAP activity toward ras and rap GTPases. *Journal of Biological Chemistry* 290:4908–4927.

Wallace ML, Burette AC, Weinberg RJ, Philpot BD (2012) Maternal Loss of Ube3a Produces an Excitatory/Inhibitory Imbalance through Neuron Type-Specific Synaptic Defects. *Neuron* 74:793–800.

Wallace RH, Wang DW, Singh R, Scheffer IE, George AL, Phillips HA, Saar K, Reis A, W.johnson E, Sutherland GR, Berkovic SF, Mulley JC (1998) Febrile seizures and generalized epilepsy associated with a mutation in the Na + -channel β1 subunit gene SCN1B. *Nature Genetics* 19:366–370.

Walz N, Mühlberger A, Pauli P (2016) A Human Open Field Test Reveals Thigmotaxis Related to Agoraphobic Fear. *Biological Psychiatry* 80:390–397.

Wang AK, Miller BJ (2018) Meta-analysis of Cerebrospinal Fluid Cytokine and Tryptophan Catabolite Alterations in Psychiatric Patients: Comparisons between Schizophrenia, Bipolar Disorder, and Depression. *Schizophrenia Bulletin* 44:75–83.

Wang H, Wu LJ, Zhang F, Zhuo M (2008) Roles of calcium-stimulated adenylyl cyclase and calmodulin-dependent protein kinase IV in the regulation of FMRP by group I metabotropic glutamate receptors. *Journal of Neuroscience* 28:4385–4397.

Wang LW, Berry-Kravis E, Hagerman RJ (2010) Fragile X: Leading the way for targeted treatments in autism. *Neurotherapeutics* 7:264–274.

Wang Y, Markram H, Goodman PH, Berger TK, Ma J, Goldman-Rakic PS (2006) Heterogeneity in the pyramidal network of the medial prefrontal cortex. *Nature Neuroscience* 9:534–542.

Warburton EC, Brown MW (2015) Neural circuitry for rat recognition memory. *Behavioural Brain Research* 285:131–139.

Watanabe K, Al-Bassam S, Miyazaki Y, Wandless TJ, Webster P, Arnold DB (2012) Networks of Polarized Actin Filaments in the Axon Initial Segment Provide a Mechanism for Sorting Axonal and Dendritic Proteins. *Cell Reports* 2:1546–1553.

Watson C, Hoeft F, Garrett AS, Hall SS, Reiss AL (2008) Aberrant brain activation during gaze processing in boys with fragile X syndrome. *Archives of General Psychiatry* 65:1315–1323.

Wefelmeyer W, Puhl CJ, Burrone J (2016) Homeostatic Plasticity of Subcellular Neuronal Structures: From Inputs to Outputs.

Weiergräber M, Kamp MA, Radhakrishnan K, Hescheler J, Schneider T (2006) The Cav2.3 voltage-gated calcium channel in epileptogenesis-Shedding new light on an enigmatic channel.

Weiler IJ, Irwin SA, Klintsova AY, Spencer CM, Brazelton AD, Miyashiro K, Comery TA, Patel B, Eberwine J, Greenough WT (1997) Fragile X mental retardation protein is translated near synapses in response to neurotransmitter activation. *Proceedings of the National Academy of Sciences of the United States of America* 94:5395–5400.

Weiler N, Wood L, Yu J, Solla SA, Shepherd GM (2008) Top-down laminar organization of the excitatory network in motor cortex. *Nature Neuroscience* 11:360–366.

Wen Y, Li W, Choudhury GR, He R, Yang T, Liu R, Jin K, Yang SH (2013) Astroglial PTEN loss disrupts neuronal lamination by dysregulating radial glia-guided neuronal migration. *Aging and Disease* 4:113–126.

Wermter AK, Kamp-Becker I, Strauch K, Schulte-Körne G, Remschmidt H (2008) No evidence for involvement of genetic variants in the x-linked neuroligin genes NLGN3 and NLGN4X in probands with autism spectrum disorder on high functioning level. *American Journal of Medical Genetics, Part B: Neuropsychiatric Genetics* 147:535–537.

Wijetunge LS, Angibaud J, Frick A, Kind PC, Nägerl UV (2014) Stimulated emission depletion (STED) microscopy reveals nanoscale defects in the developmental trajectory of dendritic spine morphogenesis in a mouse model of fragile X syndrome. *Journal of Neuroscience* 34:6405–6412.

Williams MR, De-Spenza T, Li M, Gulledge AT, Luikart BW (2015) Hyperactivity of newborn pten knock-out neurons results from increased excitatory synaptic drive. *Journal of Neuroscience* 35:943–959.

Willsey AJ, Sanders SJ, Li M, Dong S, Tebbenkamp AT, Muhle RA, Reilly SK, Lin L, Fertuzinhos S, Miller JA, Murtha MT, Bichsel C, Niu W, Cotney J, Ercan-Sencicek AG, Gockley J, Gupta AR, Han W, He X, Hoffman EJ, Klei L, Lei J, Liu W, Liu L, Lu C, Xu X, Zhu Y, Mane SM, Lein ES, Wei L, Noonan JP, Roeder K, Devlin B, Sestan N, State MW (2013) XCoexpression networks implicate human midfetal deep cortical projection neurons in the pathogenesis of autism. *Cell* 155:997.

Wilmar Saldarriaga, Flora Tassone, Laura Yuriko González-Teshima, Jose Vicente Forero-Forero, Sebastián Ayala-Zapata RH (2014) Fragile X syndrome. *Colombia Médica* 45:190–8.

Wilson BM, Cox CL (2007) Absence of metabotropic glutamate receptor-mediated plasticity in the neocortex of fragile X mice. *Proceedings of the National Academy of Sciences of the United States of America* 104:2454–2459.

Wimmer VC, Reid CA, So EY, Berkovic SF, Petrou S (2010) Axon initial segment dysfunction in epilepsy.

Winckler B, Forscher P, Mellman I (1999) A diffusion barrier maintains distribution of membrane proteins in polarized neurons. *Nature* 397:698–701.

Wiśniowiecka-Kowalnik B, Nesteruk M, Peters SU, Xia Z, Cooper ML, Savage S, Amato RS, Bader P, Browning MF, Haun CL, Duda AW, Cheung SW, Stankiewicz P (2010) Intragenic rearrangements in NRXN1 in three families with autism spectrum disorder, developmental delay, and speech delay. *American Journal of Medical Genetics, Part B: Neuropsychiatric Genetics* 153:983–993.

Wood L, Shepherd GM (2010) Synaptic circuit abnormalities of motor-frontal layer 2/3 pyramidal neurons in a mutant mouse model of Rett syndrome. *Neurobiology of Disease* 38:281–287.

Woolsey TA, Van der Loos H (1970) The structural organization of layer IV in the somatosensory region (S I) of mouse cerebral cortex. The description of a cortical field composed of discrete cytoarchitectonic units. *Brain Research* 17:205–242.

Worby CA, Dixon JE (2014) PTEN. *Annual Review of Biochemistry* 83:641–669.

World Health Organization (1992) ICD10 - version:2016.

Wright CF, McRae JF, Clayton S, Gallone G, Aitken S, FitzGerald TW, Jones P, Prigmore E, Rajan D, Lord J, Sifrim A, Kelsell R, Parker MJ, Barrett JC, Hurles ME, FitzPatrick DR, Firth HV (2018) Making new genetic diagnoses with old data: iterative reanalysis and reporting from genome-wide data in 1,133 families with developmental disorders. *Genetics in Medicine* 20:1216–1223.

Writzl K, Knegt AC (2013) 6p21.3 microdeletion involving the SYNGAP1 gene in a patient with intellectual disability, seizures, and severe speech impairment. *American Journal of Medical Genetics, Part A* 161:1682–1685.

Xiong Q, Oviedo HV, Trotman LC, Zador AM (2012) PTEN regulation of local and long-range connections in mouse auditory cortex. *Journal of Neuroscience* 32:1643–1652.

Xu K, Zhong G, Zhuang X (2013) Actin, spectrin, and associated proteins form a periodic cytoskeletal structure in axons. *Science* 339:452–456.

Xu X, Xiong Z, Zhang L, Liu Y, Lu L, Peng Y, Guo H, Zhao J, Xia K, Hu Z (2014) Variations analysis of NLGN3 and NLGN4X gene in Chinese autism patients. *Molecular Biology Reports* 41:4133–4140.

Xu ZH, Yang Q, Feng B, Liu SB, Zhang N, Xing JH, Li XQ, Wu YM, Gao GD, Zhao MG (2012) Group i mGluR antagonist rescues the deficit of D1-induced LTP in a mouse model of fragile X syndrome. *Molecular Neurodegeneration* 7.

Yamada R, Kuba H (2016) Structural and Functional Plasticity at the Axon Initial Segment. *Frontiers in Cellular Neuroscience* 10:1–7.

Yamashita T, Vavladeli A, Pala A, Galan K, Crochet S, Petersen SS, Petersen CC (2018) Diverse long-range axonal projections of excitatory layer 2/3 neurons in mouse barrel cortex. *Frontiers in Neuroanatomy* 12.

Yang DW, Pan B, Han TZ, Xie W (2004) Sexual dimorphism in the induction of LTP: Critical role of tetanizing stimulation. *Life Sciences* 75:119–127.

Yang S, Ben-Shalom R, Ahn M, Liptak AT, van Rijn RM, Whistler JL, Bender KJ (2016) β-Arrestin-Dependent Dopaminergic Regulation of Calcium Channel Activity in the Axon Initial Segment. *Cell Reports* 16:1518–1526.

Yang Y, Tao-Cheng JH, Reese TS, Dosemeci A (2011) SynGAP moves out of the core of the postsynaptic density upon depolarization. *Neuroscience* 192:132–139.

Yang Y, Ogawa Y, Hedstrom KL, Rasband MN (2007) βIV spectrin is recruited to axon initial segments and nodes of Ranvier by ankyrinG. *Journal of Cell Biology* 176:509–519.

Yang Y, Tao-Cheng JH, Bayer KU, Reese TS, Dosemeci A (2013) Camkii-Mediated Phosphorylation Regulates Distributions of Syngap-α1 and -α2 at the Postsynaptic Density. *PLoS ONE* 8.

Yin L, Rasch MJ, He Q, Wu S, Dou F, Shu Y (2017) Selective Modulation of Axonal Sodium Channel Subtypes by 5-HT1A Receptor in Cortical Pyramidal Neuron. *Cerebral cortex (New York, N.Y. : 1991)* 27:509–521.

Ylisaukko-oja T, Rehnström K, Auranen M, Vanhala R, Alen R, Kempas E, Ellonen P, Turunen JA, Makkonen I, Riikonen R, Nieminen-von Wendt T, von Wendt L, Peltonen L, Järvelä I (2005) Analysis of four neuroligin genes as candidates for autism. *European Journal of Human Genetics* 13:1285–1292.

Yoon L, Somerville LH, Kim H (2018) Development of MPFC function mediates shifts in self-protective behavior provoked by social feedback. *Nature Communications* 9.

Yoshimura T, Rasband MN (2014) Axon initial segments: Diverse and dynamic neuronal compartments.

Yu FH, Mantegazza M, Westenbroek RE, Robbins CA, Kalume F, Burton KA, Spain WJ, McKnight GS, Scheuer T, Catterall WA (2006) Reduced sodium current in GABAergic interneurons in a mouse model of severe myoclonic epilepsy in infancy. *Nature Neuroscience* 9:1142–1149.

Yuen RK, Merico D, Bookman M, Howe JL, Thiruvahindrapuram B, Patel RV, Whitney J, Deflaux N, Bingham J, Wang Z, Pellecchia G, Buchanan JA, Walker S, Marshall CR, Uddin M, Zarrei M, Deneault E, D'Abate L, Chan AJ, Koyanagi S, Paton T, Pereira SL, Hoang N, Engchuan W, Higginbotham EJ, Ho K, Lamoureux S, Li W, MacDonald JR, Nalpathamkalam T, Sung WW, Tsoi FJ, Wei J, Xu L, Tasse AM, Kirby E, Van Etten W, Twigger S, Roberts W, Drmic I, Jilderda S, Modi BM, Kellam B, Szego M, Cytrynbaum C, Weksberg R, Zwaigenbaum L, Woodbury-Smith M, Brian J, Senman L, Iaboni A, Doyle-Thomas K, Thompson A, Chrysler C, Leef J, Savion-Lemieux T, Smith IM, Liu X, Nicolson R, Seifer V, Fedele A, Cook EH, Dager S, Estes A, Gallagher L, Malow BA, Parr JR, Spence SJ, Vorstman J, Frey BJ, Robinson JT, Strug LJ, Fernandez BA, Elsabbagh M, Carter MT, Hallmayer J, Knoppers BM, Anagnostou E, Szatmari P, Ring RH, Glazer D, Pletcher MT, Scherer SW (2017) Whole genome sequencing resource identifies 18 new candidate genes for autism spectrum disorder. *Nature Neuroscience* 20:602–611.

Yuste R (2011) Dendritic spines and distributed circuits.

Zahir FR, Baross A, Delaney AD, Eydoux P, Fernandes ND, Pugh T, Marra MA, Friedman JM (2008) A patient with vertebral, cognitive and behavioural abnormalities and a de novo deletion of NRXN1α. *Journal of Medical Genetics* 45:239–243.

Zeng M, Shang Y, Araki Y, Guo T, Huganir RL, Zhang M (2016) Phase Transition in Postsynaptic Densities Underlies Formation of Synaptic Complexes and Synaptic Plasticity. *Cell* 166:1163–1175.e12.

Zernig G, Pinheiro BS (2015) Dyadic social interaction inhibits cocaine-conditioned place preference and the associated activation of the accumbens corridor.

Zhang W, Vazquez L, Apperson M, Kennedy MB (1999) Citron binds to PSD-95 at glutamatergic synapses on inhibitory neurons in the hippocampus. *Journal of Neuroscience* 19:96–108.

Zhang Y, Bonnan A, Bony G, Ferezou I, Pietropaolo S, Ginger M, Sans N, Rossier J, Oostra B, LeMasson G, Frick A (2014) Dendritic channelopathies contribute to neocortical and sensory hyperexcitability in Fmr1-/y mice. *Nature Neuroscience* 17:1701–1709.

Zhao MG, Toyoda H, Ko SW, Ding HK, Wu LJ, Zhuo M (2005) Deficits in trace fear memory and long-term potentiation in a mouse model for fragile X syndrome. *Journal of Neuroscience* 25:7385–7392.

Zheng J, Winkeler A, Peyronneau MA, Dollé F, Boisgard R (2016) Evaluation of PET Imaging Performance of the TSPO Radioligand [18F]DPA-714 in Mouse and Rat Models of Cancer and Inflammation. *Molecular Imaging and Biology* 18:127–134.

Zhong G, He J, Zhou R, Lorenzo D, Babcock HP, Bennett V, Zhuang X (2014) Developmental mechanism of the periodic membrane skeleton in axons. *eLife* 3.

Zhou D, Lambert S, Malen PL, Carpenter S, Boland LM, Bennett V (1998) Ankyrin(G) is required for clustering of voltage-gated Na channels at axon initial segments and for normal action potential firing. *Journal of Cell Biology* 143:1295–1304.

Zhu JJ, Qin Y, Zhao M, Van Aelst L, Malinow R (2002) Ras and Rap control AMPA receptor trafficking during synaptic plasticity. *Cell* 110:443–455.

Zoghbi HY, Bear MF (2012) Synaptic dysfunction in neurodevelopmental disorders associated with autism and intellectual disabilities. *Cold Spring Harbor Perspectives in Biology* 4.

Zollino M, Gurrieri F, Orteschi D, Marangi G, Leuzzi V, Neri G (2011) Integrated analysis of clinical signs and literature data for the diagnosis and therapy of a previously undescribed 6p21.3 deletion syndrome. *European Journal of Human Genetics* 19:239–242.

Zori RT, Marsh DJ, Graham GE, Marliss EB, Eng C (1998) Germline PTEN mutation in a family with Cowden syndrome and Bannayan-Riley-Ruvalcaba Syndrome. *American Journal of Medical Genetics* 80:399–402.

Zweier C, de Jong EK, Zweier M, Orrico A, Ousager LB, Collins AL, Bijlsma EK, Oortveld MA, Ekici AB, Reis A, Schenck A, Rauch A (2009) CNTNAP2 and NRXN1 Are Mutated in Autosomal-Recessive Pitt-Hopkins-like Mental Retardation and Determine the Level of a Common Synaptic Protein in Drosophila. *American Journal of Human Genetics* 85:655–666.